SQT

DOE/NASA/0168-80/1
NASA CR-165178
DDA EDR 10327

ADVANCED GAS TURBINE (AGT) POWERTRAIN SYSTEM DEVELOPMENT FOR AUTOMOTIVE APPLICATIONS

First semi-annual report for work performed from October 1, 1979 — June 30, 1980

DETROIT DIESEL ALLISON
DIVISION OF GENERAL MOTORS CORPORATION

May 1981

Prepared for
NATIONAL AERONAUTICS AND SPACE ADMINISTRATION
Lewis Research Center
Cleveland, Ohio 44135
Under Contract DEN 3-168

for
U. S. DEPARTMENT OF ENERGY

Conservation and Solar Energy
Office of Transportation Programs
Washington, D. C.

(NASA-CR-165178) ADVANCED GAS TURBINE (AGT) POWERTRAIN SYSTEM DEVELOPMENT FOR AUTOMOTIVE APPLICATIONS Semiannual Report, 1 Oct. 1979 - 30 Jun. 1980 (Detroit Diesel Allison, Indianapolis, Ind.) 235 p HC A13/MF A01 CSCL 13F

N83-12431

G3/37 00775 Unclas

NOTICE

FOREWORD

This report presents a technical summary of the Detroit Diesel Allison (DDA) project to develop an automotive gas turbine powertrain system under NASA Contract DEN 3-168 (Department of Energy funding). It covers the 9-month period October 1979 through June 1980. Future reports will cover 6-month periods.

The basic objective of this project is to develop and demonstrate, by May 1985, an advanced automotive gas turbine powertrain system that will, when installed in a 1985 Pontiac Phoenix vehicle of 1360 kg (3000 lbm) inertia weight, achieve a fuel economy of 18 km/L (42.5 mpg), meet or exceed the 1985 emission requirements, and have alternate fuel capability.

Several General Motors Divisions and other companies are major contributors to this effort. They are: Pontiac Motor Division--vehicle, Delco Electronics Division--electronic control, Harrison Radiator Division and Corning Glass Works--regenerator, Hydra-Matic Division--transmission, The Carborundum Company and GTE--ceramics.

The DDA Program Manager for the AGT 100 is H. E. Gene Helms; design effort is directed by James Williams; materials effort is directed by Dr. Peter Heitman and project effort is directed by Richard Johnson. The Pontiac effort is headed by J. Kaufeld, and the Delco Electronics work is managed by Robert Kordes. The NASA AGT 100 Project Manager is Paul T. Kerwin and Assistant Project Manager is James Calogeras.

TABLE OF CONTENTS

LIST OF ILLUSTRATIONS

LIST OF TABLES

SUMMARY

Detroit Diesel Allison (DDA), Division of General Motors Corporation, has recently initiated a 68 month Advanced Gas Turbine Powertrain System Development project under contract DEN 3-168 to NASA Lewis Research Center, sponsored with funds from the Department of Energy Office of Transportation Programs.

The objective of the project is to develop an experimental powertrain system that demonstrates; (1) a combined cycle fuel economy of 17.9 km/L (42.5 mpg) using diesel fuel No. 2 in a 1984 Pontiac Phoenix of 1364 kg (3000 lbm) weight on a 15°C (59°F) day; (2) emission levels less than federal research standards; and (3) the ability to use a variety of fuels. It is intended that the technology demonstrated through this project could assist the automotive industry in making a go/no go decision leading to production engineering development of gas turbine powertrains.

While meeting the project objective, designs are constrained to: (1) achieve reliability and life in the turbine powertrain comparable to 1985 vehicles; (2) achieve initial and life cycle powertrain costs competitive with 1985 powertrains; (3) demonstrate vehicle acceleration suitable for safety and manueverability; and (4) meet 1985 federal vehicle noise and safety standards.

The Pontiac Phoenix 1984 X-body automobile has been selected as the demonstration vehicle with a Hydra-Matic four-speed transmission. A Delco Electronics control system, using a basic automotive electronic control to be introduced in early 1980 General Motors cars, will be modified to service the turbine engine. Harrison Radiator Division will supply the regenerator system for the engine. The Corning Glass Company (regenerator disks and other parts), the Carborundum Company (most hot flow path parts), and the GTE Sylvania Company (ceramic rotors) will supply the ceramic components.

Key elements of the project are developing small, high-performance turbine engine components as well as ceramic components to meet engine requirements. Emphasis on component aerodynamic and ceramic component development initiated this project.

This report covers the work for the time period October 1979 through June 1980. The major accomplishments for this period are given in the succeeding paragraphs.

VEHICLE SYSTEM DEVELOPMENT

The main thrust of the design work at Pontiac has been to integrate the powertrain with the vehicle. Preliminary layouts have been made for the exhaust system, air induction system, and battery installation. Points of interference have been identified and resolved by altering either the vehicle or engine designs.

ENGINE/POWERTRAIN DEVELOPMENT

An engine general arrangement has evolved as a result of studies to meet the vehicle engine compartment constraints while minimizing the duct pressure losses and the heat rejection. A power transfer system (between gasifier and power turbines) has been developed to maintain nearly constant temperatures throughout the entire range of engine operation.

An advanced four-speed automatic transmission has been selected to be used with the engine.

Performance calculations comparing the current fixed geometry reference powertrain design (RPD)* engine with an earlier conceptual design (ref. 2) using variable geometry show improvements in component efficiencies and an increase in fuel economy from 18.1 to 18.3 km/L (42.5 to 43.1 mpg).

COMPRESSOR DEVELOPMENT

A 4.5:1 R_c, single-stage centrifugal compressor design has been completed and released for procurement. The impeller has 16 full blades and 16 splitters. The maximum power efficiency goal (15°C, 59°F) is 82.8%. The collecter is designed to maintain a circumferentially constant static pressure at design point, and the low exit velocity minimizes losses in the regenerator ducting. The compressor rig layout design is complete, and rig testing will be started during the next reporting period.

GASIFIER TURBINE DEVELOPMENT

Development activity concentrated on preliminary design of the RPD gasifier turbine and transition duct, preliminary design of the Mod I gasifier turbine, bench testing of the interturbine transition duct, layout and fabrication of the gasifier turbine test rig, and turbine facility checkout. Aerodynamic design details for the RPD flow path, scroll, vanes, and the rotor are presented. Initial design details of the Mod I turbine are also given. In the Mod I flow path, effort has been made to minimize aerodynamic penalties when exchanging metal and ceramic components. A cold flow test of a metal interturbine duct is described.

A layout of the current mechanical design of the gasifier scroll is presented and the revised design is discussed. The design of the metal Mod I rotor is presented with a design discussion of the ceramic rotor.

The gasifier turbine aerodynamic rig activity has consisted of the design and fabrication of parts for the first turbine rig assembly and test.

POWER TURBINE DEVELOPMENT

Effort has focused on preliminary design of the RPD power turbine and exhaust duct, preliminary design of the Mod I power turbine, layout and fabrication of the interturbine duct/scroll bench rig, and layout of the power turbine test rig.

The RPD and Mod I rotors are both designed for efficient high-response operation and ease of manufacture.

The Mod I (metal) rotor design is underway. A potential inducer bending problem has been eliminated, and calculations show a stress-rupture life greater than 50,000 h for this design. Finite element analyses and dynamic analyses of the ceramic rotor are progressing. The design of both the RPD and Mod I scrolls is in progress.

*The RPD is presented as a "Concept" of a fully developed production engine. It will be updated as the project continues. The Mod II demonstrator engine will converge toward the RPD as the project nears completion.

COMBUSTOR DEVELOPMENT

The aerodynamic and mechanical designs of the RPD and Mod I combustors are presented. Both these designs are low-emission combustors in which the fuel is mixed and vaporized in a prechamber before being ignited in the main burning zone. The temperature control required is maintained by adjusting the division of primary and dilution air.

The RPD layout is complete. The Mod I layout and detailed drawings are complete, and parts are on order for fabrication.

A new combustor rig has been designed and a layout is presented. Also a prechamber test is described, and test data are presented.

REGENERATOR DEVELOPMENT

The layout describing the RPD regenerator is complete; excerpts are presented in this report. A thermal analysis of the disk is partially complete, and disk temperatures have been calculated for idle, 100% engine speed, and 32% engine speed (48.3 km/h (30 mph) vehicle speed). The effects of variation in inlet gas flow distribution have been examined and are shown at 100% engine speed. Mechanical designs of both hot and cold seals are discussed.

The Mod I regenerator system has been designed and varies only slightly from the RPD design.

Several rigs are required for the regenerator program. A hot test rig has been designed, and fabrication of parts has started. A cold flow distribution rig is in the design layout phase. The capability will exist to simulate both air and gas sides of the regenerator with this latter rig. A sealing leaf leakage test rig layout has been started.

SECONDARY SYSTEMS

Four general areas are treated here--the block and insulation, gearbox and power transfer, rotor bearings, and secondary airflow system and thrust balance.

The mechanical design of the block is strongly influenced by the need to control metal temperatures and heat rejection by insulation. Because of the high temperatures expected in some localized areas, a nickel alloy (Ni-Resist) has been selected for the initial block material to ensure dimensional stability and minimize risk in the development engines.

The gearbox is described, and the principal features of the power turbine and gasifier gear trains are identified. The starter geartrain is also described.

Operating lives have been predicted for the four main bearings. These range from 1780 h for the No. 3 bearing to 730,000 h (infinite life) for the No. 4 bearing. The lives of bearings No. 1 and No. 2 are 4500 and 3000 h, respectively.

Secondary flow losses are defined and tabulated for the entire gas path, and the thrust balances are also tabulated. Five engine conditions from idle to full power are considered.

MATERIALS DEVELOPMENT

The DDA design support effort and the Carborundum effort are discussed. DDA work has concentrated on defining the materials for the RPD and Mod I designs. Carborundum is the principal ceramic supplier, and its unique work is described. In the rotor development effort, it has been shown that reaction-bonded SiC is stable and compatible with engine operating conditions. Ultrasonic machining methods have been successful, but cutting rates are slow. Thixotropic casting studies on the Mod I gasifier rotor have been moderately successful. Transfer molding studies were not successful and were terminated. For stationary parts, slip casting has been selected as the primary method of fabrication, but mandrel-coating techniques are being pursued as an alternative method.

CONTROLS DEVELOPMENT

The controls effort is divided between Delco Electronics and DDA. Delco's main effort is concerned with the electronic control unit. DDA maintains overall control system responsibility. Work has been done to define interface sensors and key areas of the control system specification with Delco. The DDA effort has been in three areas--defining key hardware items, defining the control mode, and developing the necessary digital simulations and related analysis techniques.

TRANSMISSION DEVELOPMENT

A four-speed automatic transaxle transmission will be used with the AGT 100 engine. Output power requirements range from 0.79 kW (1.055 hp) at 16 km/h (10 mph) to 14.9 kW (20 hp) at 96 km/h (60 mph). This transmission gives maximum fuel economy at steady state road load by utilizing the power transfer system to minimize engine output shaft speed.

SUPPORTIVE MANUFACTURING, COST, AND MARKETABILITY

Pontiac has been assessing manufacturing feasibility of components as the designs are finalized to assess manufacturing feasibility. The studies concentrate in three areas--analysis for machinability and assembly, recommended changes to improve producibility, and tooling and piece-rate studies to determine production costs.

INTRODUCTION

This is one of a series of semi-annual reports documenting work performed on an Advanced Gas Turbine (AGT) powertrain system development project for automotive applications. The work is performed under NASA/DOE contract DEN3-168. The objective of the project is to develop an experimental powertrain system that demonstrates: (1) a combined cycle fuel economy of 17.9 km/L (42.5 mpg) using diesel fuel No. 2 in a 1984 Pontiac Phoenix of 1364 kg (3000 lbm) weight on a 15.5°C (59°F) day, (2) emission levels less than federal standards, and (3) the ability to use a variety of fuels. It is intended that the technology demonstrated through this project would assist the automotive industry in making a go/no go decision regarding the production engineering development of gas turbine powertrains.

In meeting the project objective, the design is constrained to: (1) achieve reliability and life comparable to conventional 1985 vehicles, (2) achieve initial and life cycle powertrain costs competitive with 1985 powertrains, (3) demonstrate vehicle acceleration suitable for safety and manueverability, and (4) meet 1985 federal vehicle noise and safety standards.

A team concept is used in this project, with many of the team members being General Motors Divisions. Detroit Diesel Allison is the prime contractor and team leader with responsibility for the overall powertrain and controls. Pontiac Motor Division (PMD) has vehicle responsibility. Delco Electronics will develop the electronic control, and Delco Remy will develop the starter/boost system for the engine. Hydra-matic Division will produce the four-speed automatic transmission that will be used with the engine, and Harrison Radiator Division (HRD) is involved in the regenerator design and fabrication. The primary non-GM groups on the team are Carbordundum and GTE, both of whom are involved in the ceramic effort.

Prior to this contract, DDA and PMD conducted a gas turbine powertrain concept study (contract DEN3-28). In July 1979 the results of the concept study (ref. 1) were published by DDA. In this study, several configurations had been evaluated and a two-shaft regenerative engine, coupled with a conventional automatic transmission, was recommended as providing the potential for meeting the established goals. Further results of the concept study were published in March 1980 (ref. 2) wherein the long-lead technology development tasks required to support the design and development of an Experimental Advanced Gas Turbine Powertrain were presented. Both these studies were funded through NASA contract DEN3-28.

The current project became effective October 1979. As shown in Figure 1 the program is 68 months long, and divided into two phases. Phase I is 45 months long and Phase II is 23 months. Establishing and maintaining a Reference Powertrain Design (RPD) is a continuing activity, as is component development effort. In addition, two experimental powertrain versions will be designed, fabricated and tested. Mod I, the first, is the early version and is a stepping stone to Mod II, which is the final project version. Powertrain testing will be conducted on an engine dynamometer, as well as in vehicles.

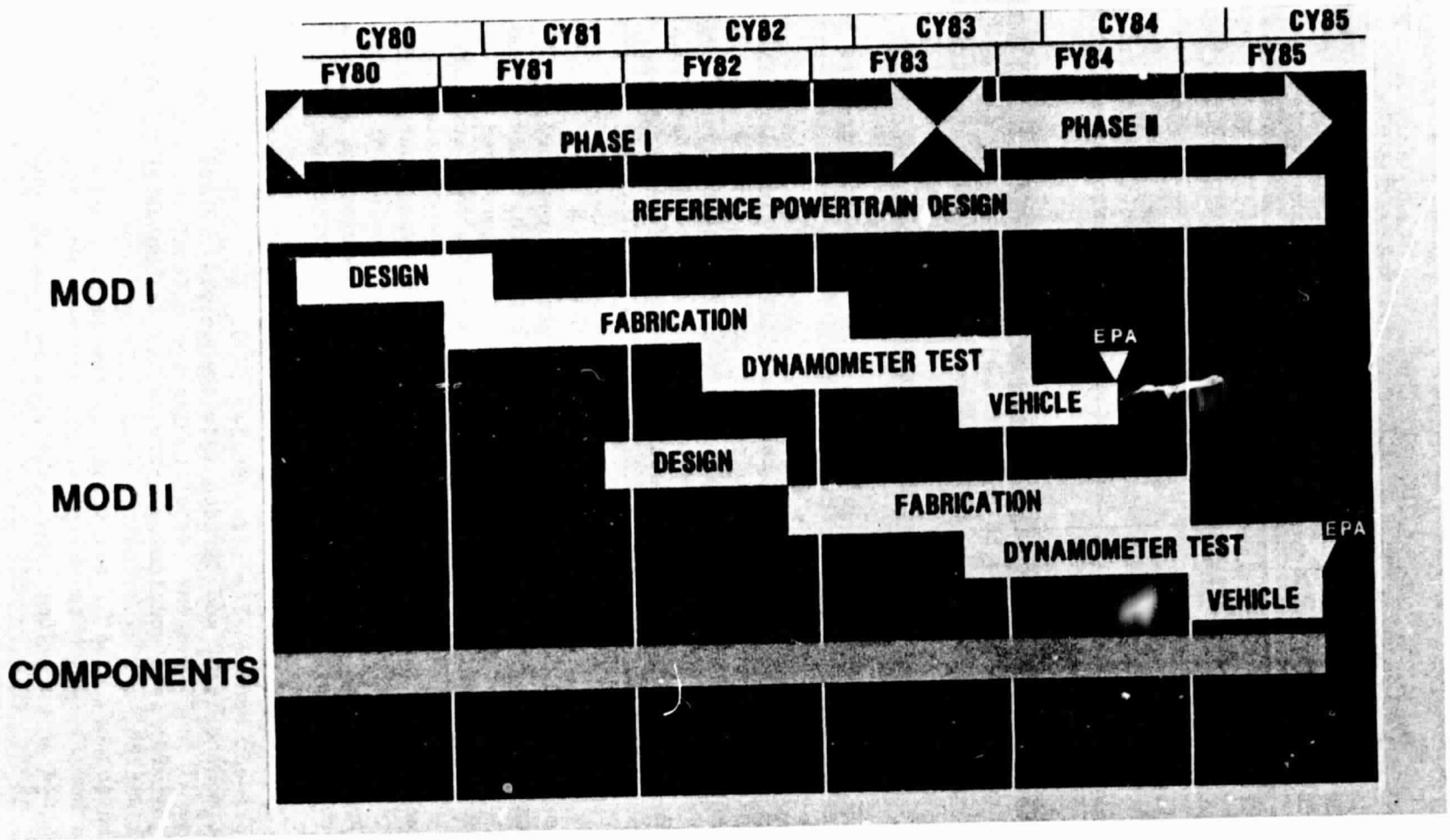

Figure 1. - AGT-100 Powertrain Development Schedule.

A Reference Powertrain Design (RPD) is a preliminary engineering design of the powertrain system that has the best potential for meeting the goals and objectives of the project. The RPD can incorporate timely emerging technologies, and it will be updated as project activity progresses.

The RPD in this current program evolved from the earlier studies identified previously. The RPD is presented as a "concept" of a fully developed production powertrain. The Mod I and Mod II experimental engines should converge toward the RPD as this development project proceeds.

The main development challenges in the program are in building small, high-performance gas turbine components and developing ceramic components for the required high engine cycle temperatures. Because of the small size engine, 0.35 kg/s (0.77 lbm/sec) airflow, extensive rig testing is planned for component development. A major ceramic component development program is being pursued, and the ultimate success of the engine depends heavily on the success of this activity.

This report is structured on a component priority basis (e.g., all work relating to the gasifier turbine rotor, including rig work and ceramic rotor development, is discussed as a part of the gasifier turbine section). Exceptions to this are functional areas that are not peculiar to any one major component. Engine Subsystems cover structures, gearbox and power transfer, rotor bearings, shafts/seals, and secondary flow. There are separate sections for materials development and controls development.

The report treats the largest item, the vehicle, first, then the engine/powertrain, then the major components of the powertrain, followed by the subsystems, materials, and controls. The transmission and manufacturing feasibility and cost efforts are treated last. Within each section the work discussed is identified as it pertains to the RPD, Mod I, or Mod II designs.

I. VEHICLE SYSTEM DEVELOPMENT

1.1 VEHICLE DESIGN

The main thrust of the design work at Pontiac has been to integrate the powertrain with the vehicle. Preliminary layouts have been made for the exhaust system, air induction system, and battery installation. Interference points have been identified and resolved by either altering the vehicle or the engine designs.

Vehicle Specifications

Compact sedan	Wheelbase 2.654 m (104.5 in.)
Vehicle accessories	Power steering, power brakes, heater/air conditioning
Vehicle drive train	Transverse-mounted engine, torque converter with lockup clutch, four-speed automatic transmission, 2.84 rear axle ratio, 185/80R13 tires
Vehicle weight, curb	1235 kg (2723 lb)
test	1370 kg (3021 lb)
Fuel tank	34 L (9 gal) capacity
Range	610 km (380 mi)
Roominess index	7018 mm (276.3 in.)
Luggage capacity	0.37 m^3 (13.1 ft^3)

Exhaust System

The basic layout of the exhaust system has been completed relative to the vehicle installation with only the connector between the duct and the engine yet to be completed. The duct will be 194 cm^2 (30 $in.^2$) in cross-sectional area with turns designed to minimize flow restriction. The rear section of the duct passes under the rear seat, over the rear axle beam, and exits under the bumper at the right rear. The floor of the car has been modified to provide a tunnel large enough to accommodate the large exhaust duct. However, this has not affected the design of either the front or rear seats, and has maintained ample foot well area for two passengers front and three passengers rear, consistent with the current passenger capacity of the front wheel drive X-body car.

Engine Air Induction System

The induction system initial design includes two separate air cleaner assemblies. The AGT-100 engine has airflow of 0.349 kg/s (0.77 lbm/sec) with a required air filter area of approximately 0.226 m^2 (350 $in.^2$). Several schemes were studied to optimize the air inlet and the air cleaner size. Results as proposed for the RPD are shown by the schematic in Figure 2 and the layout in Figure 3. Air flows into the air cleaner through an opening in the inner fender skirt, through poly foam filters, and into the compressor air inlet through a plastic duct system. The ducts will be attached to the air inlet with flexible connectors to accommodate the relative motion between the engine on its mounts and the ducts, which are attached to the vehicle.

Battery Installation

Space utilization suggests that the battery, 330.2 mm long x 172.0 mm wide x 238.8 mm high (13.0 in. long x 6.8 in. wide x 9.4 in. high), be initially relocated to the rear cargo area. The spare tire well was redesigned to accommodate the battery with the necessary hold down clamps. The cover of the battery compartment is sealed, and the battery is vented to outside air. The electrical connections are via an 0-gage positive cable from the battery to the starter and short ground cables from the body to the battery and body to the engine similar to the system used on the General Motors Corvette since 1968. The spare tire is then mounted on top of the battery cover in the cargo area. The schematic for this system is shown in Figure 4. Additional installation studies are being conducted.

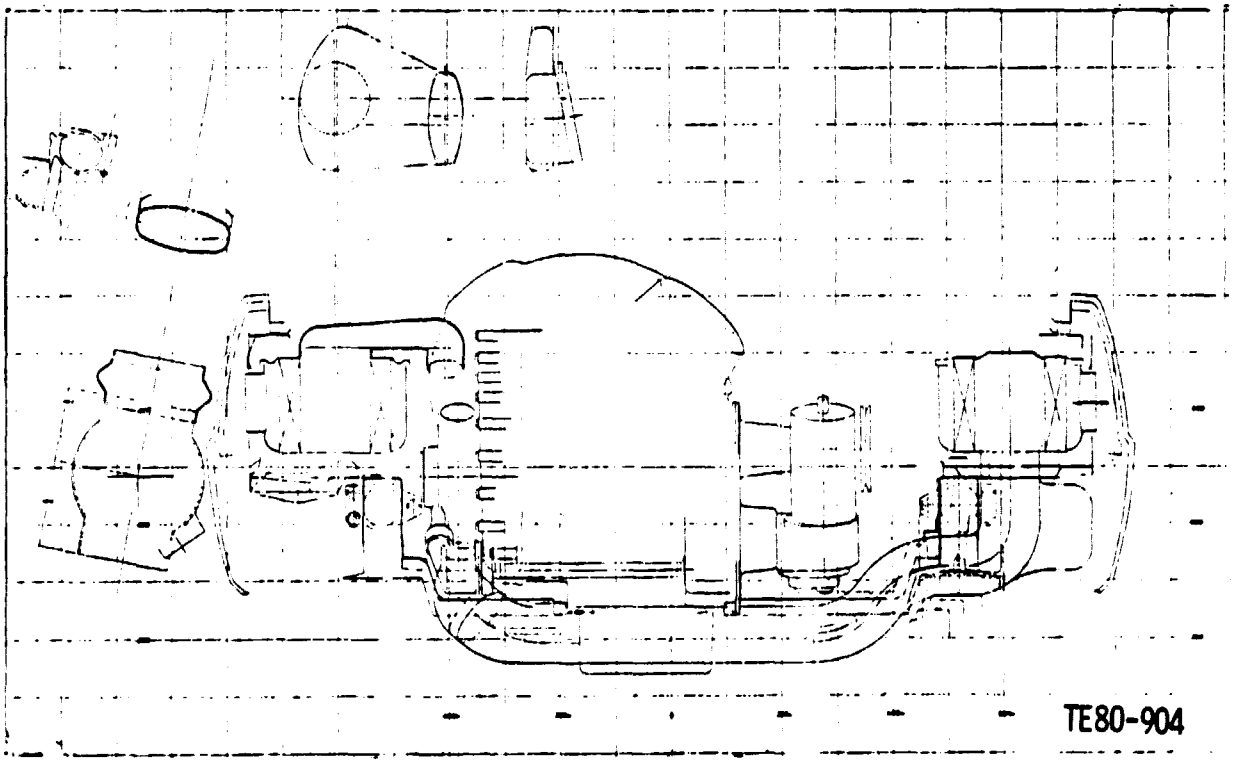

Figure 2. - Induction System Schematic--Conventional (Outside-In) Flow.

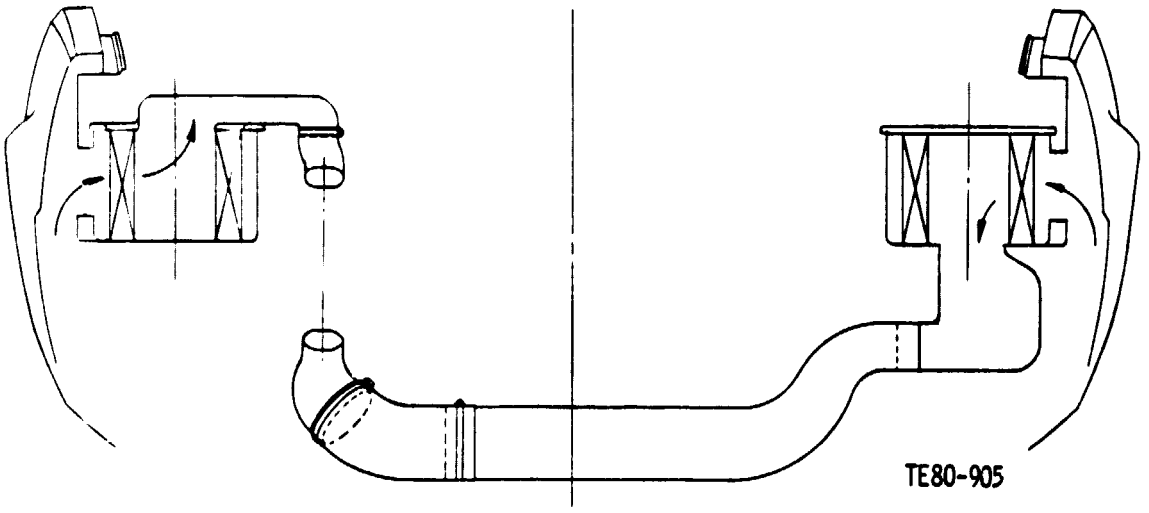

Figure 3. - AGT-100 Induction System.

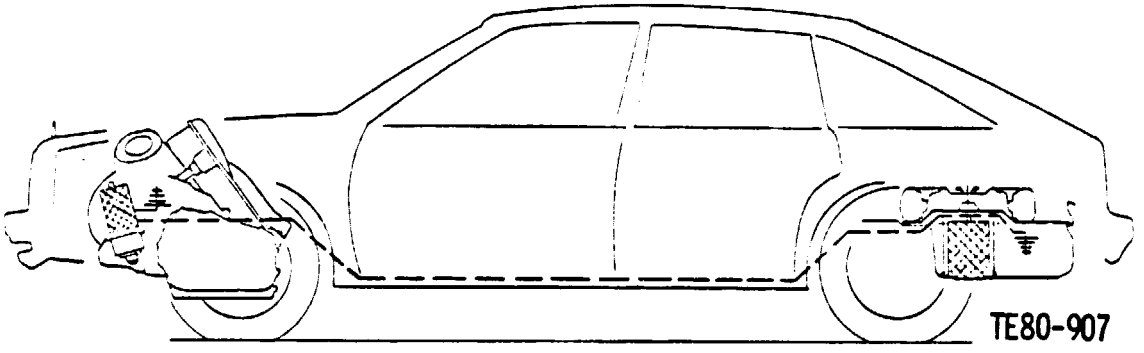

Figure 4. - AGT-100 Vehicle Battery/Starter Schematic.

II. ENGINE/POWERTRAIN DEVELOPMENT

2.1 REFERENCE POWERTRAIN DEVELOPMENT

General Arrangement

An engine general arrangement evolved as a result of studies (ref. 1) to meet the vehicle engine compartment constraints while minimizing the duct pressure losses and engine heat rejection.

The general arrangement was also impacted by decisions to:

- o Add power transfer and reduce the number of variable geometry elements--This change precipitated further study to use the space vacated by the variable geometry mechanisms for lower loss ducting and improved insulation.
- o Modify and enlarge the starter to provide a power boost to the gas generator rotor during accelerations thereby providing improved transient response--The engine driven accessory locations and drives were modified to accommodate this change.
- o Relocate the transmission--The engine was modified by shortening the engine gearbox and reducing the length of the gasifier-to-power turbine interconnecting duct.

The general arrangement that resulted from these studies and changes is shown in Figure 5. The arrangement is also being used as a basis for the Mod I engine design, accessory mounting, and installation studies.

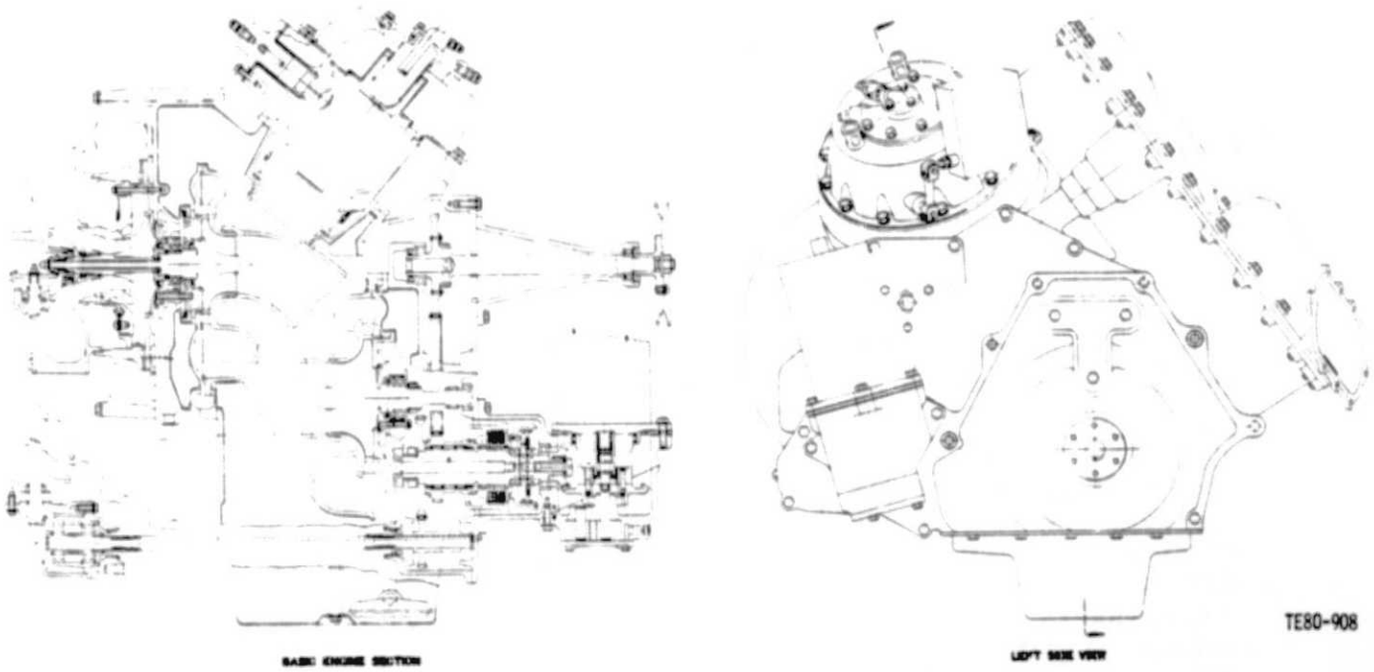

Figure 5. - RPD Engine General Arrangement.

Performance

At the beginning of this reporting period a review of the AGT-100 design concept (ref. 2) was conducted. Detailed design work and supplier cost analysis had indicated a high degree of risk and cost associated with the proposed ceramic fully variable geometry configuration relative to the gasifier and power turbine variable nozzle vanes. The objective of the review was to define a lower risk and cost fixed geometry configuration with little or no driving cycle fuel economy loss compared with the proposed fully variable configuration.

The configuration selected was a two-shaft engine with power transfer. Turbines and compressor outlet are of fixed geometry design and variable geometry is retained in the combustor and the compressor inlet guide vanes.

Combustor variable geometry is required for emission control, and variable compressor inlet guide vanes provide low power modulation. By modulating inlet guide vanes at low power airflow, the gasifier idle speed can be raised from that required for an all fixed geometry engine while minimizing fuel consumption. The higher gasifier idle speed results in improved vehicle acceleration performance.

Table I is a tabulation of max power cycle parameters, predicted driving cycle fuel economy, and predicted wide open throttle vehicle response for both the fully variable geometry and the fixed geometry configurations. Table I shows the fixed geometry engine to have 1.4% better driving cycle fuel economy than the variable geometry engine, due primarily to improved component efficiencies and a slower idle speed. Vehicle response (in time to 96.6 km/hr), is reduced to an unacceptable level.

Several methods for improving vehicle response were investigated. Table II is a summary of the results of this investigation including estimated fuel economy penalty associated with each method for improving vehicle response. The methods investigated are described below:

- o Gasifier rotor boost--Uses the engine starting motor to assist the acceleration of the gasifier rotor. Estimated usage is 152 one-second pulses per 161 km (100 mi) of combined EPA driving cycle mileage. The fuel economy penalty is based on a continuous battery recharging load of 0.33 kW (0.44 hp).
- o Gasifier rotor boost and scheduled power transfer--The specifications are the same as above but with the addition of power transfer at the beginning of the acceleration. The transfer is reduced to zero when gasifier rotor speed increases to 60%. The transfer retards the gasifier rotor acceleration and reduces the 4.0-second vehicle response but improves the 1.0-second response. The driving cycle fuel economy is the same as with rotor boost alone.
- o 55% gasifier idle speed--Gasifier rotor acceleration time is reduced, and, consequently, vehicle response is improved by increasing gasifier idle speed. However, an alternate method must be used to reduce steady-state power to acceptable idle level. Two methods of doing this are 1) throttled

compressor inlet or 2) exhaust gas recirculation to the compressor inlet. Either method results in a loss of driving cycle fuel economy, the throttled inlet being somewhat worse.

TABLE I. AGT-100 RPD ENGINE/VEHICLE PERFORMANCE

	Engine Concept			
	Fully variable geometry	Fixed geometry with power transfer	Change from variable to fixed	Comments
o Max power cycle parameters				
Altitude/ambient temp, °C (°F)	SL/15 (59)	SL/15 (59)		
Shaft power, kW (hp)	74.6 (100)	74.6 (100)		
Specific fuel consumption, mg/W·h (lbm/hp·h)	214.5 (0.3527)	198.1 (0.3257)	-7.7%	Improved cycle performance
Compressor inlet air flow, kg/s (lbm/s)	0.37 (0.81)	0.34 (0.76)	-8.2%	To maintain 74.6 kW (100 hp)
Compressor pressure ratio	4.5	4.5		
Gasifier turbine inlet temp, °C (°F)	1288 (2350	1288 (2350)		
Component efficiency				
o Compressor (T-S), %	80.1	82.8	+2.7 pts.	Reduced aerodynamic losses
o Regenerator, %	94.1	94.7	+0.6 pts.	Reduced flow
o Burner	99.9	99.9		
o Gasifier turbine (T-T), %	83.6	84.6	+1.0 pts.	Reduced aerodynamic losses
o Power turbine (T-T), %	85.6	86.7	+1.1 pts.	Reduced aerodynamic losses
Total duct pressure loss, %	15.9	15.0	-0.9 pts.	Reduced flow and improved design
Secondary flow, %	8.0	7.0	-1.0 pts.	Reduced turbine vane leakage
Primary flow path heat rejection, kW (Btu/m)	4.6 (261.4)	2.6 (15.0)	-44%	Improved insulation
Mechanical loss, kW (hp)	6.0 (8.0)	5.8 (7.8)	-2.5%	Improved bearing and spin losses
o Driving cycle fuel economy				
Gasifier idle speed, %	60	50		
Driving cycle fuel economy*, km/L (mpg)	18.1 (42.5)	18.3 (43.1)		
o Wide open throttle vehicle response				
Gasifier idle speed, %	60	50		
Max gasifier turbine inlet temp, °C (°F)	1343 (2450)	1343 (2450)		
Rotor accel time, idle to 100%, s	1.5	2.9		
Gasifier rotor inertia, kg·m^2 (lbm·in.^{2})	0.00056 (1.92)	0.00071 (2.43)		
Engine output inertia kg·m^2 (lbm·in.^{2})	0.1875 (640.7)	0.2583 (882.8)		
Vehicle performance				
o Distance in 1.0 sec, m (ft)	1.04 (3.4)	0.30 (1.0)		*DF#2, SL 15°C (59°F)
o Distance in 4.0 sec, m (ft)	28.7 (94)	14.6 (48)		
o Time to 96.6 km/hr (60 mph), s	13.0	15.3		

TABLE II. AGT-100 RPD ENGINE/VEHICLE WIDE OPEN THROTTLE RESPONSE AND DRIVING CYCLE FUEL ECONOMY

	Gasifier Idle speed %	Gasifier rotor boost	Scheduled power transfer	Distance in 1.0 s, m (ft)	Distance in 4.0 s, m (ft)	Time to 96.6 km/hr (60 mph), s	Rotor accel time s	Driving cycle fuel econ,* km/L (mpg)
Base fixed geometry w/power transfer	50	No	No	0.30 (1.0)	14.6 (48)	15.3	2.90	18.3 (43.1)
o Gasifier rotor boost	50	Yes	No	0.39 (1.3)	20.1 (66)	14.6	2.00	17.6 (41.4)
o Gasifier rotor boost and scheduled power transfer†	50	Yes	Yes	0.46 (1.5)	19.2 (63)	14.7	2.15	17.6 (41.4)
o 55% idle, throttled inlet	55	No	No	0.43 (1.4)	18.6 (61)	14.7	2.40	17.6 (41.3)
o 55% idle, exhaust gas recirculation	55	No	No	0.43 (1.4)	18.6 (61)	14.7	2.40	17.9 (42.1)

*DF#2 SL 15°C (59°F)

†This case selected for RPD.

Optimization of compressor inlet guide vane schedule for best driving cycle fuel economy is shown in Table III. The optimum schedule shows a 1.0% fuel economy improvement relative to the base 0° IGV schedule.

TABLE III. AGT-100 RPD INLET GUIDE VANE OPTIMIZATION FOR FUEL ECONOMY

DF#2 SL 15°C (59°F)

Point No.*	Engine power, kW	(hp)	Gasifier speed, %	Nominal IGV Driving cycle time/161 km (100 mi), h	0-deg Fuel rate, kg/hr	(lbm/h)	20-deg Fuel rate, kg/h	(lbm/h)	40-deg Fuel rate, kg/h	(lbm/h)	60-deg Fuel rate, kg/h	(lbm/h)	Optimized Fuel rate, kg/h	(lbm/hr)
1	35	(47)	71	0.038	6.92	(15.25)	6.96	(15.35)	7.32	(16.14)	8.02**	(17.67)	6.92	(15.25)
2	25	(33)	73	0.098	4.87	(10.74)	4.87	(10.73)	4.96	(10.94)	5.64	(12.44)	4.87	(10.73)
3	19	(25)	75	0.151	4.31	(9.51)	4.21	(9.29)	4.05	(8.93)	4.21	(9.29)	4.05	(8.93)
4	19	(25)	60	0.271	3.93	(8.66)	3.93	(8.67)	3.98	(8.77)	4.32	(9.52)	3.93	(8.66)
5	12.3	(16.5)	61	0.425	2.77	(6.10)	2.75	(6.06)	2.82	(6.22)	2.89	(6.37)	2.75	(6.06)
6	10.4	(14)	52	0.406	2.49	(5.50)	2.48	(5.46)	2.50	(5.52)	2.60	(5.73)	2.48	(5.46)
7	9.33	(12.5)	41	0.207	2.44	(5.39)	2.44	(5.37)	2.47	(5.42)	2.56	(5.65)	2.44	(5.37)
8	5.2	(7)	41	0.719	1.54	(3.40)	1.52	(3.36)	1.52	(3.36)	1.59	(3.50)	1.52	(3.36)
9***	1.3	(1.8)	23	1.449	0.84	(1.86)	0.84	(1.86)	0.84	(1.86)	0.84	(1.86)	0.84	(1.86)
	Fuel used per 161 km (100 mi), kg (lbm)				7.48	(16.50)	7.44	(16.40)	7.48	(16.48)	7.84	(17.29)	7.41	(16.34)
	Fuel economy, km/L (mpg)				18.32	(43.10)	18.42	(43.35)	18.34	(43.14)	17.48	(41.11)	18.50	(43.51)
	Percent change from base				Base		+0.6		+0.1		-4.6		+1.0	

*Nine steady state points representative of the combined Federal Driving Cycle

**50-deg IGV

***All idle points at 60-deg IGV

Figure 6 is a study of vehicle creep speed at 50 and 55% gasifier idle speed showing estimated creep speeds of 14.5 km/h (9.0 mph) at 50% idle and 19.3 km/h (12 mph) at 55% idle.

Figure 7 shows estimated engine braking power versus vehicle speed in each transmission gear range. A 1980 Pontiac Phoenix spark ignition engine braking chart is shown for comparison.

A digital computer program, which combines the engine component matching program with vehicle simulation and control simulation programs, is being developed. The engine simulation has been updated to include heat rejection, heat storage, and volume dynamics. The program will be used for control mode studies and to predict vehicle driving cycle fuel economy and transient performance.

Mod I

Estimates of AGT-100 Mod I performance indicate that fuel economy will be 11.1 km/L (26 mpg) with 70% gasifier idle speed. Wide open throttle vehicle response from idle is:

Distance in 1 s	0.5 m (1.7 ft)
Distance in 4 s	14.3 m (47 ft)
Time to 96.6 km/h (60 mph)	29.7 s
Rotor accel time (idle to 100%)	1.8 s
Gasifier rotor boost	Yes
Scheduled power transfer	Yes

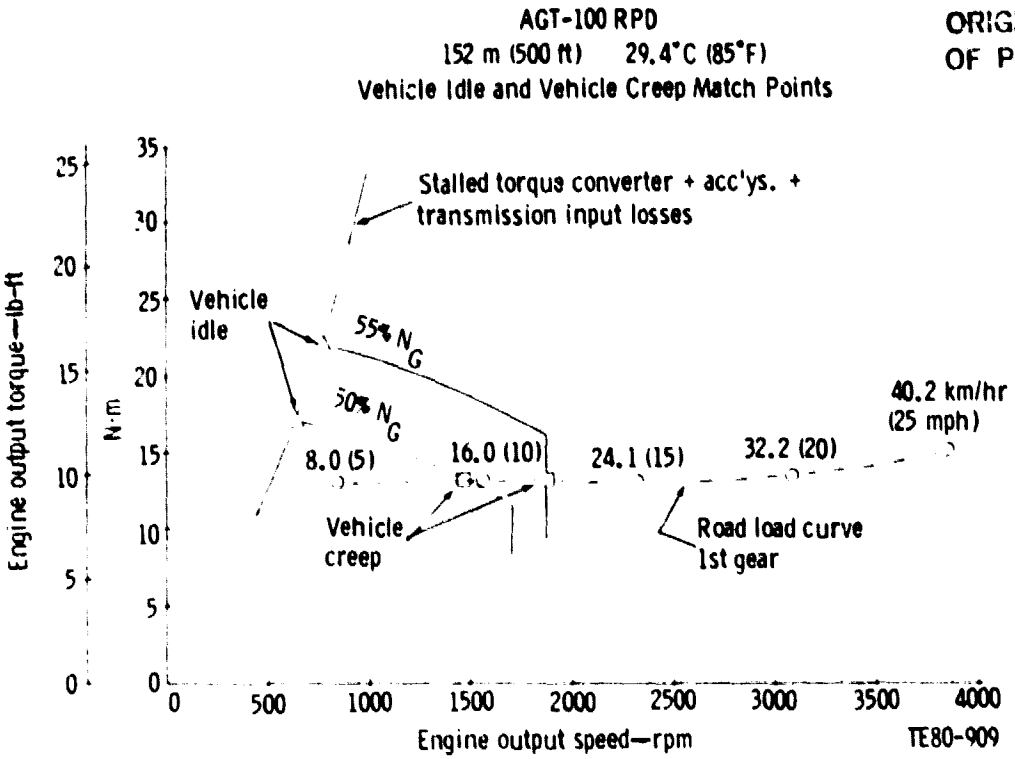

Figure 6. - Vehicle Idle and Creep Match Points.

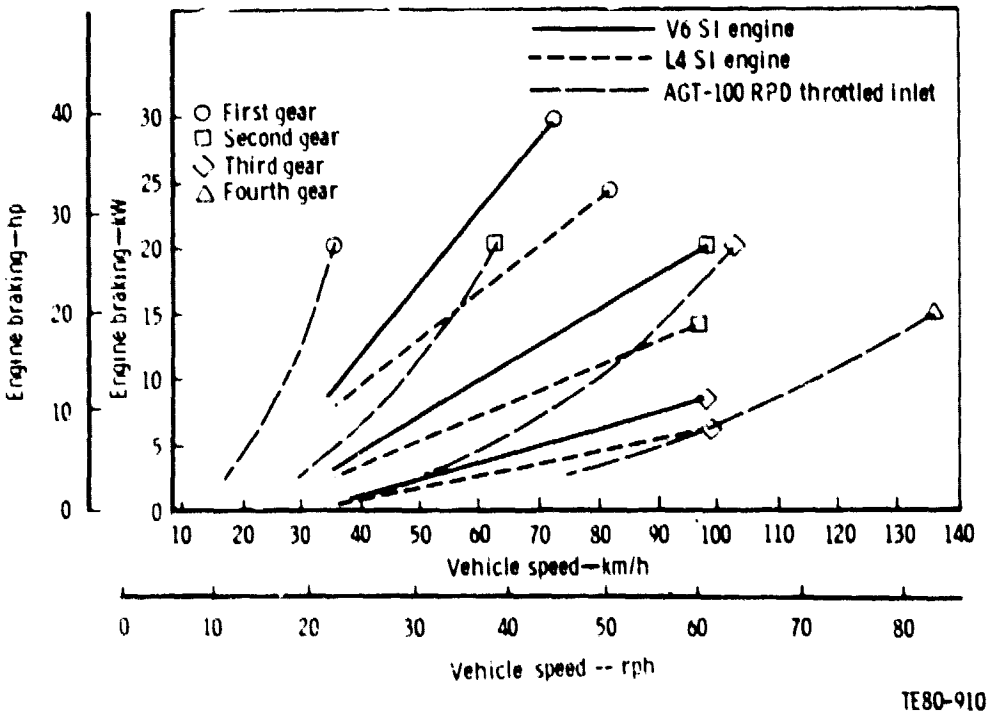

Figure 7. - Estimated Instantaneous Engine Braking.

Work is continuing to further refine the Mod I cycle by incorporating updated component performance and secondary flow system characteristics.

2.2 MOD I

Design

The Mod I engine design is essentially the same as the RPD except in areas where technology advancements require demonstration before committing to engine hardware. These consist of some of the ceramic flow path components including the turbine rotors.

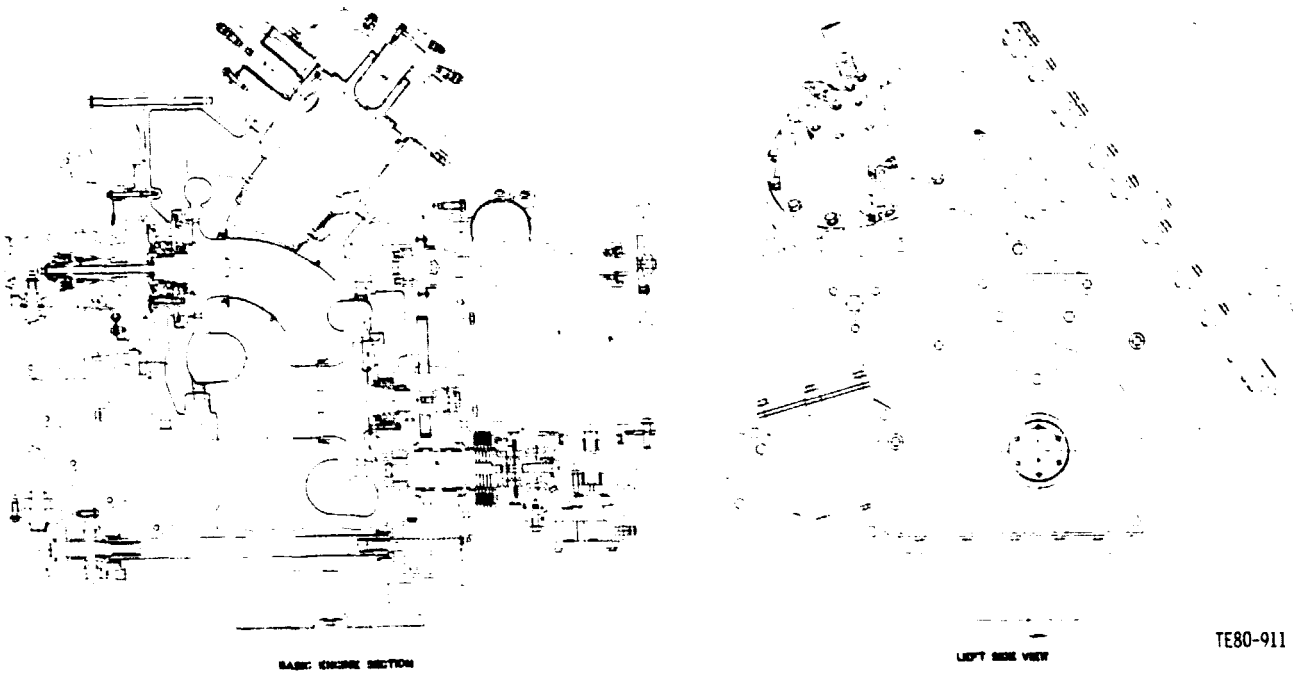

Figure 8. - Mod I General Arrangement.

The close similarity of the RPD and Mod I engines allowed the Mod I detailed design layouts to be initiated from the RPD general arrangement. The Mod I general arrangement has recently been completed and is shown in Figure 8.

Accessory mounting and external arrangement work, as well as installation in the vehicle, has been accomplished to date based on the general arrangement, individual design layouts, and sketches.

Fabrication

Tooling for selected engine parts and long lead time items have been ordered. These items include:

- o Metric cutters for gears
- o Gears
- o Compressor impeller assembly
- o Inlet duct

- o Compressor scroll
- o Compressor shroud
- o Metric bolts, washers, seals
- o Bearings
- o Assembly tooling

Compressor impeller blanks were ordered and have been delivered. Machining on these items has been initiated.

In addition to the above, engine block casting and casting tooling vendors are being selected with tooling release expected during the next reporting period.

III. COMPRESSOR DEVELOPMENT

3.1 COMPRESSOR AERODYNAMIC DEVELOPMENT

This section describes the aerodynamic design of the single-stage centrifugal compressor engineered for use in the AGT-100 engine. This compressor design as well as three inlet variations, has been released for hardware procurement. Compressor rig testing and development are scheduled to begin during the next semi-annual reporting period.

The AGT-100 compressor illustrated in cross section in Figure 9 satisfies all automotive installation requirements and incorporates DDA's latest technology. It also makes use of variable inlet guide vanes (IGV) to enhance low-power engine performance. The aerodynamic design features and background rationale used in the compressor design are included in this document.

Design

The AGT-100 compressor must satisfy a wide range of operating requirements. The engine was sized to provide sufficient power for suitable driveability and high-altitude operation even though operation occurs mostly at low power settings. Table IV outlines compressor operation through the range of steady-state driving conditions.

TABLE IV. AGT-100 COMPRESSOR OPERATING POINTS

	Idle	48 km/h (30 mph)	80 km/h (50 mph)	Design point, standard day, max power
Equivalent flow, $\frac{W\sqrt{\theta}}{\delta}$, kg/sec (lbm/sec)	0.105 (0.231)	0.107 (0.235)	0.134 (0.295)	0.347 (0.764)
Equivalent speed, $N/\sqrt{\theta}$, rad/s (rpm)	4405 (42065)	4405 (42065)	5290 (50513)	9027 (86200)
Equivalent speed, Percent of design	48.8	48.8	58.6	100
Pressure ratio Total/static	1.41:1	1.54:1	1.84:1	4.5:1
Efficiency goal, η_{T-S}	74.9	80.1	81.6	82.8
IGV induced preswirl, deg from axial	60	0	0	0

The compressor design point is the maximum power operating condition, with parameters biased selectively for part power operation. Review of the current state of the art, as represented by the DDA Industrial Gas Turbine (IGT), reveals that the efficiency goals of the AGT-100 are quite aggressive. Ad-

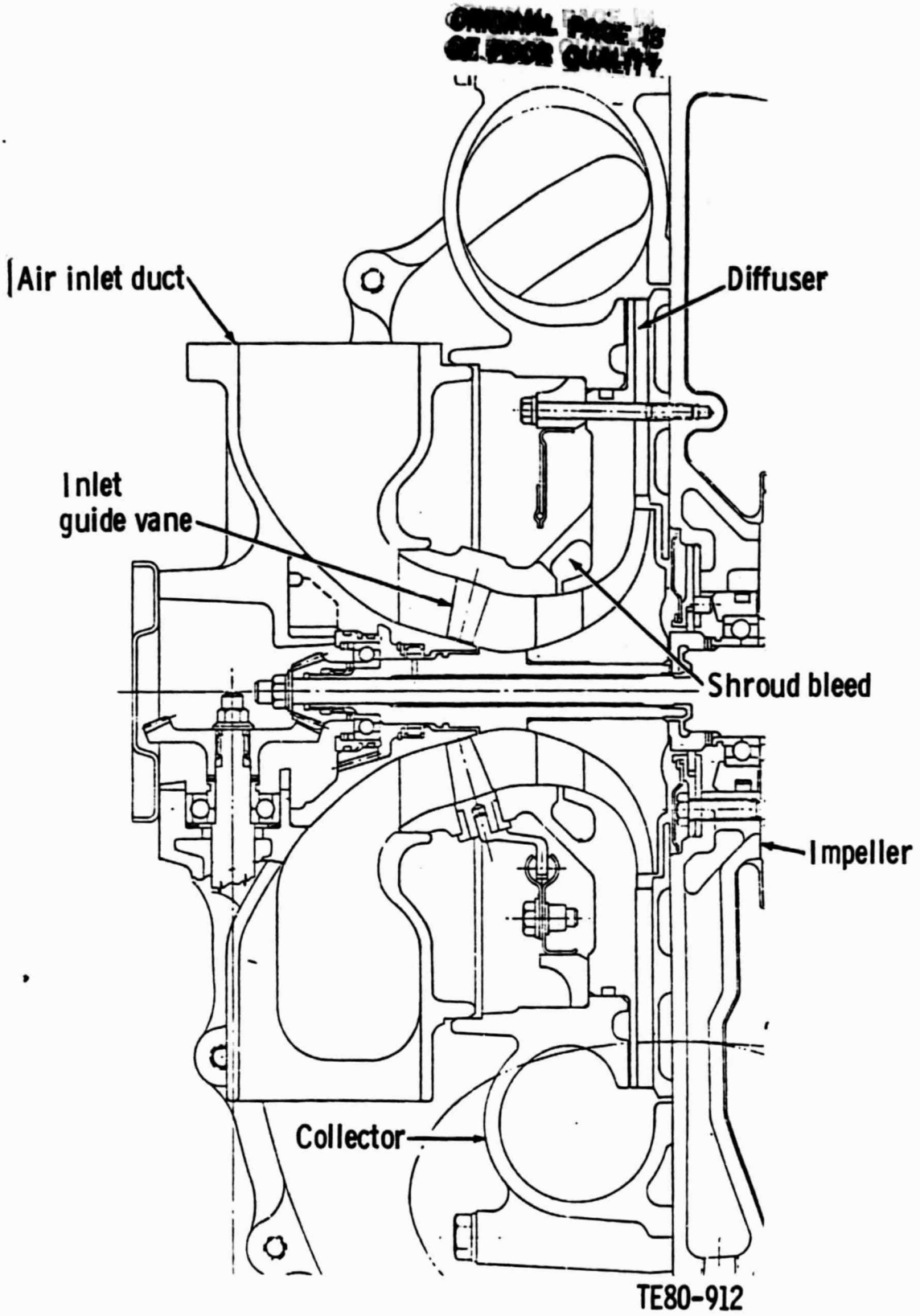

Figure 9. - AGT-100 Compressor Cross Section.

justment of the IGT compressor performance for size effects in Table V reveals that a 2.5% efficiency improvement will be required during the program.

TABLE V. AGT-100 COMPRESSOR PERFORMANCE CHALLENGE

83.0%	η_{T-S} @ 4.5:1, $W\sqrt{\theta}/\delta$ = 2.0 kg/s (4.5 lbm/sec) - IGT compressor
-2.7	Size effect to 0.34 kg/s (0.76 lbm/sec)
80.3%	state of the art at 4.5:1, $W\sqrt{\theta}/\delta$ = 0.34 kg/s (0.76 lbm/sec)
82.8%	AGT-100 efficiency goal
2.5%	Improvement required

To meet the goals of Table IV, an efficiency fall off with reducing speed must be minimized. The AGT-100 compressor design uses the philosophy incorporated in the IGT compressor. Use of this technology should enhance design point performance and provide for a very favorable efficiency-speed lapse as demonstrated by the IGT. While this flat lapse-rate enhances the AGT-100 low-power fuel economy, variable inlet guide vanes are also employed to meet the lowest power efficiency goals. These vanes provide preswirl in the direction of rotation to efficiently reduce impeller work and flow. Cycle simulations indicate that the vanes improve fuel economy at steady-state operation below 48 km/h (30 mph). The compressor also uses DDA's patent-pending inducer shroud bleed. The bleed slot is positioned a short distance aft of the impeller leading edge and communicates with ambient conditions. At low speed, pressure rise in the inducer causes flow out of the slot. Therefore, more flow is generated through the inducer, which reduces inducer incidence and alleviates stall if it exists. At high speed, near choke, the static pressure in the inducer is less, and flow occurrs inward through the slot. This flow bypasses the throat, which effectively increases the impeller flow capacity. For a given flow requirement, the inducer can, therefore, be closed slightly, which further improves low flow performance.

The AGT-100 compressor configuration is challenged in its automotive application. Constraints result from the operational environment, underhood space limitations, and engine features incorporated to enhance fuel economy and response. Major constraints include:

- o Provisions for air filtration
- o Length and diameter restrictions
- o Bearing span and shaft geometry configured to satisfy critical speed requirements
- o Engine configured for power transfer
- o Engine configured for regeneration

The specific impact of these considerations is discussed in the following design section.

Inlet/IGV

Three IGV configurations and two inlets have been designed. Two of the IGV configurations are axial and are designed for use in the same axial duct. One of these, designated the prime design, has low camber and should provide good performance from the axial setting through 40 or 50 deg of preswirl. The alternate axial IGV design has increased camber for more preswirl capability. The third IGV configuration is a radial design and is intended for use with the second inlet configuration. This inlet is a modification of the basic design.

The inlet configuration is a compromise between available space and aerodynamic considerations. Underhood space limitations precluded the use of a large single-element air filter and an axial air inlet. As shown in Figure 10, two smaller air cleaners are used to achieve adequate filtration with acceptable pressure loss. Each of these is ducted to individual ports of a bifurcated compressor inlet. These ports are perpendicular to the compressor centerline and are located opposite of each other. The use of two opposed ports is felt to reduce the probability of inlet distortion compared to use of a single port asymmetric inlet. Pollution considerations require that all engine leakage air be routed through the gearbox and ducted back to the inlet providing positive internal ventilation. This vent air enters halfway between the ports on the left side (see Figure 11).

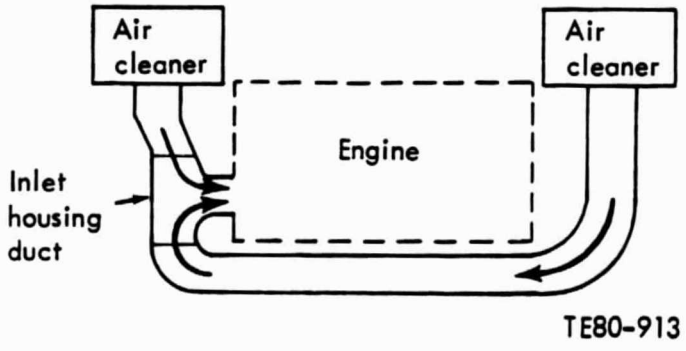

Figure 10. - AGT-100 Air Inlet Ducting.

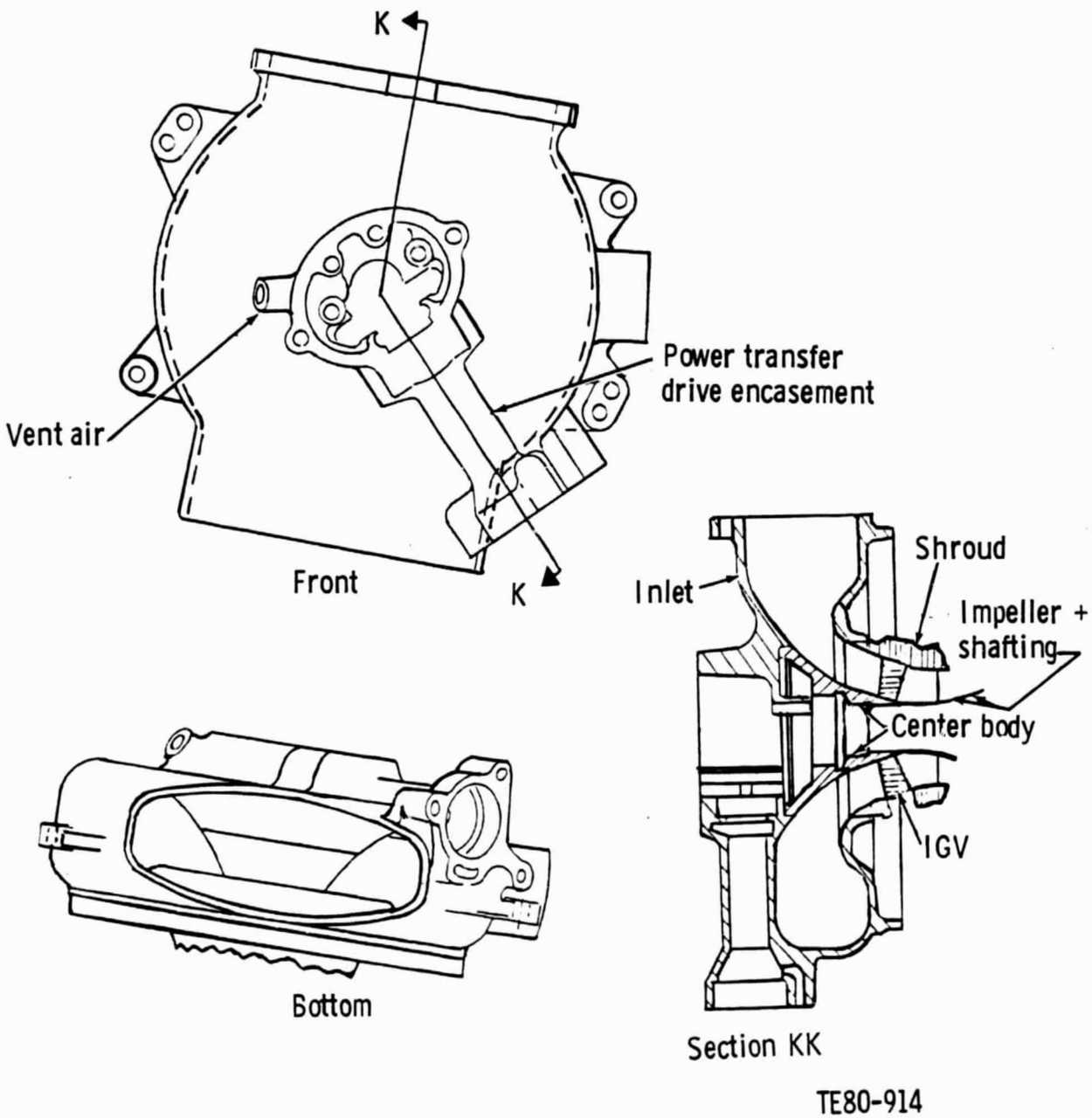

Figure 11. - AGT-100 Axial IGV Air Inlet Duct.

The inlet has an annular plenum in the plane of the ports, which feeds the axisymmetric ducting ahead of the impeller. This plenum is symmetric from port to port with the exception of an internal bump that encases the power transfer drive. This drive is perpendicular to the compressor centerline and the output shafting. Viewed from the front this drive is located 45 deg counterclockwise from the center of the bottom port.

The inlet system is shown in Figure 11. The compressor shroud forms the tip wall contour forward of the impeller. The hub wall is formed by a centerbody piloted in the inlet duct and by the shafting just forward of the impeller.

Several design compromises were necessary to satisfy shafting critical speeds. For example, the inlet duct length was minimized to shorten the bearing span at the expense of increased local surface diffusion. Also, restrictions on the centerbody diameter in the region of the front bearing constrained the hub flow path.

Despite these compromises, an iterative definition of wall shapes provided for duct flow with no evidence of boundary layer separation. Boundary layer calculations using design point duct surface velocities shown in Figure 12 indicate that neither these flow conditions nor those resulting from low-power operation should produce any separations.

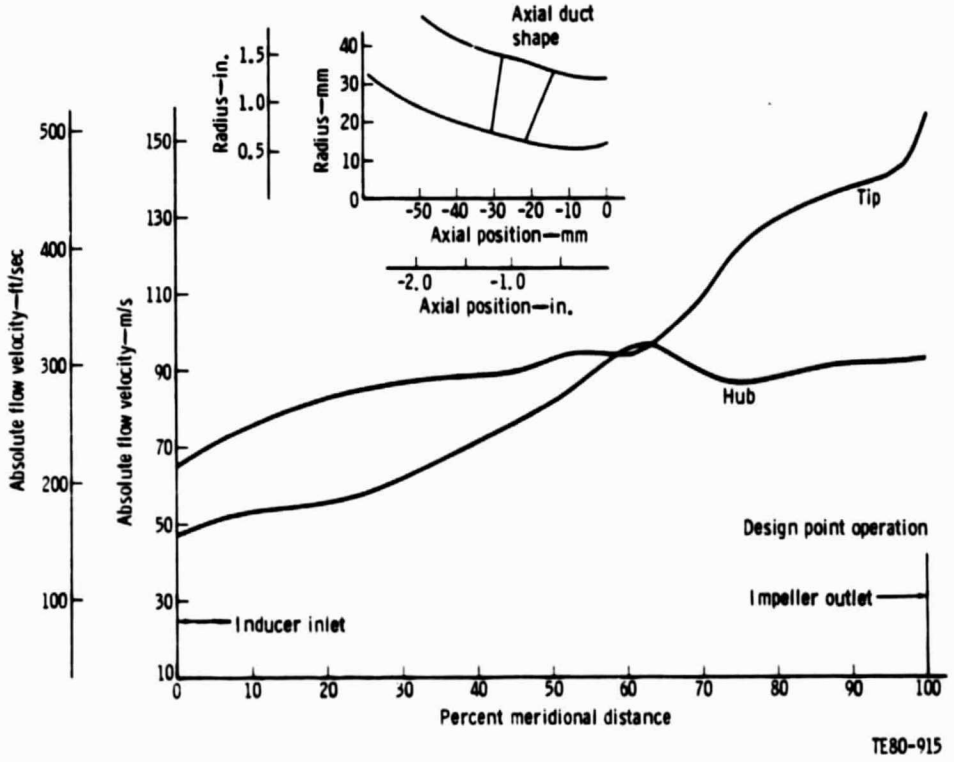

Figure 12. - AGT-100 Axial Duct Velocities.

The axial IGV's have a rotational axis that is canted 15 deg off a radial line in the meridional plane. Vanes are located approximately 19 mm (0.75 in.) ahead of the impeller. They are cantilevered from a full chord length button. The button employs a modified spherical shape to avoid any projections into the tip flow path as the vane is reset. The vane hub section opposes a conical flow path to minimize arc drop clearance increase as the vane is reset. The vane hub chord has been minimized to further reduce arc drop effects.

The prime IGV design incorporates fifteen vanes having 15 degrees of camber and is shown in Figure 13. The vane profile was generated using an analytical curvature specification procedure. Vane surface velocities were generated for conditions spanning the range of intended usage. Vane shapes were selected using an iterative generation-surface velocity analysis procedure. The selected vane provides for separation-free operation at both design point and idle conditions with up to 40 deg of preswirl. Design point, idle with 20 deg, and idle with 40 deg of preswirl surface velocities are shown in Figures 14 through 16, respectively.

Alternate Axial IGV

The alternate axial IGV configuration is a direct replacement item for the prime IGV design. Its profile is shown in Figure 17. It was designed using the same procedure as the prime design. It employs 32.5 deg of camber to increase the IGV turning capability. Analysis of this vane indicates that it should be capable of more than 60 deg of turning at idle flow without any separation. The vane, however, has excessive diffusion in the design point operating mode, and a local separation is predicted near the pressure surface leading edge. Surface velocities for this vane at design point and idle with 40 and 60 deg of preswirl are shown in Figures 18 through 20, respectively.

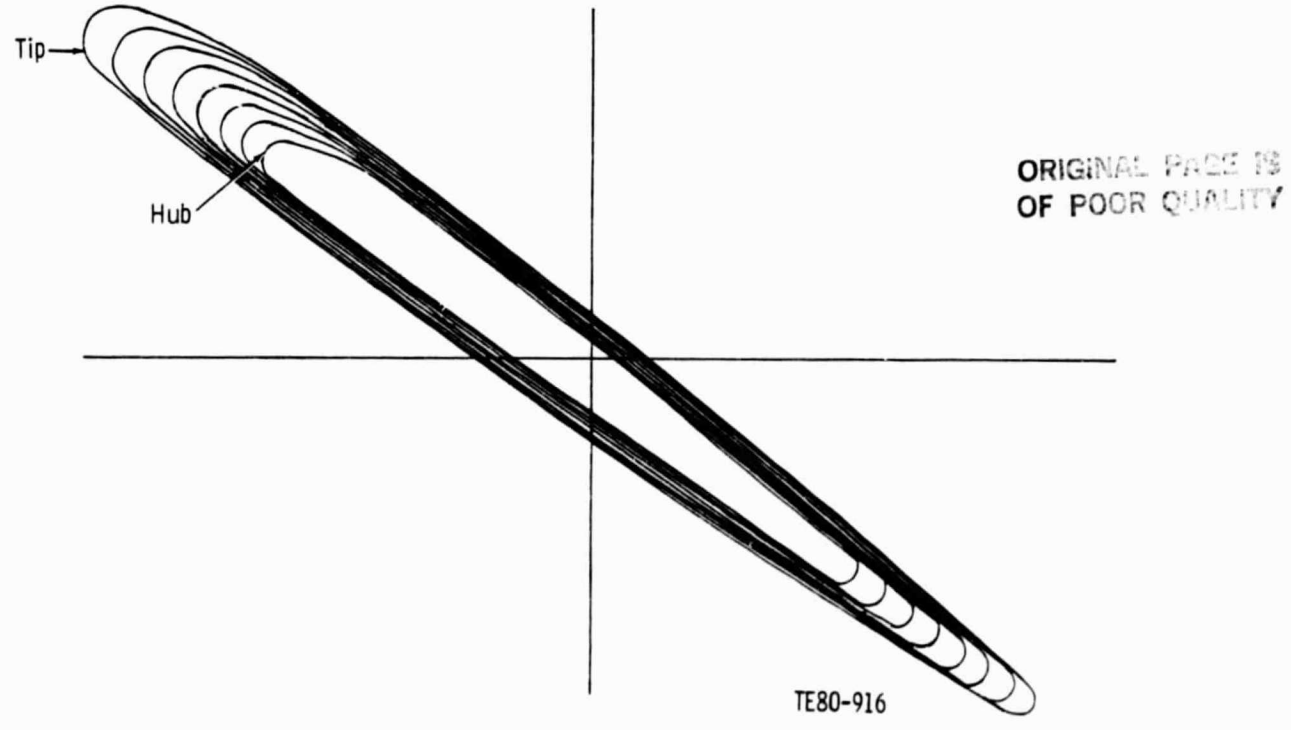

Figure 13. - Prime IGV Design Cross Section.

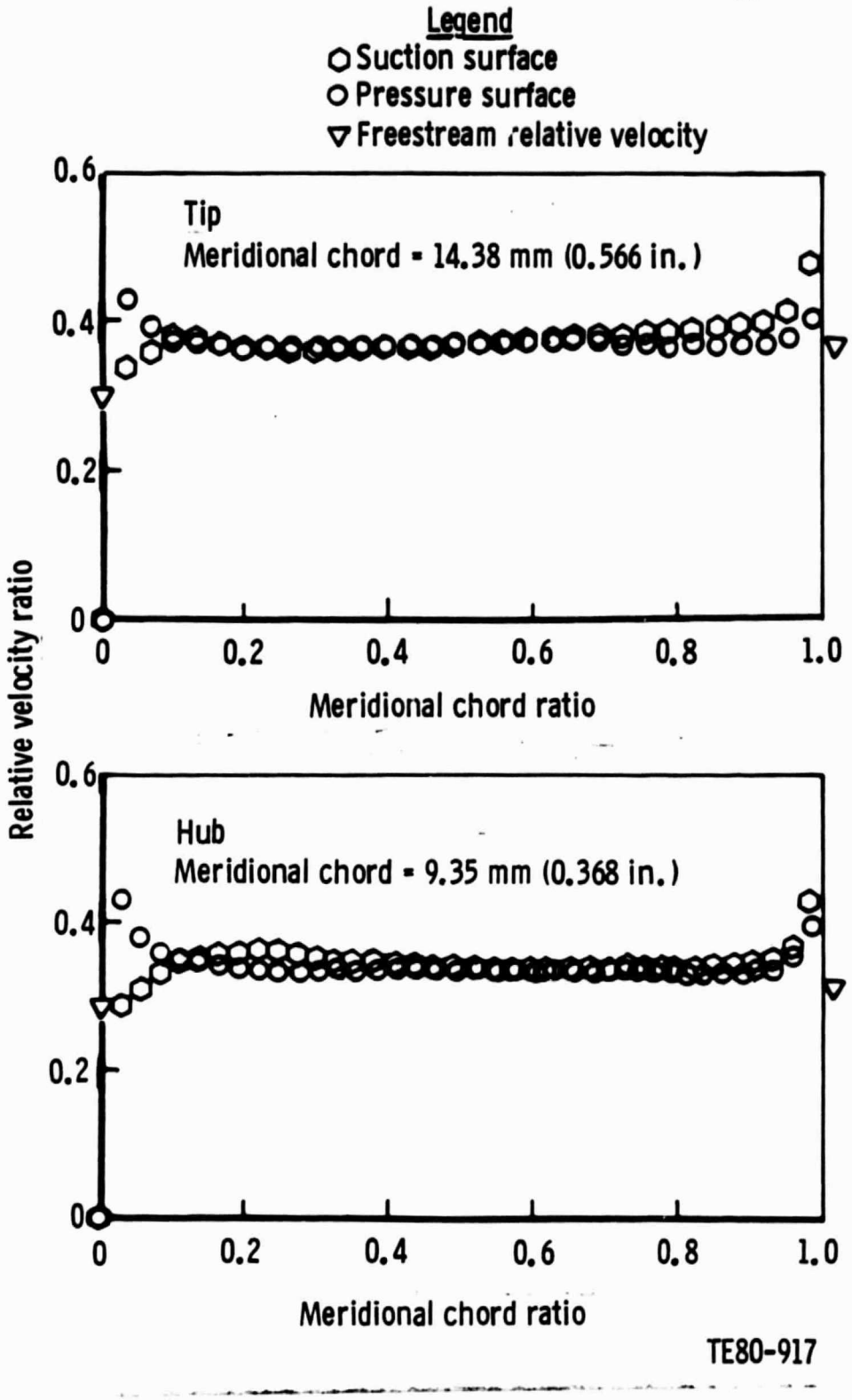

Figure 14. - Prime IGV Design Point Surface Velocities.

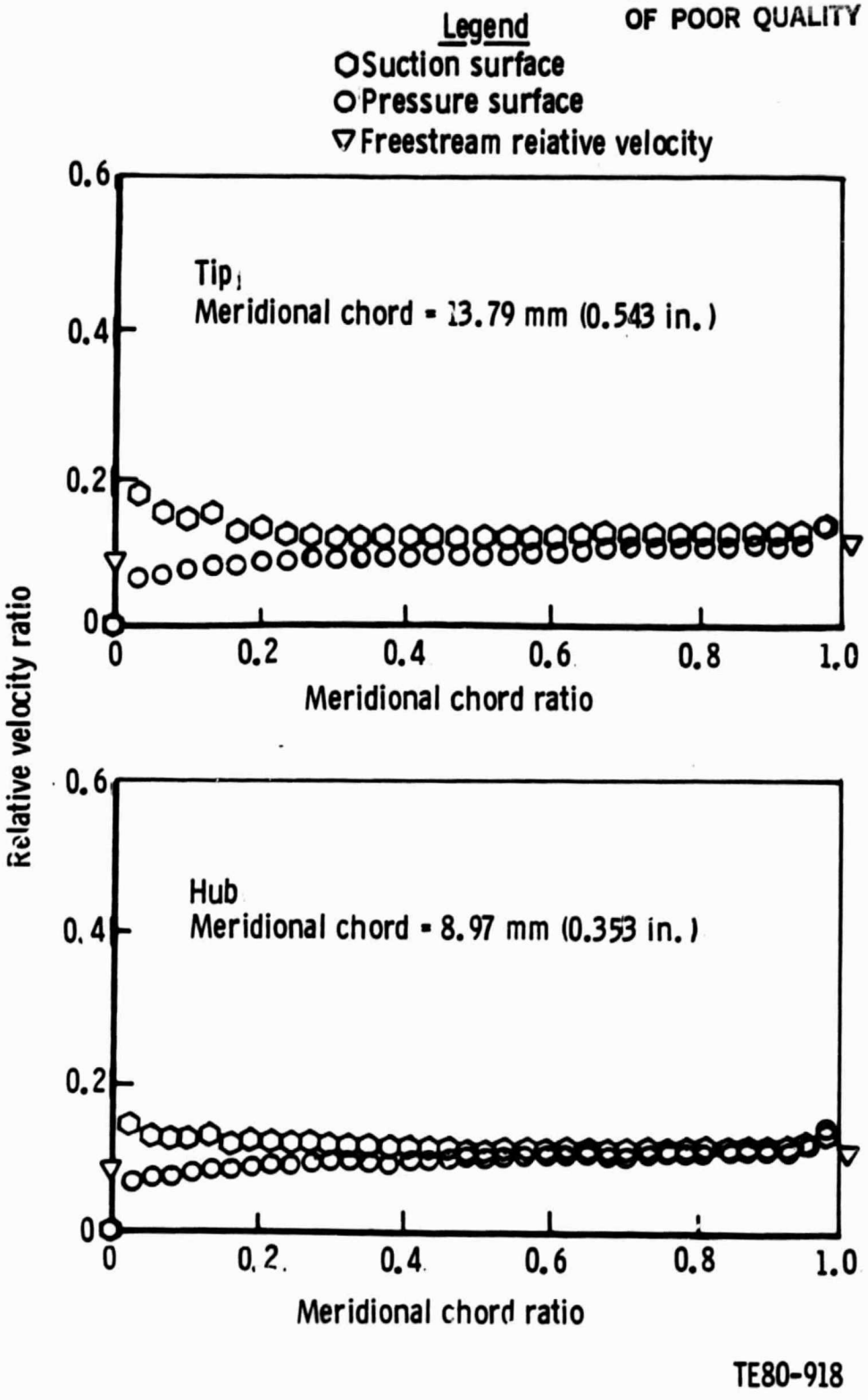

Figure 15. - Prime IGV Idle (20 deg Preswirl) Surface Velocities.

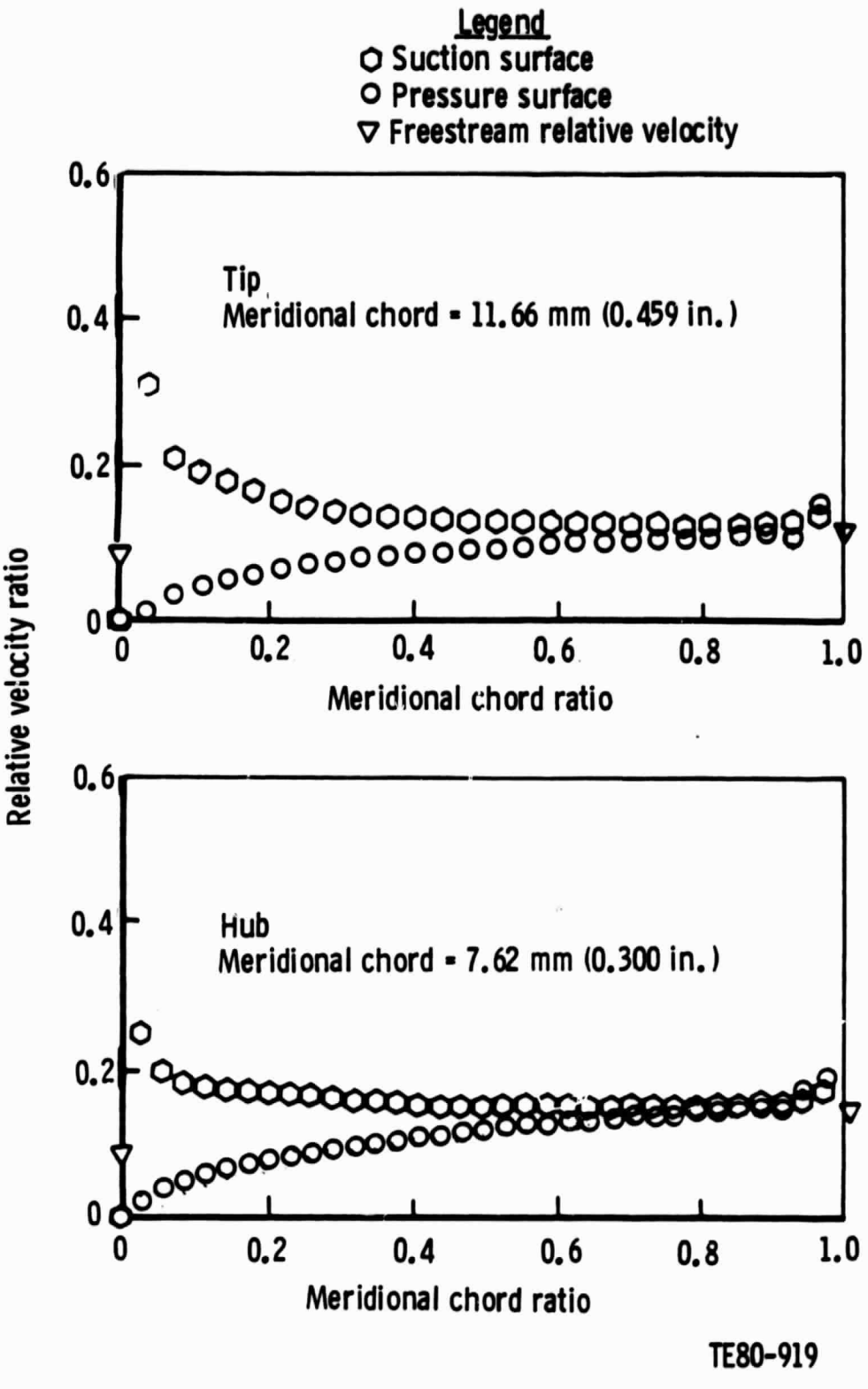

Figure 16. - Prime IGV Idle (40 deg Preswirl) Surface Velocities.

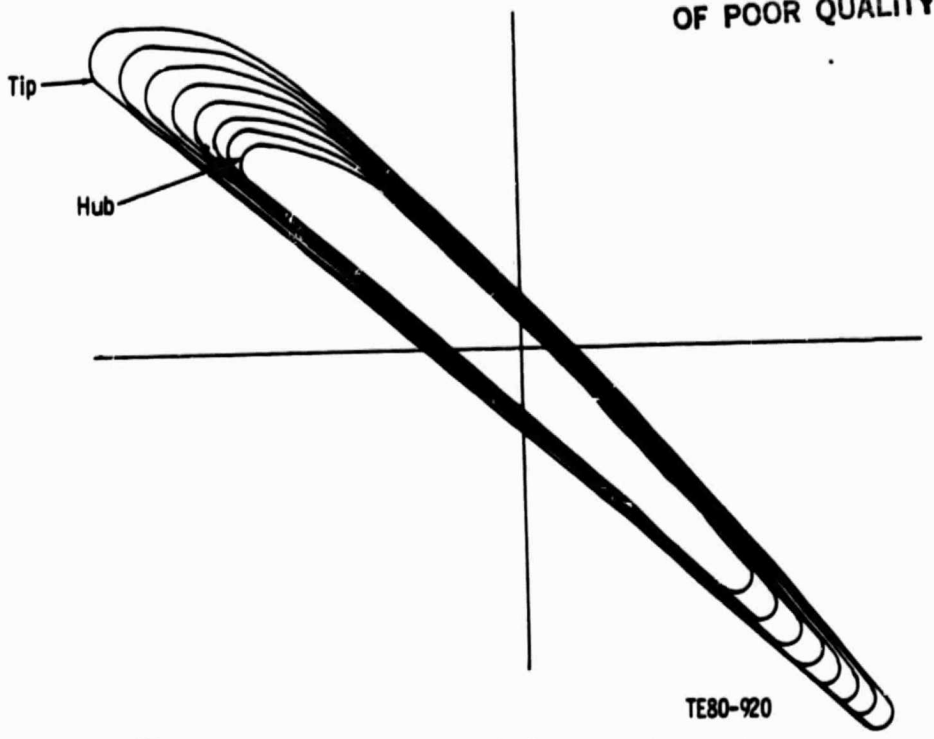

Figure 17. - Alternate Axial IGV Cross Section.

Alternate Radial Inlet/IGV

The third inlet/IGV configuration, as shown in Figure 21, is a radial design that maintains the bifurcated inlet features. The outer diameter of the guide vane cascade permits a 360° plenum to exist outboard of the cascade, but within the inlet duct. To minimize required hardware modifications, the radial duct uses as much of the axial duct contour as possible. Boundary layer analyses indicated that this modified duct should have no separation at any operating condition. Figure 22 presents the wall velocities for the radial duct at design conditions and for idle with 30 deg of preswirl.

The radial vane was generated using the same generation-analysis system as the axial vanes. The vane shape shown in Figure 23 provides for separation-free operation from design flow to idle with 40 deg of preswirl. Vane surface velocities for these design point and idle with 20 and 40 deg of preswirl are shown in Figures 24 through 26, respectively.

The effect of both radial and axial IGV's on inducer flow conditions was assessed. A comparison of inducer incidence for varied levels of preswirl out of the IGV is shown in Table VI. Both axial designs will produce the numbers listed.

DDA and external source data for compressors with IGV's, both axial and radial, show efficiencies peaked at 20 to 40 deg of preswirl for low and intermediate speeds. At the peak efficiency setting, a slight flow reduction was incurred. Larger values of preswirl produced significant flow reductions, but this was largely a result of simple pressure drop in the IGV's.

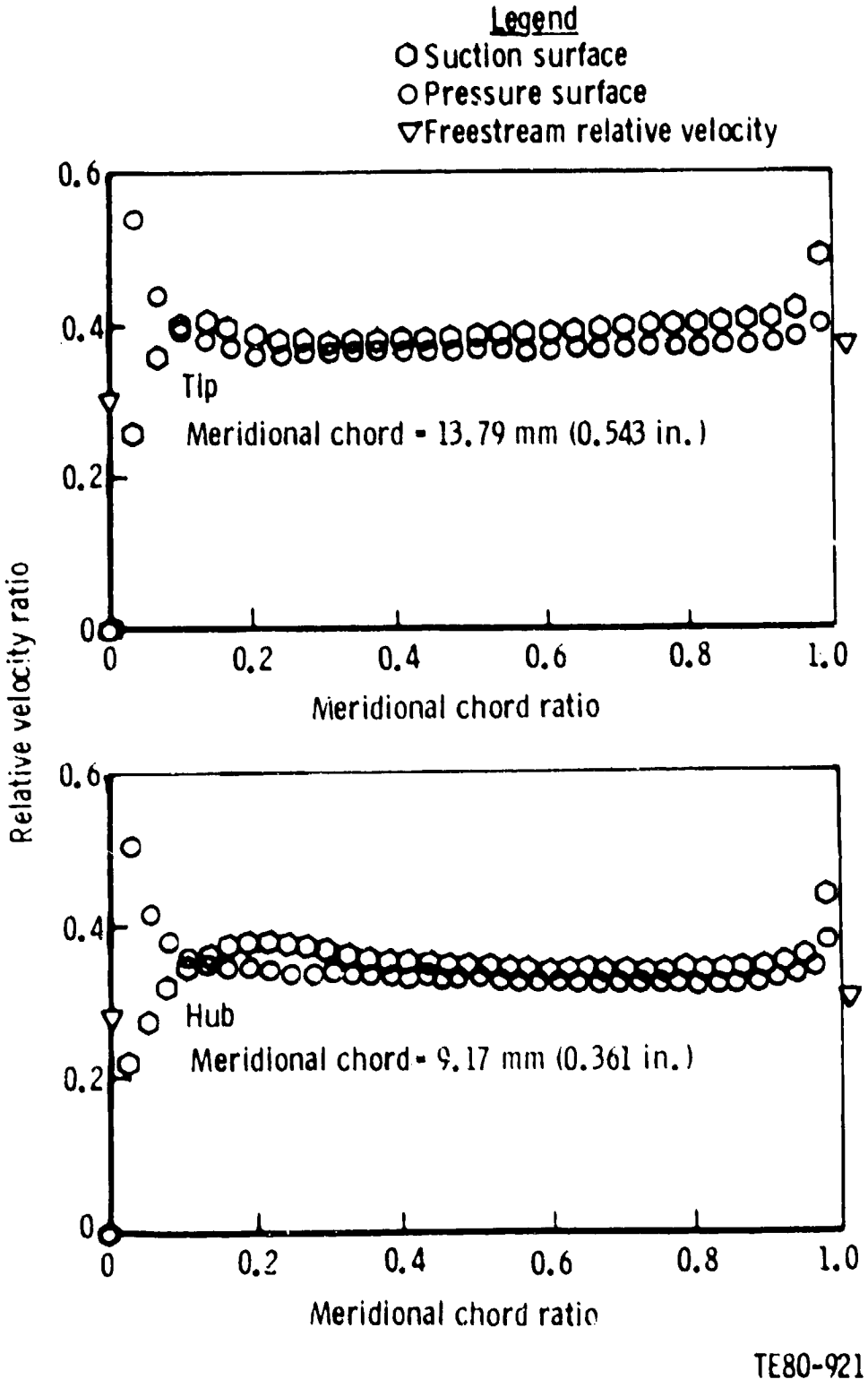

Figure 18. - Alternate Axial IGV Design Point Surface Velocities.

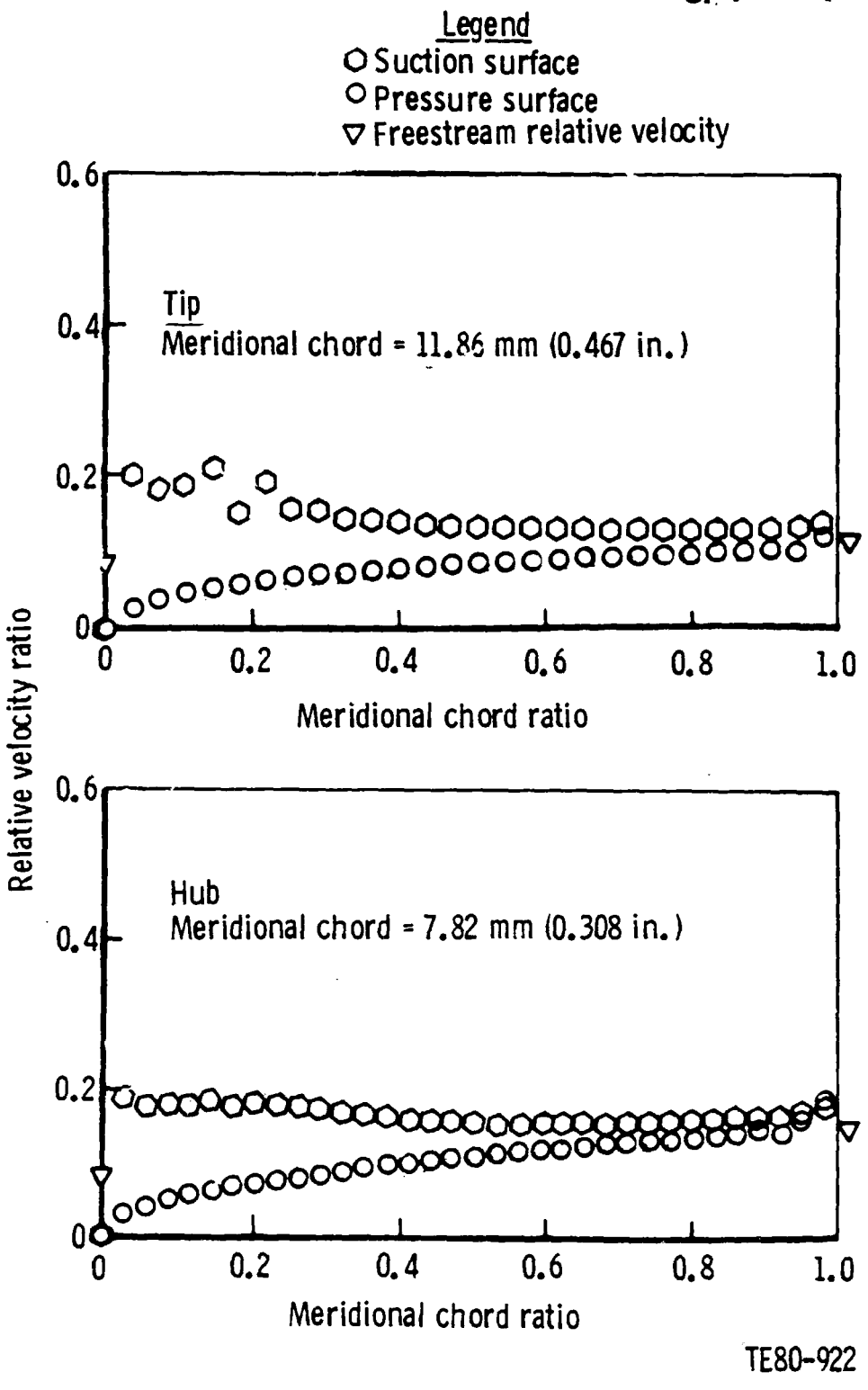

Figure 19. - Alternate Axial IGV Idle (40 deg Preswirl) Surface Velocities.

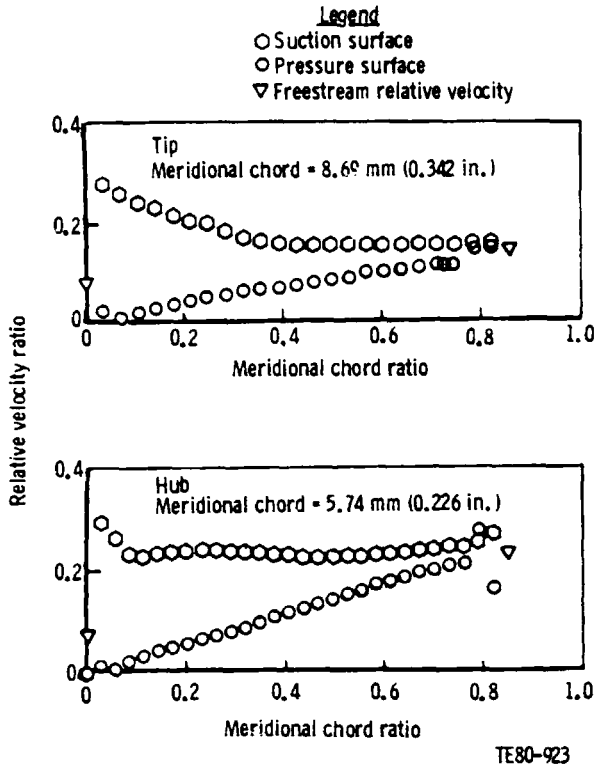

Figure 20. - Alternate Axial IGV Idle (60 deg Preswirl) Surface Velocities.

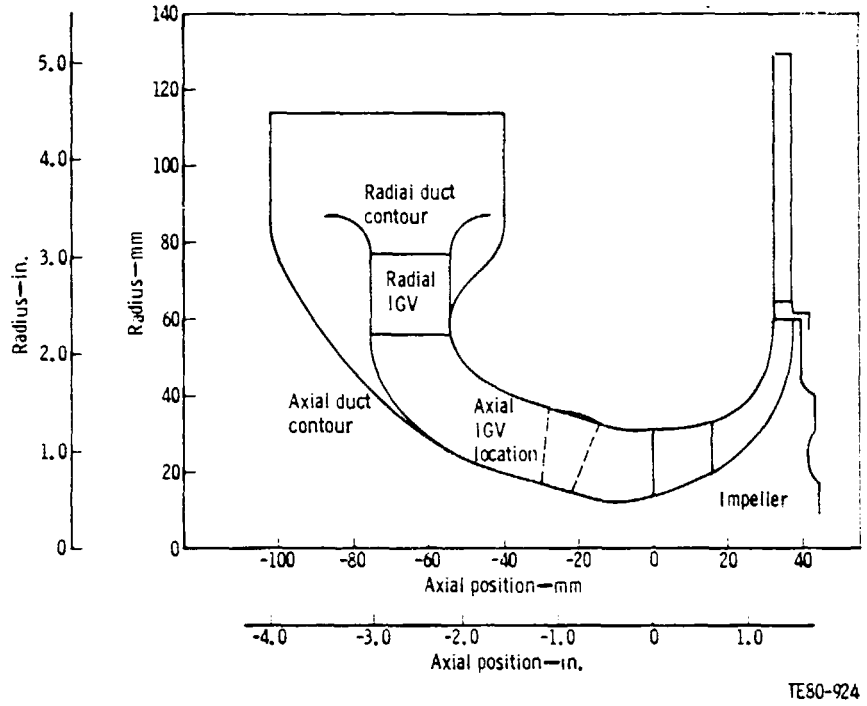

Figure 21. - Comparison of Radial and Axial IGV Inlet Configurations.

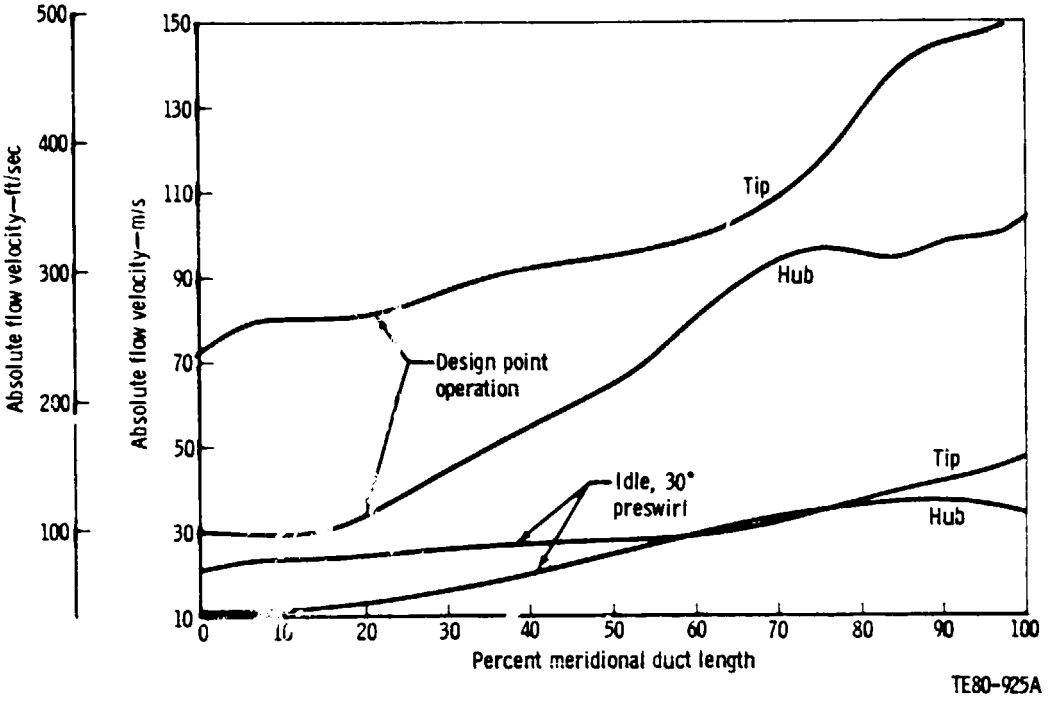

Figure 22. - AGT-100 Radial Duct Velocities.

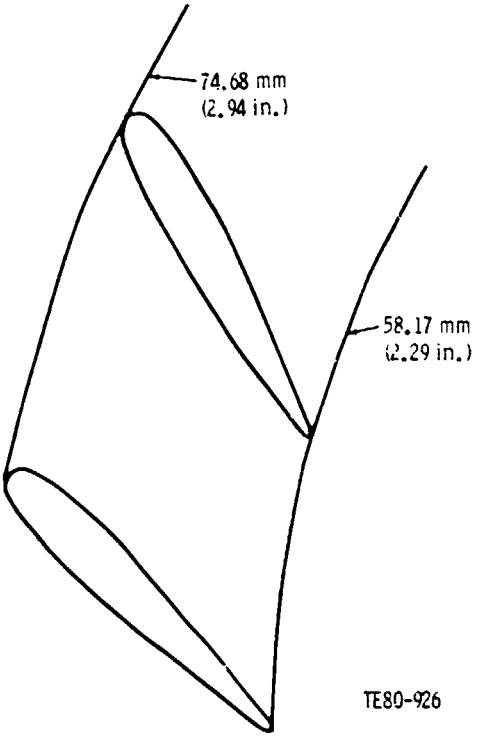

Figure 23. - Alternate Radial IGV Cross Sections.

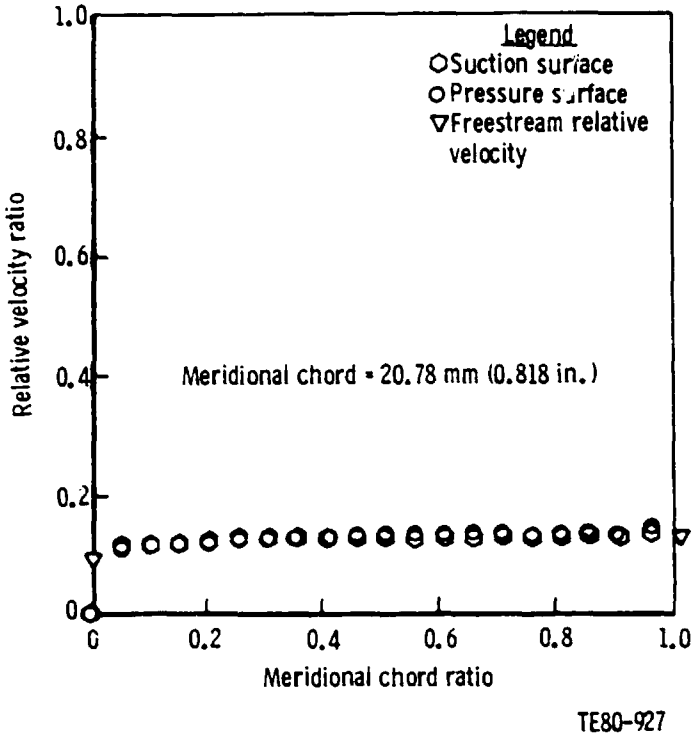

Figure 24. - Alternate Radial IGV Design Point Surface Velocities.

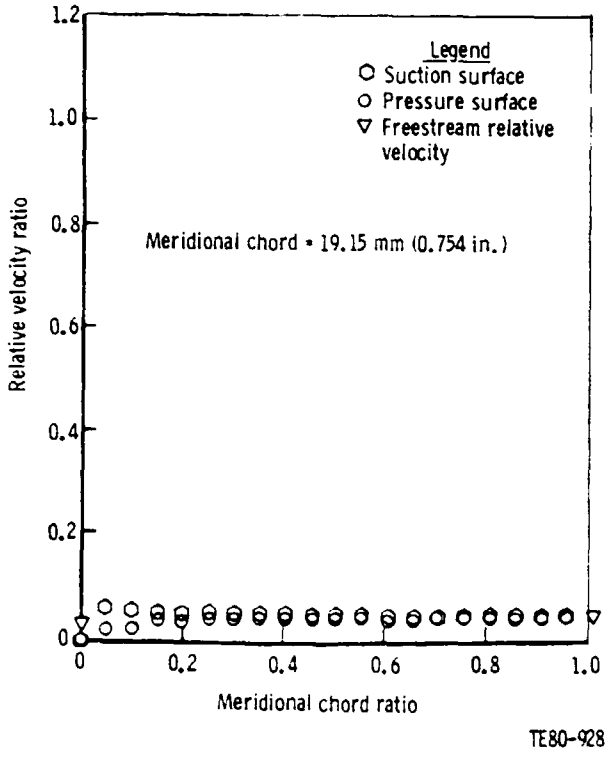

Figure 25. - Alternate Radial IGV Idle (30 deg Preswirl) Surface Velocities.

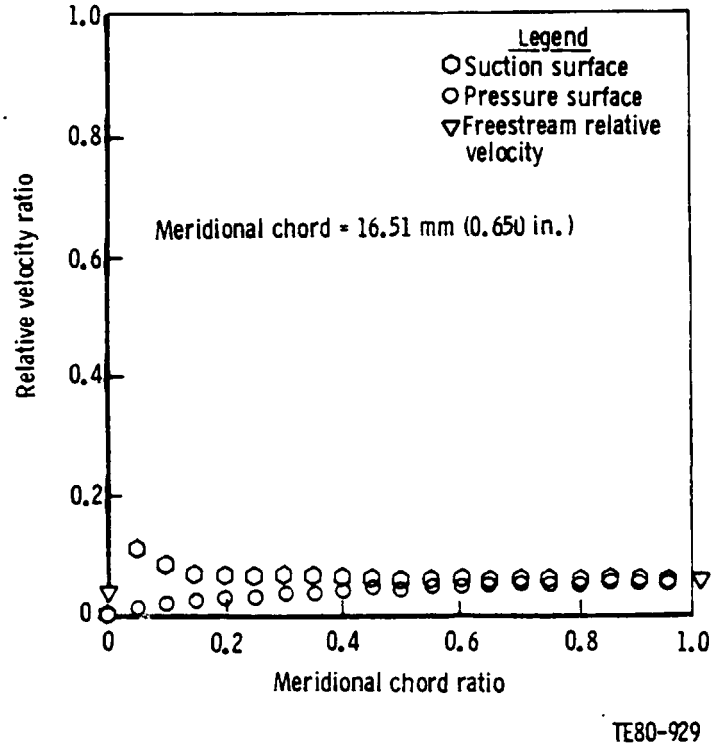

Figure 26. - Alternate Radial IGV Idle (45 deg Preswirl) Surface Velocities.

TABLE VI. INDUCER INCIDENCE AT IDLE AS A FUNCTION OF IGV PRESWIRL

Vane exit configuration/preswirl (measured from meridional)		Incidence Hub	Incidence Shroud
Radial	20 deg	+17.1 deg	+10.7 deg
Radial	30 deg	+11.8 deg	+10.3 deg
Radial	40 deg	+ 1.9 deg	+ 9.8 deg
Axial	30 deg	+10.1 deg	+10.2 deg
Axial	40 deg	+ 1.4 deg	+ 9.9 deg
Axial	50 deg	-20.9 deg	+ 9.9 deg

Experimental evaluation of the three IGV configurations will serve to:

- o Identify the IGV most effective at efficiently reducing part speed flow
- o Determine if an IGV can provide a more significant flow reduction than has been demonstrated in the past

Impeller

Basic impeller design parameters were selected using previous preliminary design studies (ref. 2) and recent DDA industrial gas turbine (IGT) compressors development experience. At the AGT-100 cycle pressure ratio, DDA experience indicates 50 deg of backsweep as being aerodynamically desirable and mechanically achievable. Preliminary design efforts resulted in selection of 16 full blades/16 splitters to achieve blade loadings comparable to those of the IGT. A compatibility study, between the compressor and turbine, resulted in a specific speed selection of 80. Compressor specific speed is defined as:

$$N\, Q^{1/2} \Big/ \left[(R_c^{(\gamma-1)/\gamma}-1)\, T_{T_1}\, C_p\, J\right]^{3/4}$$

The effect of inlet specific flow and hub/tip ratio on design-to-idle incidence growth has been assessed and is shown in Figure 27. Increasing hub/tip ratio and decreasing design point specific flow reduces the design-to-off design incidence swing. Minimization of the inducer tip relative Mach number is achieved by assigning moderate specific flows, 146-161 kg/m^2·s (30-33 lbm/ft^2-sec) and as small a hub/tip ratio as practical. The hub/tip ratio was constrained by a minimum hub value required to satisfy rotor critical speeds and impeller bore provisions. These and other aerodynamic considerations led to selection of a design point specific flow of 146 kg/m^2·s (30 lbm/ft^2-sec) and an inducer hub/tip ratio of 0.45.

Subsequent engine cycle modifications reduced the final specific inlet flow value to 143 kg/m^2·s (29.3 lbm/ft^2-sec). This value of specific flow provides for a 0.93 relative tip Mach number, relative tip flow angle of 60.7 deg, and a near minimum design-to-idle incidence swing.

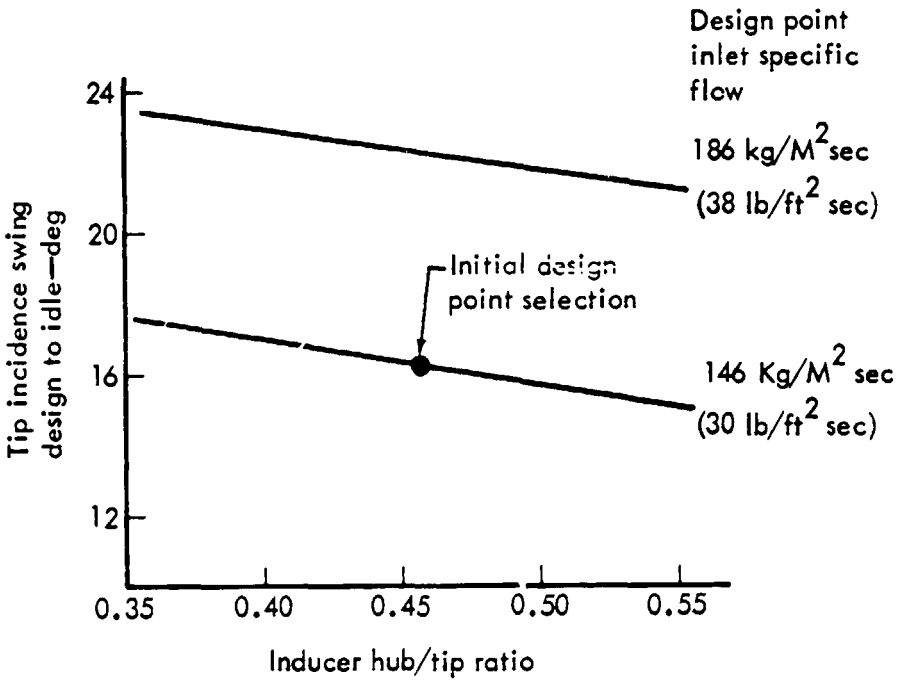

Figure 27. - The Effect of Inlet Specific Flow and Hub/Tip.

The flow-path length was selected after assessing the shroud velocity diagrams from the preliminary designs. The selected length scales closely to the IGT impeller. The length provides for moderate shroud curvatures.

The impeller exit width was selected to provide for a impeller exit absolute flow angle of 80.0 deg. This angle was felt to be a limiting design value and allows for the possibility of maximal impeller diffusion. The large exit width which results adds flexibility to the development program. Variation of the original width, the shroud contour and the exit width is included in the test rig program.

The impeller diameter was set at 60.07 mm (2.365 in.) using DDA's performance model. This model uses a jet/wake concept in which flow in the jet is considered isentropic. Flow in the wake includes the inviscid effects. The jet and wake are then mixed to arrive at impeller exit flow conditions. Basic impeller and diffuser performance parameters must be input. These are derived from empirical correlations. Assumed performance parameters were estimated conservatively since the data base is significantly smaller than that used in establishing the basic correlations. This approach should minimize the possibility of not achieving the desired pressure ratios using the original hardware.

The compressor uses DDA's inducer shroud bleed. Feasibility was demonstrated using a reduced flow capacity IGT compressor. The bleed slot location and size was scaled from that test. The slot is 4.28 mm (0.170 in.) wide and is centered at 16.5% of the shroud meridional distance.

A summary of the impeller design parameters is presented in Table VII.

TABLE VII. AGT-100 IMPELLER DESIGN PARAMETERS

Design corrected flow, kg/s (lbm/sec)	0.35 (0.76)
Stage design pressure ratio, total-to-static	4.5:1
Design corrected speed, rpm	86,200
Design specific speed	79
Design inlet specific flow, $kg/m^2 \cdot s$ (lbm/ft^2-sec)	143.1 (29.3)
Inlet hub/tip ratio	0.45
Inlet hub radius, mm (in.)	14.00 (0.551)
Inlet tip radius, mm (in.)	31.09 (1.224)
$M_{rel\ Tip_{inlet}}$ (design point)	0.93
Axial flow-path length, mm (in.)	38.10 (1.5)
Number blades/splitters	16/32
Inducer bleed location, % meridional distance	16.5
Inducer bleed width, mm (in.)	4.32 (0.170)
Impeller exit backsweep, deg	50
Exit radius, R_2, mm (in.)	60.07 (2.365)
Impeller exit width, mm (in.)	5.44 (0.214)
Impeller exit angle, deg	80

The impeller internal design parameters were assessed using a computer program which provides for an axisymmetric radial equilibrium flow solution, including the effects of enthalpy and entropy gradients. The flow-path shape, blading angles, and blading thicknesses were iteratively adjusted to alter diffusion rates, loading distributions, and stress levels.

The impeller flow path is shown in Figure 28. The leading edge of the splitters are positioned in a plane perpendicular to the centerline as indicated on this flow path.

The impeller blade thicknesses are presented in Figure 29. The thicknesses were adjusted in the inducer region to allow adequate draft for stability. They also reflect exit region thickness modifications, which reduced the impeller bore stress. Blade elements and blade normal thicknesses are linear between equal meridional locations on the hub and shroud.

The design point impeller relative velocity distributions are shown for hub and shroud sections in Figures 30 and 31, respectively. The hub distribution limits the inducer suction surface diffusion to 45 m/s (148 ft/sec). The shroud exhibits essentially linear diffusion from inlet to exit. At design point the impeller choke flow margin is 5.3%. The impeller is set to this relatively small choke margin to enhance low-speed performance and to improve the potential shroud bleed performance.

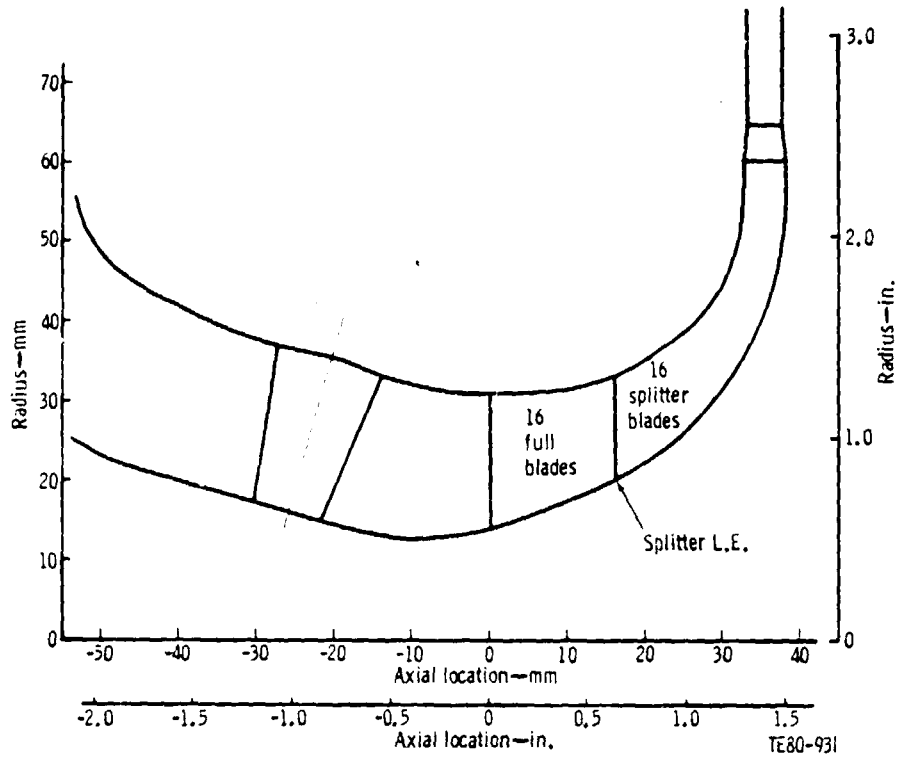

Figure 28. - AGT-100 Impeller Flow Path.

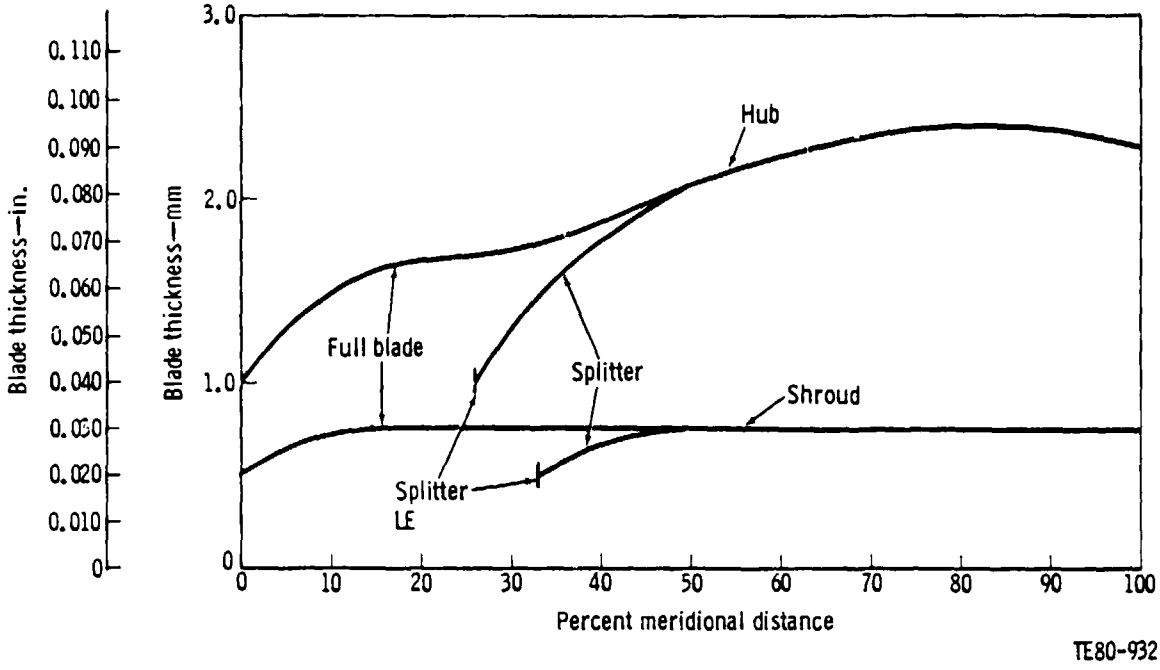

Figure 29. - AGT-100 Impeller Normal Blade Thicknesseses.

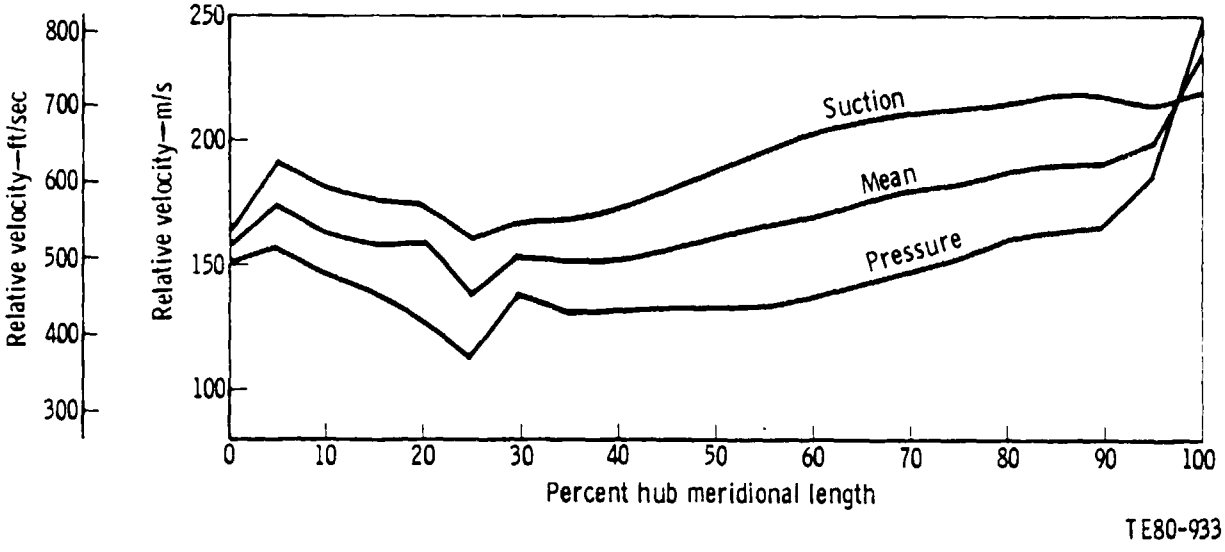

Figure 30. - AGT-100 Impeller Hub Relative Velocity Distribution, $N/\sqrt{\theta}$ = 100%.

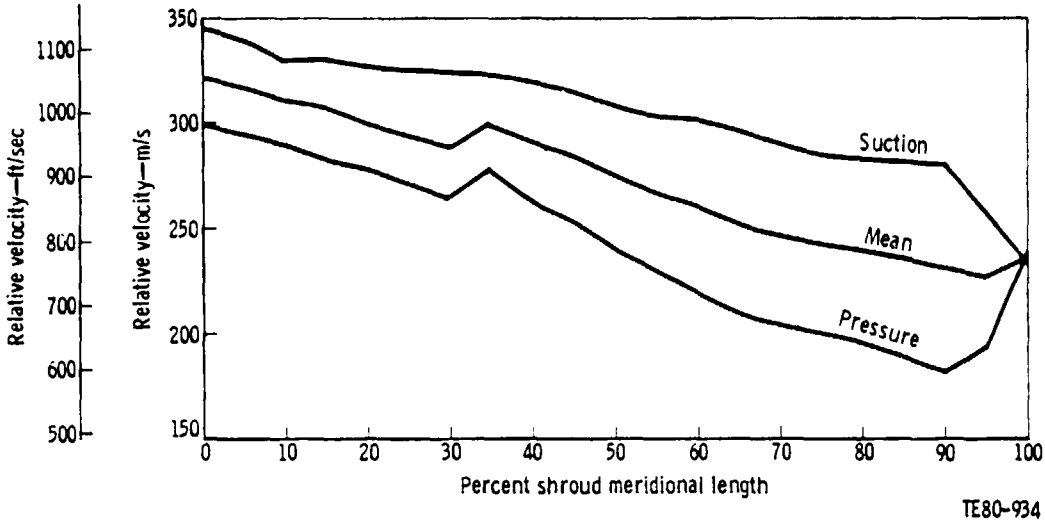

Figure 31. - AGT-100 Impeller Shroud Relative Velocity Distribution $N/\sqrt{\theta}$ = 100%.

Design running clearances are 0.076-0.18 mm (0.003-0.007 in.) over the inducer and 0.127-0.229 mm (0.005-0.009 in.) at the exit. While smaller clearances are desirable, these values were achieved only after a careful review of the mechanical configuration and stack tolerances. An abradable coating now under development may provide the potential for clearance reduction at a future time.

Diffuser

The AGT-100 uses a modified wedge, vane island diffuser. The diffuser vane cross section is shown in Figure 32. The diffuser has 21 vanes and employs a vaneless space of length equal to 8% of the impeller exit radius. The vaneless space meridional flow path has a 15% contraction, which produces an annulus area ratio between impeller exit and diffuser inlet of 0.939. The meridional vaneless space contraction allows for some impeller exit width reduction during development without incurring a smoke shelf configuration.

The flow path through the diffuser vane has a constant axial dimension so that the 4.04:1 diffuser area ratio is achieved using an 8.5-deg divergence between vane walls. The diffuser passage inlet throat, w_4, is nominally 4.31 mm (0.170 in.) and the meridional width, b_4, is equal to 4.7 2 mm (0.186 in.). Therefore, the diffuser throat aspect ratio, b/w, is 1.10. This diffuser geometry is shown in Table VIII.

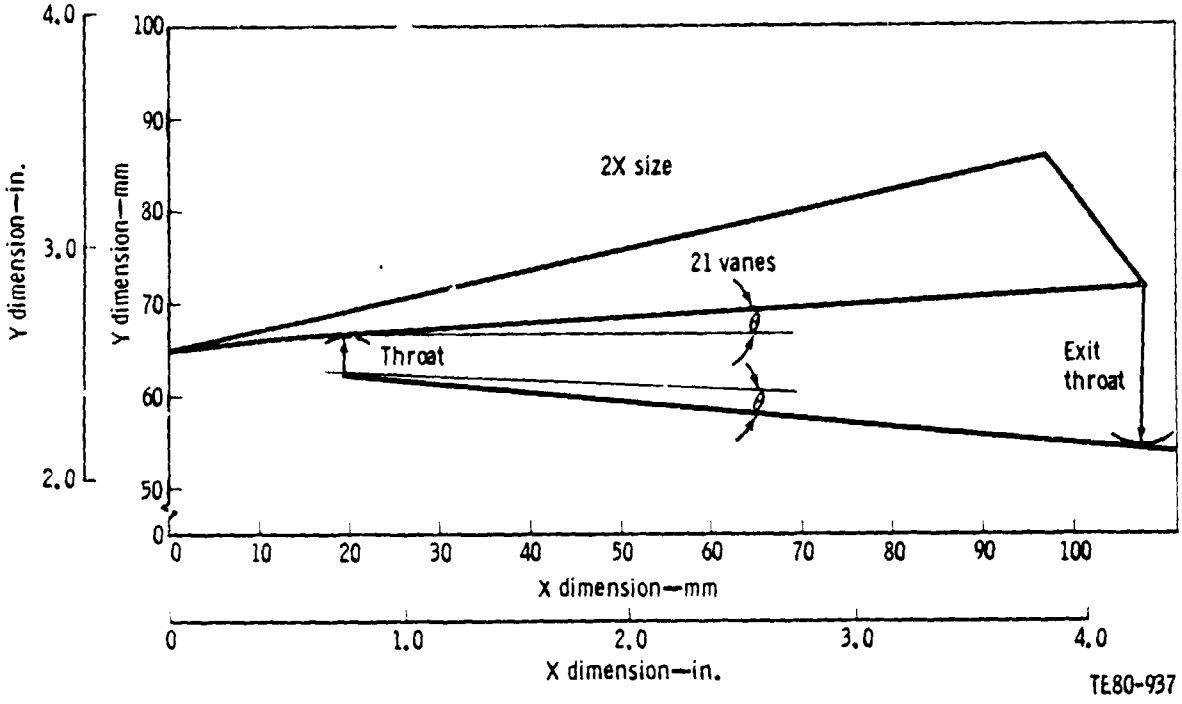

Figure 32. - AGT-100 Diffuser Vane Section.

TABLE VIII. DIFFUSER GEOMETRY

Number of vanes	21
Vane inlet radius, R_3	64.87 mm (2.554 in.)
Vane exit radius	129.5 mm (5.10 in.)
Vane leading edge radius	0.25 mm (0.010 in.)
Design incidence (pressure surface)	-0.25 deg
Suction surface radius of curvature	446.3 mm (17.57 in.)
Passage divergence angle	8.50 deg
Design inlet throat dimension	4.32 mm (0.170 in.)
Meridional width	4.72 mm (0.186 in.)
Design vaneless space, R_3/R_2	1.08
Design area ratio	4.04
Throat aspect ratio	1.10

Collector

The AGT-100 regenerative engine configuration requires a compressor exit collector. A front view and a typical cross section of the collector are illustrated in Figure 33. The collector is an overhung single exit port design. Cross sections beginning with the minimum section at the tongue or splitter are maintained as circular as possible to minimize friction losses. The mean radius of each section is placed at the diffuser exit radius. This placement is a compromise between overall size and increased loss associated with lowering the collector radius relative to the diffuser exit radius.

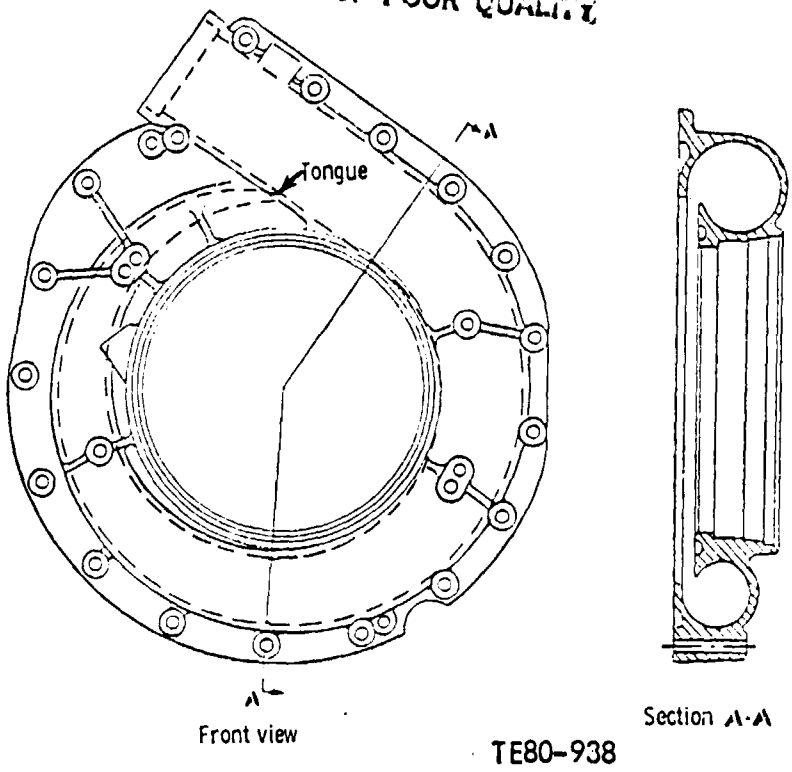

Figure 33. - AGT-100 Compressor Collector.

The collector provides for an approximate 2:1 area ratio dump for flow exiting the diffuser. This reduces the collector through-flow Mach number to minimize the pressure drop. The exit Mach number is computed to be 0.08, which is required to minimize losses in the regenerator ducting.

The collector was designed to maintain a circumferentially constant static pressure at design operation. A nearly linear area distribution was used because analysis indicated that such a distribution would closely approximate the constant pressure condition. The minimum section under the tongue has an area of 25.8 mm^2 (0.04 $in.^2$) to allow for some recirculation in order to avoid stalling or separation at this point. The collector area then increases to 3426 mm^2 (5.31 $in.^2$) at the collector exit.

Rig Design

An auxiliary gearbox is required to increase the speed capability of the DDA compressor test facility. A 3:1 step-up ratio is needed to keep gear and bearing loads and speeds within acceptable limits. This design is shown on Figure 34. The gearbox is designed for 96,000 rpm output shaft speed. All detailed drawings are completed and parts released for fabrication.

The compressor rig design is shown in Figure 35. The compressor rig will be mounted on the auxiliary gearbox and driven by a splined coupling shaft between the auxiliary gearbox output shaft and the test equipment shaft. This latter shaft replaces the gasifier turbine rotor and serves as the tiebolt for the rig rotor. The rig will use the engine inlet, which provides a bifurcated plenum. The necessary elbows and tubes will adapt through a plate to the

existing test rig inlet plenum. The inlet configuration improves accessability to the rig and should provide adequate space for mounting a strain gage signal transfer device to be required at a later time. The rig will use engine parts except in those cases where procurement could be expedited by replacing castings with machined parts or (as in the case of a number of parts in the rear bearing area) where materials with lower temperature properties can be used. The dynamic analysis of the rig indicated that use of the test equipment rear support eliminated the necessity for a mass isolator. Consequently, the rear bearing cage will be provided. The rig design permits replacement of the test equipment parts by engine parts in subsequent portions of the compressor rig program.

The engine scroll is modified to provide four tubes which port the inducer bleed air to an external control system. This will allow investigation of the effect of inducer flow rates on compressor performance during the rig testing. The external system includes an ejector, flow measurement devices, and appropriate valving that will allow a controlled variation of the inducer bleed cavity sink pressure.

The layout and most of the detailing was completed on the test equipment parts. Only a few engine parts replacements in the rear bearing area remain to be detailed.

3.2 COMPRESSOR MECHANICAL DEVELOPMENT

Design

The engine gasifier module is configured such that the compressor impeller and gasifier turbine rotor are mounted on two ball bearings. An angular contact bearing (No. 1) is forward of the impeller, and a split ball bearing (No. 2) is approximately midway between the compressor impeller and the gasifier turbine rotor. The No. 1 bearing mounts in the center body, which in turn is attached to the inlet duct. The No. 2 bearing mounts in the bearing support, which has attached to it the scroll, compressor diffuser shroud, and retaining ring. The variable geometry inlet guide vanes are assembled into the shroud and operated by a lever, ball, and separator mechanism. The power transfer drive bevel pinion attaches to the end of the compressor impeller shaft and drives through a vertical shaft, bevel gearbox, and horizontal shaft back to the power transfer clutch in the gearbox. The general arrangement of the compressor module is delineated in Figure 5, Section 2.1. (See Section VIII for further details of bearings, shafts, gears, etc.)

Compressor Rotor and Diffuser

The initial prototype impellers are machined from a solid cast billet (production impellers will have the blades and splitters processed in place). The diffuser selected is a fixed-vane channel type with 21 wedge-shaped vanes. The compressor rotor is an aluminum impeller pressed onto a steel shaft. Heat transfer and stress analysis studies are complete.

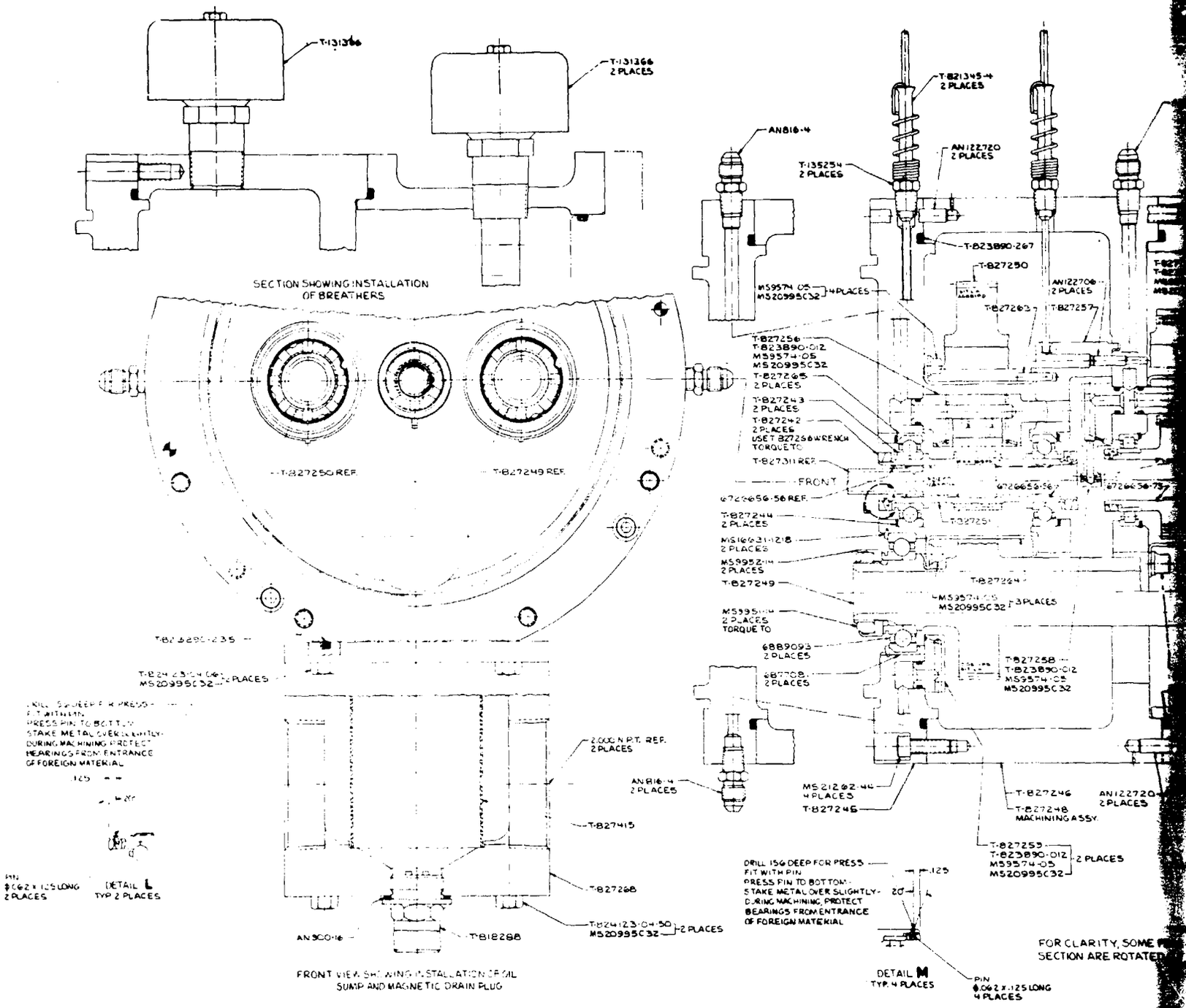

Figure 34. - Compressor Rig

FOLDOUT FRAME

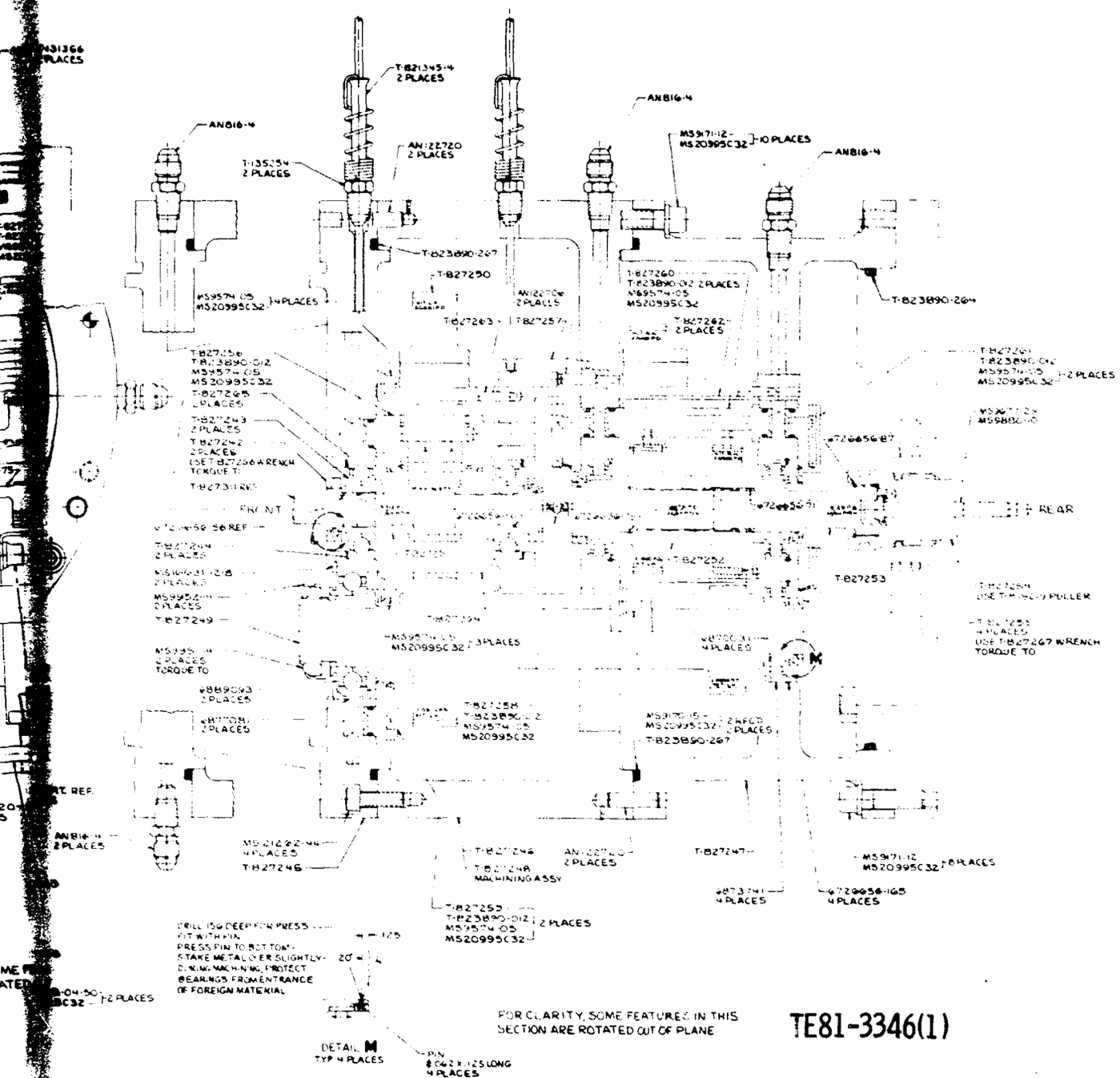

Figure 34. - Compressor Rig Design for 3:1 Step-Up Ratio.

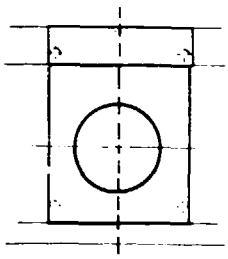

VIEW K-K

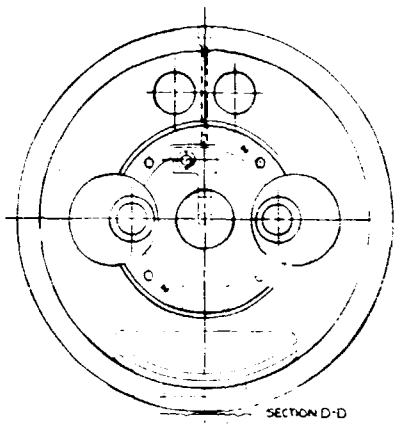

SECTION D-D

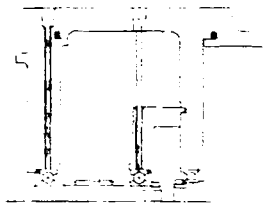

SECTION J-J

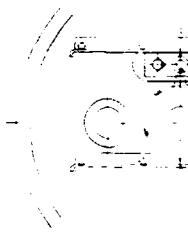

SECTION

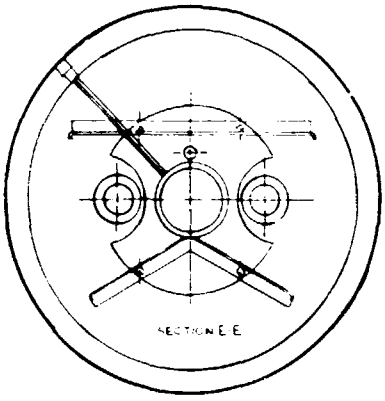

SECTION E-E

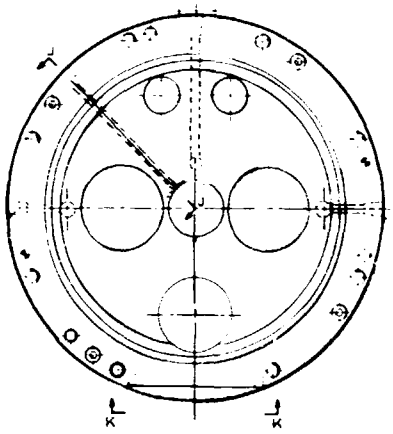

VIEW F-F

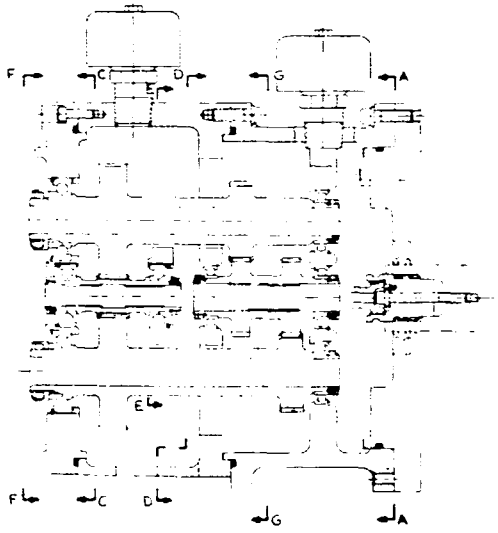

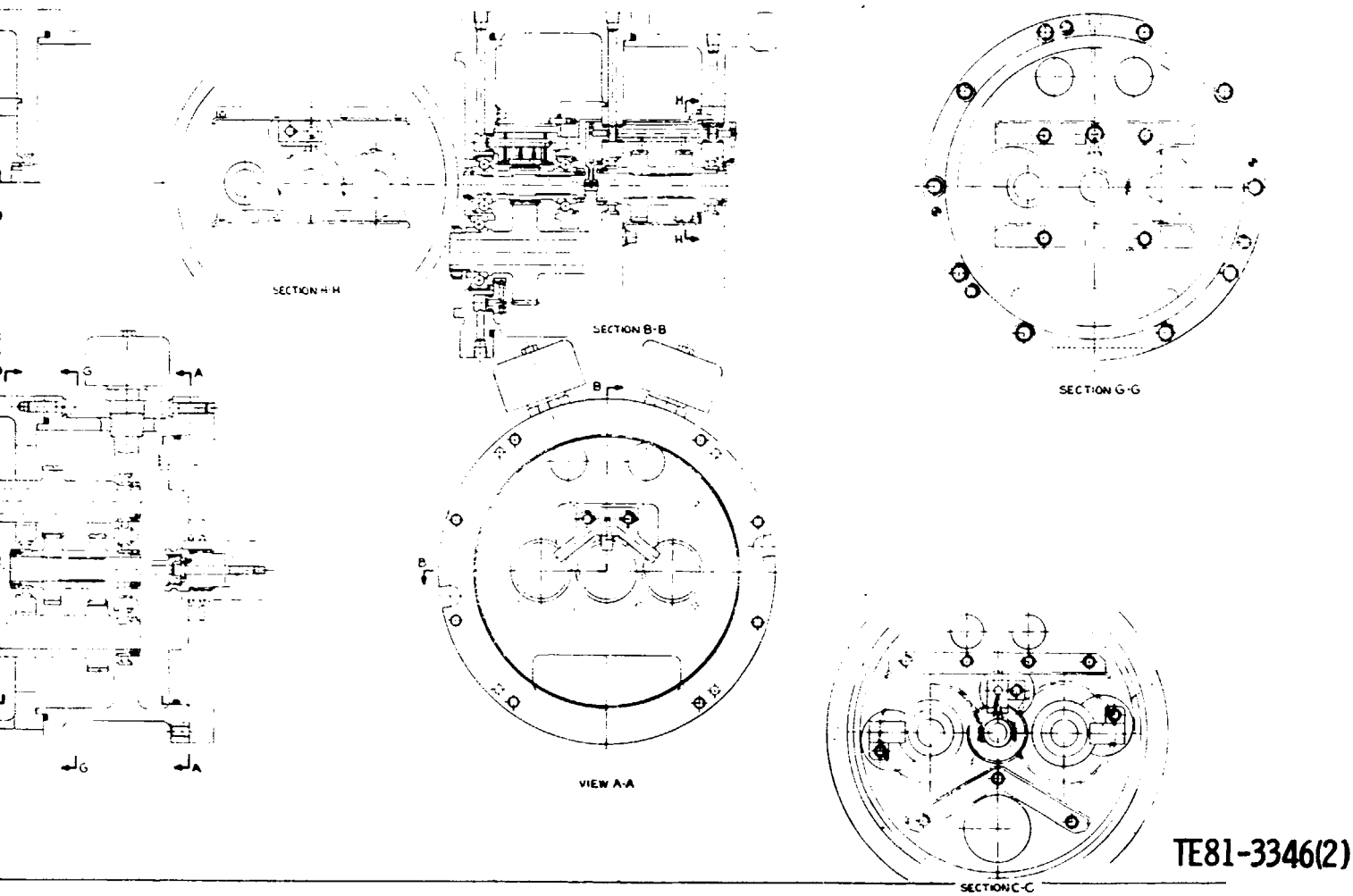

Figure 34. - Compressor Rig Design for 3:1 Step-Up Ratio. (cont)

FOLDOUT FRAME 2

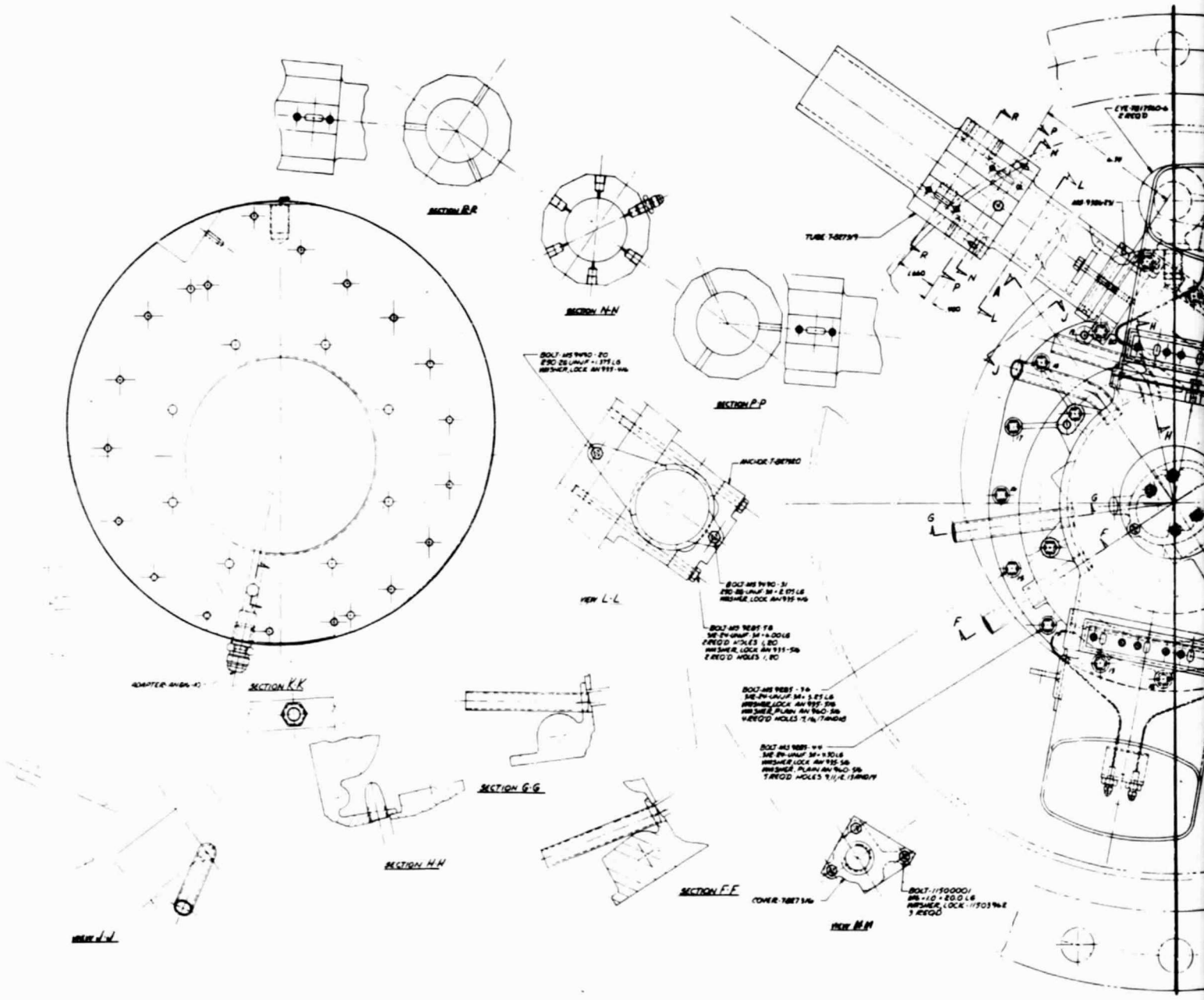

Figure 35. - Compressor Rig Desig

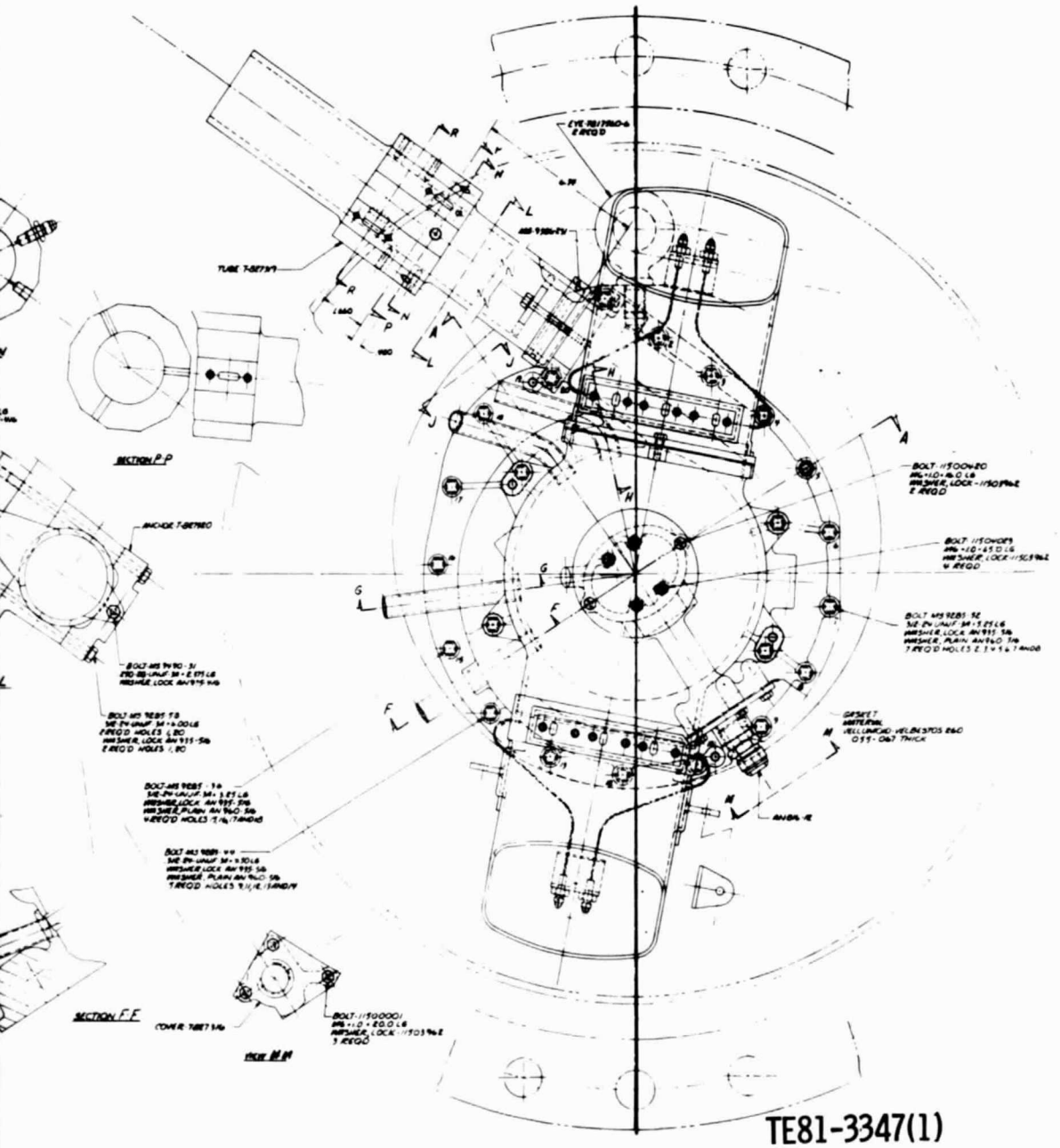

Figure 35. - Compressor Rig Design.

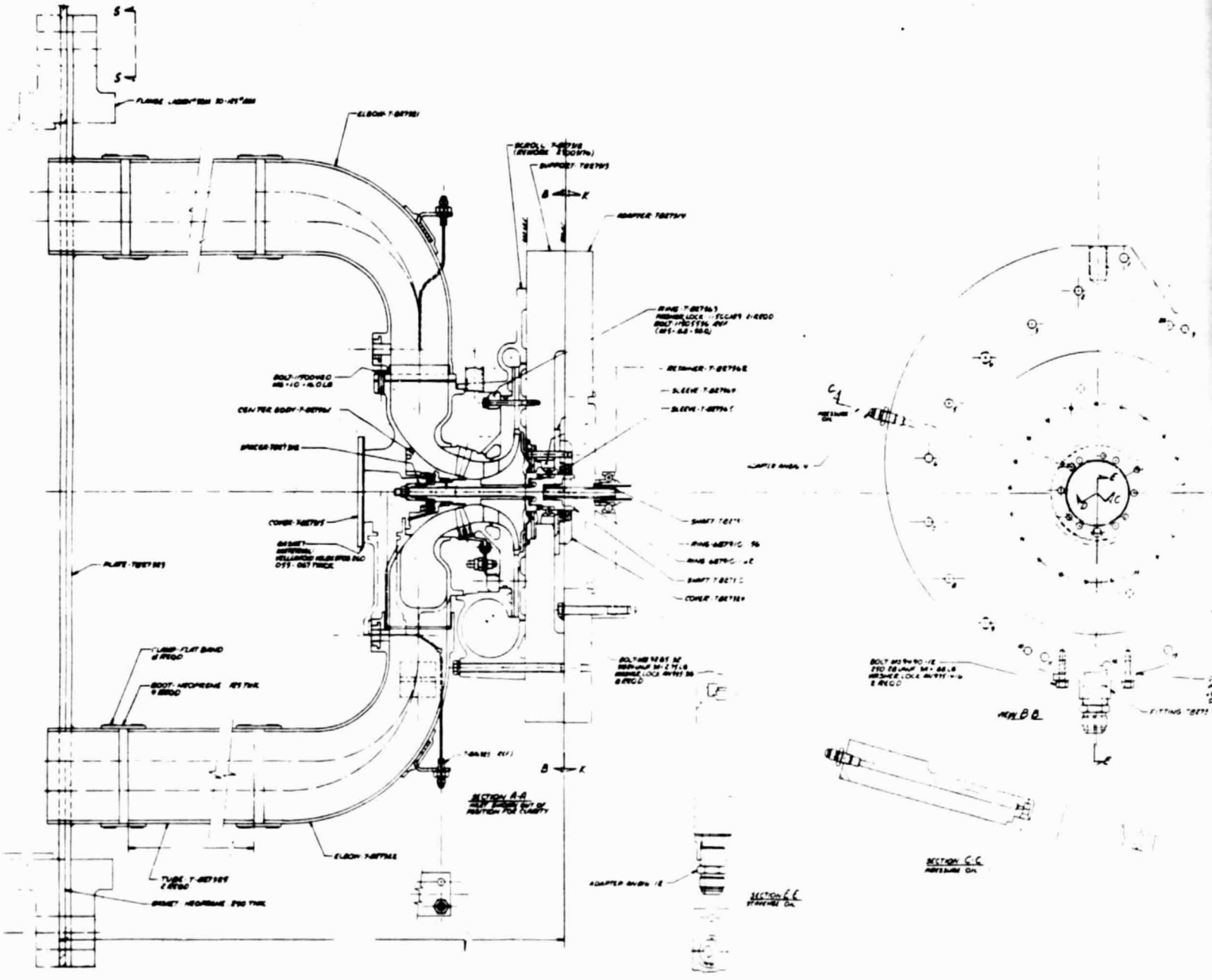

FOLDOUT FRAME

Figure

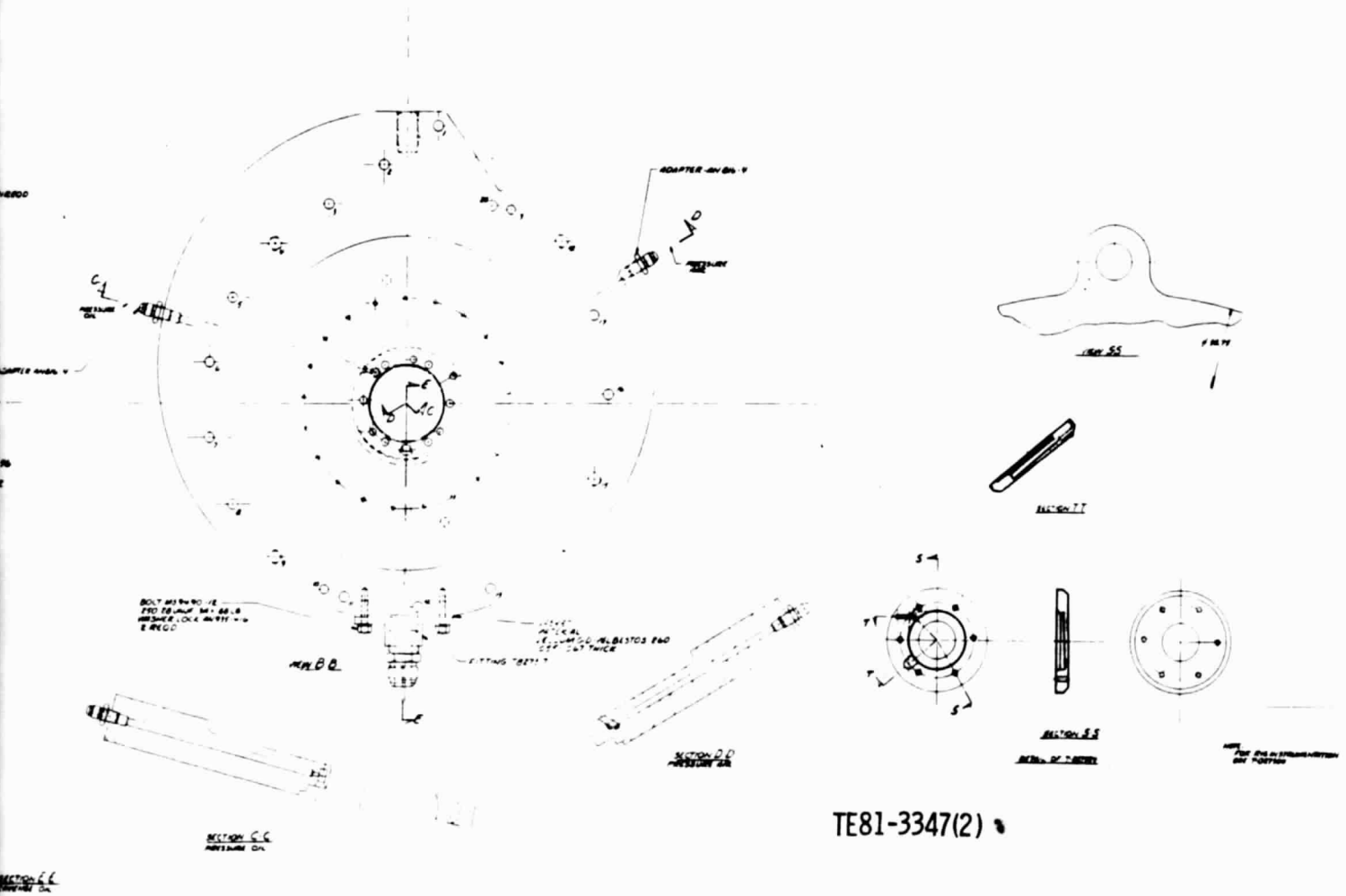

TE81-3347(2)

Figure 35. - Compressor Rig Design. (cont)

Inlet Guide Vane

The 15 variable geometry vanes have a range of 75 degrees from idle to full power. This movement is accomplished by a vane-mounted lever engaging a ball contained in a separator ring, which is moved by an externally mounted actuator. The vane bushing and lever ball are plastic material to reduce frictional losses. Work continues on the selection and mounting of the IGV actuator.

Containment

One of the design objectives of the engine program is to ensure containment of the compressor impeller should a burst occur. An analysis of the capability of the compressor cover to absorb the energy of the impeller failure was completed. The revised compressor configuration shown in Figure 5, Section 2.1, will provide containment to 150% of the impeller design speed, whereas impeller burst with -3 material will be at 144% speed. Experience on the IGT engine indicates that elastic and plastic deformation of the compressor impeller will produce rubbing with the compressor cover at speed only slightly above the design speed. This rubbing rapidly becomes self-perpetuating because of heating of the impeller and material transfer to the cover, and a rotor terminal velocity is achieved at less than 115% gasifier rotor speed. The similarity of the configurations between the IGT and AGT-100 compressors would suggest that the same sequence of events would occur and that containment capacity of the cover is more than adequate.

Work is proceeding on static deflections of the bearing support and surrounding structure to provide hot and cold compressor tip clearances. Ribs were added to the shroud support fingers to reduce the local bending stress in that area. The layout of the shroud was revised and pattern equipment is ordered.

Compressor Structural Analysis

The impeller was analyzed for three conditions:

- o Cold build, or assembly
- o Standard day ambient inlet, 100% design speed (86,200 rpm)
- o Ambient inlet temperature of 52°C (125°F), maximum overspeed of 115% (99,130 rpm)

The standard day ambient inlet, 100% speed operating condition was used to evaluate the low cycle fatigue life of the impeller and the high cycle fatigue margin of the blade. The hot day overspeed (125°F day, 115% speed) was used to evaluate the yield criteria and to determine the burst speed of the impeller. The hot day overspeed condition was also analyzed to ensure that the radial pilot between the shaft and impeller bore is maintained.

Two finite element models have been employed in analyzing the impeller wheel:

- o Triangular Plate Model - This model consists of separate blade and backplate substructures, joined together by constraint equations. The model is used for preliminary sizing of blade and backplate thicknesses, and for the final hot-to-cold geometry iterations.

- o 3-D Cube Model - This model includes the entire wheel and blade, and a detailed modeling of the fillet between wheel and blade. This model calculates the concentrated stress in the fillet, and allows determination of the stress concentration associated with the peak stress.

The low cycle fatigue goals for the AGT-100 impeller are based upon the combined urban and highway EPA driving cycle. To evaluate impeller stresses, the speed excursions associated with the driving cycles are reduced to an equivalent number of zero to max rpm cycles. The total design life of 100,000 miles is equivalent to 33,600 zero to maximum rpm cycles. The impeller material is expected to be silverless K01 aluminum (AA-206). Low cycle fatigue lives are based on smooth bar test data for that material. A material LCF model was developed from these test data.

The results listed below pertain to the final configuration impeller:

- o Low Cycle Fatigue (LCF)
  The low cycle fatigue lives of the impeller are summarized in Table IX.
- o High Cycle Fatigue
  The high cycle fatigue margins for the blade and backplate are summarized in Table X. The regions identified are areas of high mean stress, or locations of maximum vibratory stress for the computed modes.
- o Burst Speed
  The impeller wheel has a calculated burst speed of 115,000 rpm, or 133% speed using -3σ material properties. The burst speed with mean properties is 124,000 rpm, or 144% speed. Burst occurs when the average tangential stress exceeds 91% of the ultimate strength.
- o Impeller Yield
  Design criteria require that no significant volume of material exceeds yield strength, to ensure no permanent deformation of the wheel shape at 125°F ambient inlet, 115% speed. Although some local yielding occurs in the bore, this will not result in bore deformation.
- o Radial Pilot Contact
  A radial interference fit of 0.048 mm (0.0019 in.) between the impeller bore and shaft is sufficient to ensure radial contact at 125°F ambient inlet, 115% speed.

The computed average (mean) low cycle fatigue life of 12,500 cycles is not considered desirable. A materials program has been started to evaluate strength improvement by prestressing. See Section 9.1.

A thermal and stress analysis is in process to determine the structural deflections of the compressor shroud and surrounding structure that reflects on compressor blade tip clearance. Design effort continues on the power transfer bevel drive and gearbox, variable geometry inlet guide vane mechanism, and the turbine bearing support.

Power Transfer

The power transfer drive consists of a clutch in the gearbox and connecting shafting to the gasifier rotor. A horizontal quill shaft connects the main reduction gearbox to the bevel drive gearbox, which is attached to the inlet duct. The drive to the compressor rotor is accomplished by a radial shaft with bevel gears at each end. The design of the drive is nearing completion.

TABLE IX. AGT-100 COMPRESSOR IMPELLER LOW CYCLE FATIGUE

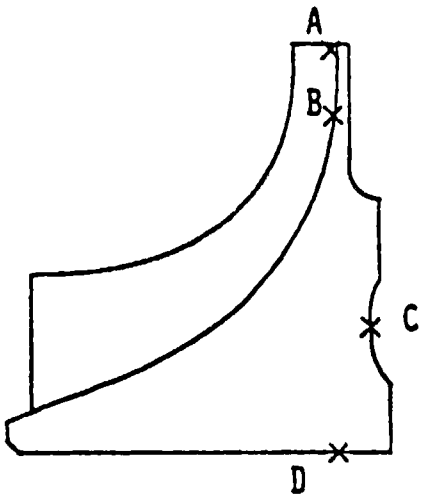

Location	Stress--MPa (ksi) Mean	Alternating	Maximum	Life-cycles Mean	-3
Blade					
A			228 (33.1)	114,000	48,900
Backplate					
B			259 (37.6)	52,200	21,400
Wheel					
C	139 (20.2)	140 (20.3)	279 (40.5)	22,500	9,100
D	371 (53.9)	98 (14.2)	470 (68.1)	12,500	6,800

Noise

An analysis to determine the amount of rotor noise reduction required to produce a comfortable near-vehicle noise level was conducted. Noise from gear mesh induced tones is not predictable and will be measured during engine test.

TABLE X. HIGH CYCLE FATIGUE MARGINS FOR THE AGT-100 IMPELLER

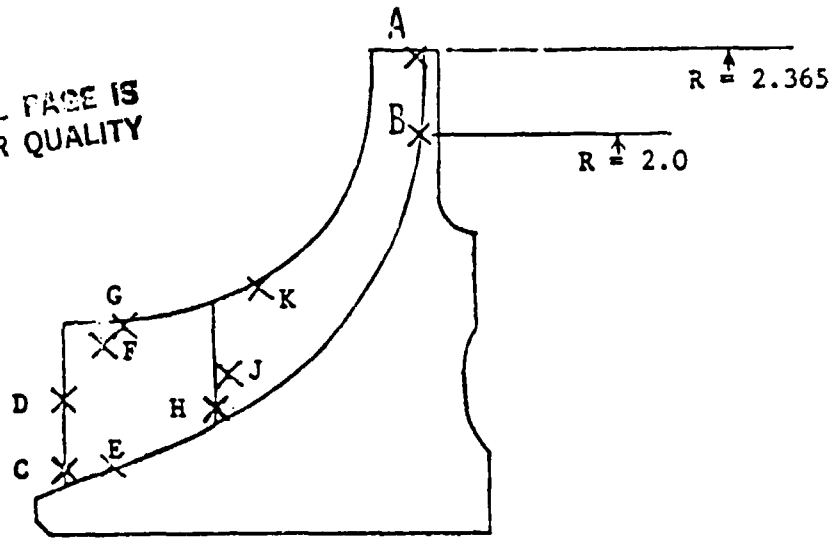

	Location	Vibration mode	Stress concentration factor	Mean equiv. stress ksi	-3 allowable vibratory stress
Blade					
	A*		1.09	19.0	5.4
	B*		1.46	22.6	4.0
	C*		3.0	9.3	3.7
	D**	4	3.0	7.3	3.9
	E**	1	1.4	13.5	5.8
	F**	5	1.0	2.3	9.2
	G**	2,3	1.0	2.7	9.1
Splitter					
	H*		3.0	7.6	3.8
	J**	1	1.0	7.0	8.3
	K**	2	1.0	5.1	8.7
Backplate					
	B*		1.29	29.1	3.3

*Locations of high steady-state stress and/or high stress concentrations due to foreign object damage

**Locations of maximum vibratory stress

IV. GASIFIER TURBINE DEVELOPMENT

4.1 GASIFIER TURBINE AND INTERTURBINE DUCT AERODYNAMIC DEVELOPMENT

High efficiency over a broad operating range is the primary goal for the gasifier turbine. Aerodynamic design to achieve this goal must be consistent with stress, heat transfer, vibration, and mechanical design requirements. To be competitive in the automotive market, this goal must be achieved with recognition of the requirement for low cost and low inertia. Achievement of high efficiency for the AGT-100 gasifier turbine is challenging because of the small size, ceramic construction, and relatively low Reynolds number.

Development activity during this period has focused on preliminary design of the RPD gasifier turbine and transition duct, preliminary design of the Mod I gasifier turbine, bench testing of the interturbine (transition) duct, layout and fabrication of the gasifier turbine test rig, and turbine facility checkout.

RPD Gasifier Turbine Design

The RPD engine cycle requirements for the gasifier turbine at the maximum power, sea level static, condition are:

Inlet temperature, °C (°F)	1288 (2350)
Inlet pressure, kPa (psia)	438.4 (63.58)
Fuel/air ratio	0.0129
Equivalent flow, $W\sqrt{\theta}_{cr}\,\epsilon/\delta$, kg/s (lbm/sec)	0.178 (0.391)
Equivalent work, $\Delta h/\theta_{cr}$, kJ/kg (Btu/lbm)	42.07 (18.09)
Equivalent speed, $N/\sqrt{\theta}_{cr}$, rpm	37630
Expansion ratio (total - total)	1.8726
Efficiency with inlet scroll (total - total)	84.7

Although the turbine operates at the maximum power point only a small fraction of the time, this point does represent the most severe steady-state structural design condition. The maximum power condition, therefore, has been selected as the design point to ensure a systematic integration of fabrication, aerodynamic, heat transfer, stress, and vibration design disciplines. The design process commences with aerodynamic definition of flow path, vane and blade contours, and thickness distribution.

Flow Path Selection

Several factors are involved in the selection of "optimum" flow-path parameters. First is the realization that part power is empnasized at the expense of full-power performance. Caution must be used, however, to avoid any severe efficiency reduction at maximum power, which would result in unacceptable vehicle response. A second major factor is the selection of aerodynamic and geometric parameters consistent with structural design for fabricability, long life, and low cost. This second factor became particularly important with respect to achieving adequate life of the ceramic wheel. A third important consideration in design relates to selection of flow-path parameters conductive to low inertia.

The gasifier turbine flow path selected to satisfy the AGT-100 turbine design criteria is illustrated in Figure 36. This turbine features a symmetrical vane with endwall contouring and a low-inertia rotor. Salient features of the turbine design are:

Vane inlet diameter, mm (in.)	147.38 (5.802)
Rotor tip diameter, mm (in.)	112.52 (4.43)
Vaneless space diameter ratio	1.078
Rotor tip width, mm (in.)	8.38 (0.330)
Exducer hub/tip radius ratio	0.30
Rotor tip diameter/exducer tip diameter ratio	1.600
Rotor tip width/rotor tip diameter ratio	0.0745

Operating at the sea level static (SLS) maximum power condition, the turbine exhibits a tip speed of 508 m/s (1667 ft/sec), an aerodynamic loading parameter (U/C - Tip Speed/Isentropic Spouting Velocity) of 0.700 and a specific speed of 75. Turbine specific speed is defined as: $N\,Q^{1/2}/(\Delta h_{is})^{3/4}$. Turbine parameters for several engine operating points under road-load conditions are presented in Table XI.

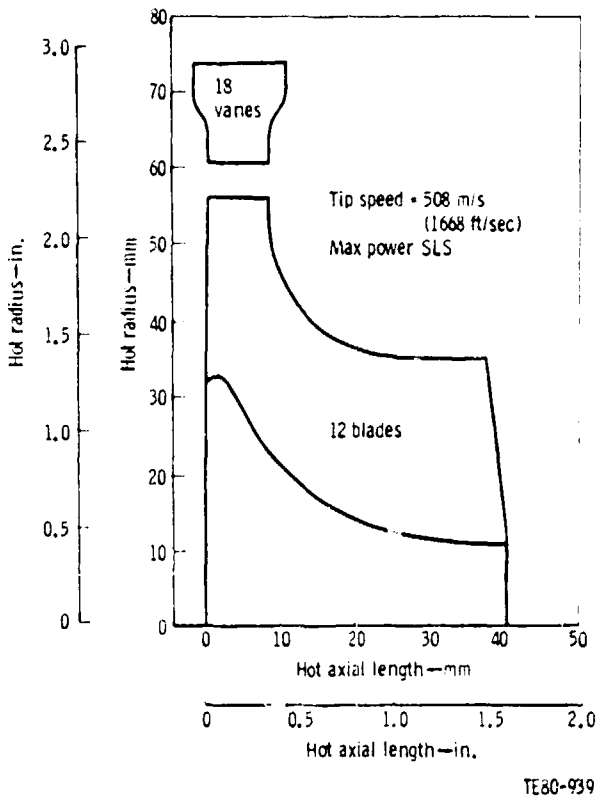

Figure 36. - RPD Gasifier Turbine Flow Path.

TABLE XI. RPD GASIFIER TURBINE PARAMETER FOR VARIOUS ENGINE OPERATING POINTS

Speed, km/h (mph)	(Idle)	32 (20)	48 (30)	80 (50)	102 (70)	Max power*	Max power (SL)**
Turbine power, kW (hp)	5.93 (8.24)	6.04 (8.10)	11.99 (16.37)	14.50 (19.45)	26.53 (35.58)	64.49 (86.48)	71.35 (95.68)
Inlet temperature, °C (°F)	683 (1261)	842 (1548)	1172 (2142)	1226 (2238)	1241 (2265)	1288 (2350)	1288 (2350)
Equivalent flow, kg s^{-1} (lbm sec^{-1})	0.128 (0.282)	0.136 (0.299)	0.141 (0.309)	0.162 (0.357)	0.172 (0.377)	0.176 (0.387)	0.178 (0.391)
Equivalent work, kJ kg^{-1} (Btu lbm)	16.40 (7.05)	15.79 (6.79)	16.30 (6.88)	23.24 (9.99)	30.49 (13.11)	39.40 (17.11)	42.08 (18.09)
Equivalent speed, %	63.5	54.4	51.9	62.2	75.8	100.00	100.00
Expansion ratio (T - T)	1.262	1.252	1.259	1.407	1.560	1.847	1.873
U/C	0.719	0.639	0.587	0.582	0.625	0.707	0.700
Mean reaction	0.515	0.425	0.446	0.393	0.439	0.514	0.510
N_S	49.7	63.8	59.8	60.7	65.7	75.2	74.9
N_{RE}	36,400	27,800	25,800	34,500	47,500	81,300	88,500
Swirl angle, deg	+16.2	+1.2	-7.8	-11.6	-8.1	-0.7	+2.4
$M_{N_{ax,t}}$	0.112	0.112	0.119	0.154	0.178	0.214	0.218

*Ambient temperature: 29°C (85°F), altitude: 152 m (500 ft).
**Ambient temperature: 15°C (59°F), altitude: sea level.

As evident in Table XI, the turbine is required to operate over a wide speed and power range. This gives rise to a substantial variation in equivalent flow and work. The aerodynamic loading parameter (U/C) varies from 0.582 to 0.719. The mean static pressure reaction ranges from 0.393 to 0.515. The maximum variation of exit swirl is +16.2 to -11.6 deg. This low turbine exit swirl range is most important for minimizing losses in the transition duct and power turbine.

The power transfer engine concept allows cycle temperatures to remain high over a wide operating range. This is accomplished by extracting additional work from the gasifier turbine, necessary work at the power turbine shaft. Figure 37 illustrates the ratio of gasifier turbine power to compressor power over the engine road-load operating range.

The flow-path selection has been verified through a sensitivity study of critical design parameters. This study included specific speed, tip diameter, vane exit angle, exducer hub/tip radius ratio, and exducer area.

Specific Speed

Proper selection of the gas generator rotative speed is important for achieving the maximum efficiency in both the compressor and turbine. Normally the RPM selection for peak efficiency is common to the compressor and turbine. The additional work of the gasifier turbine in the power transfer engine, however, results in a specific speed slightly less than the optimum value as shown in Figure 38. An increase in RPM to achieve the optimum specific speed is not warranted since it would result in reduced compressor efficiency and increased turbine blade stress.

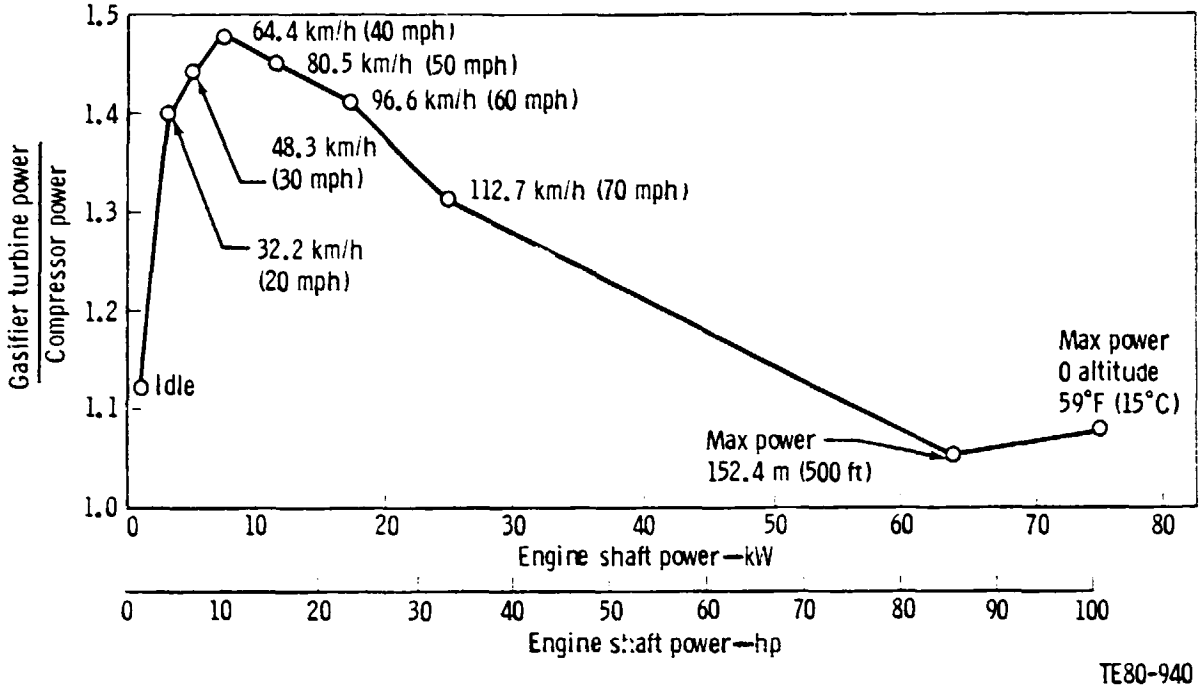

Figure 37. - Ratio of RPD Gasifier Turbine Power to Compressor Power.

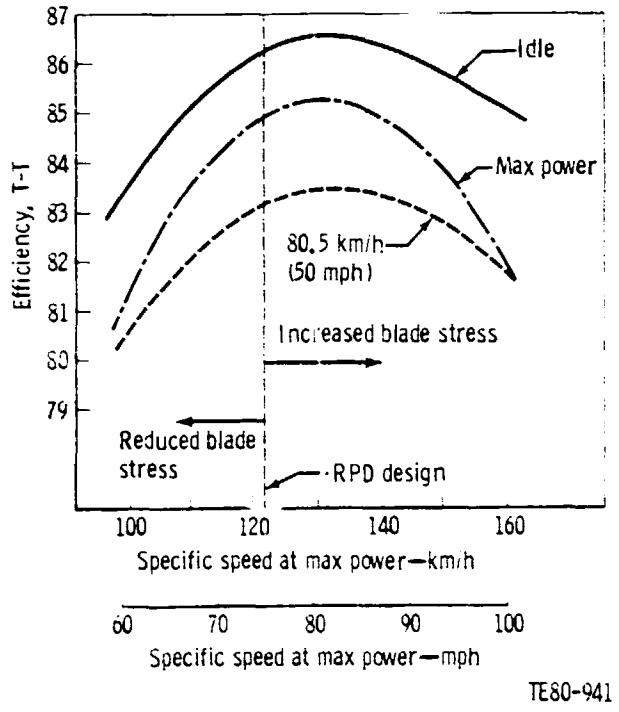

Figure 38. - Effect of Specific Speed on RPD Gasifier Turbine Efficiency.

Tip Diameter

For a specified rotative speed, tip diameter defines the tip speed and aerodynamic loading parameter (U/C). Turbine efficiency is a strong function of tip speed with peak efficiencies generally occurring at a U/C value of 0.7. Figure 39 presents the effect of tip diameter change on turbine efficiency. The RPD turbine design selection provides a good compromise between idle, 80 km/h (50 mph), and maximum power conditions.

Vane Exit Angle

Figure 40 presents the effect of vane exit angle on turbine efficiency. The RPD gasifier turbine vane angle occurs close to the predicted optimum value. Since a high reaction level is desirable to ease the aerodynamic loading of the rotor, the vane exit angle has been selected as large as possible. Further increase would result in reduced efficiency as a result of increasing vane trailing edge blockage.

Exducer Hub/Tip Radius Ratio

Low hub/tip radius ratios are desirable for attaining low inertia. Fortunately, turbine efficiency favors low hub/tip radius as illustrated in Figure 41. Further reductions in hub/tip radius ratio from the 0.3 value selected for the RPD gasifier would result in hub diameters too small for dynamic balance.

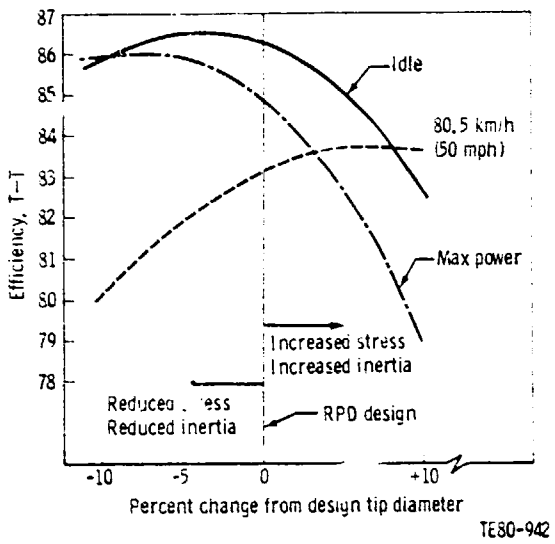

Figure 39. - Effect of Tip Diameter on RPD Gasifier Turbine Efficiency.

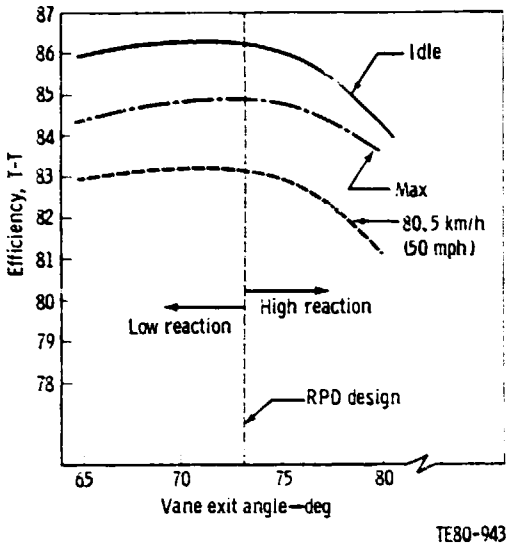

Figure 40. - Effect of Vane Exit Angle on RPD Gasifier Turbine Efficiency.

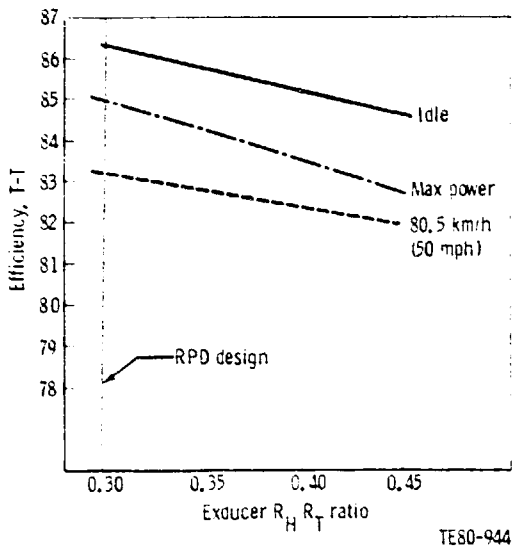

Figure 41. - Effect of Exducer Hub/Tip Rotor on RPD Gasifier Turbine Efficiency.

Exducer Area

Turbine exit area should be as large as possible to minimize the Mach number through the interstage duct. However, too large an exducer area will result in excessive blade stress, reduced first mode frequency, and low reaction. Figure 42 presents both total-to-total and total-to-static efficiency levels as a function of exducer area change. A 10% increase in exducer area would result in a slight gain in total-to-static efficiency but would create a risk in structural design and reduced turbine reaction, as well as a slight decrease in total-total efficiency. The exducer area selected for the RPD engine appears to be a good compromise between area and structural design criteria.

Gasifier Turbine Performance

The aerodynamic performance of the RPD gasifier turbine has been calculated to include the inlet scroll. The efficiency goal for the gasifier turbine is illustrated in Figure 43 as a function of engine road-load power. The lower efficiencies at 48 and 64 km/h (30 and 40 mph) reflect increased turbine loading of the power transfer system.

These engine operating points are superimposed on the equivalent torque-speed performance map illustrated in Figure 44. As can be noted, the turbine design has been tailored to emphasize part power performance. Equivalent flow, equivalent work, efficiency, exit swirl, and exit Mach numbers are illustrated in Figures 45 through 49 as a function of total-to-total expansion ratio.

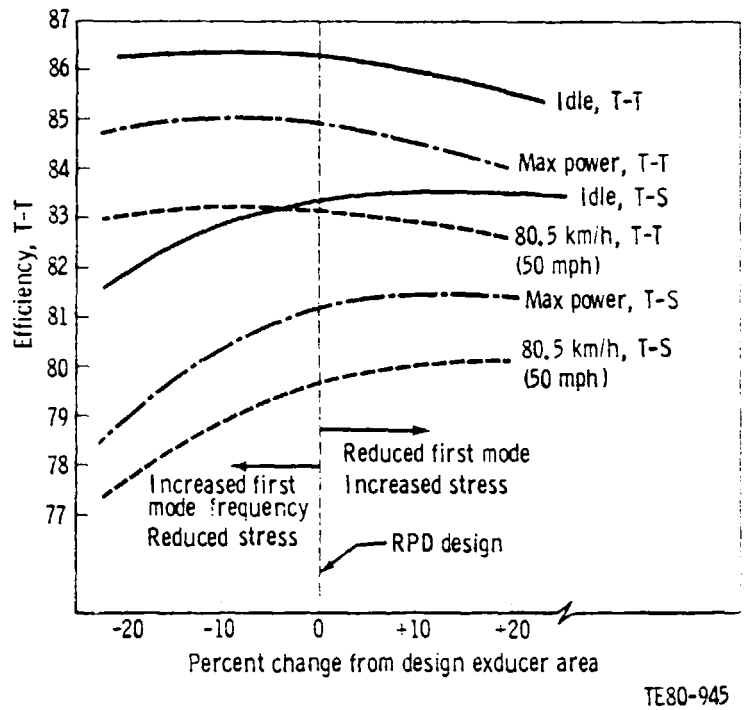

Figure 42. - Effect of Exducer Area on RPD Gasifier Turbine Efficiency.

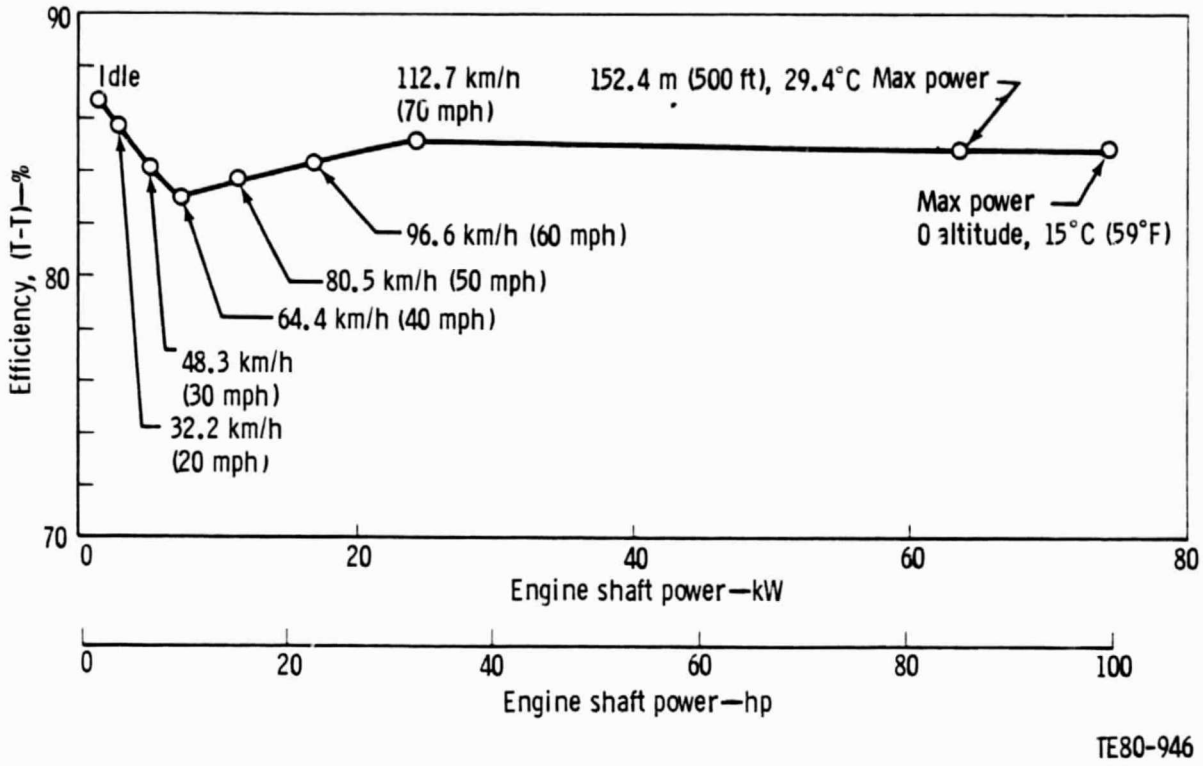

Figure 43. - Efficiency Goal--RPD Gasifier Turbine with Inlet Scroll.

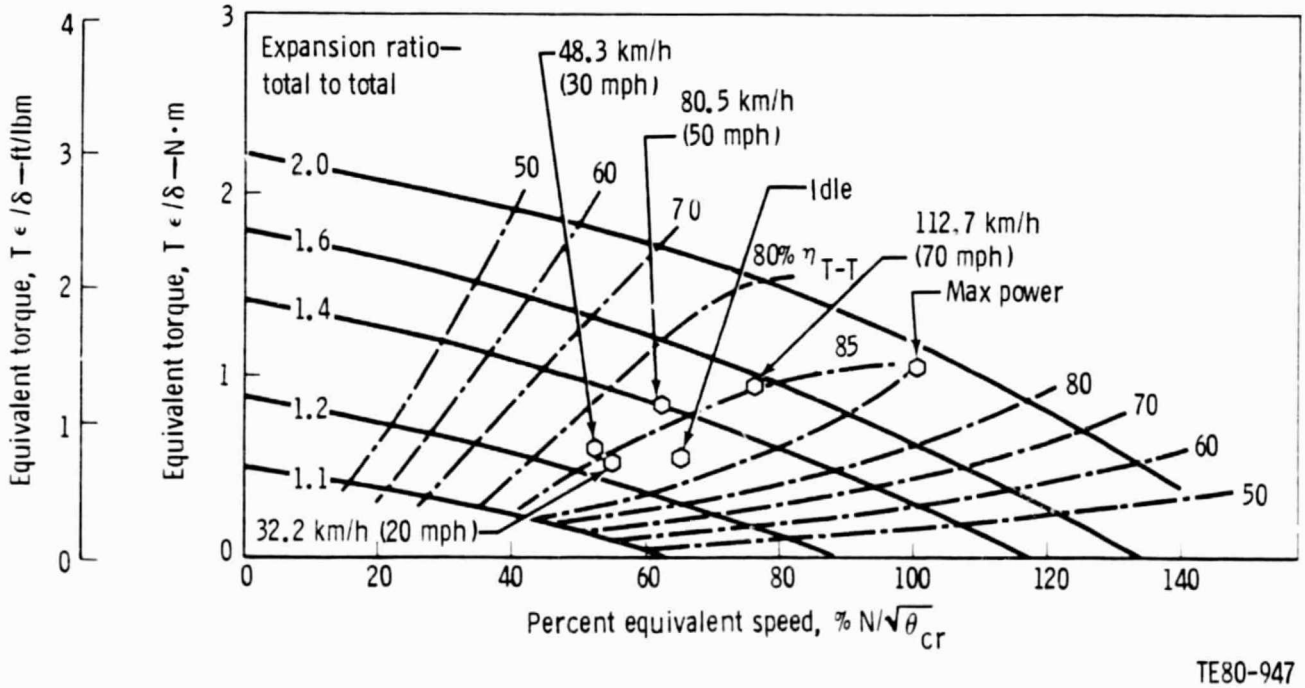

Figure 44. - Predicted Performance Map--RPD Gasifier Turbine with Inlet Scroll.

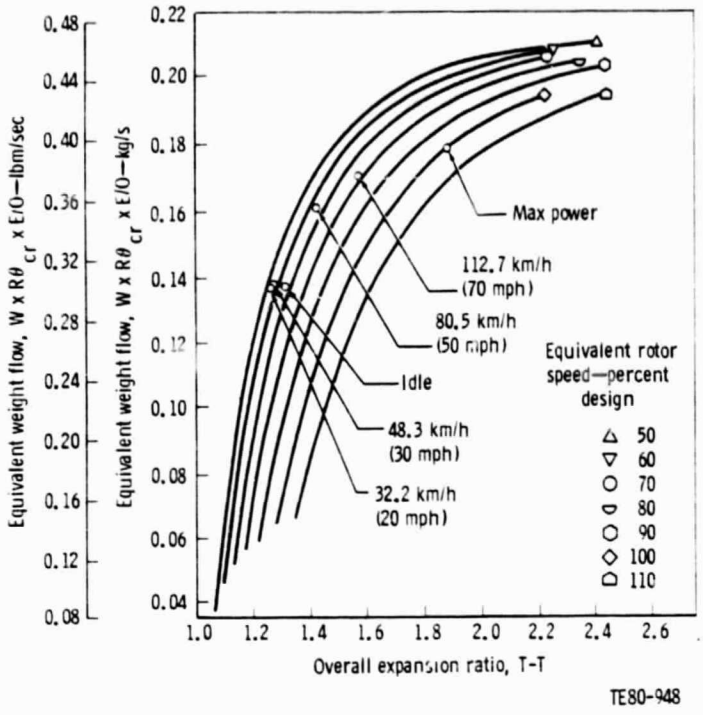

Figure 45. - Predicted Equivalent Flow--RPD Gasifier Turbine.

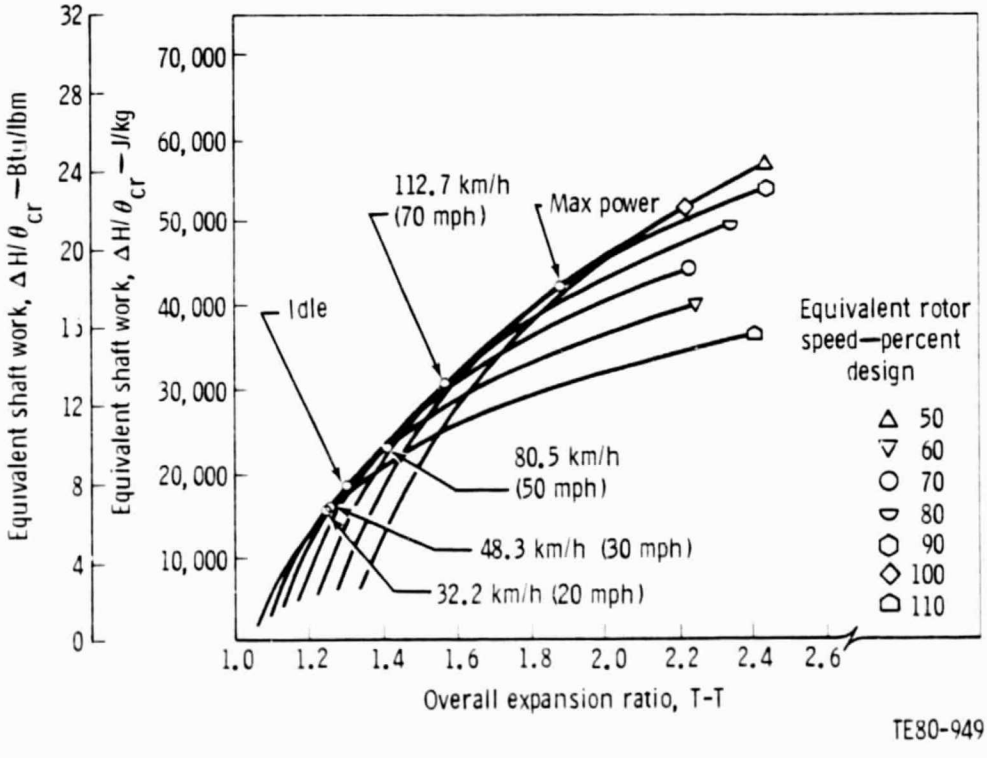

Figure 46. - Predicted Equivalent Work--RPD Gasifier Turbine.

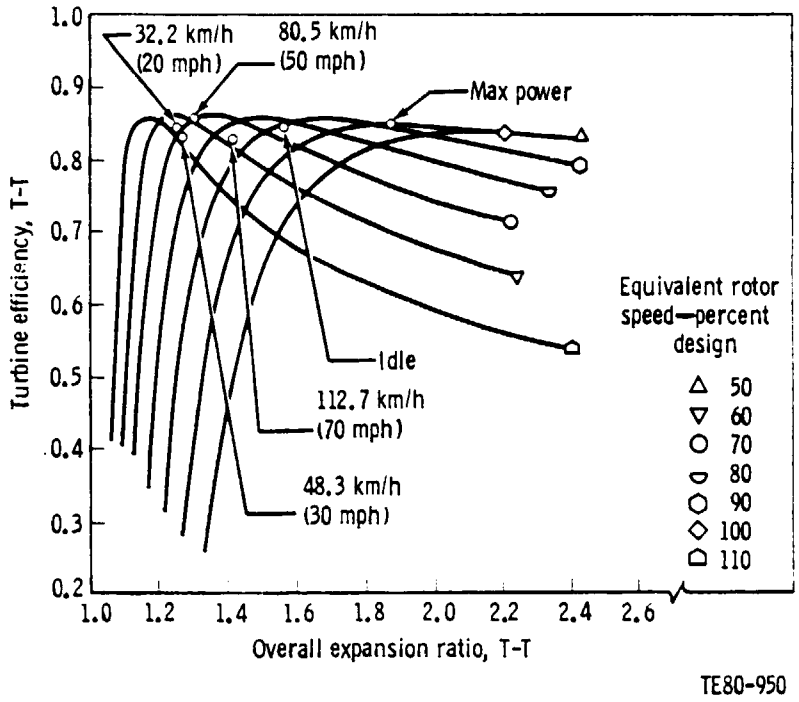

Figure 47. - Predicted Efficiency--RPD Gasifier Turbine.

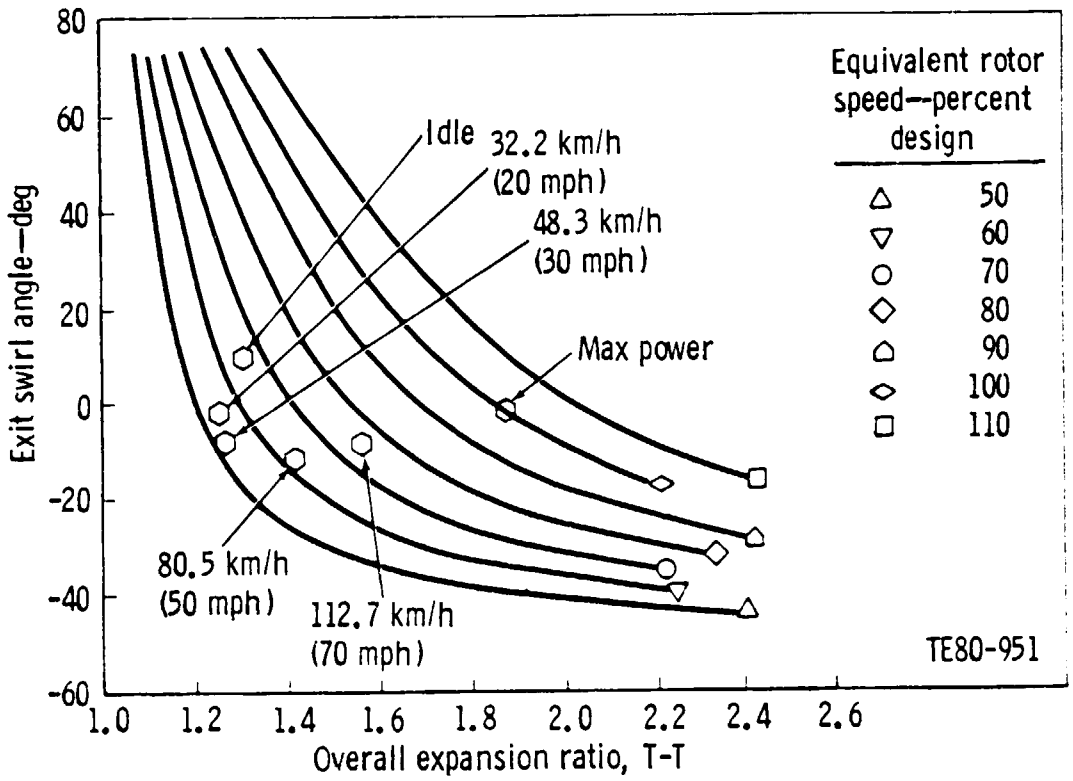

Figure 48. - Predicted Exit Swirl Angle--RPD Gasifier Turbine.

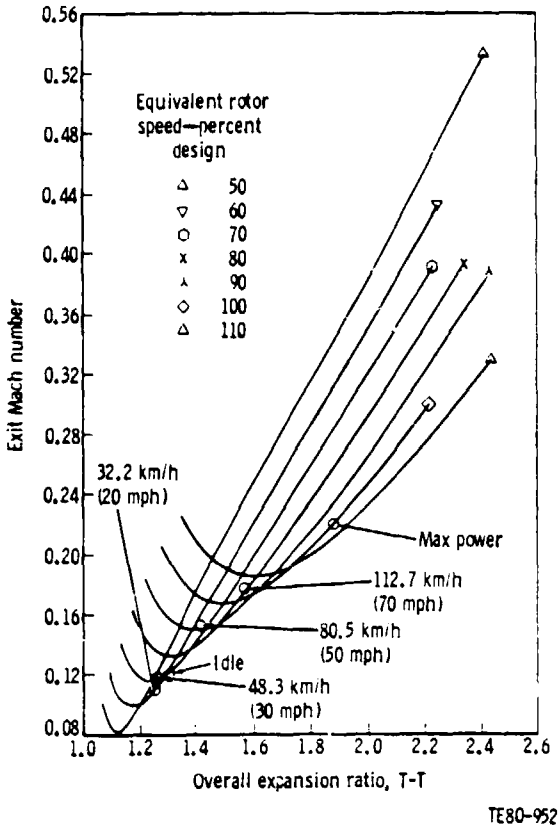

Figure 49. - Predicted Exit Mach Number--RPD Gasifier Turbine.

The preceding turbine performance estimates are calculated through the use of the DDA mean-line performance prediction program. This initial effort was followed with a more detailed design analysis using a quasiorthogonal meridional flow analysis. Meridional flow analysis Mach number diagrams for max power (SLS), 80 km/h (50 mph), 48 km/h (30 mph), and idle are presented in Figures 50 through 53.

Scroll Design

Low loss delivery combustor air to the turbine inlet is the primary goal for the design of the gasifier turbine scroll. The aero design to achieve this goal must be consistent with available space in the engine compartment and with stress, heat transfer, and mechanical design requirements.

The scroll design is based on specification of cross-sectional shape and geometry to ensure minimum loss and delivery of circumferentially uniform flow to the turbine vane row. This was accomplished by designing for low through-flow velocity and uniform exit flow angles. Engine arrangement and compartment size limit the cross-sectional area and outside diameter of the scroll. These limitations prohibited the use of circular cross sections, which provide the most favorable hydraulic diameter.

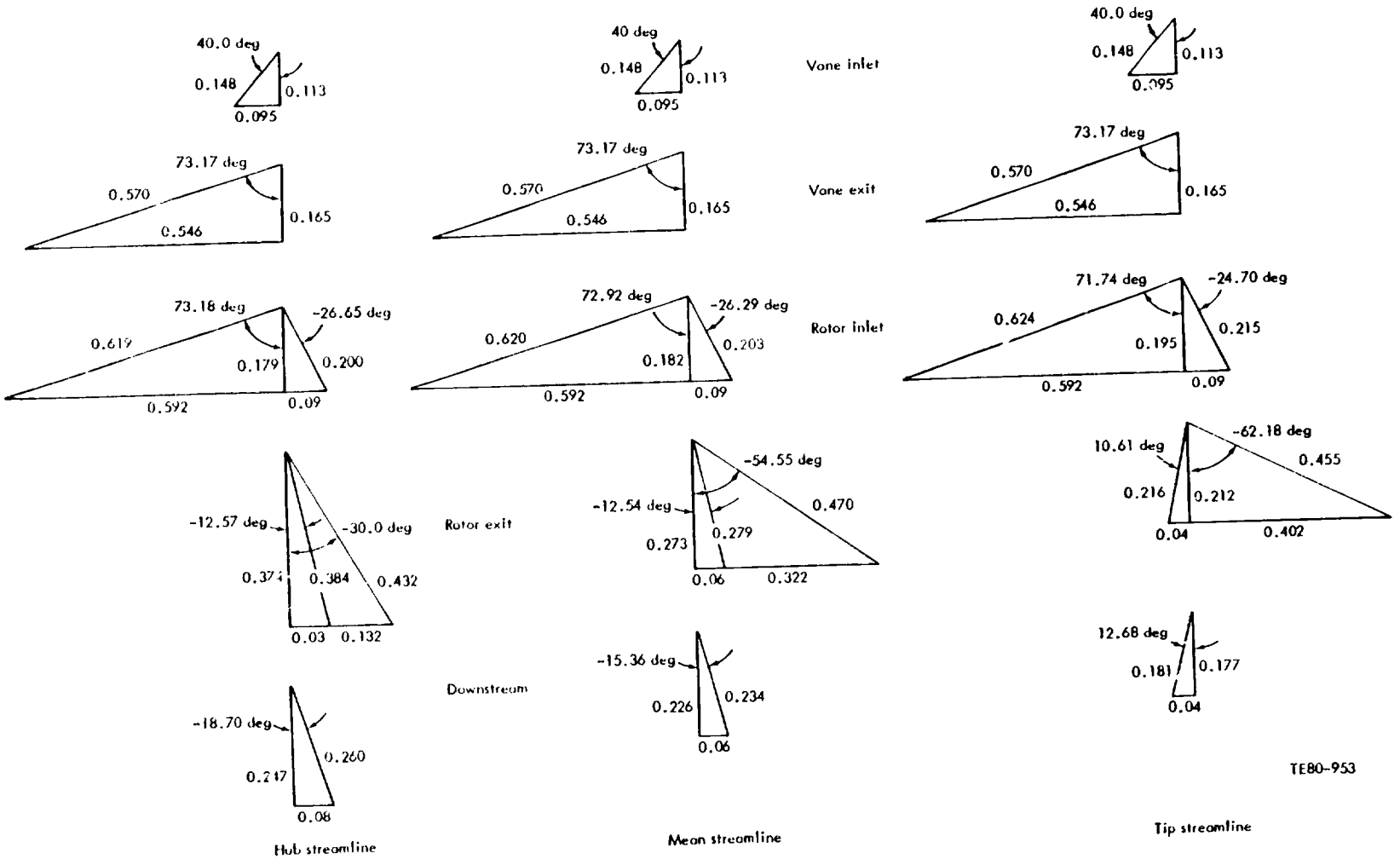

Figure 50. - Mach Number Diagrams--Max Power (SLS)--RPD Gasifier Turbine.

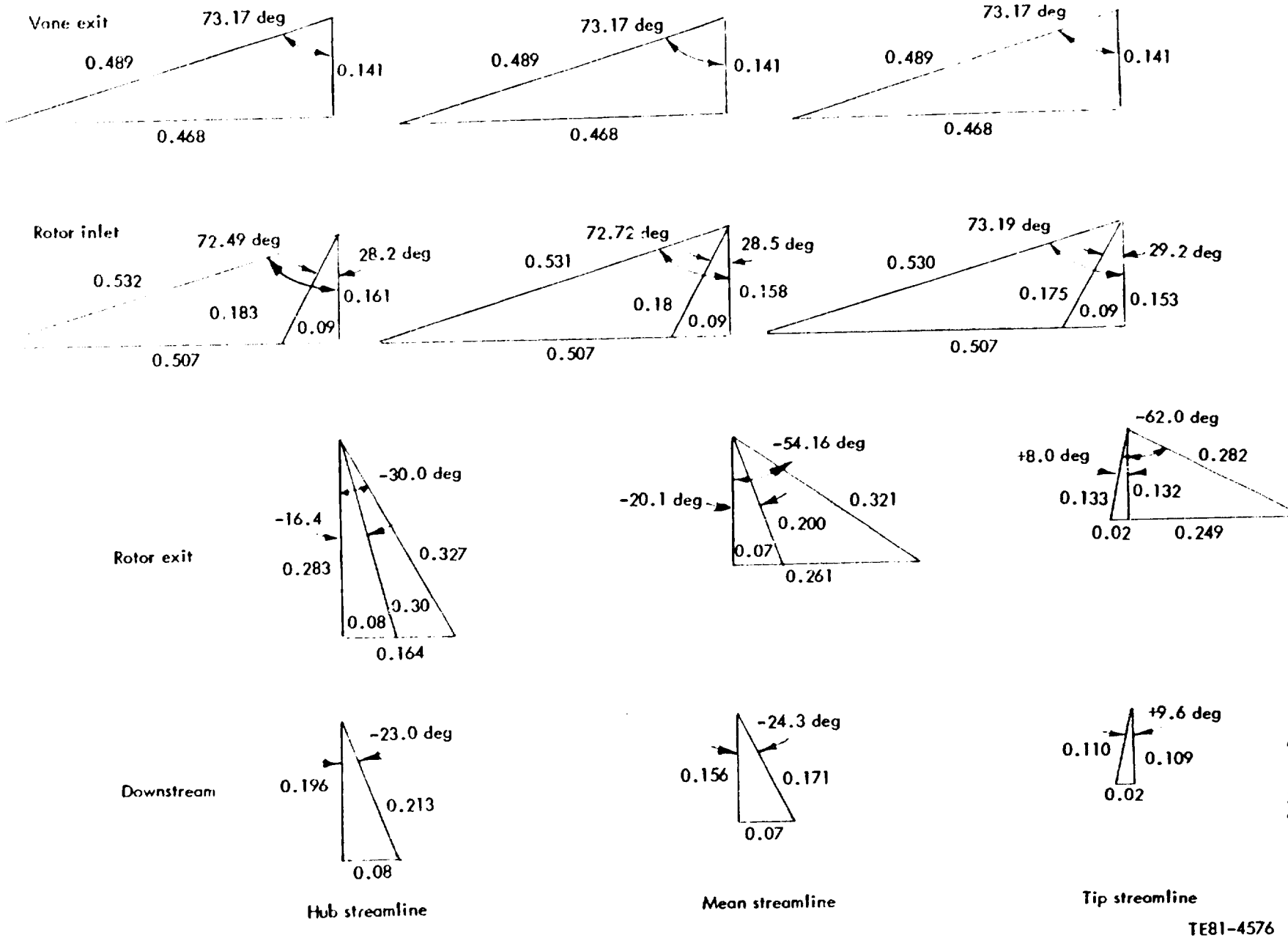

Figure 51. - Mach Number Diagrams--48 km/h (30 mph)--RPD Gasifier Turbine.

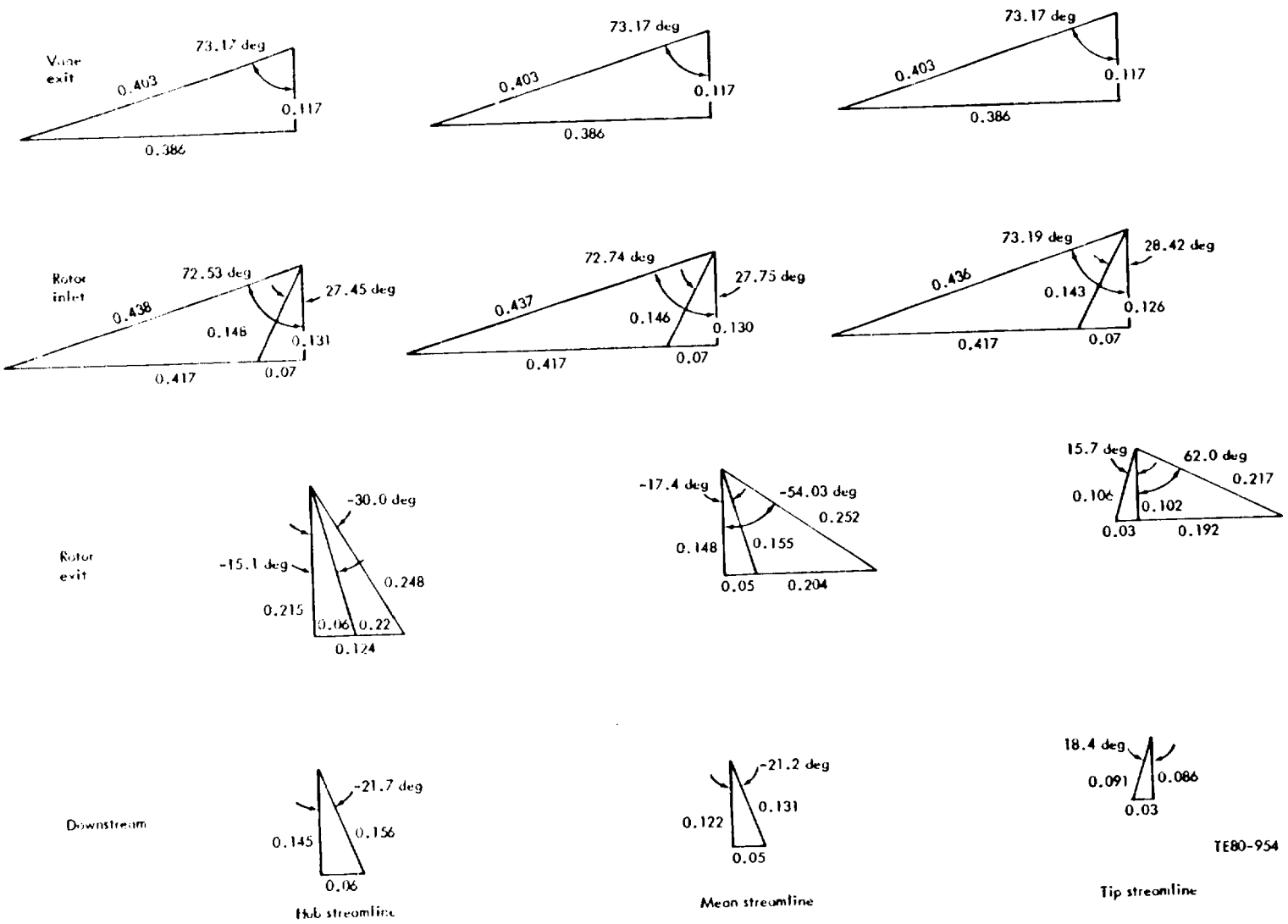

Figure 52. - Mach Number Diagrams--80 km/h (50 mph)--RPD Gasifier Turbine.

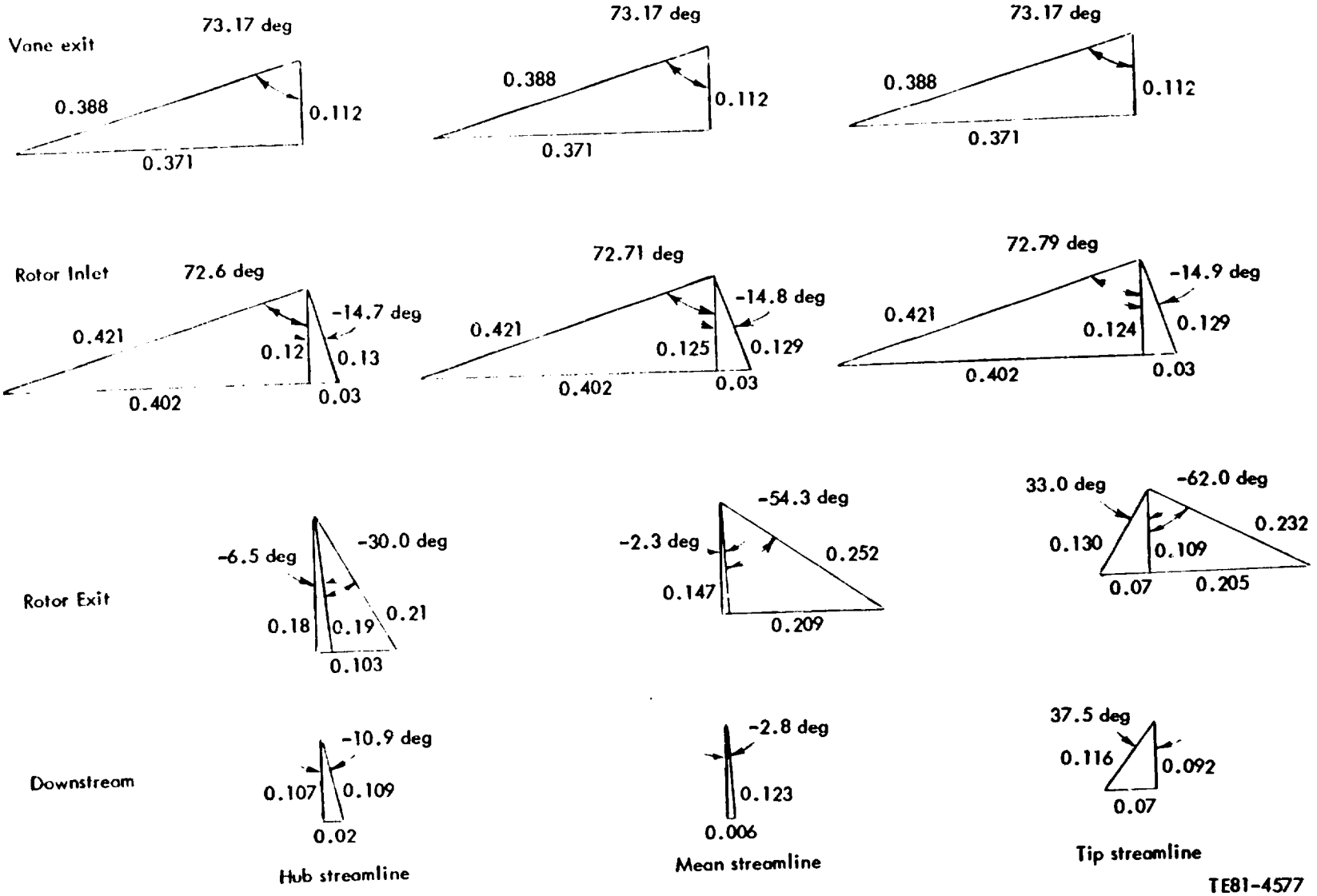

Figure 53. - Mach Number Diagrams--Idle--RPD Gasifier Turbine.

Scroll cross-sectional shapes at various angular locations are shown in Figure 54. The constraint on maximum diameter results in the scroll being approximately rectangular in cross section for the first 180 deg. Over this 180-deg arc, the scroll width has been circumferentially reduced on the shroud side. The mean flow radius of the scroll was designed to progress radially inward using an Archimedean spiral. At the location where the scroll closes (the tongue), the outer scroll surface is blended into the nearest vane. This eliminates flow crossover at the 360-deg location.

Inlet to the scroll from the combustor is illustrated in Figure 55. This inlet provides a transition from the circular cross section at the combustor exit to the scroll cross-sectional shape at the 0-deg scroll station.

The through-flow Mach numbers and scroll exit flow angles are shown in Table XII for various engine road-load operating conditions. The relatively small variation in exit flow angle is desirable to minimize vane incidence losses.

TABLE XII. SCROLL THROUGH-FLOW MACH NUMBERS AND EXIT ANGLE--RPD GASIFIER TURBINE

Operating condition	Through-flow Mach number	Exit angle from radial
Max power	0.070	48
80 km/h (50 mph)	0.079	54
48 km/h (30 mph)	0.058	50
32 km/h (20 mph)	0.056	50
Idle	0.057	49

Vane Design

The RPD vane is illustrated in Figure 56. Designed for low cost and ceramic construction, the vane exhibits a trailing edge diameter of 0.762 mm (0.030 in.), a leading edge diameter of 5.08 mm (0.20 in.), and a true chord of 26.772 mm (1.054 in.). The vane number of 18 results in a solidity of 1.265 based on true chord, a throat width of 6.3 mm (0.2480 in.), and a trailing edge blockage of 10.8%. Should future effort on ceramic vane development provide a trailing edge diameter of 0.508 mm (0.020 in.), the trailing edge blockage would be reduced to a more favorable value of 7.2%.

The vane design is symmetrical to offer cost reduction in mass production assembly through not requiring the vanes to be assembled into the wall slots with a particular orientation. The symmetrical design exhibited essentially the same aerodynamic characteristics as the cambered version.

Endwall contouring has been incorporated to improve aerodynamic loading of the vane. Suction and pressure surface velocity distributions for the SLS max power design point are illustrated in Figure 57. Suction surface diffusion has been effectively avoided through the use of endwall contouring. Boundary layer displacement thickness and incompressible form factor for each surface are illustrated in Figures 58 and 59, respectively.

DESIGN FEATURES

- LOW VELOCITY
- UNIFORM EXIT ANGLE
- UNIFORM EXIT VELOCITY
- ARCHIMEDEAN SWIRL

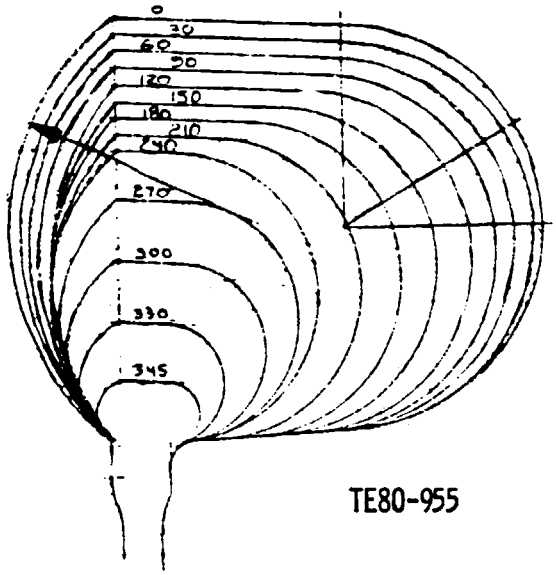

Figure 54. - Gasifier Scroll Cross-Sectional Shape.

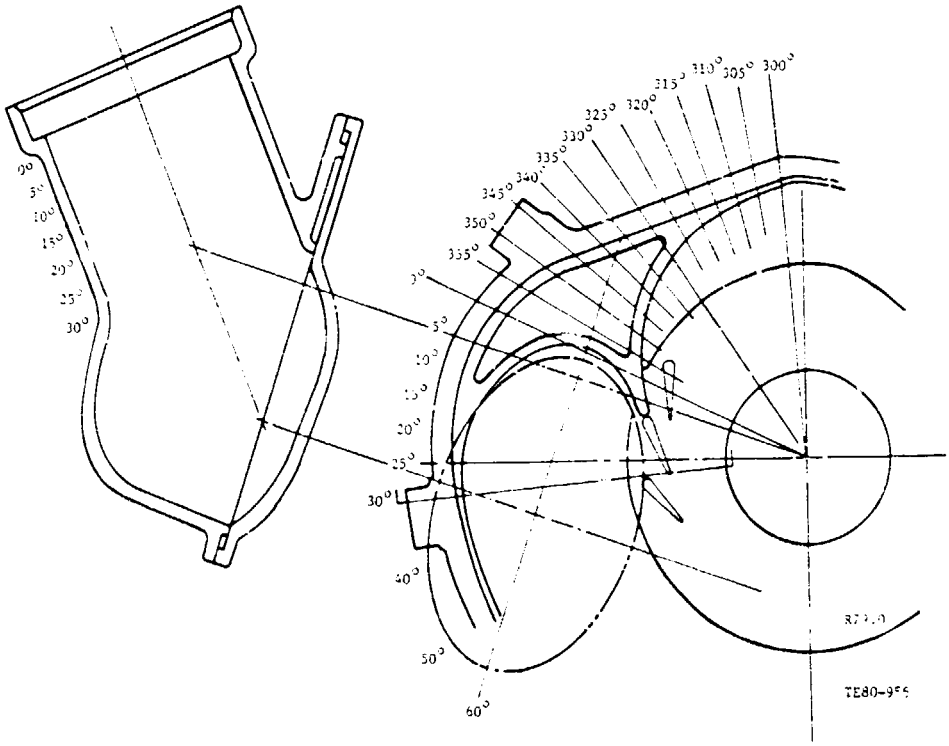

Figure 55. - Gasifier Scroll Inlet Transition.

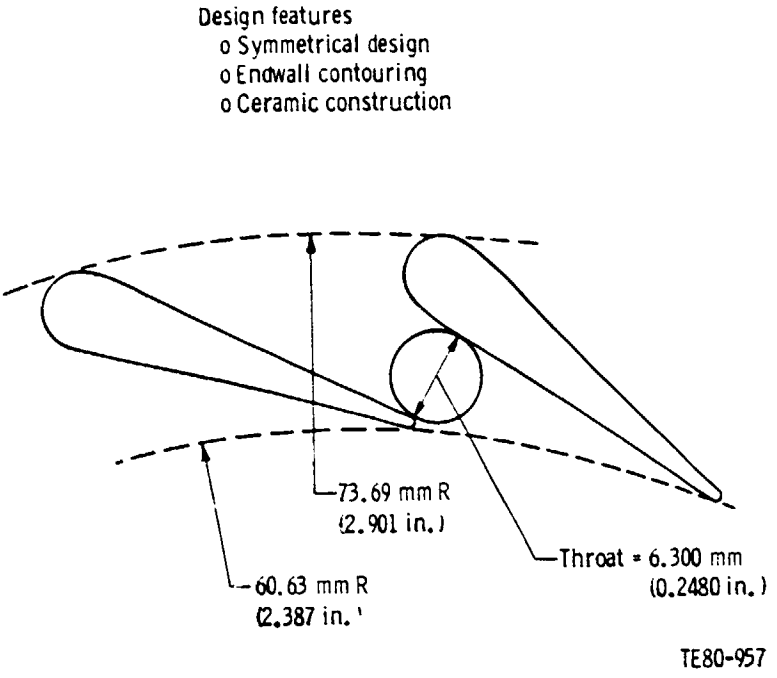

Figure 56. - RPD Gasifier Vane Design.

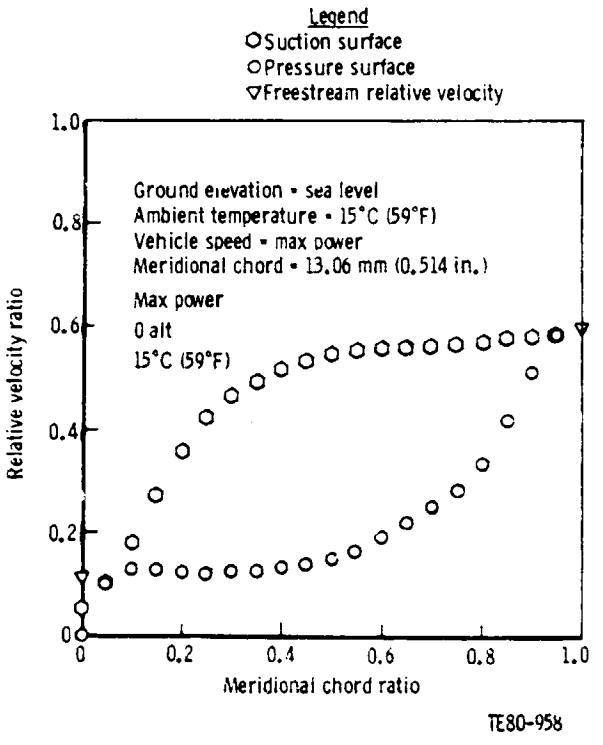

Figure 57. - RPD Vane Velocity Distribution.

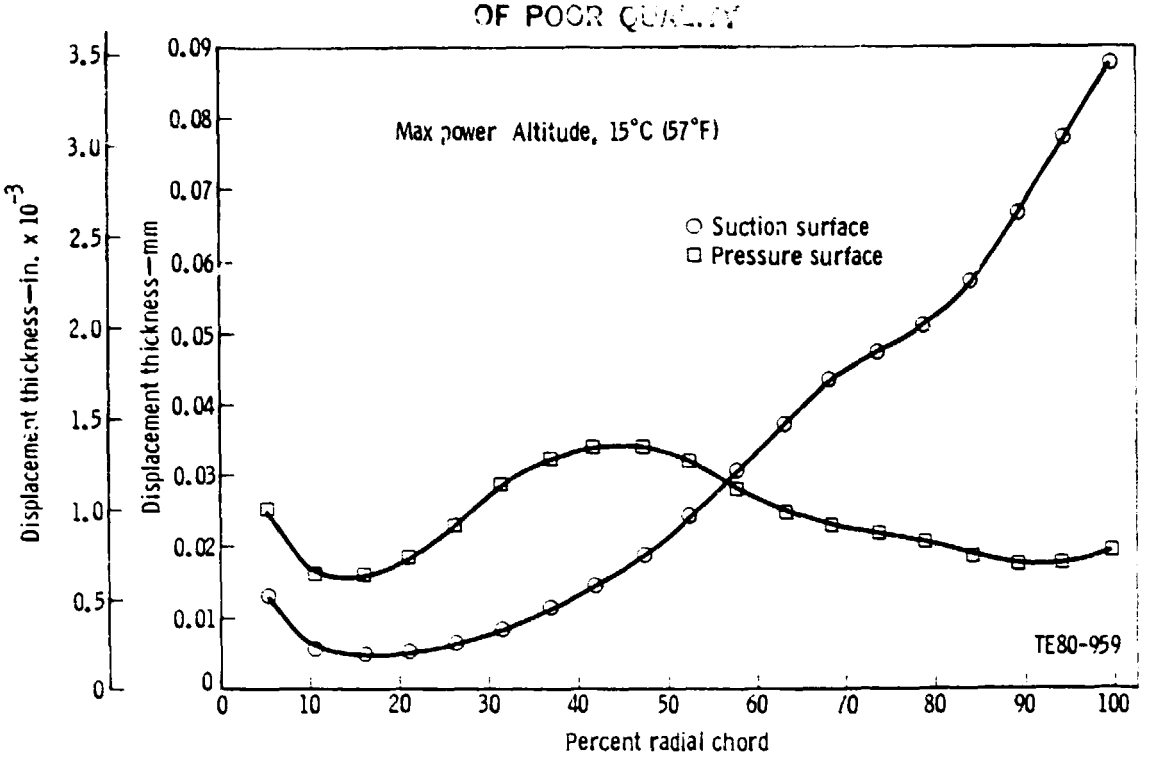

Figure 58. - Boundary Layer Displacement Thickness--RPD Gasifier Vane.

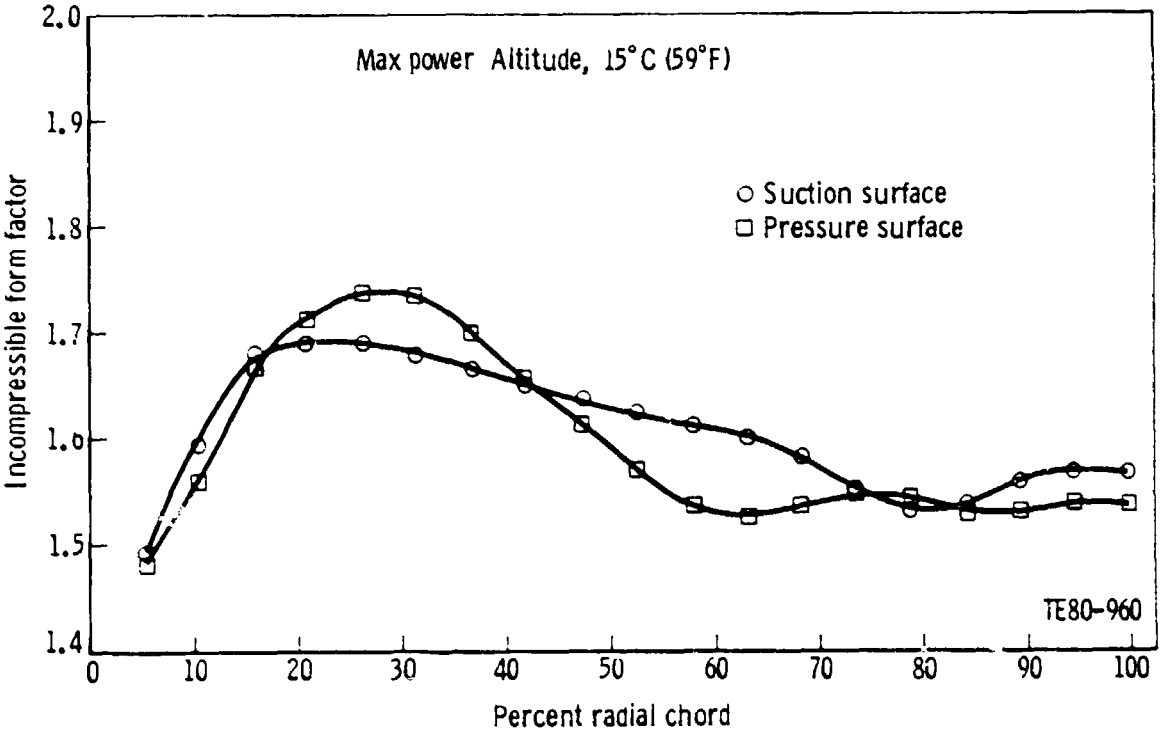

Figure 59. - Boundary Layer Form Factor--RPD Gasifier Vane.

Rotor Design

The rotor has been designed with emphasis on low cost through use of radial blading, low inertia through use of fully scalloped backplate and deeply cut hub, low exit Mach number to minimize transition duct loss and relatively high maximum power reaction to achieve a broad efficiency band. Consistent with ceramic construction, the minimum blade thickness is 0.762 mm (0.030 in.). The blade thickness distribution is that of an optimum "dog leg." At each axial location, the blade thickness is constant from the tip inward to a specified radius and then follows a logarithmic profile toward the hub. The hub contour was selected to provide balance between blade and hub stress levels.

The blade shape is illustrated by radial section cuts in Figure 60. The rotor throat, trailing edge diameter, and blade angle are presented in Figures 61 through 63.

Blade-to-blade velocity distributions for hub, mean, and shroud under SLS maximum power operation are illustrated in Figures 64 through 66. Velocity distributions for 92.6 km/h (50 mph) are illustrated in Figures 67 through 69. Idle velocity distribution are shown in Figures 70 through 72.

Rotor exit swirl and Mach number, as calculated from the meridional flow analysis program, are illustrated in Figure 73. The radial variation in turbine total-to-total efficiency is presented in Figure 74.

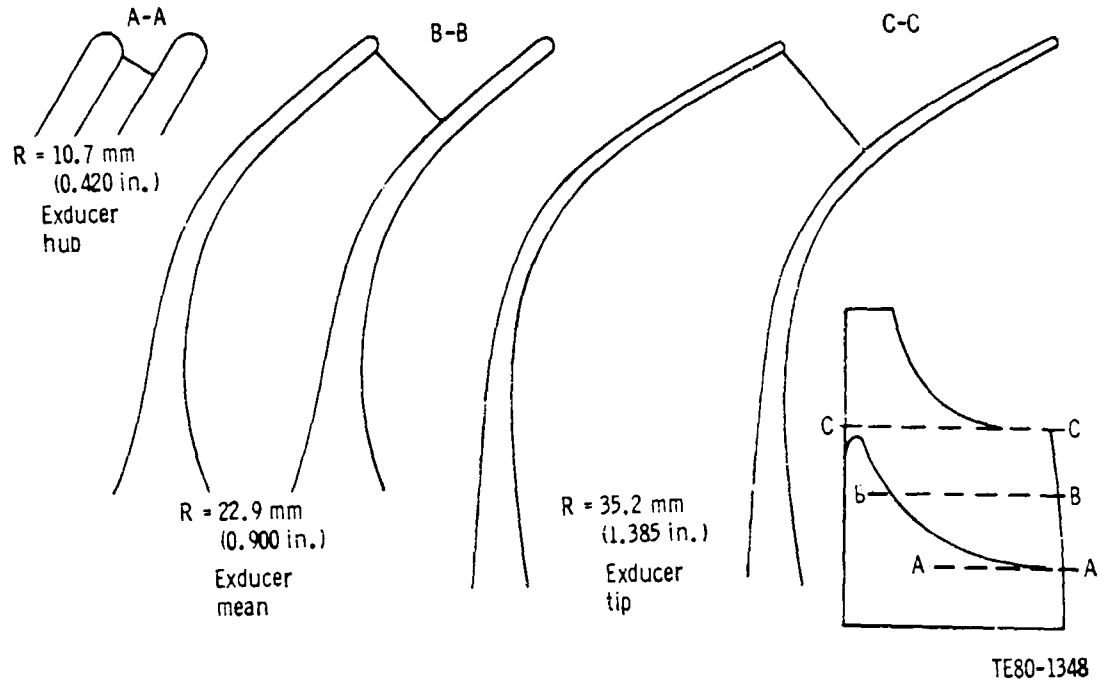

Figure 60. - RPD Gasifier Turbine Rotor Airfoil Sections.

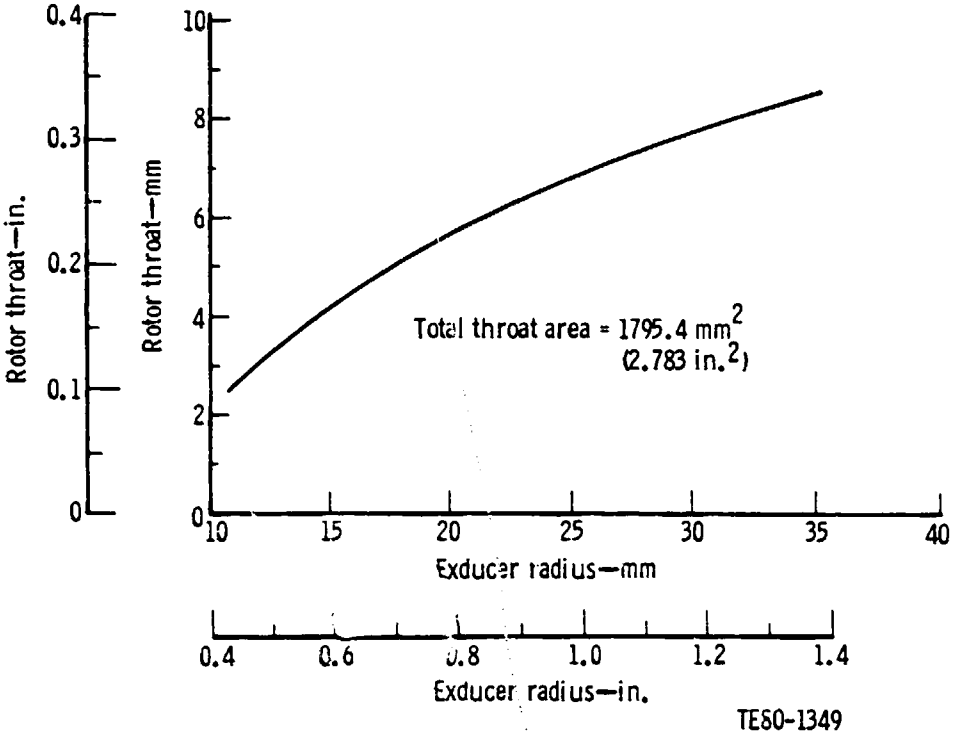

Figure 61. - RPD Gasifier Turbine Rotor Throat.

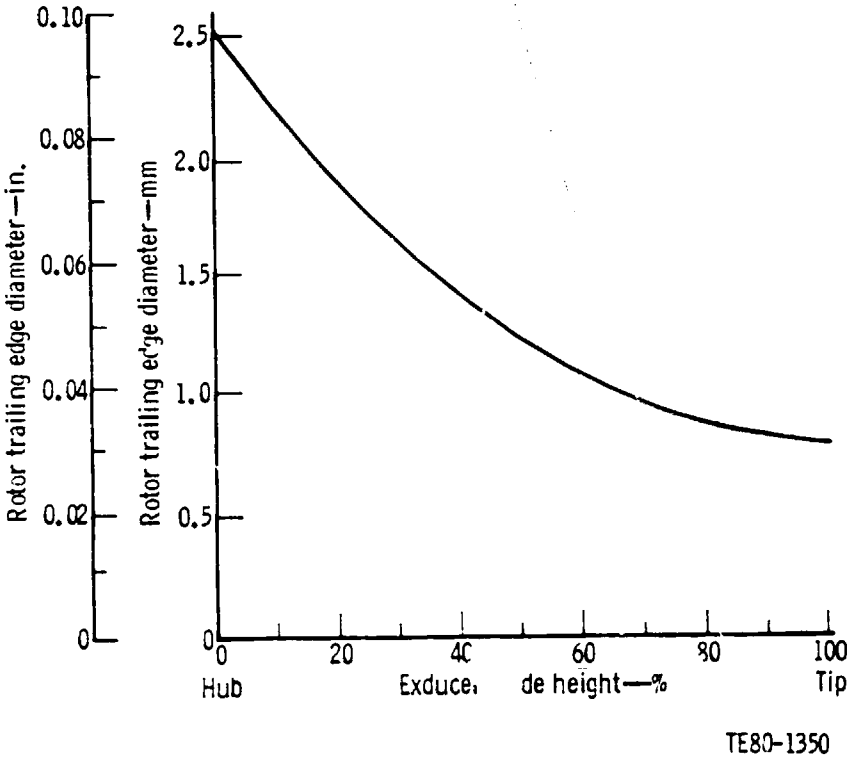

Figure 62. - RPD Gasifier Turbine Rotor Trailing Edge Diameter.

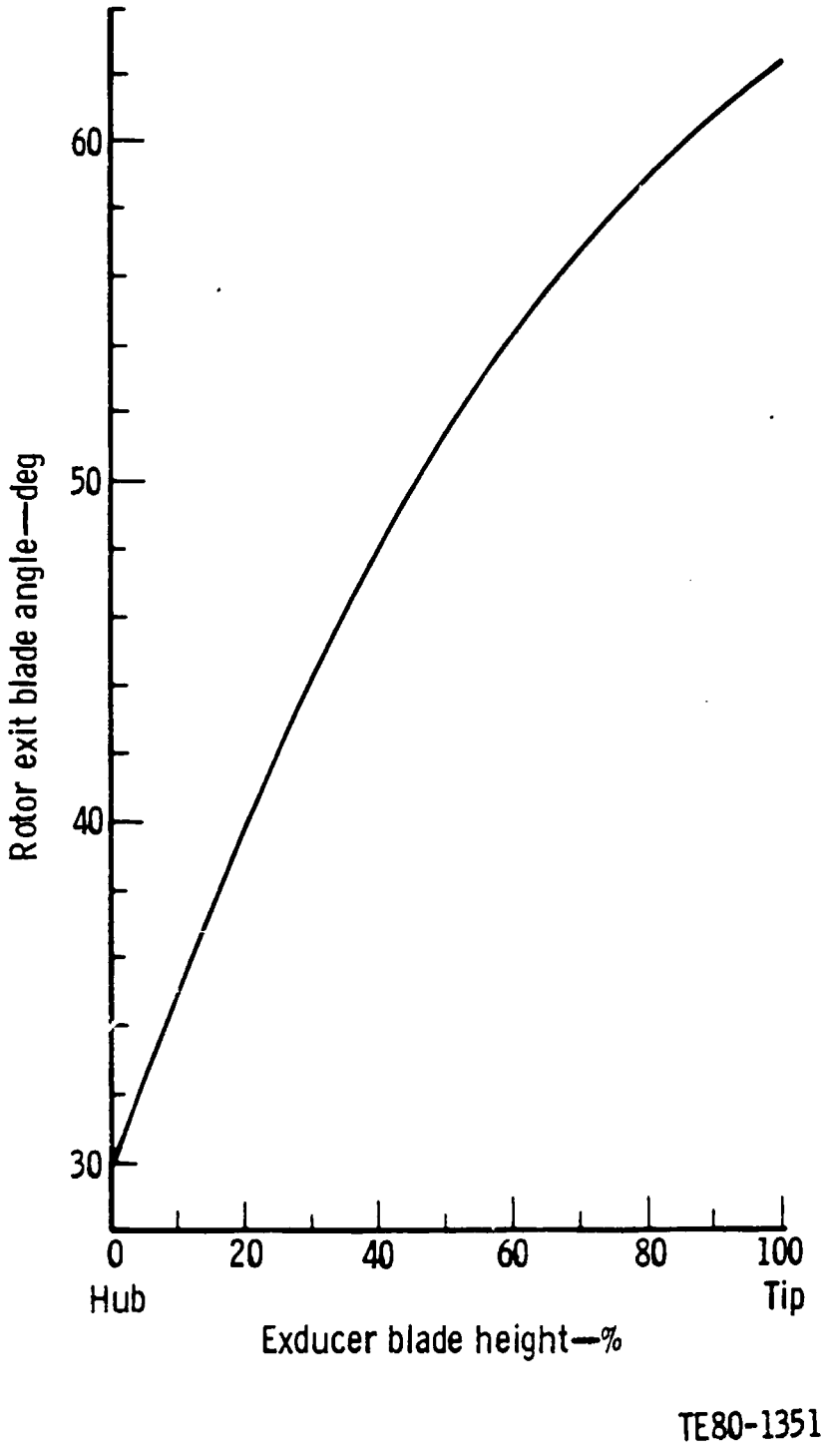

Figure 63. - RPD Gasifier Turbine Rotor Exit Blade Angle.

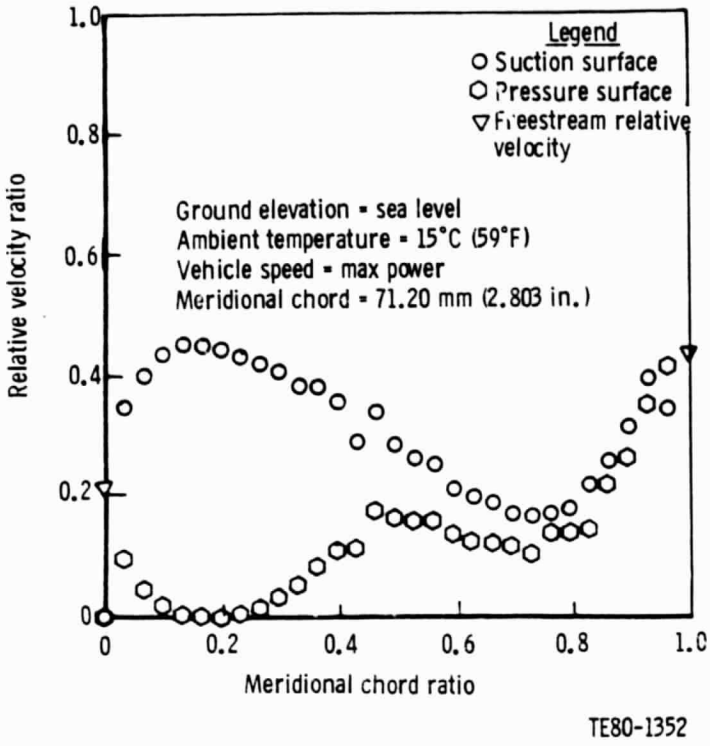

Figure 64. - RPD Gasifier Rotor Hub Velocity Distribution--Maximum Power.

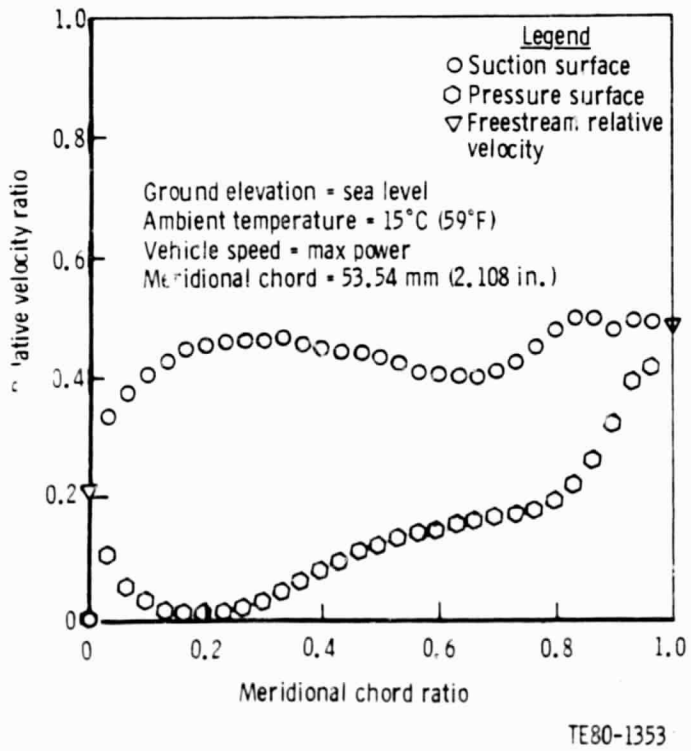

Figure 65. - RPD Gasifier Rotor Mean Velocity Distribution--Maximum Power.

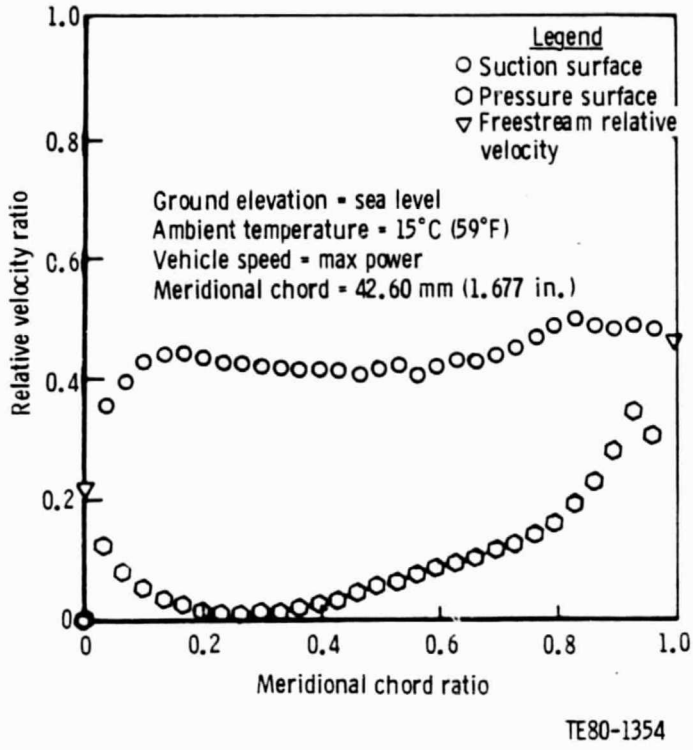

Figure 66. - RPD Gasifier Rotor Tip Velocity Distribution--Maximum Power.

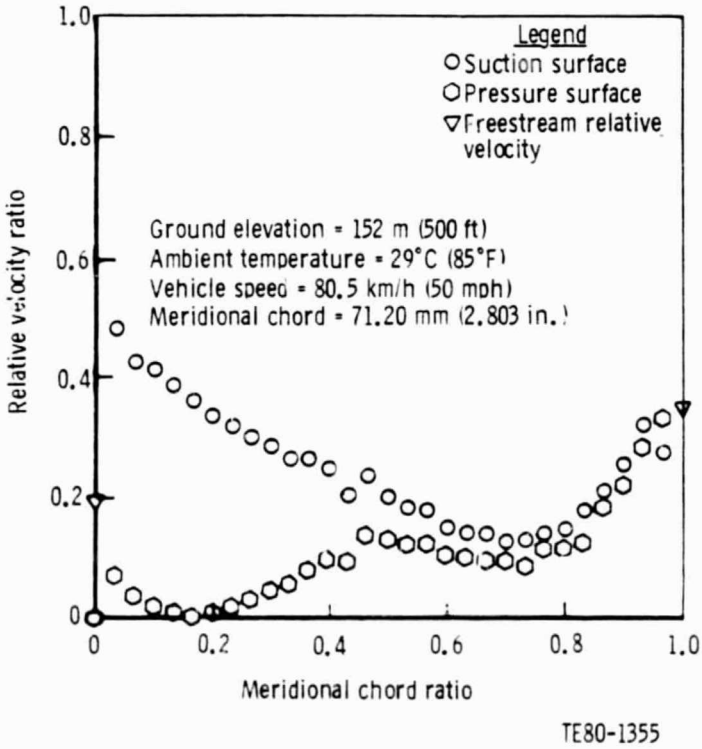

Figure 67. - RPD Gasifier Rotor Hub Velocity Distribution--80 km/h (50 mph).

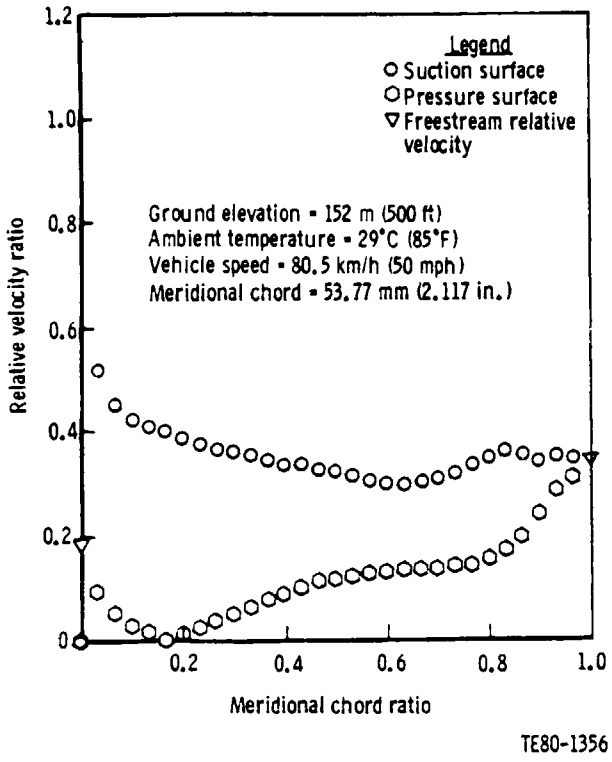

Figure 68. - RPD Gasifier Rotor Mean Velocity Distribution--80 km/h (50 mph).

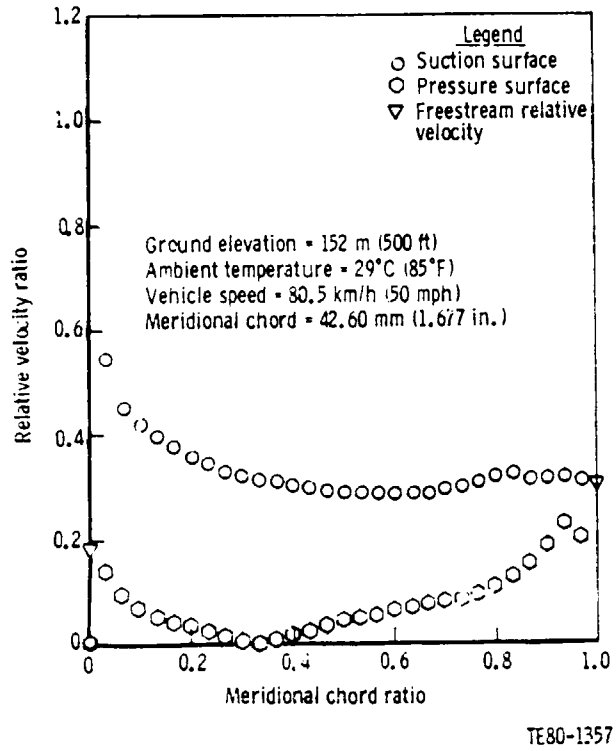

Figure 69. - RPD Gasifier Rotor Tip Velocity Distribution--80 km/h (50 mph).

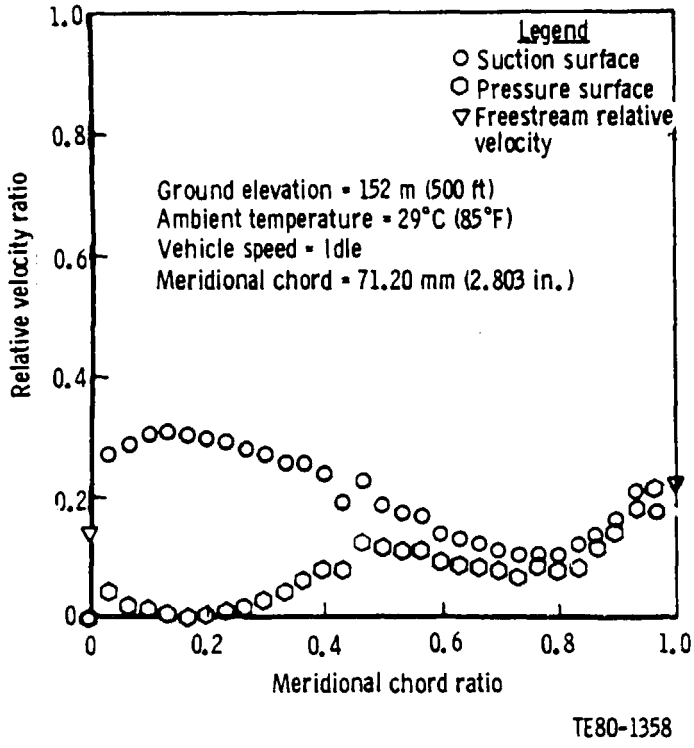

Figure 70. - RPD Gasifier Rotor Hub Velocity Distribution--Idle.

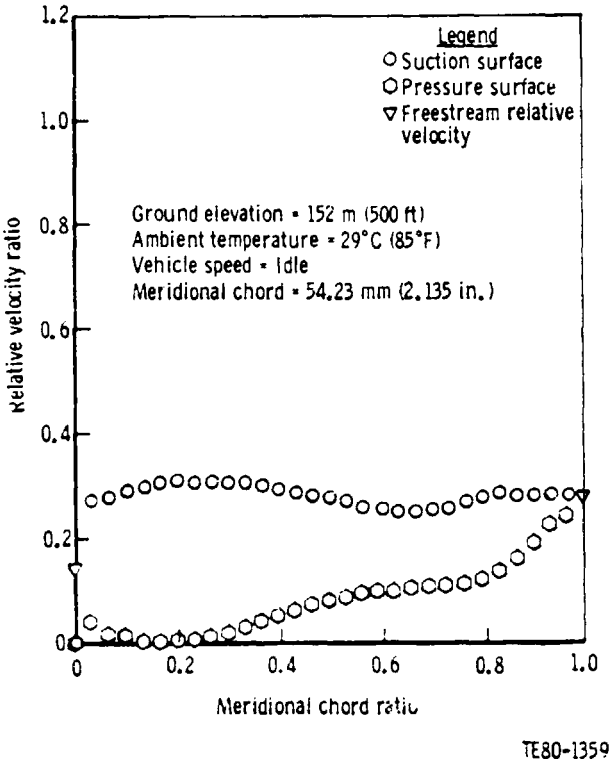

Figure 71. - RPD Gasifier Rotor Mean Velocity Distribution--Idle.

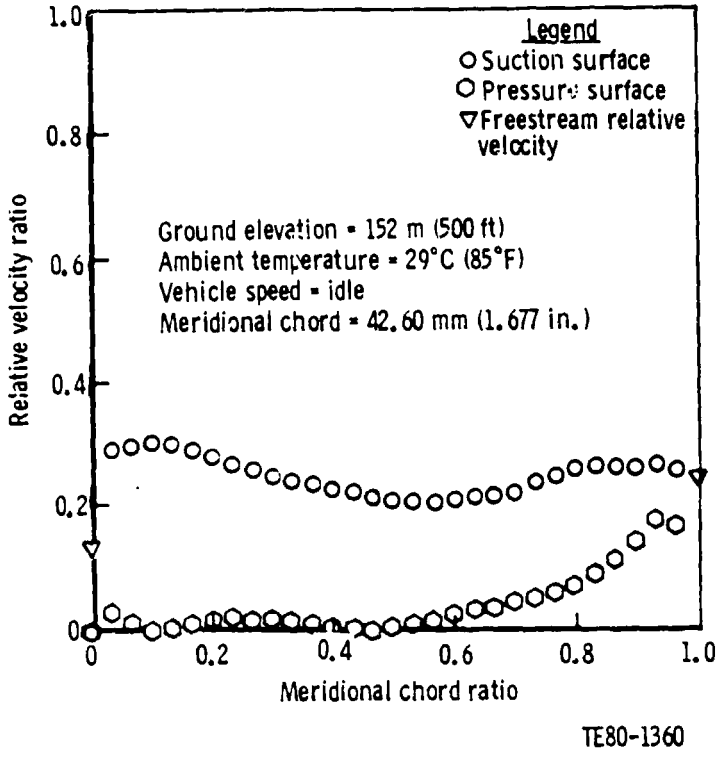

Figure 72. - RPD Gasifier Rotor Tip Velocity Distribution--Idle.

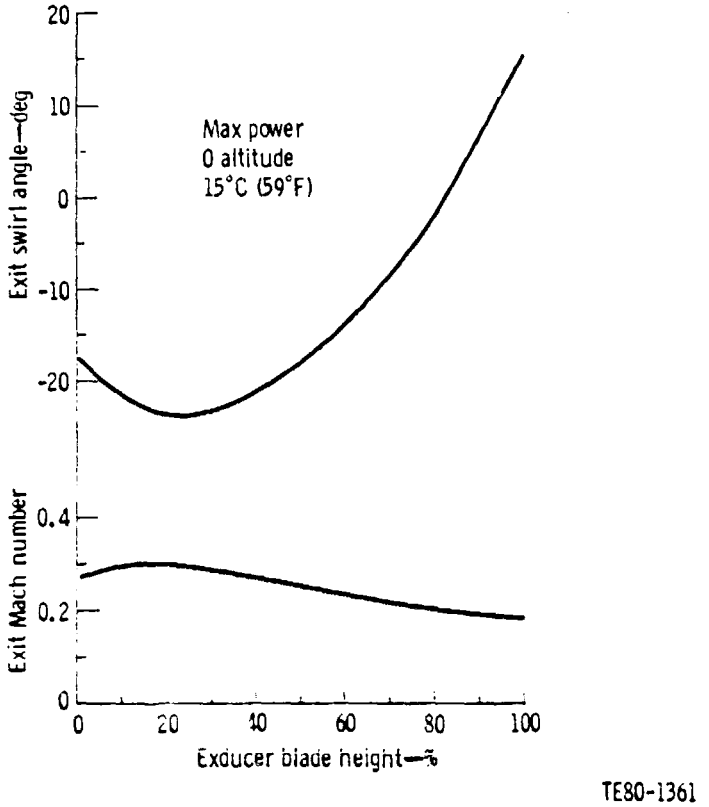

Figure 73. - Predicted Radial Distribution of Exit Swirl and Mach Number--RPD Gasifier Turbine.

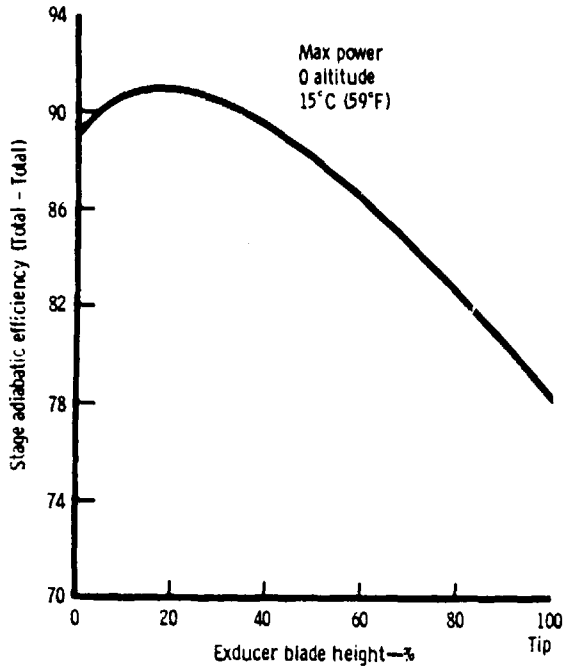

Figure 74. - Predicted Radial Distribution of Stage Efficiency--RPD Gasifier Turbine.

Interturbine Duct

The interturbine duct is the connecting flow path between the discharge of the gasifier turbine and the inlet to the power turbine scroll. The offset of the two shafts, the axial positioning of the turbine, the center discharge of the gasifier turbine, and the circumferential feed of the power turbine produced a unique three-dimensional design problem. Further complicating this design was the need to diffuse the flow, from Mach 0.25 at the gasifier turbine exit plane to Mach 0.1 at the entrance plane of the scroll (at maximum power), in order to minimize scroll losses.

Several approaches were considered in designing the interturbine ducting. These approaches are summarized in Figure 75 and include:

- o Diffusing and discharging axially into the power turbine scroll--This required either rotating the gasifier 90 deg or adding additional gearing to maintain the orientation of the power shaft.
- o Diffusing axially and dumping into a plenum having a 90-deg off-take into the power turbine scroll.
- o Using the available space to turn the flow through a diffusing 90-deg elbow with discharge into the power turbine scroll--Both the first and second approaches were eliminated because of the nonfeasibility of rotating the gasifier shaft and the inadequacy of length for diffusion prior to dumping the flow. The third approach was chosen as the most feasible for use in the AGT-100 engine.

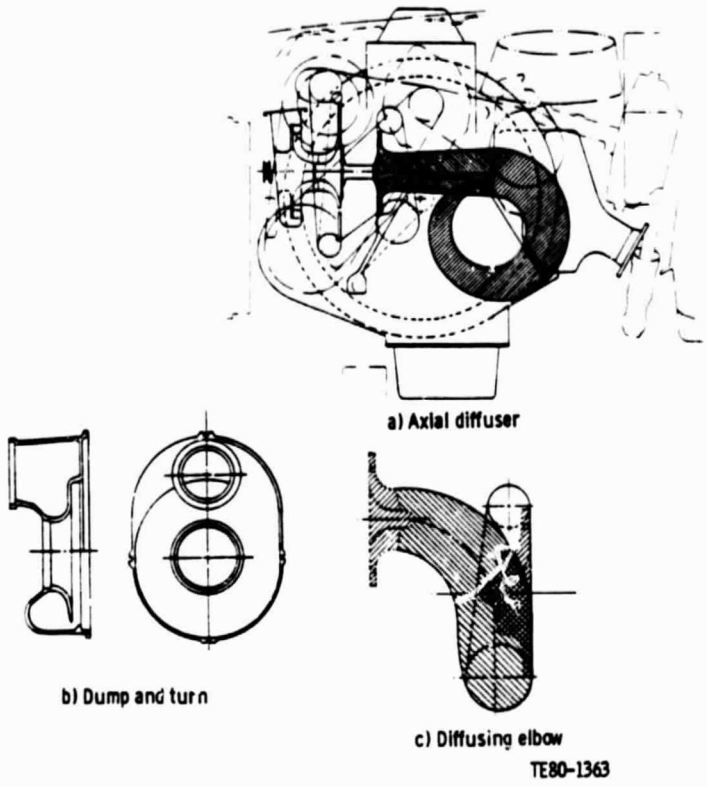

Figure 75. - Approaches to Interturbine Ducting.

Axial and radial positioning of the gasifier and power turbine within the engine was constrained primarily by available space and required location for the output shaft. This position defined the envelope of the interturbine duct. Based on work by Miller at BHRA (Reference 3), a 90-deg diffusing bend with L/D (meanline length divided by diameter), similar to the ducting that will fit in the engine envelope, would have a maximum area ratio of 1.5 for minimum loss and exit distortion. Therefore, an area ratio of 1.5 was selected, and a layout of the interturbine duct was made.

The discharge of the interturbine duct is the inlet to the power turbine scroll. This requires a transition in cross section from circular at gasifier exit to approximately rectangular at scroll inlet. Figure 76 shows the interturbine duct and presents the dimensions for defining the cross section of the transition. Inlet and discharge Mach number from the duct are summarized for various engine operating conditions in Table XIII. Projected losses for the interturbine duct based on the work by Miller are also presented in Table XIII.

TABLE XIII. INTERTURBINE DUCT PERFORMANCE--RPD ENGINE

Operating condition	Gasifier turbine exit		Interturbine duct	
	M_{NABS}	Swirl angle	Exit M_{NABS}	$\Delta P/P$, %
Idle	0.119	+10.0	0.079	0.25
32 km/h (20 mph)	0.112	+ 1.2	0.075	0.20
48 km/h (30 mph)	0.119	- 7.8	0.079	0.25
80 km/h (50 mph)	0.154	-11.6	0.102	0.50
102 km/h (70 mph)	0.178	- 8.1	0.118	0.80
Maximum power	0.219	- 2.4	0.144	1.10

Mod I Gasifier Turbine Design

Commonality with the RPD gasifier turbine is an important design factor for the Mod I turbine. Because of differing cycle conditions between the Mod I and RPD engines, an exact duplication of flow path is not possible. Consideration was, therefore, directed to a Mod I design that would provide interchangeability of metallic and ceramic hardware with the minimum aerodynamic penalty.

The Mod I engine cycle requirements for the gasifier turbine at the maximum power, sea level static, condition are:

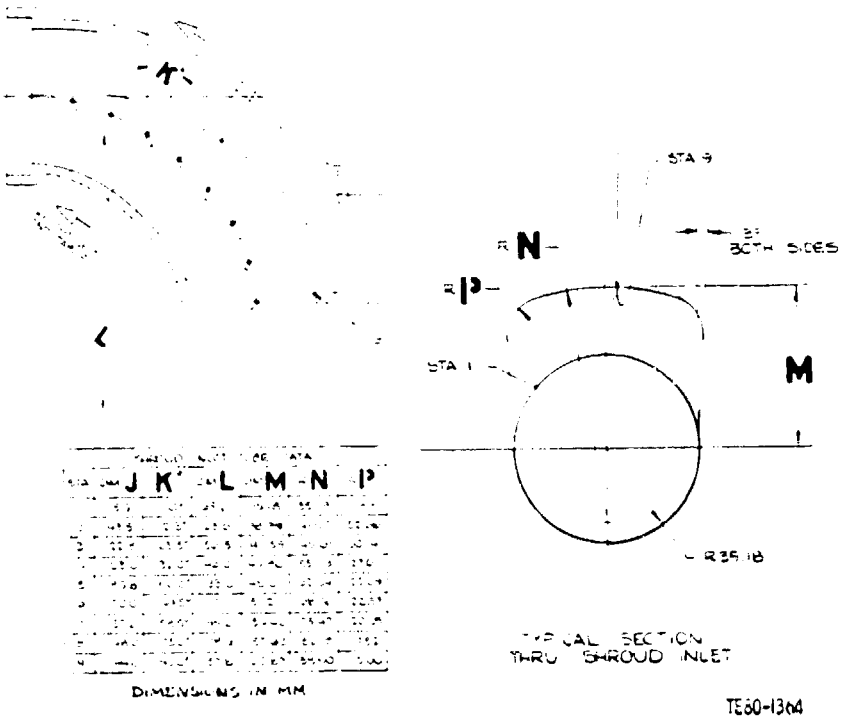

Figure 76. - Interturbine Duct Configuration.

Inlet temperature, °C (°F)	1080 (1976)
Inlet pressure, kPa (psia)	438.6 (63.62)
Fuel/air ratio	0.0110
Equivalent flow, $W\sqrt{\theta}_{cr}/\delta$ - kg/s (lbm/sec)	0.162 (0.357)
Equivalent work, $\Delta h/\theta_{cr}$ - kJ/kg (Btu/lbm)	51.73 (22.24)
Equivalent speed, $N/\sqrt{\theta}_{cr}$, rpm	40348
Expansion ratio (Total - Total)	2.2583
Efficiency with inlet scroll (Total - Total)	82.60

Flow-Path Selection

The preliminary flow path for the Mod I engine is illustrated in Figure 77. With the exception of vane height change and rotor shroud trim, the Mod I and RPD flow paths are identical. Operating at the SLS maximum power condition, the turbine exhibits a tip speed of 508 m/s (1667 ft/sec), an aerodynamic loading parameter (U/C - Tip Speed/Isentropic Spouting Velocity) of 0.666 and a specific speed of 69.2. Turbine parameters for several engine operating points under road-load conditions are presented in Table XIV. The Mod I gasifier turbine is required to produce approximately 5% more power under maximum power (SLS) conditions than the RPD. The Mod I equivalent flow is approximately 8.7% less than the RPD. Because of the higher Mod I work requirements, both the U/C and specific speed (N_s) are lower than the RPD turbine. As illustrated in Table XIV, the exit swirl values are favorable over the entire operating range.

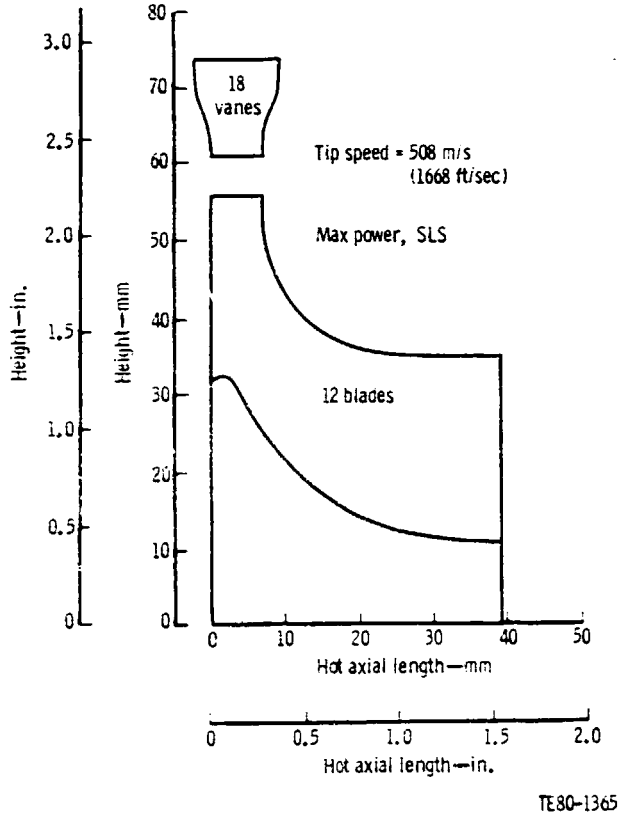

Figure 77. - Mod I Gasifier Turbine Flow Path--Preliminary.

TABLE XIV. MOD I GASIFIER TURBINE PARAMETERS FOR VARIOUS ENGINE OPERATING POINTS (PRELIMINARY)

Speed km/h (mph)	Idle	32 (20)	48 (30)	80 (50)	102 (70)	Max* power	Max** power (SLS)
Turbine power, kW (hp)	10.07 (13.51)	11.49 (15.41)	13.19 (17.68)	26.20 (35.13)	46.86 (62.84)	67.52 (90.55)	75.03 (100.6)
Inlet temperature, °C (°F)	797 (1466)	1034 (1894)	1080 (1976)	1080 (1976)	1080 (1976)	1080 (1976)	1080 (1976)
Equivalent flow, kg/s (lbm/sec)	0.135 (0.299)	0.141 (0.310)	0.145 (0.319)	0.158 (0.348)	0.162 (0.357)	0.160 (0.354)	0.162 (0.357)
Equivalent work, kJ/kg (Btu/lbm)	25.26 (10.86)	24.84 (10.68)	25.72 (11.06)	36.10 (15.52)	45.78 (19.68)	50.61 (21.76)	51.73 (22.24)
Equivalent speed, %	67.3	61.0	60.0	72.2	87.4	100.0	100.0
Expansion ratio (T-T)	1.455	1.459	1.490	1.763	2.045	2.211	2.258
U/C	0.647	0.584	0.559	0.570	0.618	0.674	0.666
Mean reaction	0.426	0.370	0.350	0.362	0.410	0.467	0.461
N_s	61.1	56.2	54.4	57.3	63.5	69.6	69.2
N_{RE}	39,400	32,300	33,800	48,000	67,900	88,700	96,400
$alpha_{swirl}$	+11.8	-0.05	-4.9	-8.1	-5.5	+0.3	-1.7
MV_{exit}	0.132	0.135	0.143	0.184	0.217	0.230	0.230

*Ambient temperature: 26°C (85°F), altitude: 152 m (500 ft).
**Ambient temperature: 15°C (59°F), altitude: sea level.

Aerodynamic Performance

The efficiency goal for the Mod I gasifier turbine including inlet scroll is illustrated in Figure 78. Efficiency levels are on the order of 1-2 percentage points lower than the RPD gasifier turbine. Work is continuing toward finalizing the Mod I gasifier design. Velocity diagrams and blade-to-blade velocity distributions for selected operating points will be generated during the next period.

Scroll Design

The flow path for the Mod I gasifier scroll is the same as that for the RPD engine. Mechanically, the main difference is that the Mod I scroll is fabricated from metal, whereas the RPD scroll is ceramic. The ceramic scroll is assembled with a circumferential flange at the maximum diameter of the scroll. A rope seal is employed at this flange to minimize flow leakage. In the Mod I engine, this joint will be welded to eliminate leakage.

Vane Design

The vane design for the Mod I gasifier turbine is identical to the RPD engine. In order to satisfy Mod I cycle requirements, the vane height must be reduced by 15.8%. Consideration was given to a vane angle reset to accommodate the Mod I engine requirements; however, this idea was discarded because of efficiency penalties associated with reduced reaction levels and increased vane trailing edge blockage.

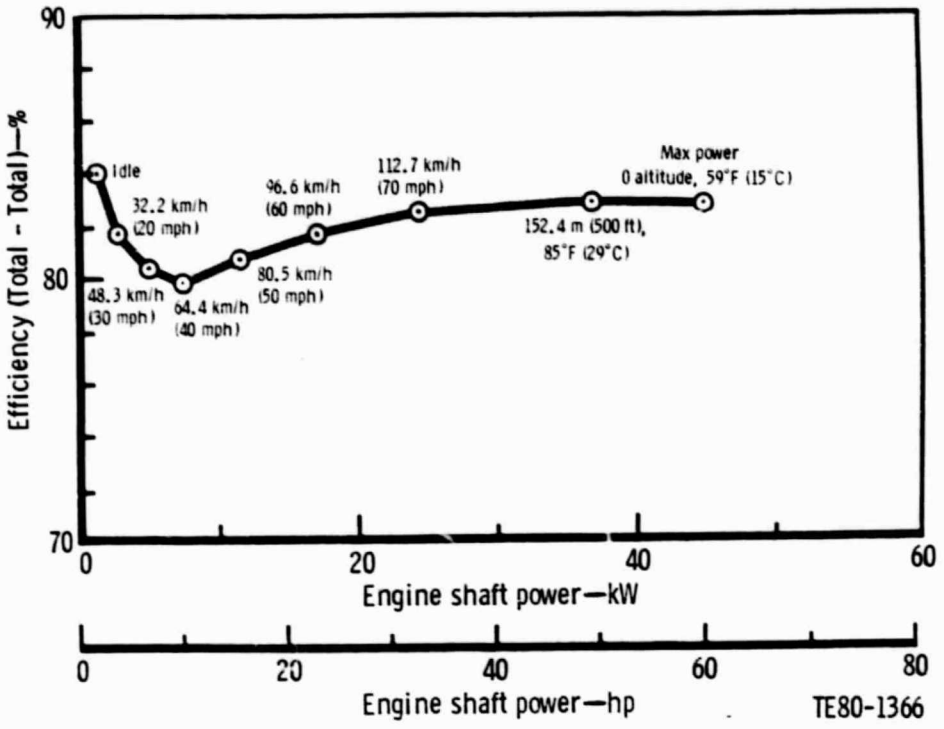

Figure 78. - Efficiency Goal--Mod I Gasifier Turbine with Inlet Scroll.

Rotor Design

Preliminary structural design studies conducted on the Mod I gasifier turbine rotor revealed that a partial backplate would be required to provide an inducer vibratory mode above fourth engine order. The preliminary studies also revealed that the stress rupture life in the inducer portion was unacceptable. These preliminary structural analyses used the same thickness distribution as employed for the RPD gasifier. In order to improve the inducer stress rupture life, a new thickness distribution was generated for the Mod I turbine. This new thickness incorporated a logarithmic taper, which began at the tip of the wheel. Thus, the constant thickness portion of the inducer, which was used for the RPD turbine, was eliminated. Not only did this new thickness distribution provide improved stress rupture life, it also provided sufficient increase in inducer stiffness to avoid the requirement for a partial backplate.

Approximate blade-to-blade velocity distributions based on the quasiorthogonal meridional flow analysis are presented in Figures 79 through 81. These preliminary Mod I distributions were generated for the SLS maximum power design point.

During the next period, the Mod I rotor design will be finalized, and master charts for engine hardware will be finalized and generated. Experimental data from the turbine development program will be incorporated into the final Mod I gasifier turbine design.

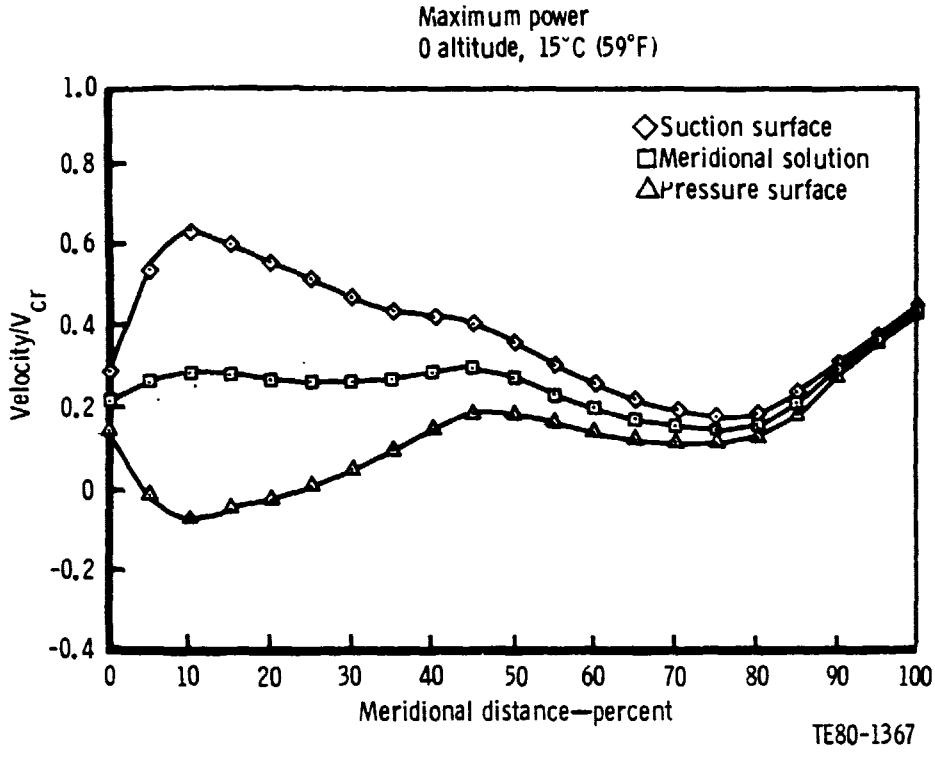

Figure 79. - Approximate Hub Velocity Distribution--Mod I Gasifier Turbine.

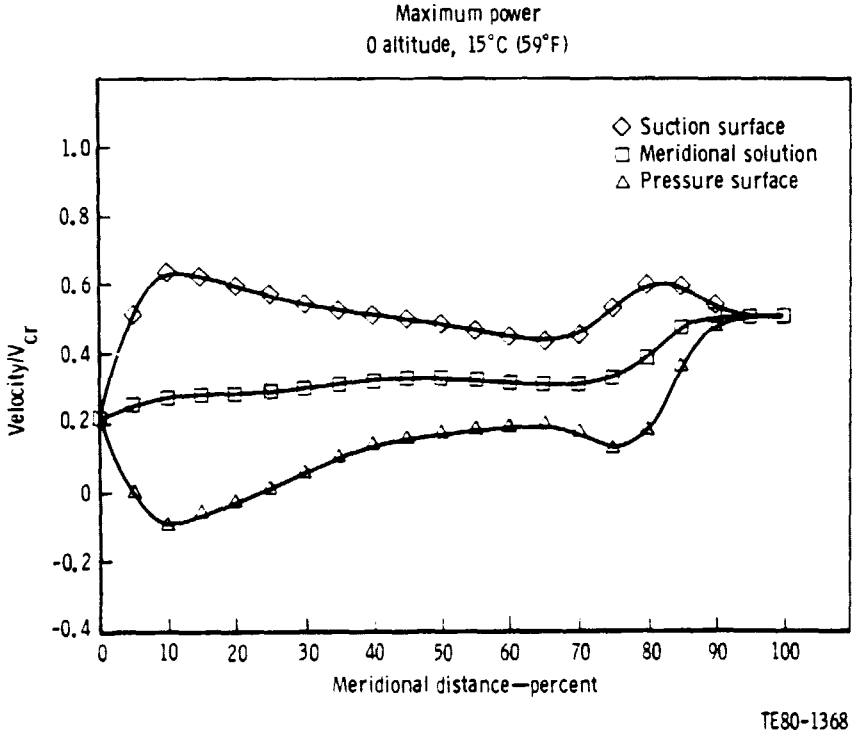

Figure 80. - Approximate Mean Velocity Distribution--Mod I Gasifier Turbine.

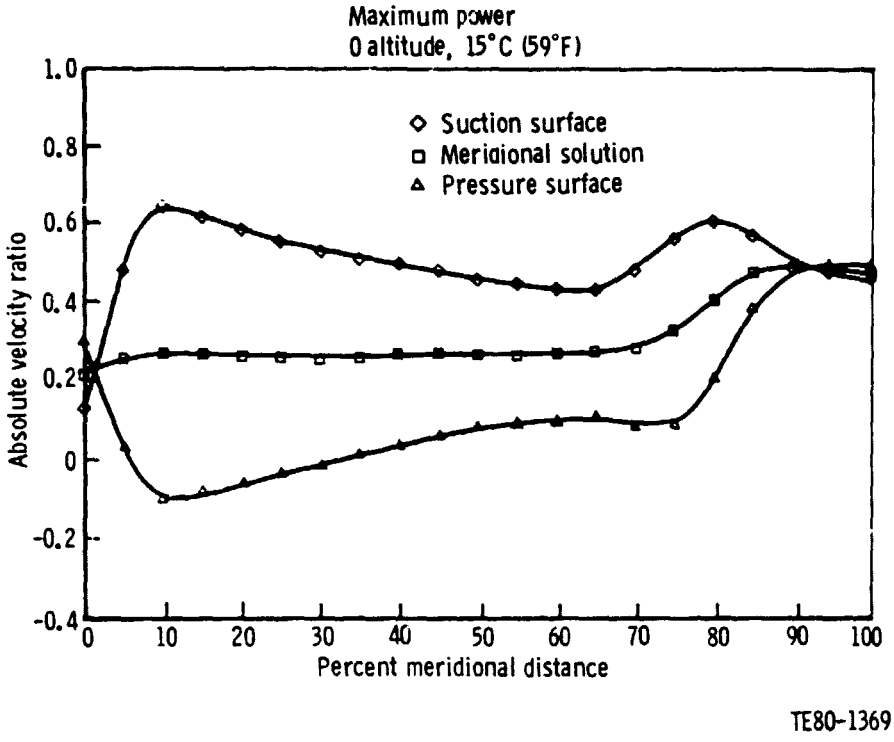

Figure 81. - Approximate Shroud Velocity Distribution--Mod I Gasifier Turbine.

Interturbine Duct

The interturbine duct for the Mod I design is essentially the same as the RPD design. The Mod I gasifier turbine exit diameter is the same as the RPD exit diameter, and, therefore, the interturbine duct inlet diameter is the same. The Mod I duct and the Mod I power turbine scroll will be fabricated from metal. The scroll through-flow area was increased by the difference in thickness of the metal walls relative to the ceramic walls due to Mod I power turbine requirements (see Section V). This results in an increase in area at interturbine duct exit of approximately 5%. The Mod I interturbine duct is being designed to accommodate this increased area ratio.

Interturbine Duct Cold Flow Testing

Overall engine length for the RPD configuration is strongly influenced by the length of the interturbine duct. This duct, a diffusing 90-deg elbow, must provide low loss flow transfer from gasifier turbine exit to the power turbine inlet scroll and must accept a range of inlet Mach numbers and swirl angles. To establish the feasibility of the diffusing bend design approach, a cold flow test rig was designed, fabricated, and tested.

The interturbine duct cold flow test rig consisted of 1) a radial inflow inlet section with variable turning vanes to provide desired swirl at duct inlet, 2) a 180-deg constant area discharge tube to simulate a constant velocity scroll at interturbine duct exit, and 3) a set of three interturbine duct models. The duct models and scroll simulator were made from epoxy with aluminum chip filler. A sketch of the test setup is shown in Figure 82, and a photo of the hardware is shown in Figure 83. The three test models covered the range of expected available length for the interturbine duct and were tested over a range of swirl from -60 to +60 deg and a range of inlet Mach number from 0.1 to 0.5. Purpose of this testing was to establish the sensitivity of duct loss to duct length and inlet conditions and to provide needed information to assist in the design of the ducting.

Each test model was circular in cross section, had an area ratio of 1.5, and turned the flow 90 deg. Duct centerline radii of curvature were 5.25, 5.75, and 6.50 in. (133, 146, and 165 mm), respectively. Prior to testing, an analytical estimate was made of the expected losses for the interturbine duct models. This estimate is shown crosshatched in Figure 84. Measured total pressure losses as a function of inlet absolute Mach number and swirl angle for the 146 mm (5.75 in.) radius of curvature duct is shown in Figure 84. At 0 and 20-deg swirl, losses for the elbow are notably less than the analytical estimate. At higher swirl (40 deg), however, the measured loss approaches the analytical estimate. The effect of length on loss is of second order but not insignificant. With the fixed geometry AGT-100 configuration, maximum expected swirl variation is from -10 to +10 deg.

Figures 85 and 86 are examples of the wall static pressure measurements for the 146 mm (5.75 in.) radius elbow. Figure 85 is for 0-deg swirl, and Figure 86 is for 40-deg inlet swirl. A comparison of these plots reveals a significant change in the static pressure recovery on the bend side radius and in the overall recovery to the end of the elbow. This decrease in recovery corresponds to the increase in loss seen in Figure 84.

Some difficulty was experienced in measuring elbow exit total pressure and swirl angle at high inlet swirl angles. This measurement difficulty resulted from a highly distorted flow field at the elbow exit. In order to evaluate the degree of flow distortion qualitatively, the cold flow rig was modified to include a 6-in. clear plastic straight section downstream of the elbow. Wool tufts were traversed across the passage and regions of high turbulence and stalled flow were identified. Results are illustrated in Figure 87. A possible separated flow region is present on the inside of the bend at zero swirl, which was not present at 40-deg swirl. In both cases, however, a strong vortex was noted near the outside of the bend, which apparently is the remains of a vortex shed from the centerbody of the turbine.

Conclusions drawn from the interturbine duct testing follow:

- o Measured elbow losses were less than expected for swirl angles less than 20 deg.
- o Duct length did not have a strong influence on loss magnitude.
- o Exiting flow from the elbow was highly distorted.
- o Static pressure variation through the elbow is influenced by swirl.

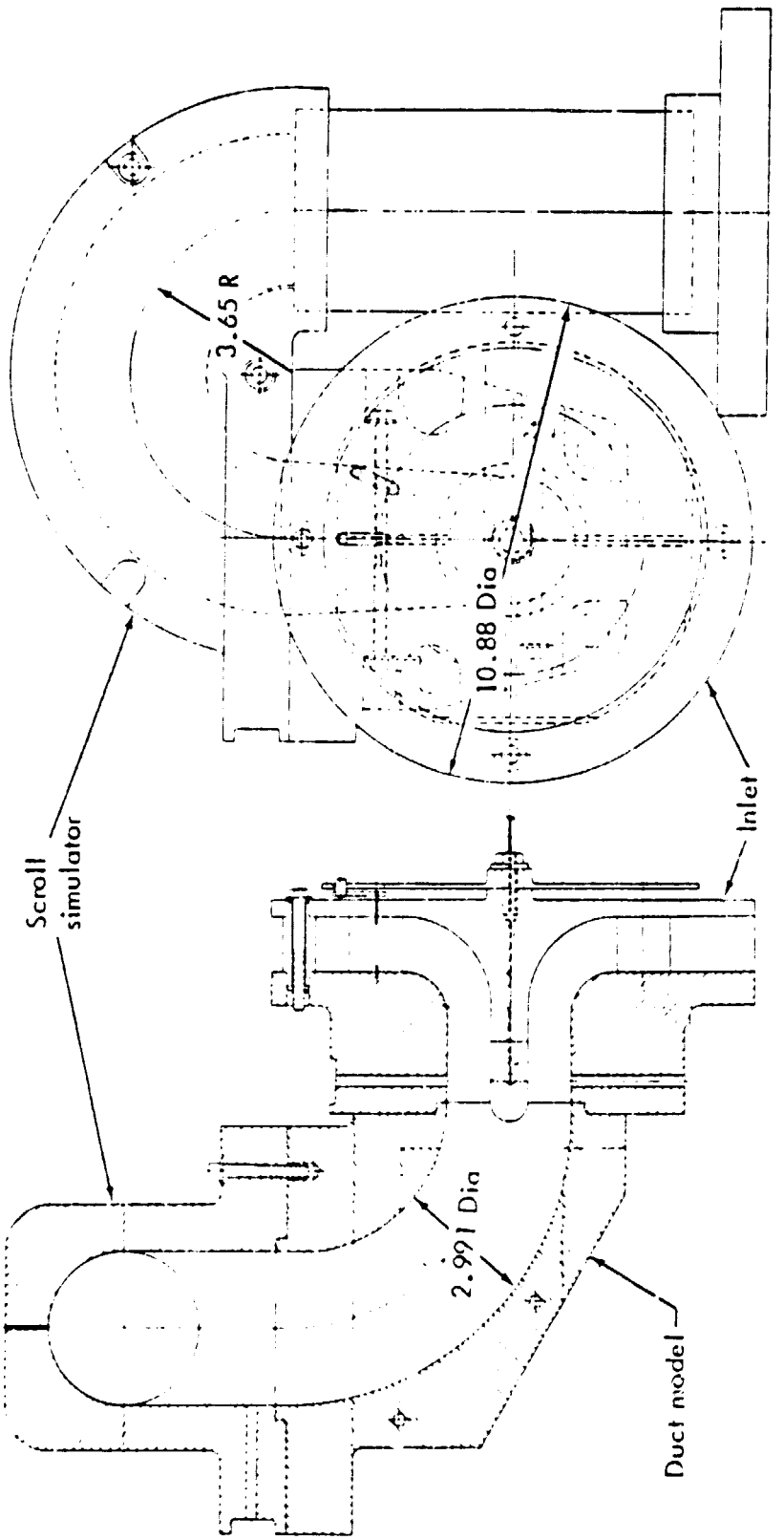

TE80-85

Figure 82. - Interturbine Duct Cold Flow Rig.

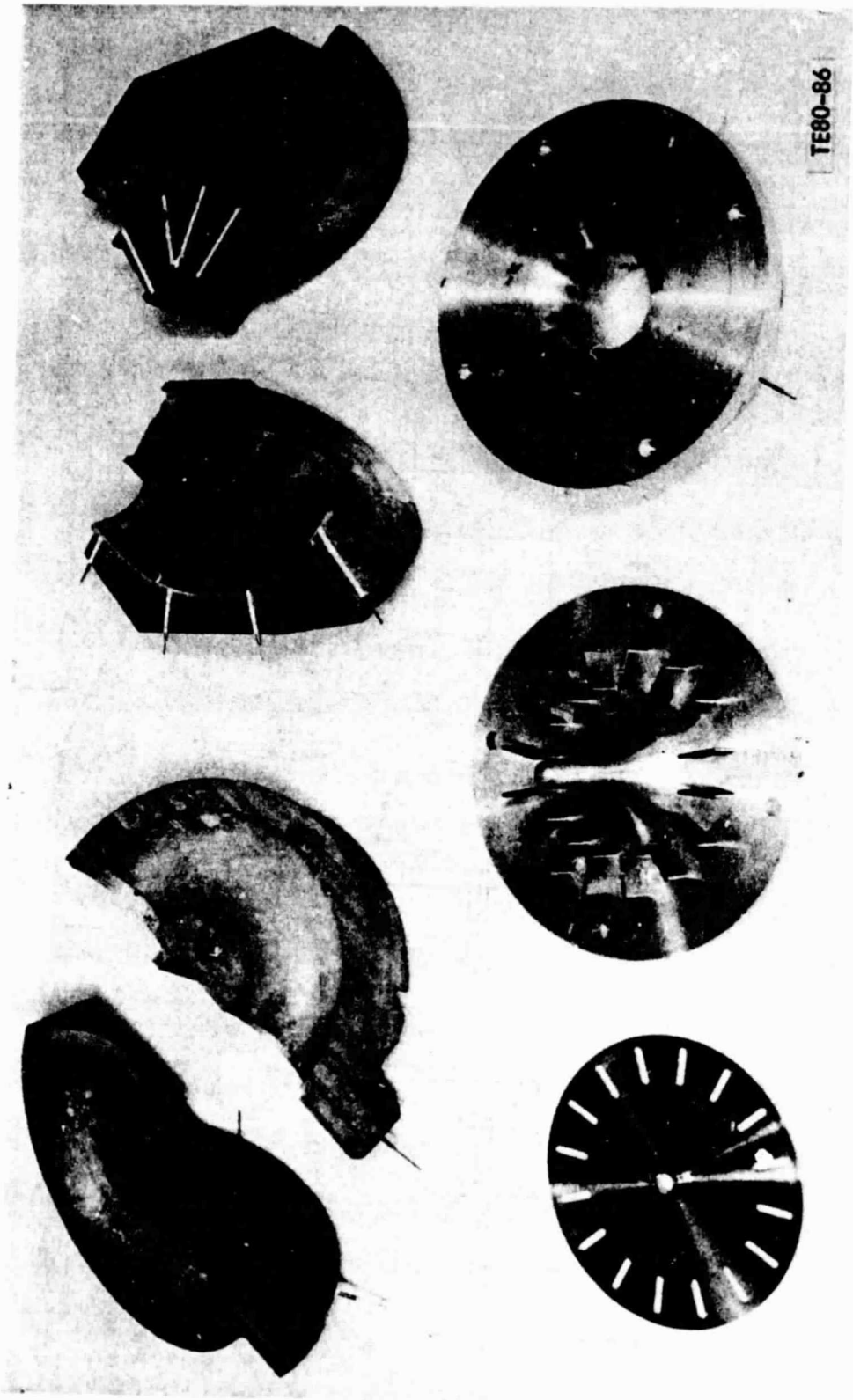

Figure 83. - Interturbine Duct Test Rig.

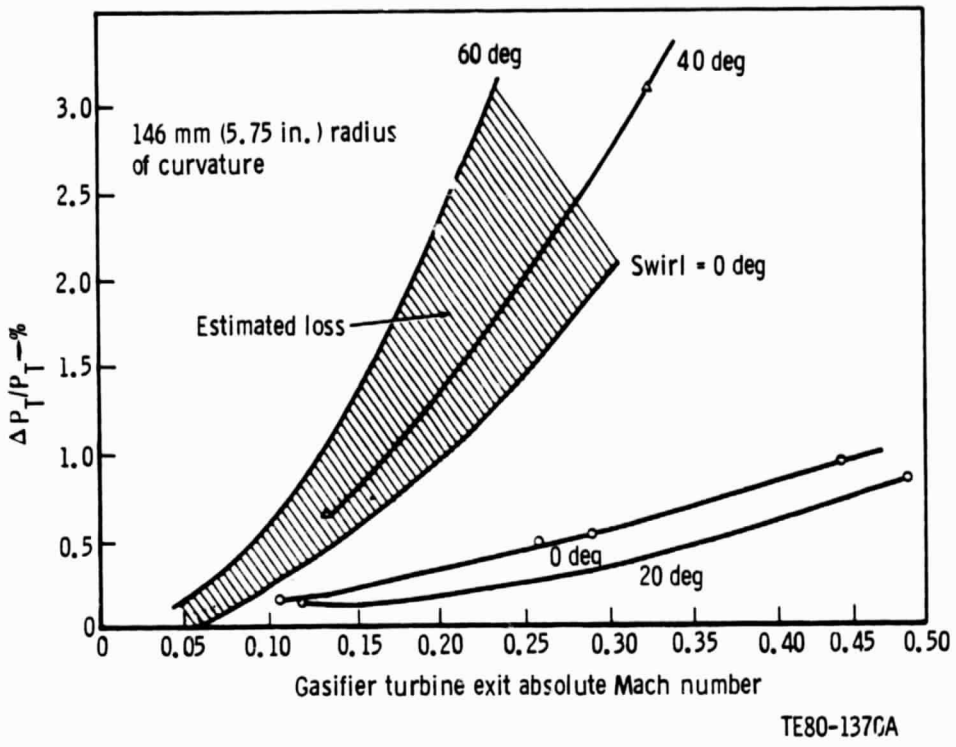

Figure 84. - AGT-100 Interturbine Duct Losses.

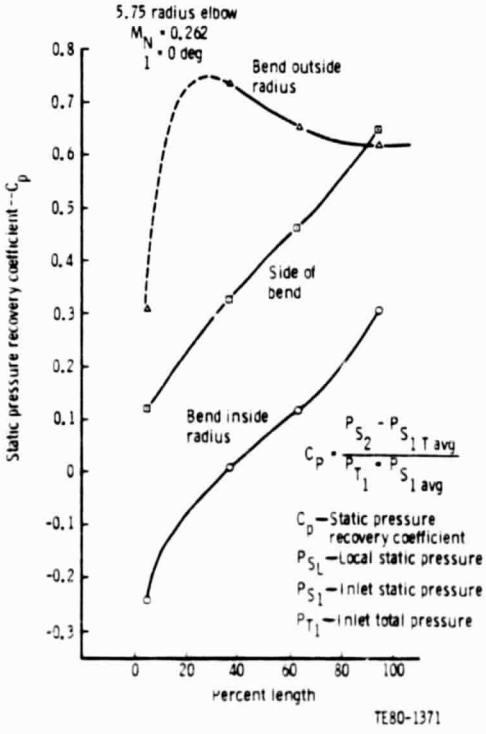

Figure 85. - AGT-100 Interturbine Duct Cold Flow Data--Zero Swirl.

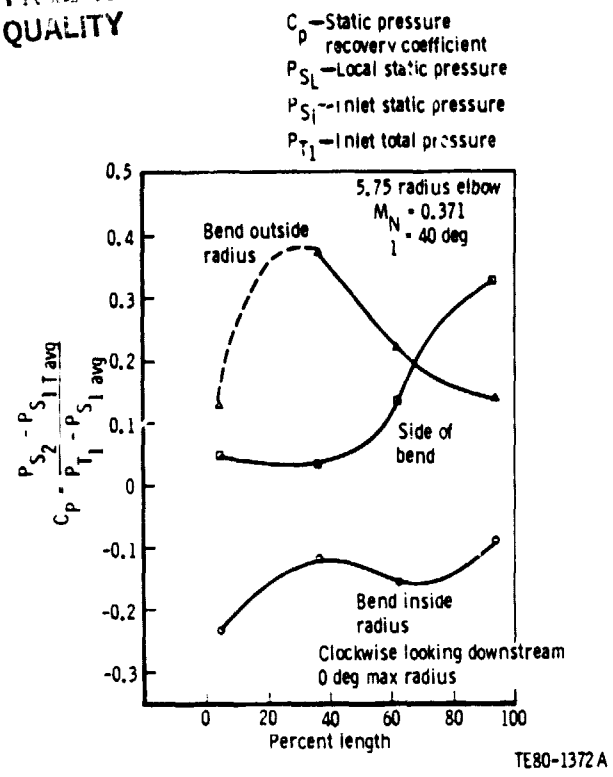

Figure 86. - AGT-100 Interturbine Duct Cold Flow Data--40-deg Swirl.

Based on this testing, the decision was made to design and fabricate a similar test rig to evaluate the specific configuration of the RPD engine. In order to include the effect of flow distortion at the duct exit and determine its influence on duct/scroll performance, the new rig is being designed to include 1) the interturbine duct with transition in cross-sectional shape, 2) the RPD scroll configuration, and 3) the power turbine inlet vane row to simulate proper flow distribution at scroll exit. A cross-section of the rig is shown in Figure 88. This cold flow test rig will include swirl generation at the interturbine duct inlet to simulate engine conditions and turbine inlet vanes at the scroll discharge to simulate back pressure. Instrumentation will include static pressure taps on the interturbine duct and scroll walls, total pressure and swirl measurement at the duct inlet, and a circumferential total pressure survey using a Kiel probe at the vane exit. The rig is being constructed from epoxy with aluminum chip filler. The back wall will be constructed with clear plexiglass to permit visual observation of the flow field. Tufts of wool and/or smoke may be used for flow visualization. Testing is planned to include a range of inlet Mach numbers and swirl angles to cover the expected environmental engine conditions. Testing will be accomplished at ambient pressure and temperature.

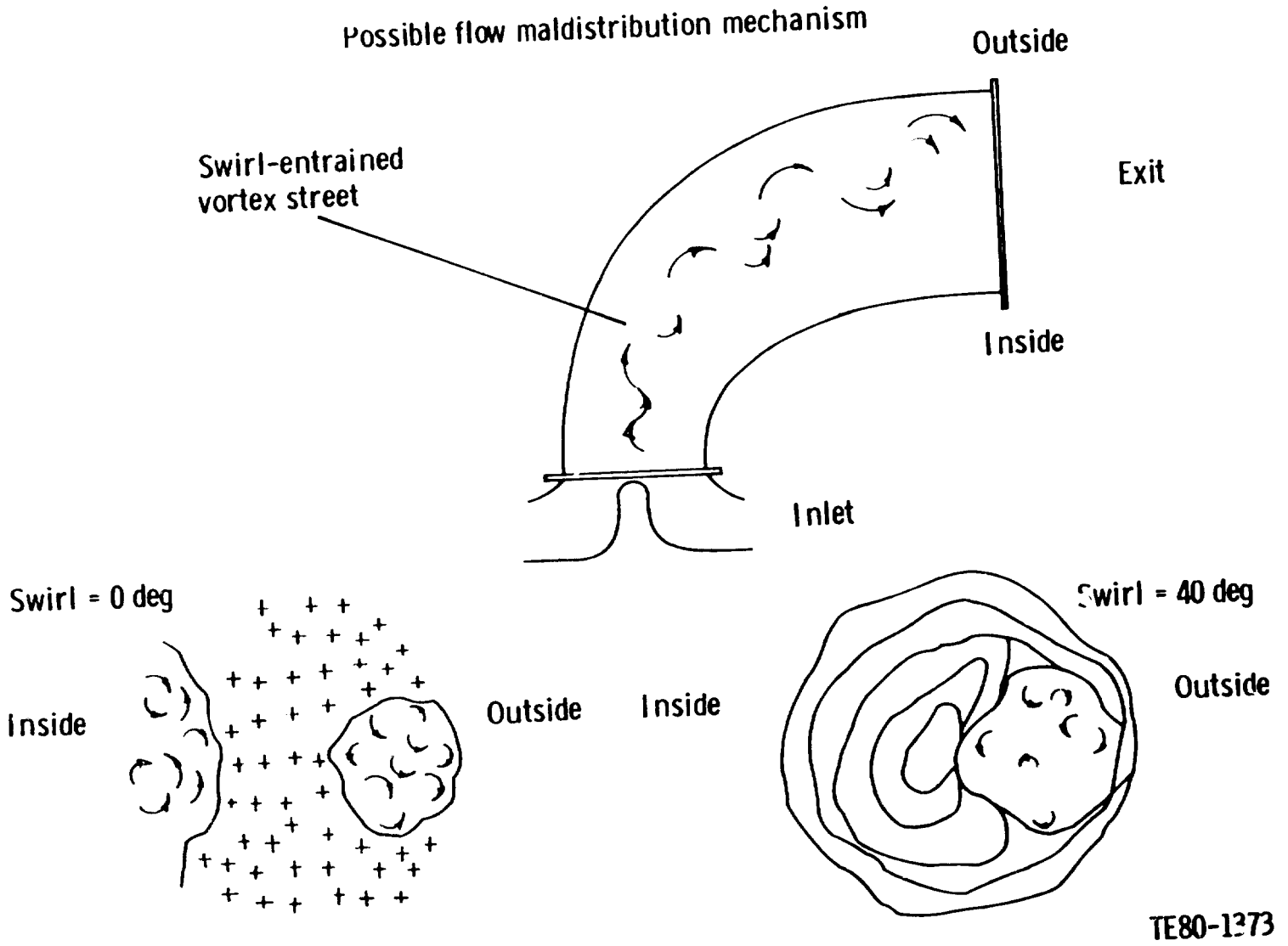

Figure 87. - Flow Visualization Results--AGT-100 Interturbine Duct.

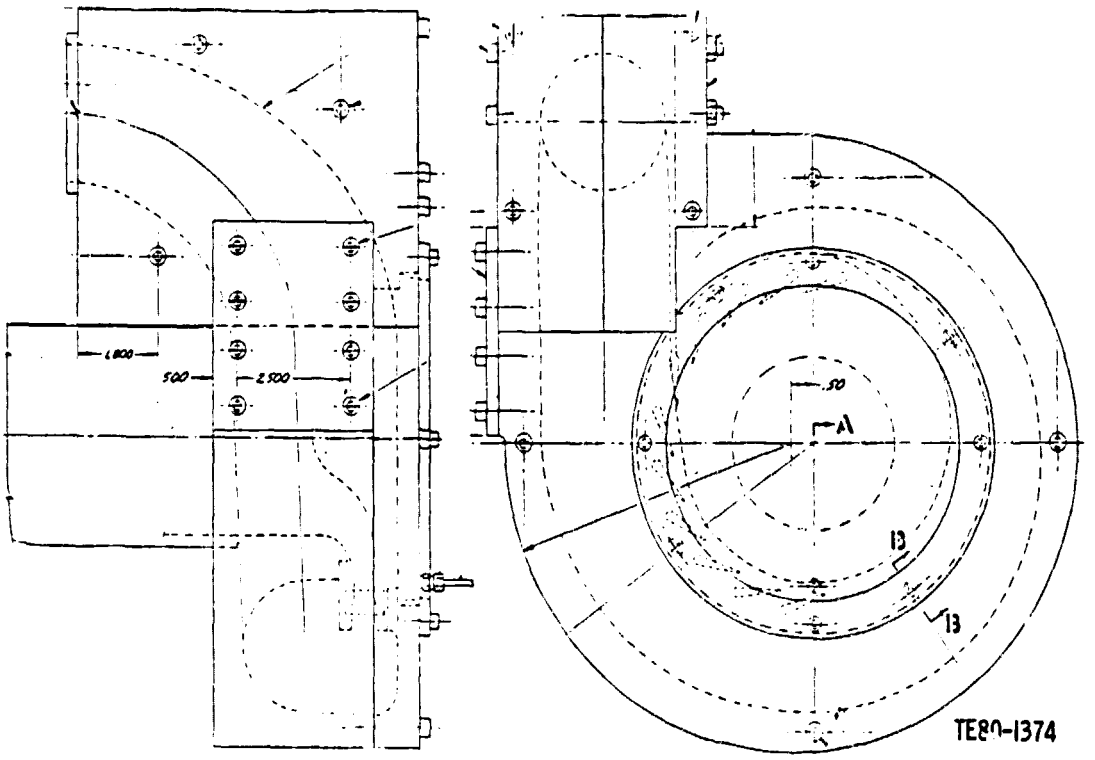

Figure 88. - Interturbine Duct/Power Turbine Scroll Test Rig.

Gasifier Turbine Aerodynamic Development Rig

The gasifier turbine rig activity consisted of the design and fabrication of parts for the first buildup. Coincident with parts fabrication for the first buildup, the inlet scroll and the interturbine duct designs were completed and released for fabrication.

Parts for the turbine rig have been fabricated and instrumented for test. The turbine wheel was machined on a tape-controlled 5-axis milling machine. Figure 89 shows this wheel as it was removed from the milling machine, and Figures 90 and 91 show the wheel after finish machining. This wheel is made from a 410 series stainless steel hardened for improved machining characteristics.

The gasifier nozzle vanes shown in Figure 92 are also made from 410 series stainless. They are assembled by inserting into pockets in the fore and aft walls as a freely supported structure. This design permits easy rework of the wall contours by simply removing the vanes. Three vanes have a hole through the center of the leading edge radius to permit the installation of adjustable tiebolts. The tiebolts permit small adjustments in the wheel-to-shroud clearance using the temporarily installed dial indicator gages as parallel and passage width indicators. Matched machined plugs replace these indicators during the tests. The tiebolts further restrain the walls from changing clearance as a result of the pressure and temperature forces. A shimming arrangement allows a close clearance setup to minimize the adjustment required with these tiebolts. This serves to limit the tensile stress in the bolts during testing to approximately 480 kPa (70,000 psi). The bolts are made of Type A286 stain-

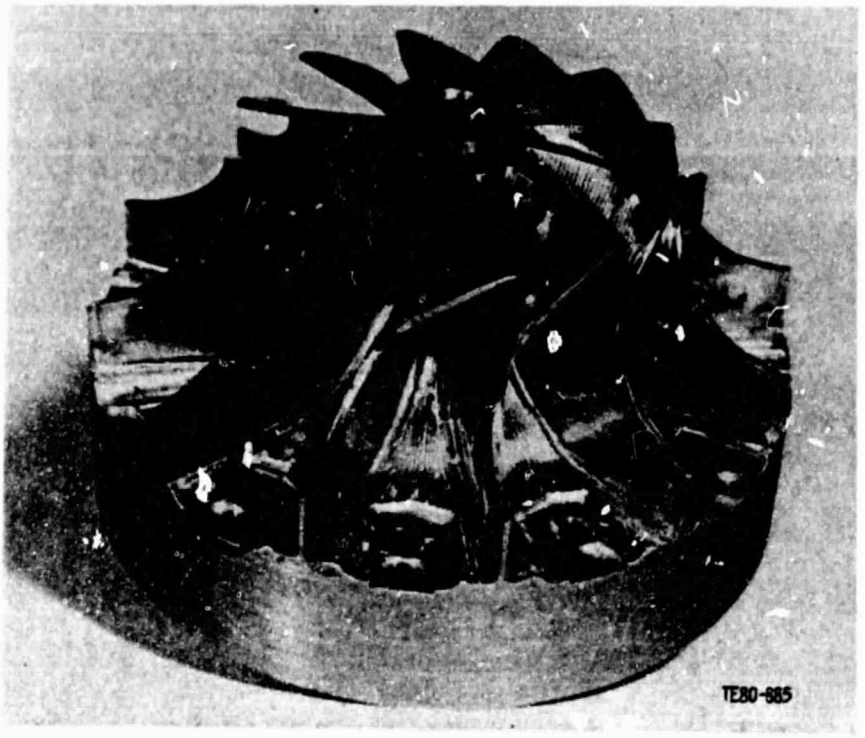

Figure 89. - Photo of Rough-Machined Gasifier Turbine Wheel.

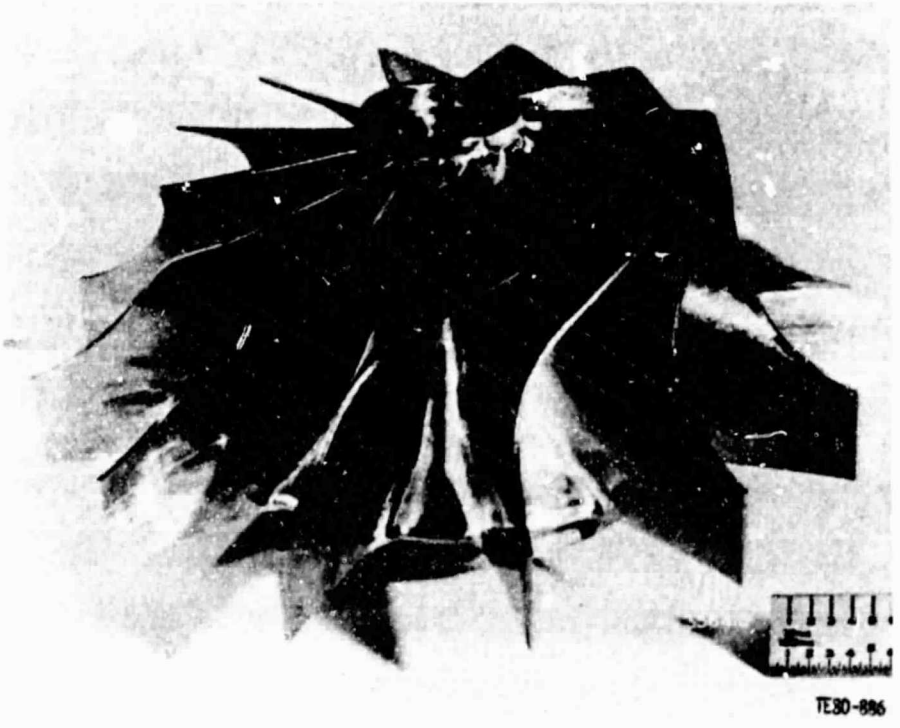

Figure 90. - Photo of Finish-Machined Gasifier Turbine Wheel (top).

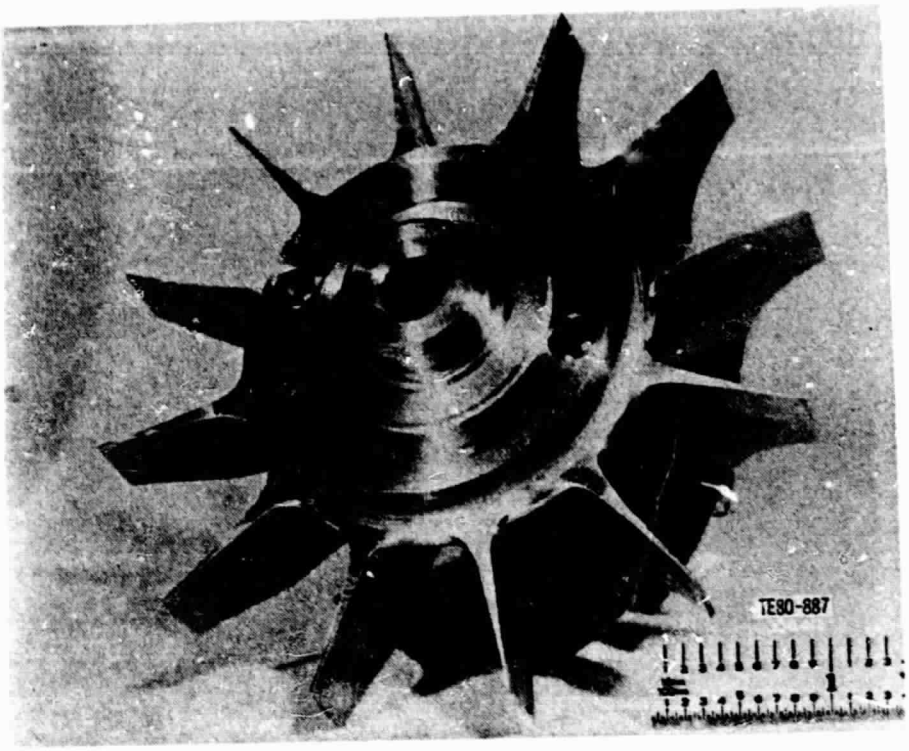

Figure 91. - Photo of Finish-Machined Gasifier Turbine Wheel (bottom).

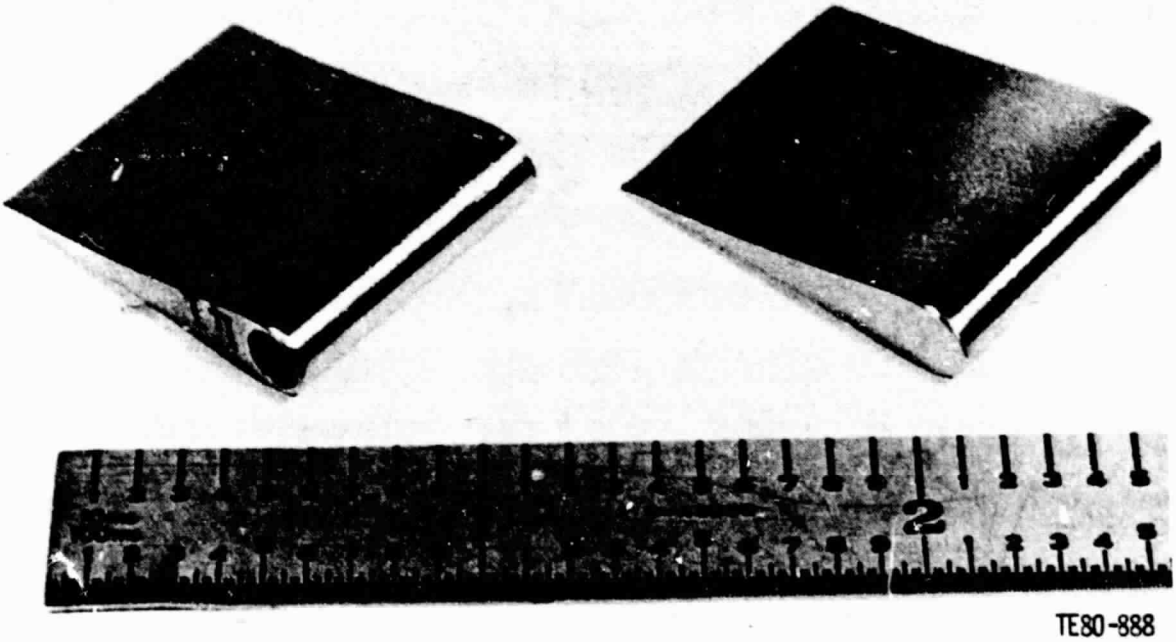

Figure 92. - Photo of Gasifier Nozzle Vanes.

less steel with a minimum yield of 590 kPa (85,000 psi) at the operating temperature of 149°C (300°F). The normal pressure forces tend to separate the walls thus opening the clearance and applying a tensile load to the bolts. Placement of the rear piston ring seal between shroud support and cover helps to minimize this effect by minimizing the area subjected to pressure difference.

Instrumentation in the flow path consists of wall static pressures, adjustable Kiel-type total pressure and temperature probes installed at the inlet and a traversing yaw probe survey at the exhaust. Provisions have been made to permit control of the backplate pressure and, if desired, the flow-path leakage in that area. A system of tubes leading back through the module mounting flange allows pressure or vacuum control of the backplate. A leaf spring mass isolator system over the roller bearing moves an objectionable natural frequency reasonance out of the operating speed range at 55,000 rpm.

Testing has been conducted using the proposed AGT-100 module and drive system to evaluate potential dynamic problems. Natural frequencies up to 55,000 rpm have been charted by running with and without the gasifier turbine wheel installed. A gearbox extension mount was installed to reduce a resonance amplitude at approximately 30,000 rpm.

The new low-torque, high-speed torquemeter assembly is ready for installation. A dynamic calibration will be made when a new high-speed water brake dynamometer unit is delivered. A previous dynamic calibration of the existing torquemeter has been made with a similar water brake dynamometer capable of speeds up to 20,000 rpm. These tests indicated the feasibility of using this approach to verify accurate repeatable torque readings. Since the turbines to be tested for the AGT-100 program are very small and have low torque [under 27 N·m (20 ft-lbm)], the dynamometer drive system motors the reduction gearbox, and because temperature differential measurements could contain inaccuracies because of leakage flows, a new turbine torque measuring system is essential to obtain the accuracies required.

The turbine system is designed to permit the interchangeability of the gasifier or power turbine configurations without removal of the module or drive system from the test facility. The wheels are attached to a common shaft in the module, and balancing of the rotor is accomplished by using a dummy balance shaft. This system permits the various turbine configurations to be changed on the test facility in a shorter period of time.

An inlet scroll uses a removable fiberglass insert to simulate inlet conditions into the turbine. This insert is mounted to the inlet casing with aluminum bulkheads imbedded in the insert and supported by the existing structure. The inlet instrumentation is designed to be rotated to the anticipated air inlet angles when running with or without this scroll installed. Addi tional wall static pressure taps are provided for flow evaluations of the scroll.

An interturbine duct on the rig exhaust simulates the engine design and replaces the standard cylindrical exhaust diffuser. The exhaust spool is replaced by an adapter plate to allow the larger diameter telescoping exhaust header to be moved forward over the duct. This modification permits the exhaust flow to leave the rig unrestricted. Additional configurations will be defined after aerodynamic evaluations of these tests.

4.2 GASIFIER TURBINE MECHANICAL DEVELOPMENT

RPD

Scroll Design

The gasifier turbine scroll takes gas from the combustor, distributes it, and then directs it through a series of vanes into the gasifier turbine rotor.

The RPD gasifier turbine scroll assembly design has been initiated. The design was influenced by the manufacturing processes agreed upon between DDA and Carborundum. Figure 93 shows a cross-sectional view of the scroll assembly. Carborundum is to produce the scroll/shroud by the slip casting process. The upper backplate will be made by the mandrel coating method. No process has been selected as yet for the lower backplate, but the simple shape lends itself to many choices. These three parts will be made of alpha silicon carbide.

The cross key arrangement, which secures the scroll assembly to the block, is basically the same as for the power turbine and is described in Section 5.2. Figure 94 describes the scroll assembly.

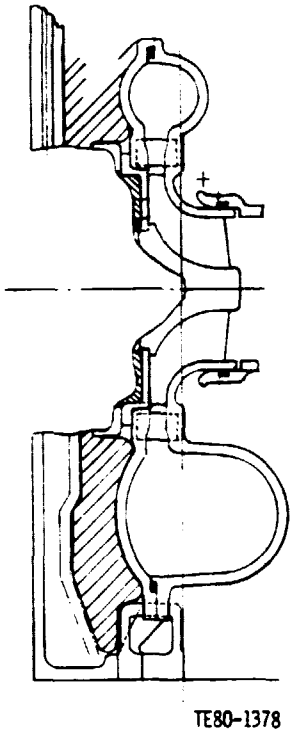

Figure 93. - Cross Section of Gasifier Turbine.

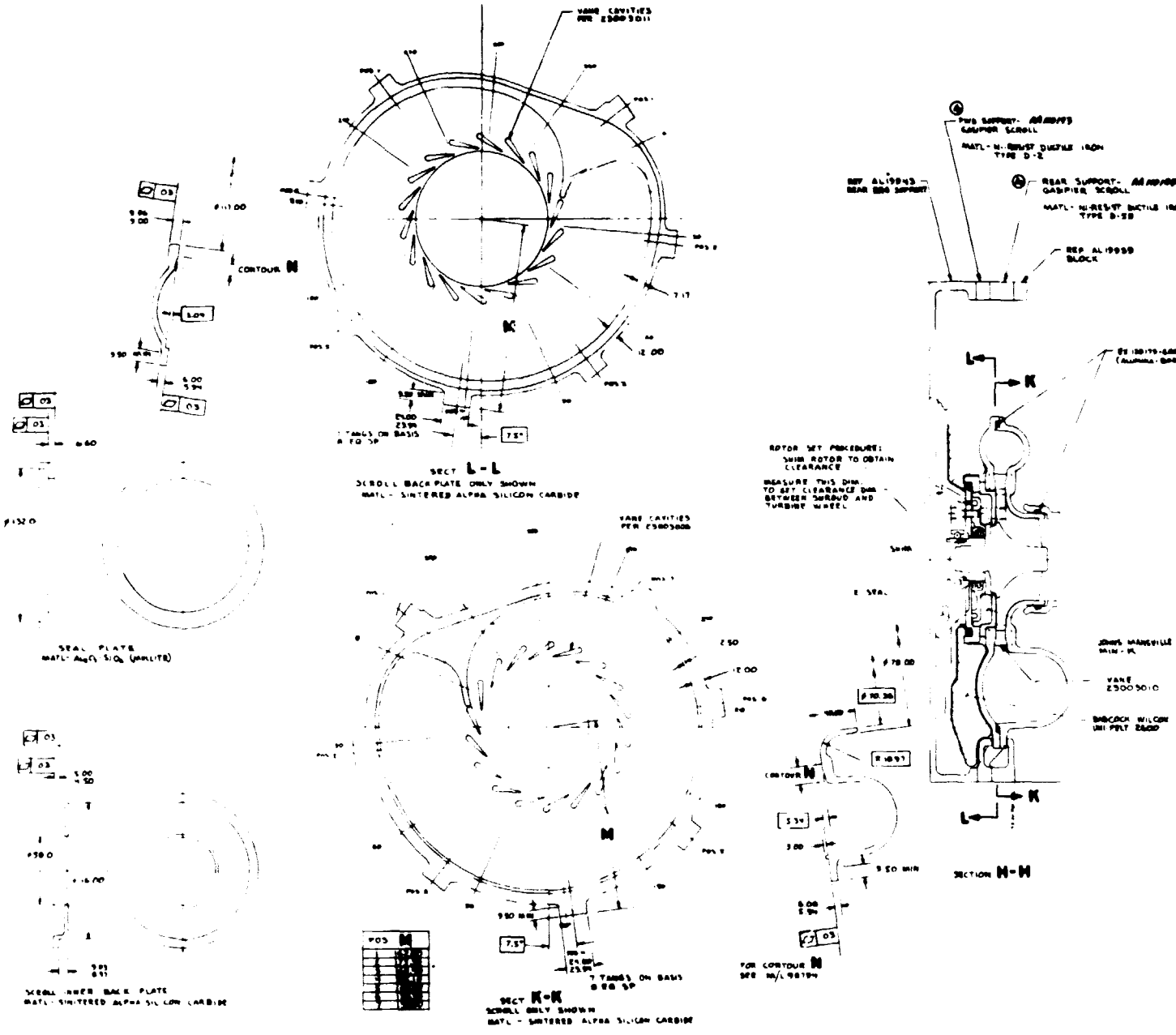

FOLDOUT FRAME

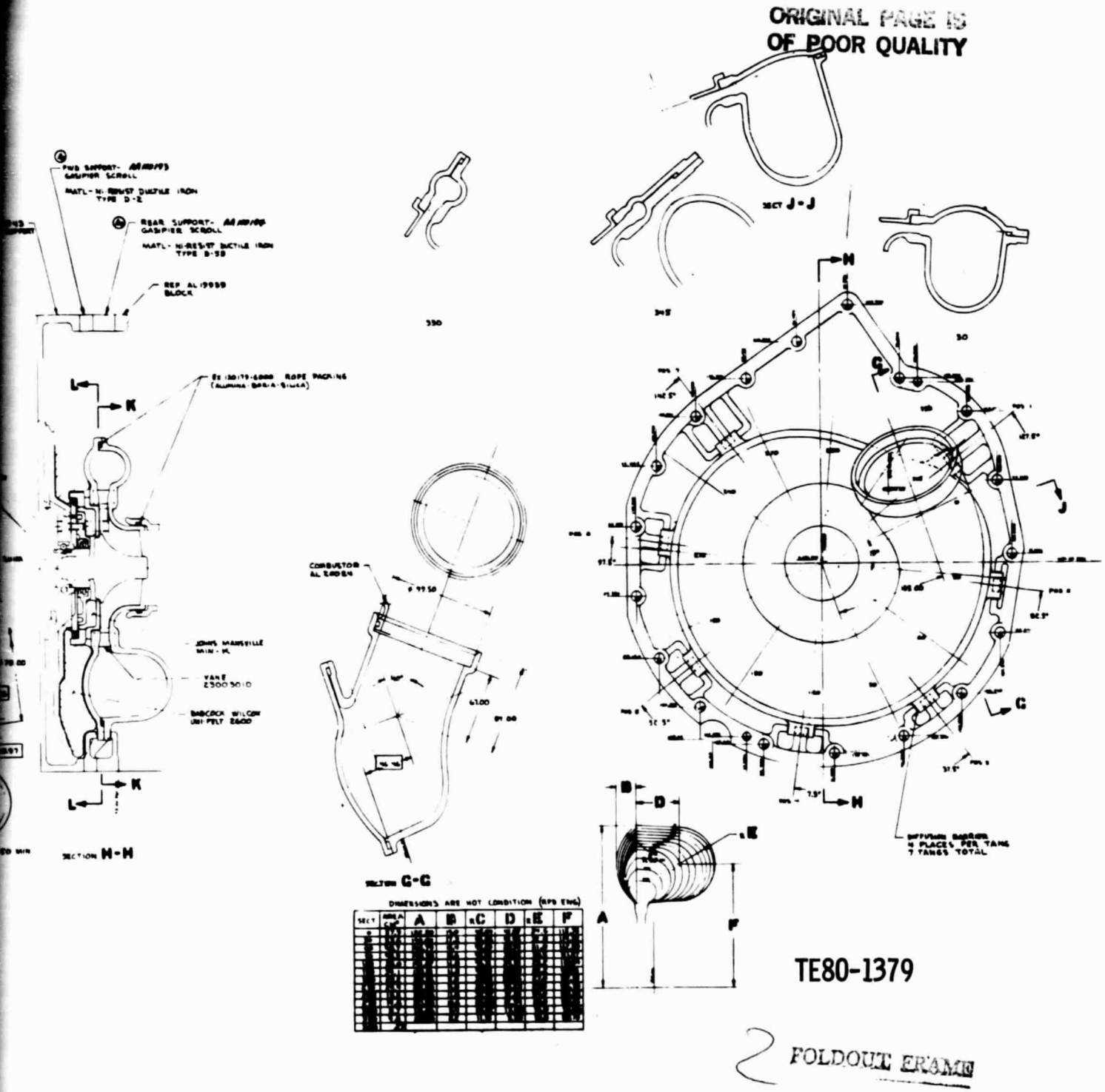

Figure 94. - Layout of Gasifier Turbine Scroll.

To a large extent, the basic cross-sectional shape of the scroll assembly was determined with the aid of a two-dimensional finite element model. This approach defined the basic shape and uncovered problems that should be eliminated early in the design prior to building a more detailed three-dimensional model. A study was made of axisymmetric sections at various locations through the scroll assembly. It was found that a section about 120 deg into the scroll yielded the highest stresses and deflections. This location was then used to define the two-dimensional model that was common to all later analyses.

A heat transfer analysis was run at the section under study for maximum power steady-state and transient conditions. Points were analyzed every 10 seconds from 0 to 200 seconds corresponding to a cold start followed by an acceleration to maximum power. Figure 95 shows the time versus gas temperature used in this analysis. An early section is shown in Figure 96 and Figures 97 and 98 present the steady-state temperature and principal stress plate of that section. As shown, the stress levels were not too severe at the steady-state condition.

The most severe stresses in the transient were found to occur at 60 seconds into the transient run. Figures 99 and 100 present plots of the transient temperatures and stresses. The stresses were found to be unacceptably high

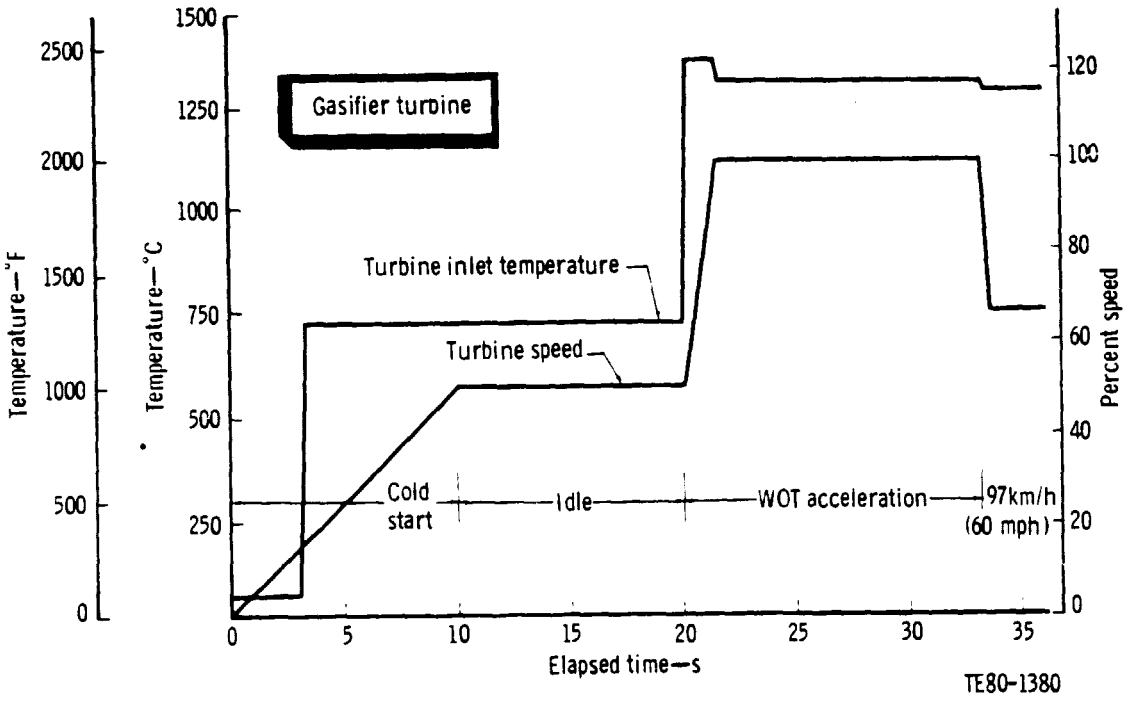

Figure 95. - Temperature vs Time Plot Used in Scroll Analysis.

PRECEDING PAGE BLANK NOT FILMED

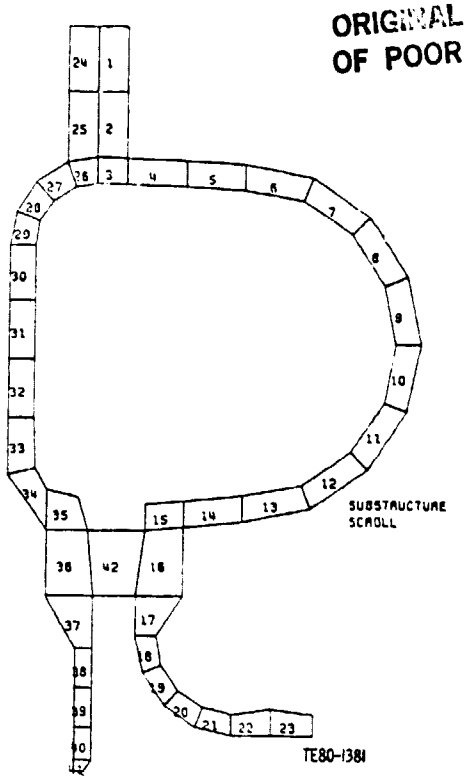

Figure 96. - Early Two-Dimensional Finite Element Analysis.

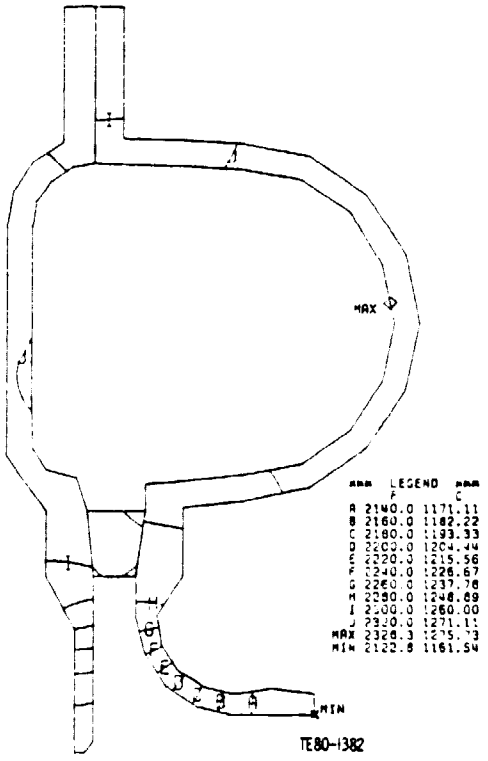

Figure 97. - Temperature Distribution of Early Model.

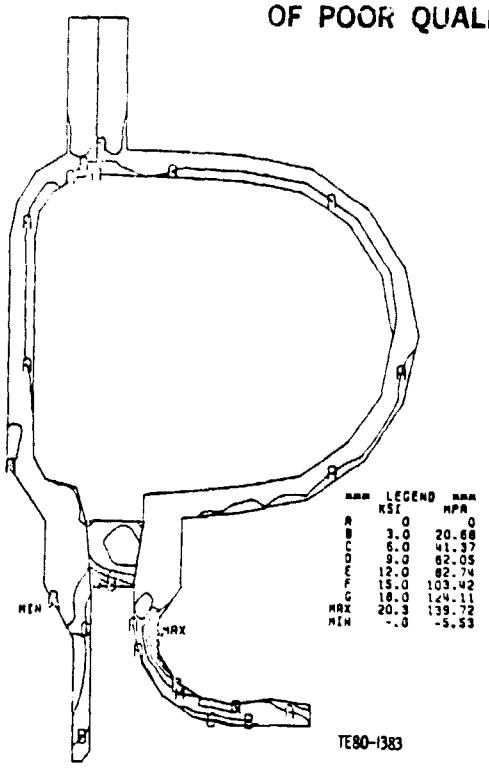

Figure 98. - Principal Stress of Early Model.

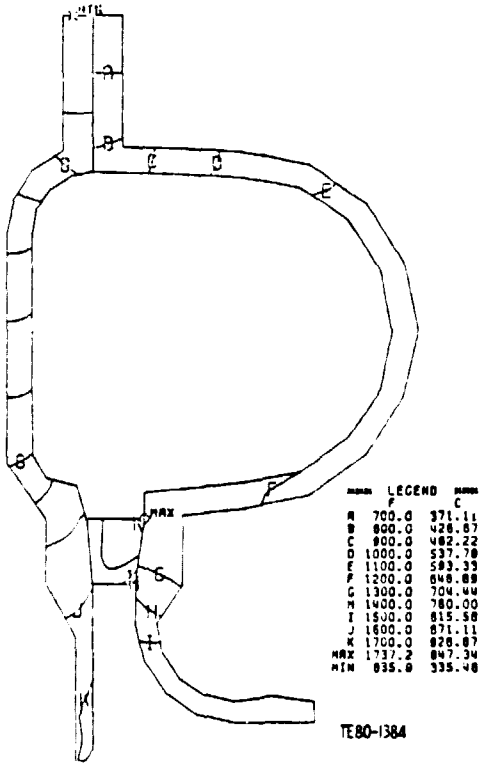

Figure 99. - Sixty-Second Transient Temperature Distribution of Early Model.

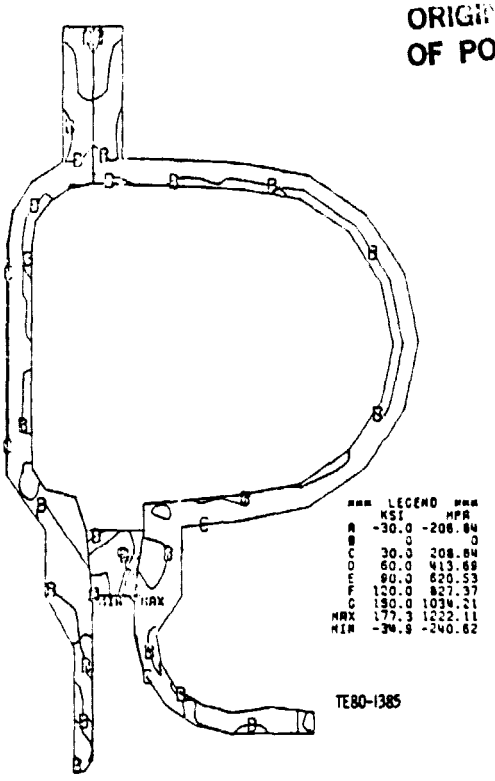

Figure 100. - Sixty-Second Principal Stress of Early Model.

(1222 MPa (177 kpsi)), and, therefore, it was necessary to change the scroll geometry to reduce the stresses. Some of the major changes were:

- o Removal of the continuous flange at the top of the scroll to allow for more even heating and thereby to reduce thermal stresses
- o Rounding backplate side to add some spring effect
- o Split backplate to lower stresses throughout the upper plate and to eliminate a deflection problem that existed throughout the transient run (This also resulted in a much easier assembly process, which is explained in Section 5.2.)

The configuration shown in Figure 101 evolved from these changes. The temperature distribution and principal stresses at steady-state conditions are shown on Figures 102 and 103. The same information for the 60 seconds transient point, which still yielded the highest transient stresses, are presented in Figures 104 and 105. The maximum principal stress occurs in the transient analysis and is an acceptable 236.48 MPa (34.3 ksi).

The scroll assembly layout drawing was then completed using this shape. A three-dimensional finite element model was started at the completion of the RPD layout and is in the final stages of modeling. Final alterations and/or acceptance will be accomplished with the three-dimensional finite element model.

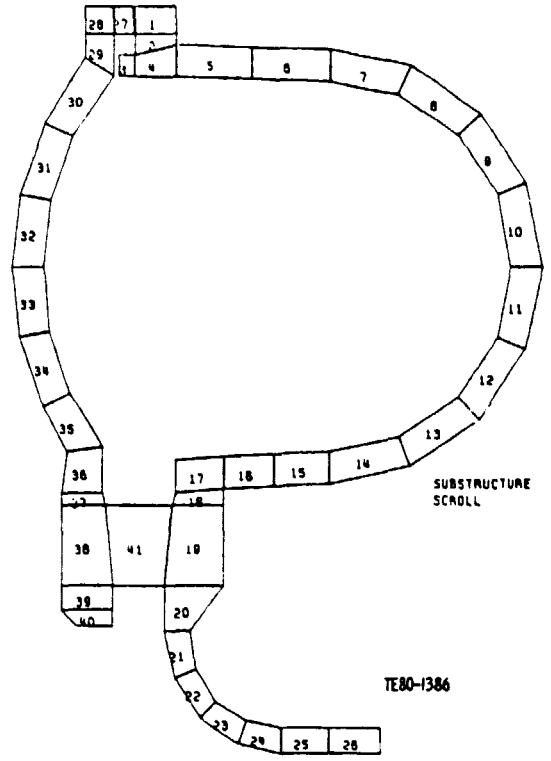

Figure 101. - Final Two-Dimensional Finite Element Section.

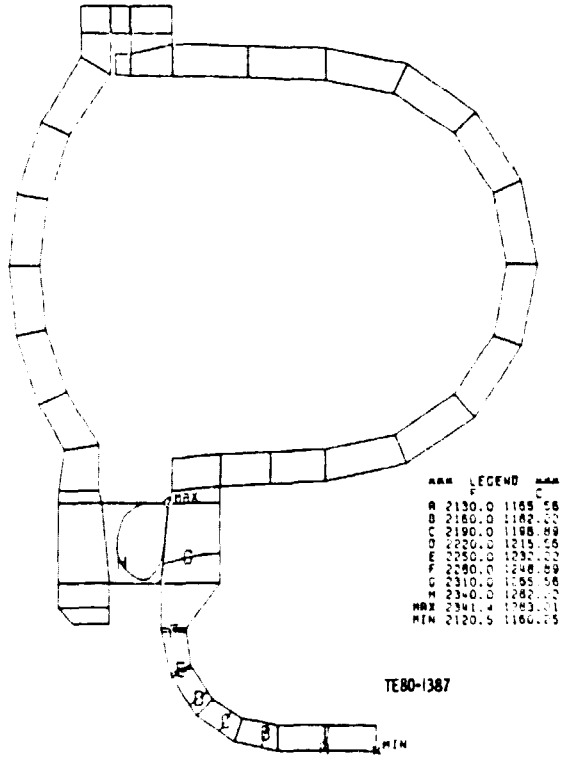

Figure 102. - Steady-State Temperature Distribution.

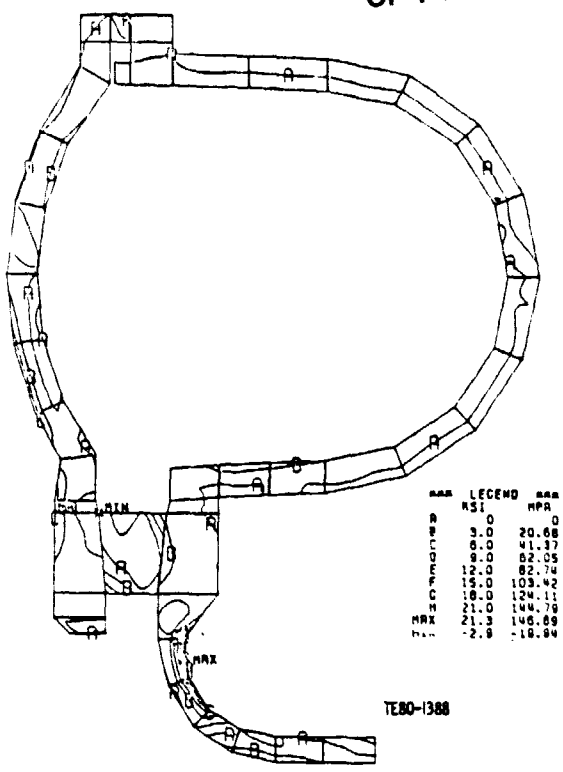

Figure 103. - Steady-State Principal Stress.

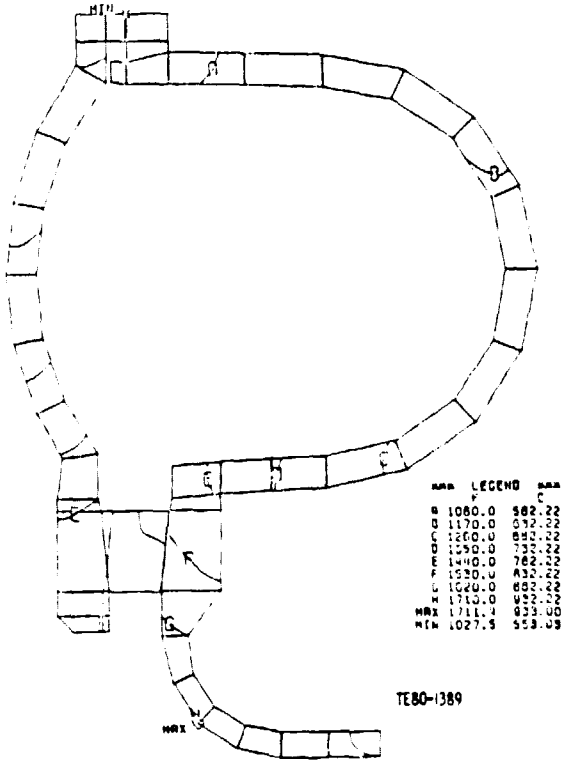

Figure 104. - Transient Temperature Distribution.

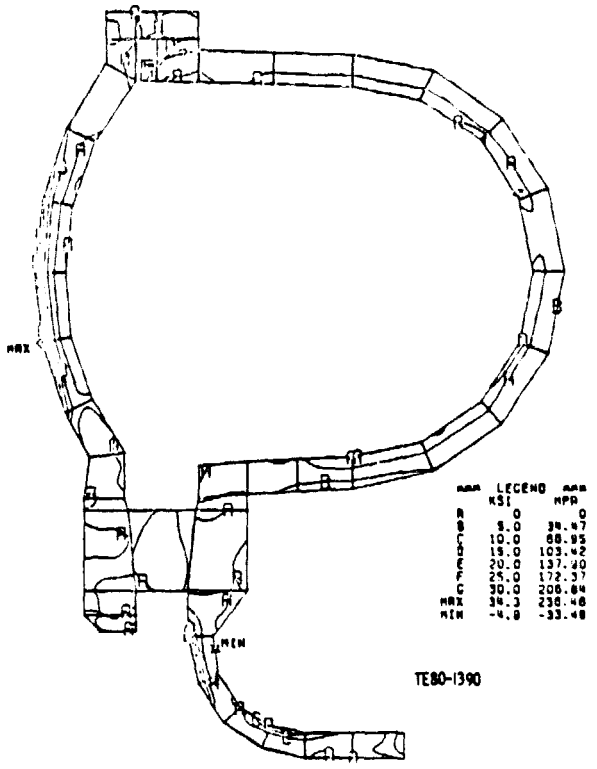

Figure 105. - Transient Principal Stress.

Mod I

Rotor

The design of the Mod I (metal) gasifier turbine is in progress. Previous analytical work indicated satisfactory disk stress levels but fairly low blade stress-rupture life, even though the properties of Mar-M246 were assumed in the analysis. An additional problem was an inducer vibratory mode that necessitated a partial backplate to stiffen the blade.

A new blade thickness distribution has been devised to increase blade thickness and thereby increase stress-rupture life and eliminate the need for a partial backplate. The resulting speed-frequency diagram is shown in Figure 106. The first inducer bending mode (mode 2) is above the fourth engine order and thus satisfies one of the design criteria.

Heat transfer and stress analyses were performed using a two-dimensional axisymmetric finite element model. The results at the maximum power (steady-state) condition are shown in Figures 107 and 108.

Stress-rupture life has also been calculated, including the effects of off-design operation. The time distribution at various gasifier rotor speeds was estimated using power demand during the combined Federal Driving Cycle (FDC) and the output power characteristic of the Mod I engine. The distribution indicates a significant amount of time (approximately 40%) at idle or at low power settings where the turbine inlet temperature is less than maximum. Cal-

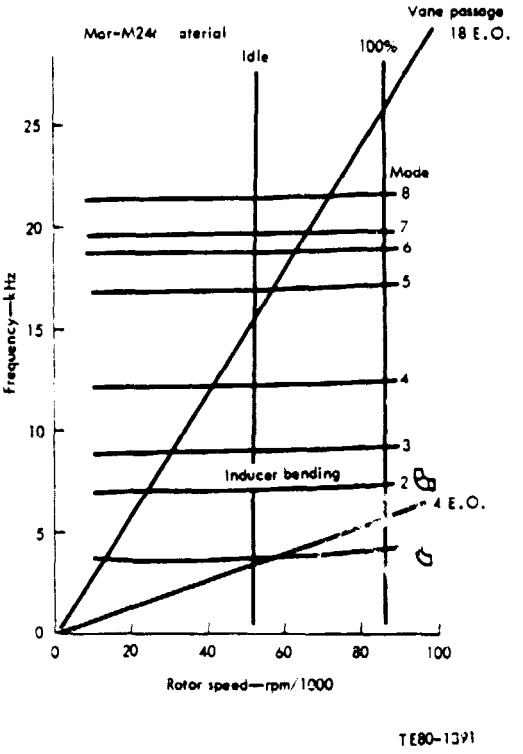

Figure 106. - Speed Frequency Diagram for Mod I Metal Gasifier Turbine.

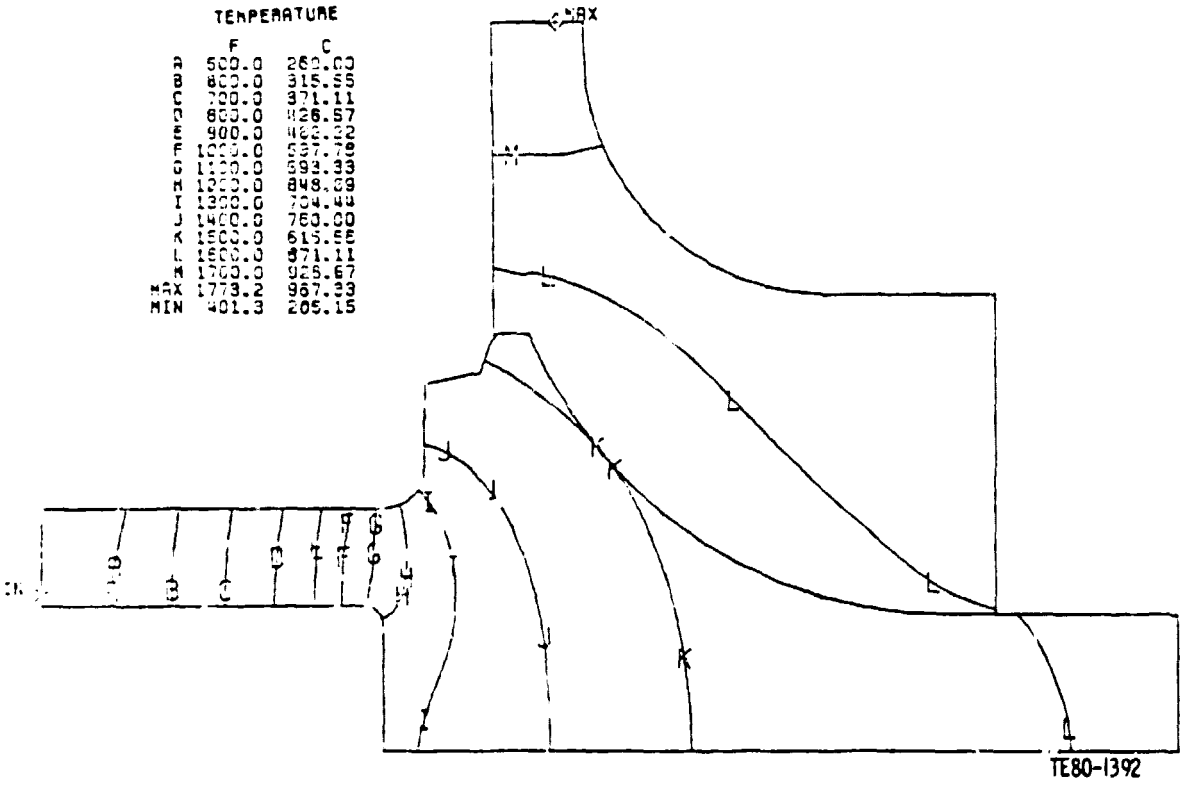

Figure 107. - AGT Mod I Gasifier Turbine Temperature Distribution at Maximum Power.

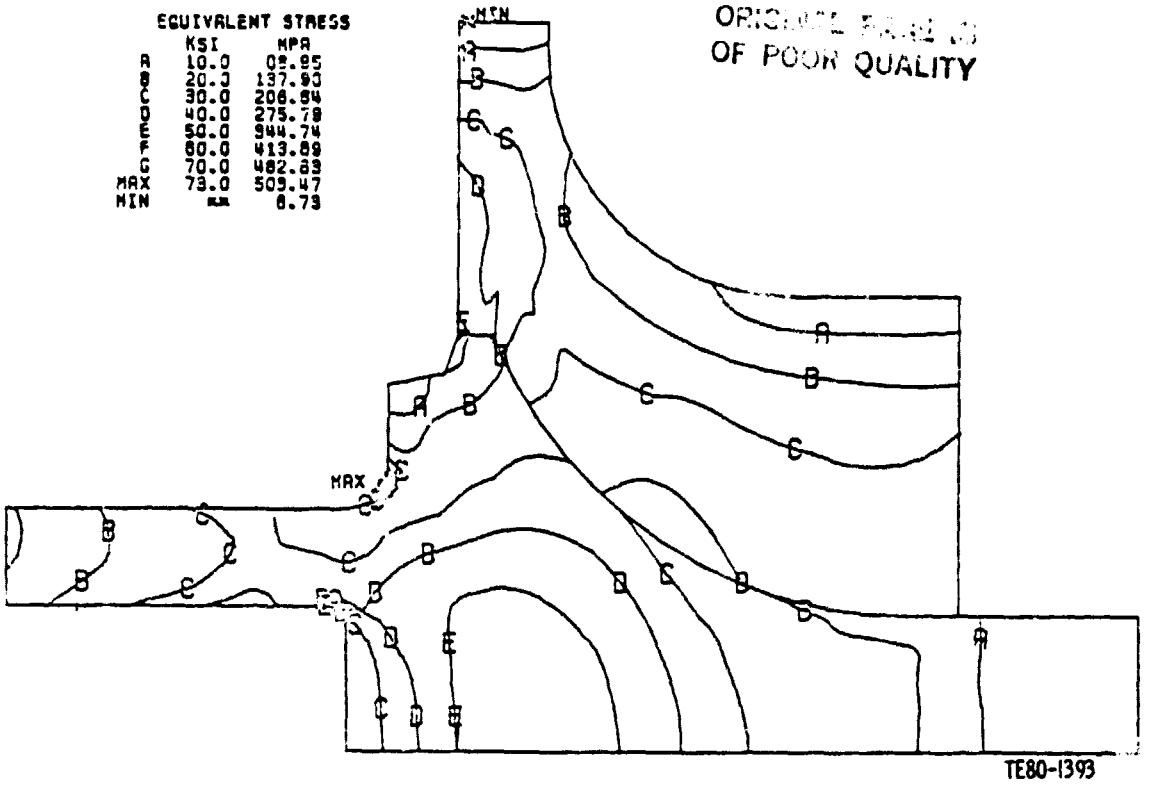

Figure 108. - AGT Mod I Gasifier Turbine Stress Distribution at Maximum Power.

culations indicate very long stress-rupture life at these conditions. The distribution of operating time at the rated turbine inlet temperature of 1080°C (1976°F) follows:

Gasifier speed, %	Combined FDC time fraction, %
100	.6%
95	1.5
90	1.3
85	6.7
80	8.6
75	13.8
70	28.7

Using this distribution the estimated mean stress-rupture life on the combined FDC is 779 hours. At the design point operating condition, the mean life is 210 hours. The relatively small improvement in life at offdesign conditions is attributed to the increase in blade metal temperature resulting from the increase in total relative gas temperature at lower rotor speeds. Thus, the increased metal temperature partially offsets the effect of reduced stress at lower speeds.

The maximum individual engine test time accumulation planned for the Mod I version is 250 hours, thus the design life meets the requirement.

Scroll Design

The layout of Mod I metal back-up parts is nearing completion. Construction and running of a three-dimensional finite element model for these parts will start shortly. This model will be somewhat less detailed than the RPD model as the primary concern is deflection during transients. The three-dimensional analysis should be completed during the next reporting period.

Rotor Dynamics

The initial RPD gasifier turbine rotor critical speed analysis was presented in Ref 2. The geometric representation of the rotor system is shown in Figure 109. Subsequent analyses were performed using this model to predict rotor responses to component unbalances. Responses were computed for in-phase and out-of-phase unbalances at the compressor and turbine of 0.000933 N-m (0.000826 lbm-in.) and 0.000726 N-m (0.000643 lbm-in.), respectively. These unbalances are commensurate with a 0.0254 mm (0.001 in.) offset of the component center of gravity from the center of rotation. The maximum response levels computed for the steady-state operating speed range were found to be 0.102 mm (4 mils) at the turbine blade tip and 0.051 mm (2 mils) at the compressor blade tip. Use of a squeeze film damper at the compressor end bearing provides enough damping to reduce the lower mode response, which occurs in the transient speed range because of the out-of-phase unbalance. Calculated bearing dynamic loads resulting from out-of-balance indicate that the front bearing load is sensitive to out-of-phase unbalance while the rear bearing load is sensitive to in-phase unbalance. The maximum computed dynamic loads in the operating speed range because of the assumed unbalances are 222.4 N (50 lbf) at the front bearing and 333.6 N (75 lbf) at the rear bearing.

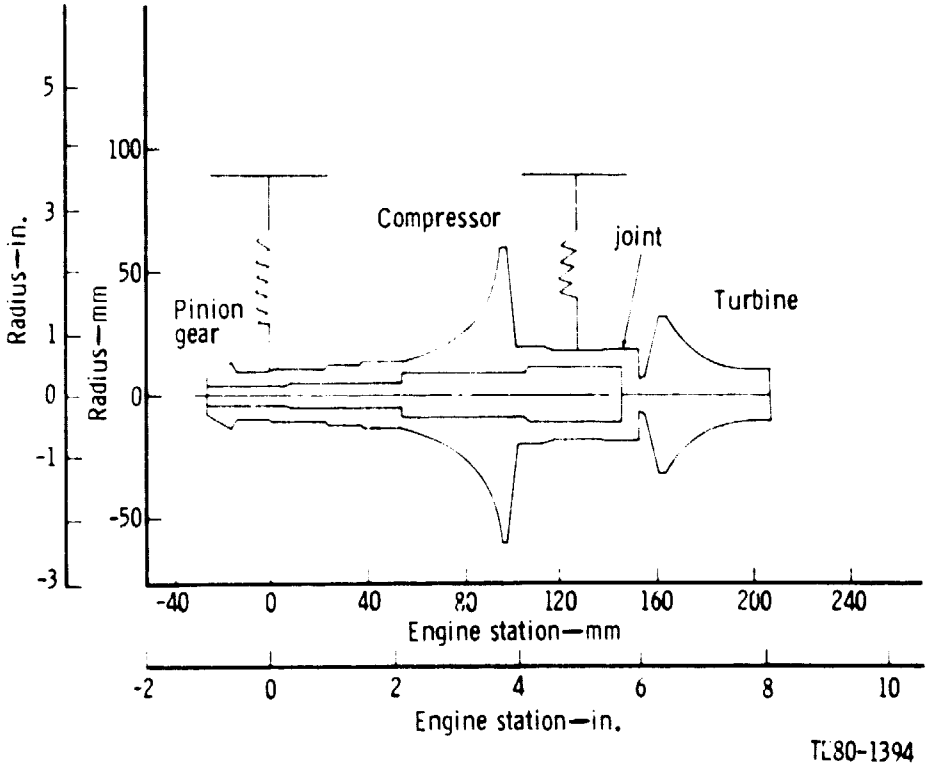

Figure 109. - AGT-100 RPD Gasifier Turbine Rotor System Geometric Representation.

Following these calculations, a change was made in design philosophy, which resulted in a modified gasifier turbine rotor configuration. A change to the power transfer arrangement allowed the shortening of the rotor shaft overhang from the compressor end bearing by 20.32 mm (0.80 in.). Additionally, the material of the interface joint between the steel shaft and ceramic turbine was changed. The modified geometric schematic is shown in Figure 110. Figure 111 shows the computed critical speeds and mode shapes for the rotor supported with a 3.5 MN/m (20,000 lbf/in.) spring rate at the front bearing and a 10.5 MN/m (60,000 lbf/in.) rate at the rear bearing. These rates provide a steady-state operating speed range free of critical speeds. Table XV shows the computed critical speeds of the first three modes for three values of joint stiffness. The third mode (shaft bending mode) is not sensitive to this change in stiffness.

TABLE XV. SENSITIVITY OF FREQUENCIES RESULTING FROM ROTOR/SHAFT JOINT STIFFNESS FOR AGT-100 RPD GASIFIER ROTOR

Temperature	Modulus of elasticity	Mode No.	Frequency, cpm
538°C (1000°F)	1.21×10^5 MPa (17.5×10^6 psi)	1	29,283
		2	33,921
		3	142,237
760°C (1400°F)	0.917×10^5 MPa (13.3×10^6 psi)	1	29,281
		2	33,921
		3	142,139
982°C (1800°F)	0.758×10^5 MPa (11.0×10^6 psi)	1	29,279
		2	33,920
		3	142,003

Further analyses have been initiated to include the asymmetric coupling between the gasifier turbine rotor and the power take-off drive train. Preliminary results from this three-plane simulation indicate that coupled critical speed exists in the gasifier operating speed range. Design perturbations are being investigated to synthesize a viable configuration.

4.3 CERAMIC GASIFIER TURBINE ROTOR

The gasifier and power turbine wheels for the RPD engine have been defined and are undergoing detailed design analysis. Because the gasifier turbine is expected to operate in a more severe thermal environment and at higher speeds, much of the initial analysis has concentrated on this rotor.

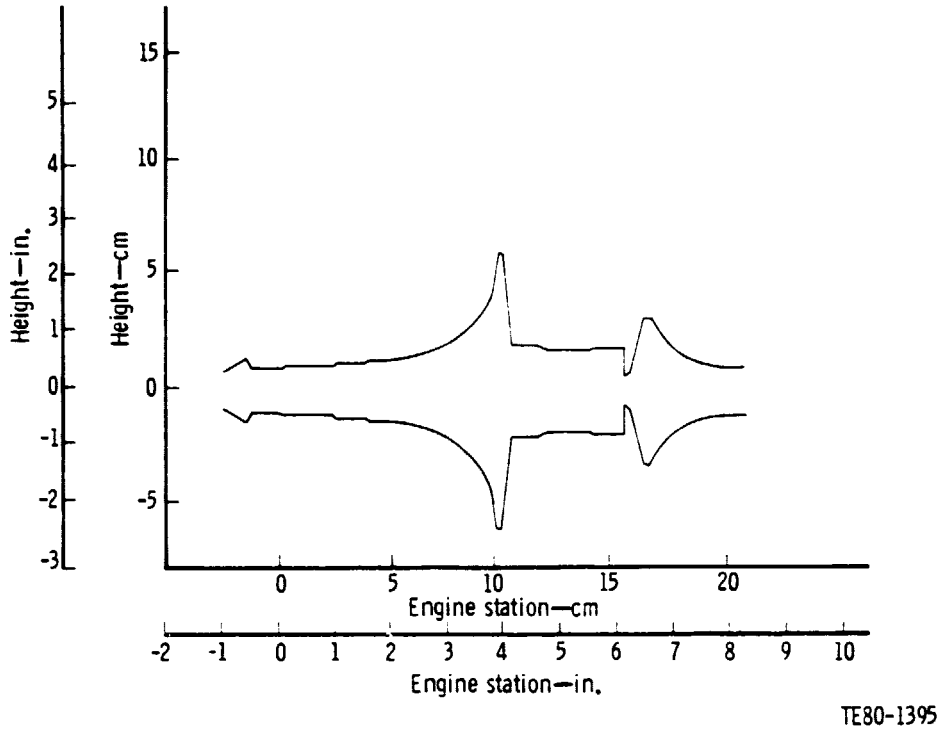

Figure 110. - AGT-100 RPD Gasifier Turbine Rotor for RPD Power Transfer Design.

Work accomplished was in four areas. These are summarized below and detailed later in this section.

- o Proof testing--The existing two-dimensional model was used to examine the effect of proof tests on increasing survival probability. This work is applicable in concept to both gasifier and power turbines.
- o Three-dimensional finite element model--A computer routine generates a three-dimensional finite-element model of any radial turbine given flow-path coordinates and blade thickness data. Two- and three-dimensional results for the gasifier turbine compare favorably.
- o Shaft joint analyses--Three design schemes have been investigated which would apply to either the gasifier or power turbine rotors.
- o Revised two-dimensional analytical models--The models have been revised to reflect power transfer, balance stock, gas recirculation, and joint effects in the current RPD designs of both turbines.

Proof Testing

Work has been performed to predict analytically the impact of proof testing on probability of survival. The existing two-dimensional model and Weibull statistics were used for these studies. Previous analyses of a severe cold start to maximum power transient indicated that high strengths (mean strengths) were

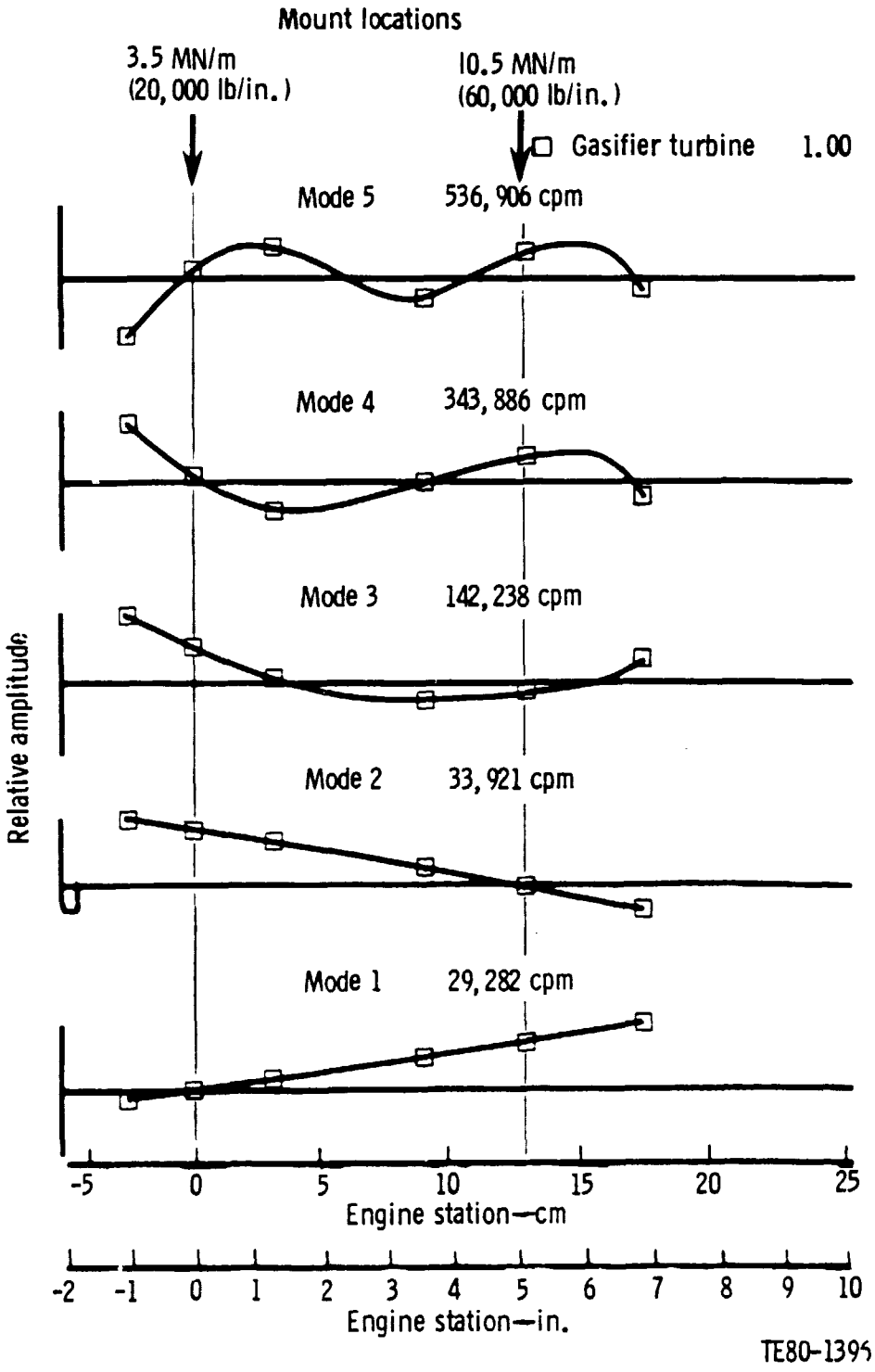

Figure 111. - AGT-100 RPD Gasifier Turbine Rotor Critical Speeds and Mode Shapes.

required to meet reliability goals because of the wide scatter in strength data. The use of cold spin testing had been proposed as a proof test to eliminate the low-strength rotors. This would have permitted the use of material with lower-than-desired mean strength and still achieve the desired survival probability. However, studies to date indicate cold spin testing is not effective for these purposes because it does not test the most critical failure parameter--stressed volume--adequately.

The computed rejection rate for cold spin proof testing of the gasifier turbine is shown in Figure 112 for three material strength levels. Assuming the rotor has been proof tested to the stress state occurring in a cold spin, the probability of survival has been computed for the maximum transient condition. The results are shown in Figure 113 for the same three material strength levels.

For low rates of proof test rejection (less than 20%), negligible improvement in the transient probability of survival was computed. As an example, if a 20% cold spin test rejection rate is assumed, the proof test speed would be 115 x 10^3 rpm (Figure 112) for 413.4 MPa (60-ksi) material. That test speed has only increased the maximum transient survival probability from 0.63, at 80 x 10^3 rpm, to 0.70, at 115 x 10^3 rpm (Figure 113). This effect is apparently the result of the dissimilarity between a cold spin stress state and that created during an engine transient. The probability of survival is a function of stressed volume, and the stress distribution is more uniform for a cold spin test compared to the transient. Figure 114 shows the relative stress levels for each condition. It can be seen that the solid disk portion of the wheel is more highly stressed relative to the blade for the cold spin case (A/B is low). Duplicating the peak stress level in the blade root that occurs in the transient would result in a very high proof test rejection.

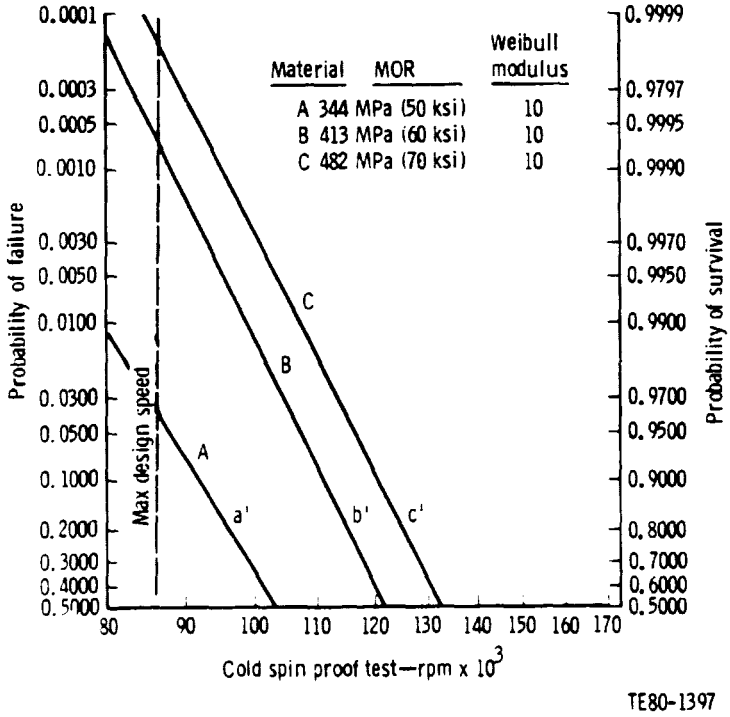

Figure 112. - Proof Test Rejection Rate for AGT Gasifier Turbine.

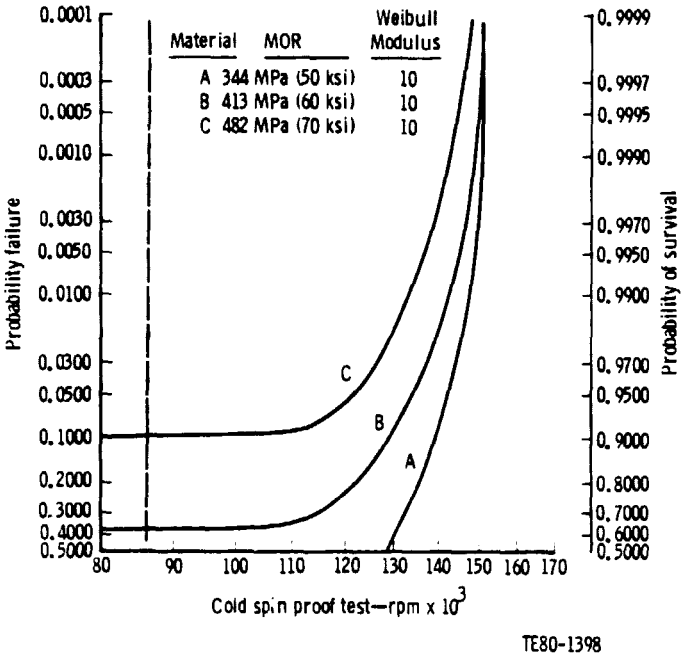

Figure 113. - Maximum Transient Failure Rate After Proof Test.

Sintered alpha-silicon carbide material

	A max blade stress	B Max disk stress	A/B
Mech only (86,240 rpm)	105 MPa (15.3 ksi)	92 MPa (13.4 ksi)	1.14
Max steady state	125 MPa (18.2 ksi)	104 MPa (15.1 ksi)	1.20
Max transient	260 MPa (37.8 ksi)	998 MPa (28.8 ksi)	1.31

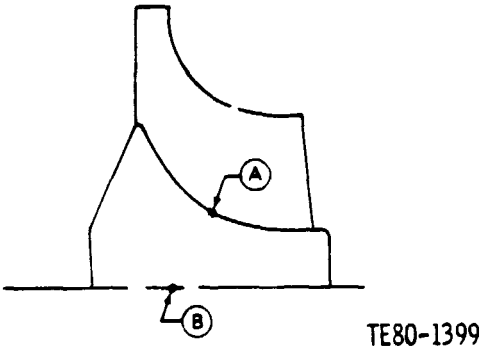

Figure 114. - Stress Distribution Variation.

The cold spin proof test cannot, therefore, significantly reduce material strength requirements. However, it is still useful as an independent verification of material strength in the wheel.

Three-Dimensional Finite Element Model

A computer routine has been developed to automatically generate a three-dimensional finite element model of the radial turbine, given flow-path coordinates and blade thickness data. This program reduces the amount of manual effort in constructing this complex model. The model uses 20 noded solid elements and generates a one-blade sector of the wheel. An example is shown in Figure 115.

A direct comparison has been made between axisymmetric (two-dimensional) and three-dimensional models of the gasifier turbine. The axisymmetric model element mesh was defined to simulate the three-dimensional mesh closely. Heat transfer and stress analyses were performed at the maximum power steady-state condition, and a probability of survival computed using the properties of sintered silicon carbide material. The results are shown in Figure 116.

The results show excellent agreement even when individual element probability of survival is compared. It was anticipated that some difference in the surface probability of survival would be noted because the three-dimensional model includes the surface area between blades. However, the surface probability of survival is not as significant as the volume probability of survival for the gasifier turbine. The small difference in volume probability of survival is primarily a result of the addition of fillets in the blade root of the three-dimensional model.

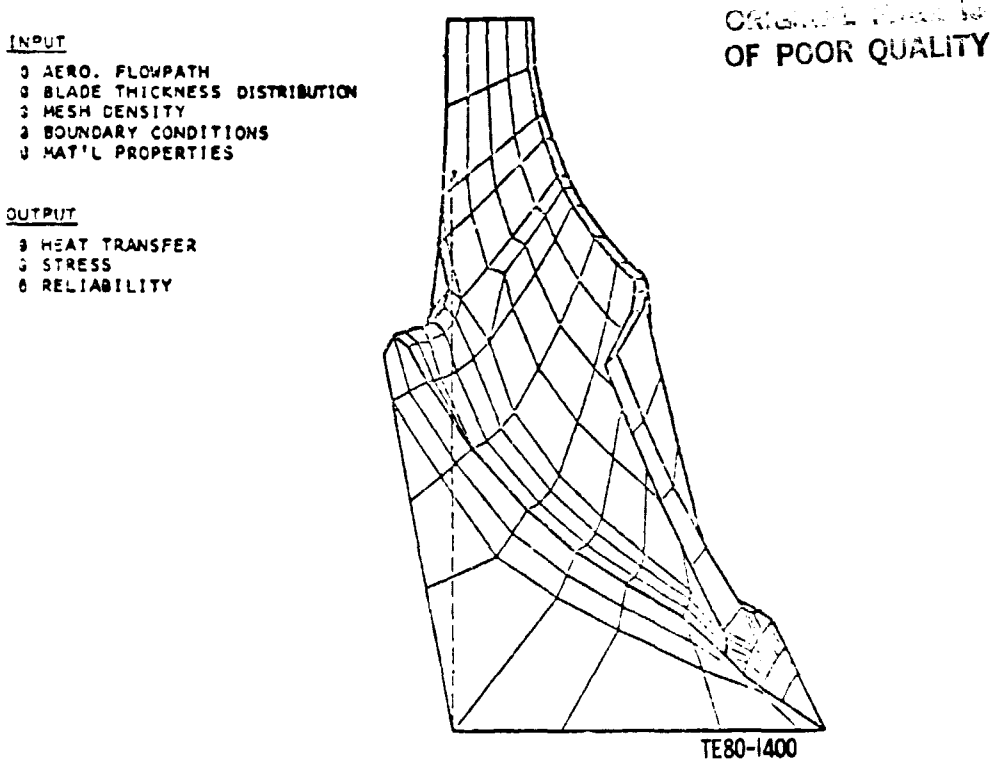

Figure 115. - Three-Dimensional Finite Element Model of Radial Turbine.

Finite element analysis at max power steady state
(sintered alpha silicon carbide, MOR = 50 ksi, m = 8)

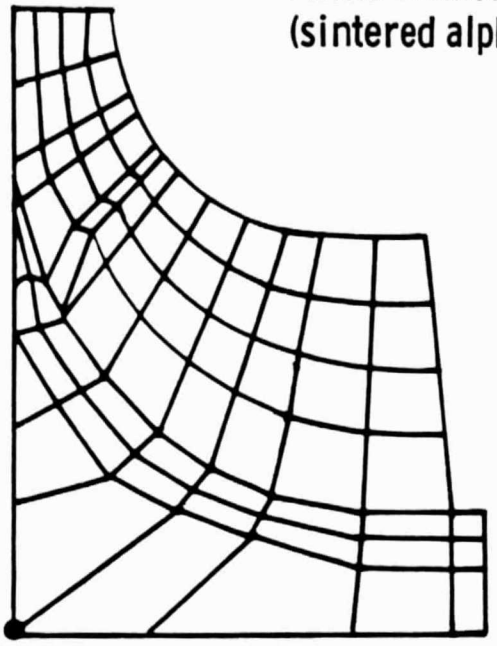

Axisymmetric (2D) model

Probability of survival

Surface	0.9974
Volume	0.8333
Total	0.8312

- Max principal stress 170 MPa (24.7 ksi)

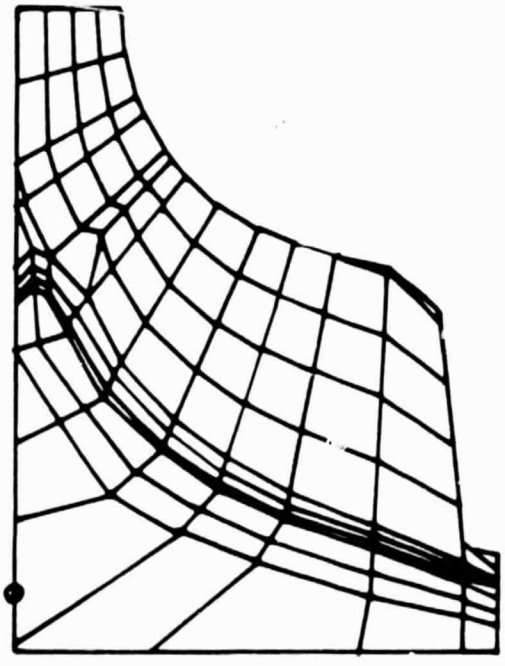

3-D Model

Probability of Survival

Surface	0.9955
Volume	0.8100
Total	0.8063

- Max principal stress 169 MPa (24.6 ksi)

TE80-1401

Figure 116. - Comparison of Two- and Three-Dimensional Finite Element Model--Results for Ceramic RPD Gasifier Turbine.

Shaft Joint Analysis

The attachment of the ceramic rotors to metal shafts has been investigated, and several approaches have been defined for further analysis. One configuration uses a slotted spool of an intermediate expansion material (e.g., Columbium) to adapt the ceramic wheel to the metal shaft. The proposed adaptor material has to have a relatively high temperature capability because of the high conductivity of silicon carbide, which is a candidate rotor material.

Without modification, the joint temperature would be in excess of 870°C (1600°F). However, a temperature below 650°C (1200°F) is required to minimize the oxidation problem and permit the use of low expansion superalloys such as Incoloy 903. Possible means of lowering this joint temperature have been investigated.

One approach would be to cool the joint region with compressor discharge air. But analysis of this approach indicates an unacceptable level (4%) of engine airflow would be required to lower the peak joint temperature to 650°C (1200°F), as shown in Figure 117. This is again a result of the high conductivity of the silicon carbide rotor, which transmits the heat to the joint interface.

Another approach would be to reduce the heat conducted to the joint by interposing a low conductivity thermal barrier. This approach appears promising and is currently being followed.

Revised Two-Dimensional Analysis Results

Refinements have been made to the two-dimensional finite element models of both the gasifier and power turbine to reflect the power transfer configuration, the addition of balance stock, the effects of gas recirculation resulting from backface pumping, and the new joint configuration. The steady-state maximum power results are shown in Figure 118. In addition, transient schedules shown in Figure 119 were used to generate thermal conditions for a severe engine transient.

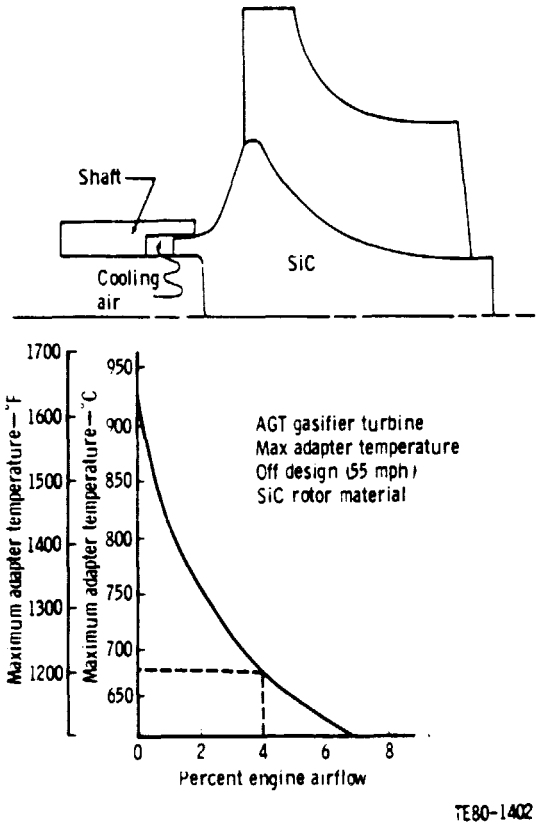

Figure 117. - Effect of Cooling Air on Joint Temperature.

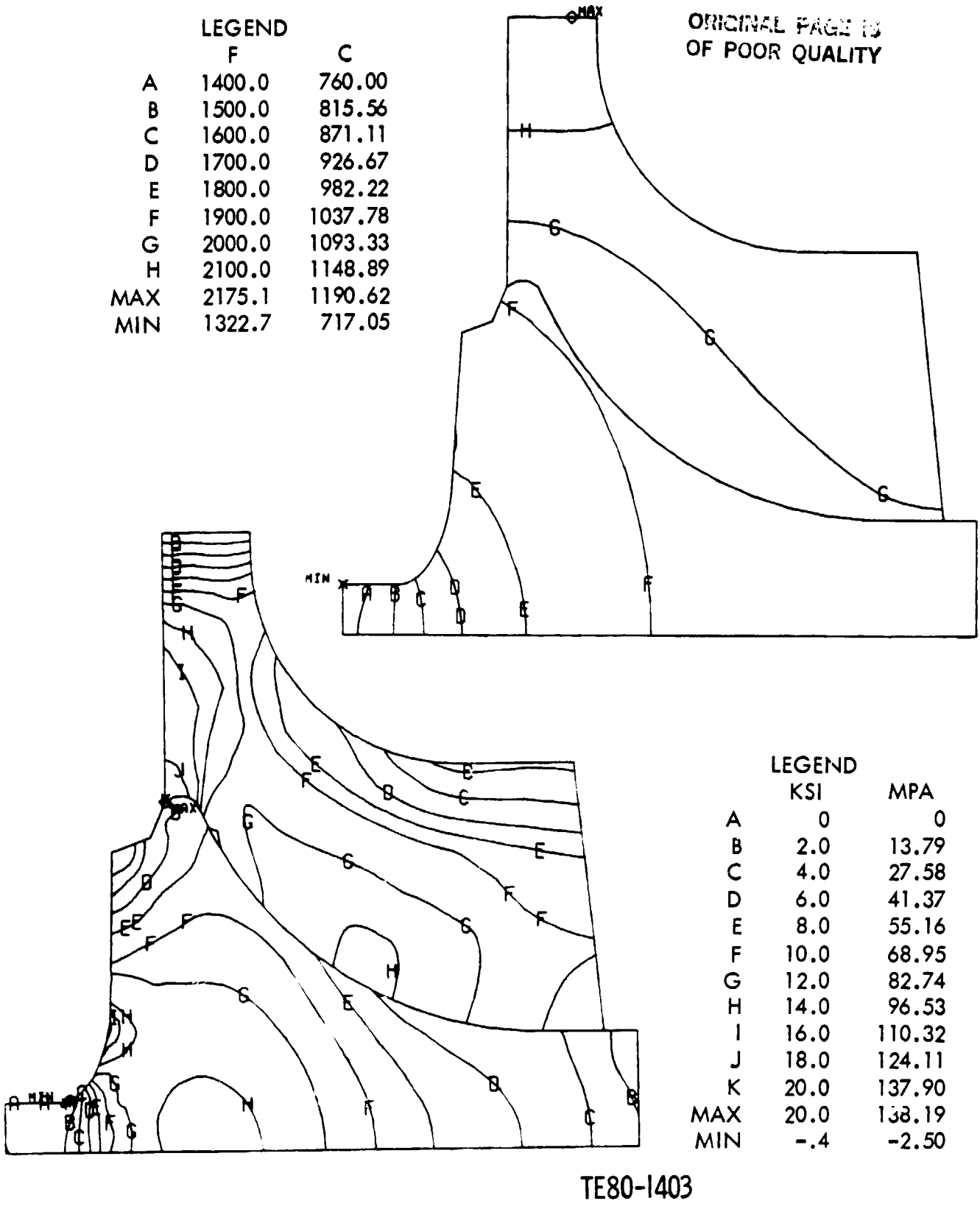

Figure 118. - AGT RPD Gasifier Turbine, Steady-State, Maximum Power Results.

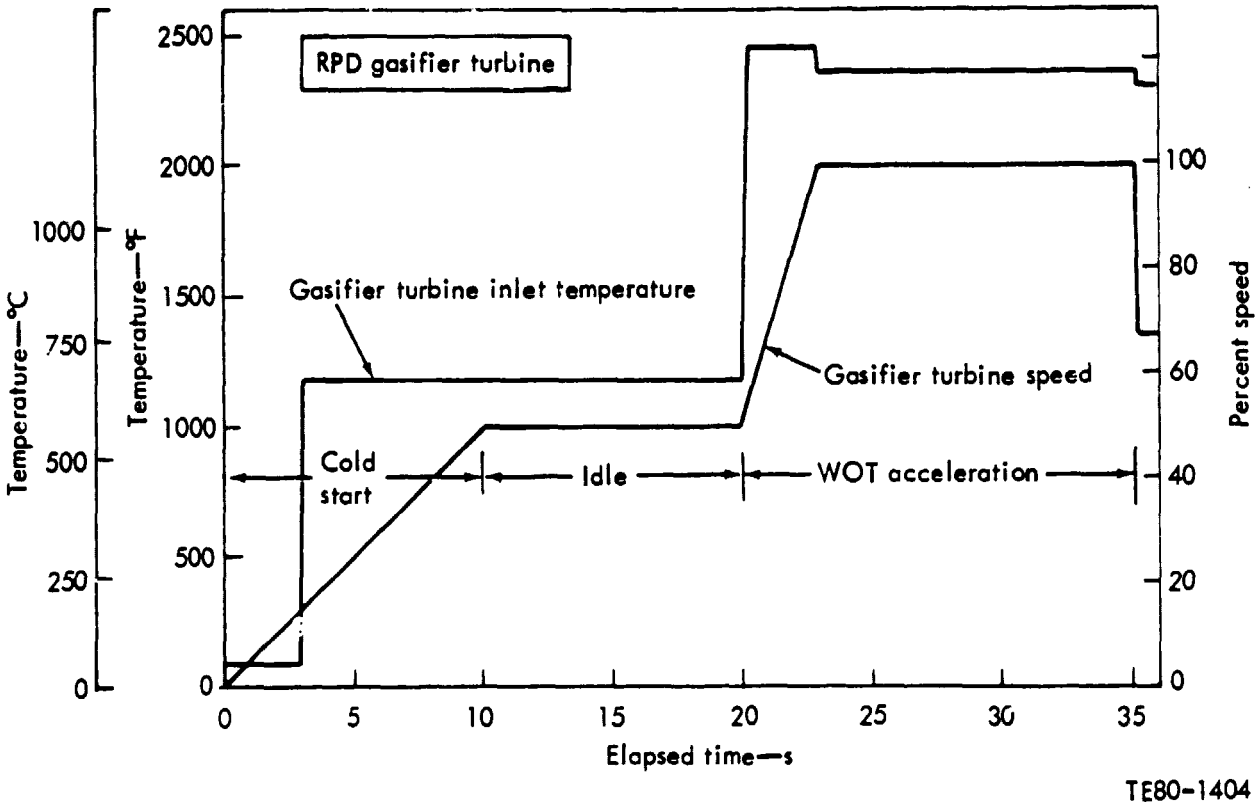

Figure 119. - AGT-100 Cold Start to Maximum Transient.

Calculation of the gasifier rotor's probability of survival using Weibull material parameters indicate a minimum point is reached at the 32 seconds elapsed time. The corresponding stress and temperature results are shown in Figure 120.

The transient analysis results have also been used to establish the required material strength for each wheel to achieve the design probability of survival goal. Figure 121 compares the required strength levels for s ed alpha silicon carbide for both rotors. The gasifier turbine requirement is slightly less than the level reported previously. Even though the power turbine operates at a higher tip speed, the material strength requirement is less than that for the gasifier. This is explained by reduced thermal stresses in the power turbine as a result of lower operating temperatures and reduced thermal gradients.

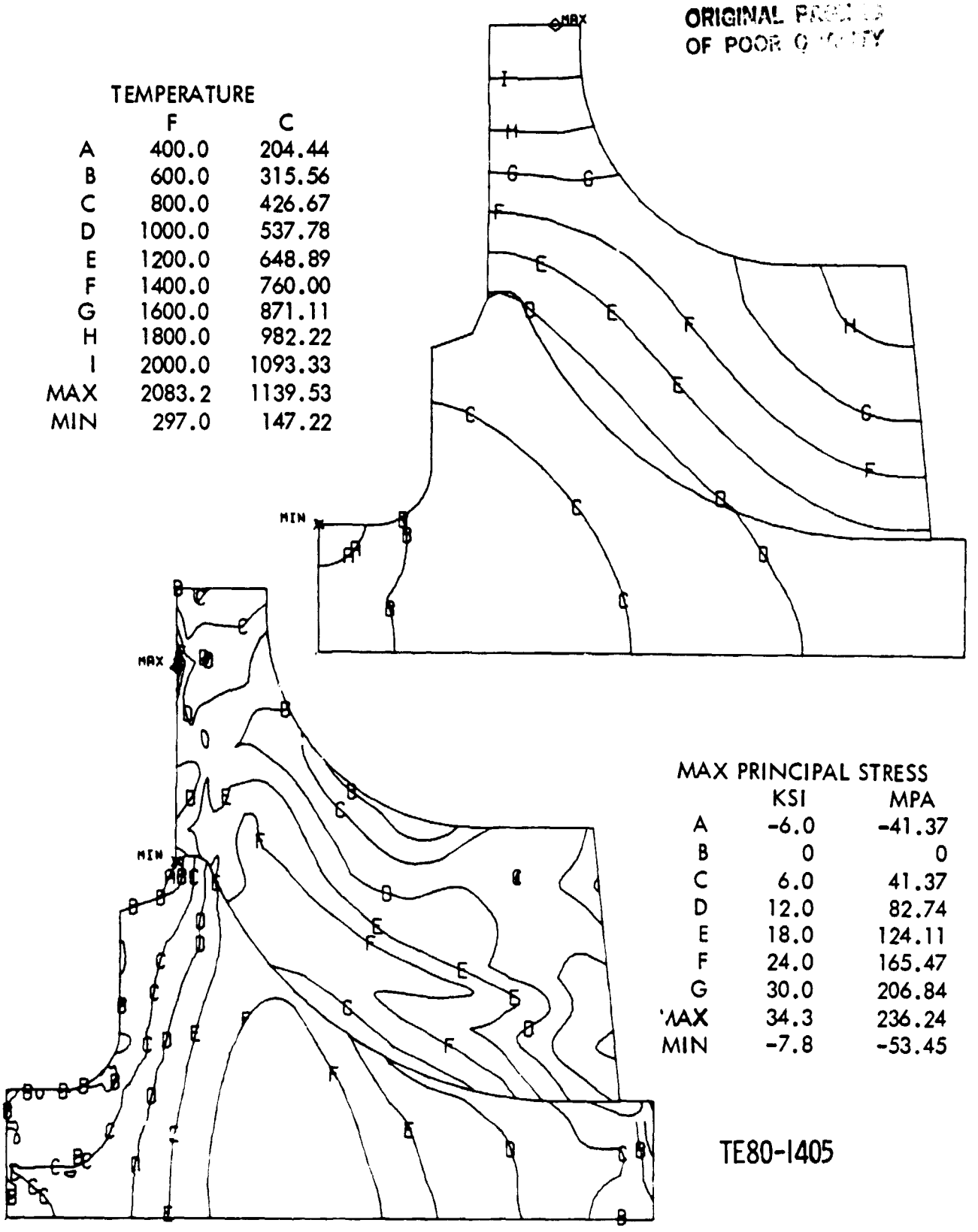

Figure 120. Ceramic Gasifier Turbine Maximum Transient Results.

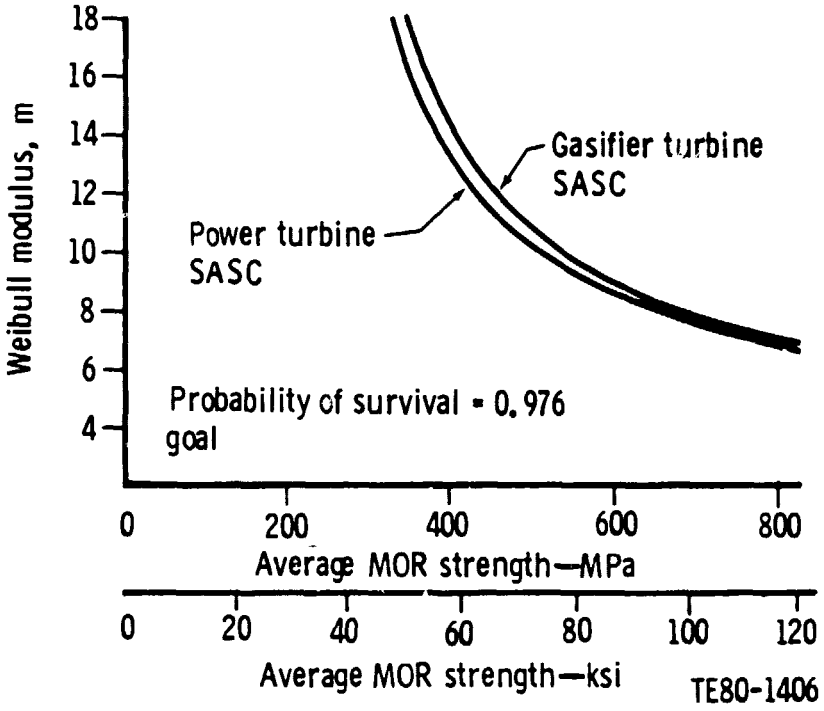

Figure 121. - Material Strength Requirements for Ceramic Turbines.

V. POWER TURBINE DEVELOPMENT

5.1 POWER TURBINE AERODYNAMIC DEVELOPMENT

Similar to other AGT-100 components, the power turbine is required to operate over a wide range with high efficiency. Aerodynamic design to achieve this goal must be consistent with stress, heat transfer, vibration, and mechanical design requirements. To be competitive in the automotive market, the high efficiency must be achieved with recognition of the requirement for low cost and low inertia. Although larger than the AGT-100 gasifier turbine, the design of the power turbine is challenging because of small size, ceramic construction, and relatively low Reynolds number.

Development activity during this period has focused on design of the RPD power turbine and exhaust duct, preliminary design of the Mod I power turbine, layout and fabrication of the interturbine duct/scroll bench rig, and layout of the power turbine test rig.

RPD Power Turbine Design

The RPD engine cycle requirements for the power turbine at the maximum power, sea level static, condition are:

Inlet temperature, °C (°F)	1109 (2028)
Inlet pressure, kPa (psia)	229.06 (33.22)
Fuel/air ratio	0.0129
Equivalent flow, $W\sqrt{\theta}_{cr}\,\epsilon/\delta$, kg/s (lbm/sec)	0.322 (0.707)
Equivalent work, h/θ_{cr}, kJ/kg (Btu/lbm)	49.24 (21.17)
Equivalent speed, $N/\sqrt{\theta}_{cr}$, rpm	31,450
Expansion ratio (Total - Total)	2.064
Efficiency without inlet scroll (Total - Total)	86.70

Although the turbine operates at the maximum power point only a small fraction of the time, this point does represent the most severe steady-state structural design condition. The maximum power condition, therefore, has been selected as the design point to ensure a systematic integration of fabrication, aerodynamic, heat transfer, stress, and vibration design disciplines. The design process commences with aerodynamic definition of flow path, vane and blade contours, and thickness distribution.

Flow Path Selection

Several factors are involved in the selection of "optimum" flow-path parameters. First is the realization that part power is emphasized at the expense of full-power performance. Caution must be used, however, to avoid any severe efficiency reduction at maximum power, which would result in unacceptable vehicle response. A second major factor is the selection of aerodynamic and geometric parameters consistent with structural design for long life and low cost. This second factor becomes particularly important with respect to achieving adequate life of the ceramic wheel. A third important consideration in design relates to selection of flow-path parameters conductive to low inertia.

The power turbine flow path selected to satisfy the AGT-100 turbine design criteria is illustrated in Figure 122. This turbine features a symmetrical vane with endwall contouring and a low inertia rotor. Salient features of the turbine design are:

Vane inlet diameter, mm (in.)	186.02 (7.324)
Rotor tip diameter, mm (in.)	148.08 (5.830)
Vaneless space diameter ratio	1.06
Rotor tip width, mm (in.)	11.04 (0.4346)
Exducer hub/tip radius ratio	0.300
Rotor tip diameter/exducer tip diameter ratio	1.652
Rotor tip width/rotor tip diameter ratio	0.0745

Operating at the SLS maximum power condition, the turbine exhibits a tip speed of 527 m/s (1730 ft/sec), an aerodynamic loading parameter (U/C - Tip Speed/ Isentropic Spouting Velocity) of 0.724 and a specific speed of 80. Turbine parameters for several engine operating points under road-load conditions are presented in Table XVI.

TABLE XVI. RPD POWER TURBINE PARAMETERS FOR VARIOUS ENGINE OPERATING POINTS

Speed, km/h (mph)	Idle	32 (20)	48 (30)	80 (50)	102 (70)	Max* power	Max power** (SL)
Turbine power, kW (hp)	1.48 (1.98)	2.56 (3.44)	4.30 (5.76)	9.31 (12.49)	21.10 (28.30)	64.98 (87.14)	74.09 (99.36)
Inlet temperature, °C (°F)	634 (1174)	979 (1795)	1106 (2022)	1128 (2062)	1113 (2035)	1113 (2035)	1109 (2028)
Equivalent flow, kg/s (lbm/sec)	0.159 (0.350)	0.168 (0.369)	0.175 (0.385)	0.224 (0.493)	0.261 (0.574)	0.314 (0.691)	0.322 (0.707)
Equivalent work, kJ/kg (Btu/lbm)	5.07 (2.18)	7.02 (3.02)	10.30 (4.43)	15.96 (6.86)	26.45 (11.37)	46.87 (20.15)	49.24 (21.17)
Equivalent speed, %	24.5	32.8	47.0	53.0	74.6	99.9	100.00
Expansion ratio (T-T)	1.075	1.099	1.149	1.237	1.441	1.990	2.064
U/C	0.545	0.638	0.751	0.688	0.745	0.740	0.724
Mean reaction	0.356	0.434	0.543	0.479	0.537	0.546	0.533
N_s	55.7	63.3	71.4	68.4	74.7	80.3	79.8
N_{RE}	29,000	20,800	20,800	28,100	39,200	68,100	74,200
Swirl angle, deg	-9.9	+4.1	+23.0	+0.2	+14.0	+1.6	-2.0
$M_{N_{exit}}$	0.071	0.076	0.092	0.117	0.160	0.254	0.269

*Ambient temperature: 29°C (85°F), altitude: 152 m (500 ft).
**Ambient temperature: 15°C (59°F), altitude: sea level.

The power turbine is required to operate over a much larger range of speed and flow than the gasifier turbine. In order to accent part power performance the aerodynamic loading coefficient (U/C) was selected to be larger than optimum (U/C = 0.7) at the high power points. Mean static pressure reaction varies from 0.356 at idle to 0.546 at the maximum power condition. The exit swirl variation is from -9.9 deg at idle to +23 deg at 48.4 km/h (30 mph).

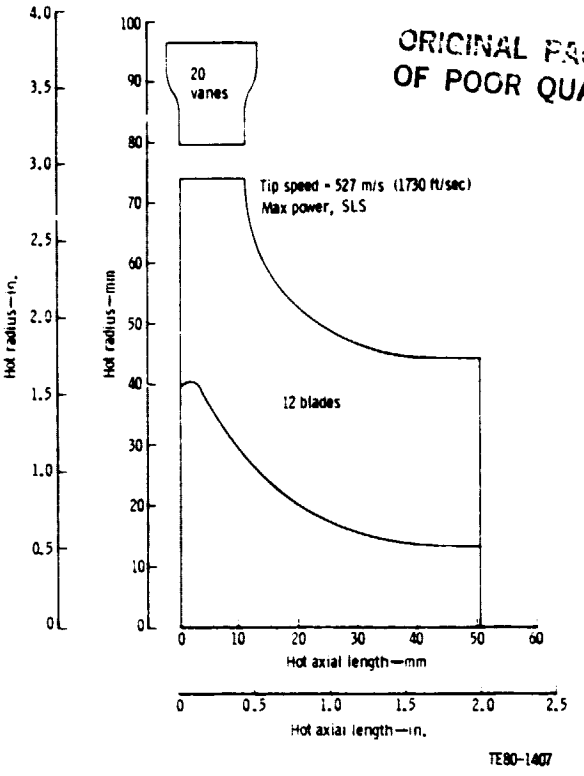

Figure 122. - RPD Power Turbine Flow Path.

The power transfer engine concept assists the power turbine. This results in a cycle component match that allows the power turbine to operate at nearly peak efficiency over most of the operating range. Figure 123 illustrates the ratio of power turbine power to the power turbine shaft power over the engine road-load operating range.

Similar to the work performed on the gasifier turbine, a sensitivity study of critical design parameters was made to verify flow-path selection. This study included specific speed, tip diameter, vane exit angle, exducer hub/tip radius ratio, and exducer area.

Specific Speed

Speed selection for the power turbine is more flexible than that encountered for the gasifier turbine since considerations for compressor performance are not present. As shown in Figure 124, the RPD design specific speed of 80 is nearly optimum. Consistent with the requirement for long life, the selection has been made toward lower specific speed to provide reduced blade stresses.

Tip Diameter

The emphasis to part power performance necessitates a tip diameter larger than that dictated by the maximum power operating point. As shown in Figure 125, the RPD design tip diameter has been selected to provide a good compromise of performance over the operating range.

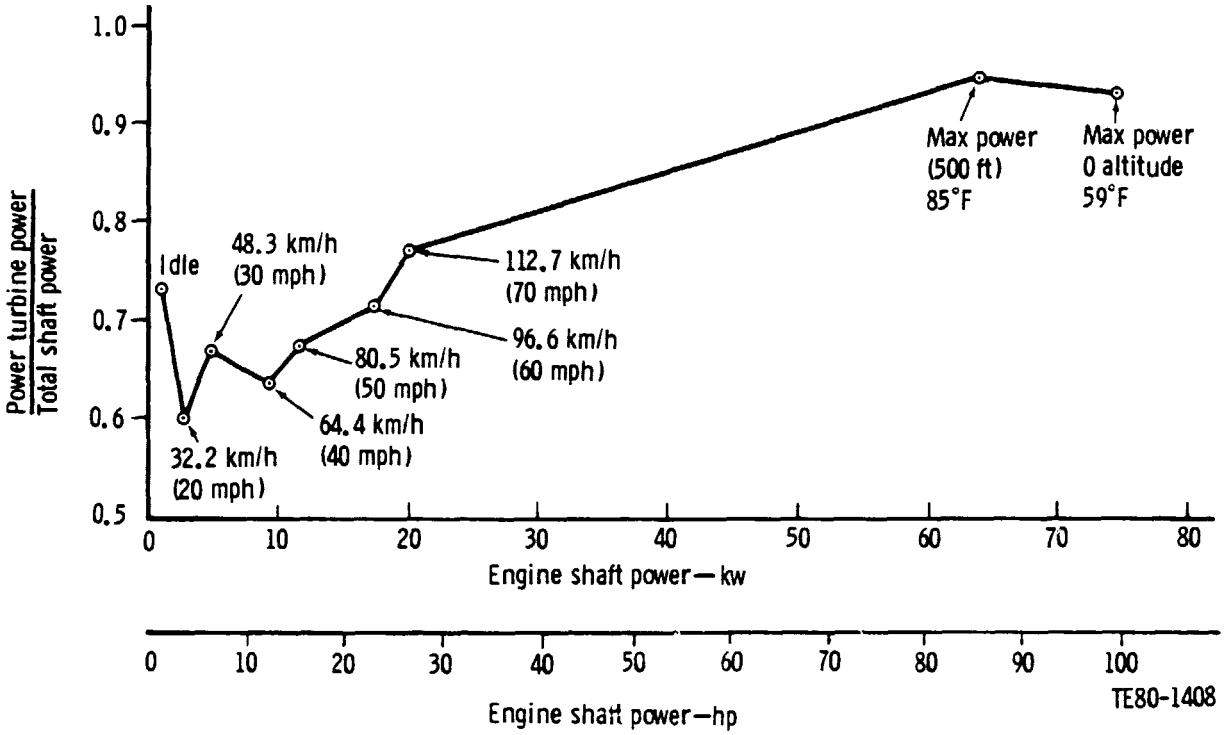

Figure 123. - Ratio of RPD Power Turbine to Total Shaft Power.

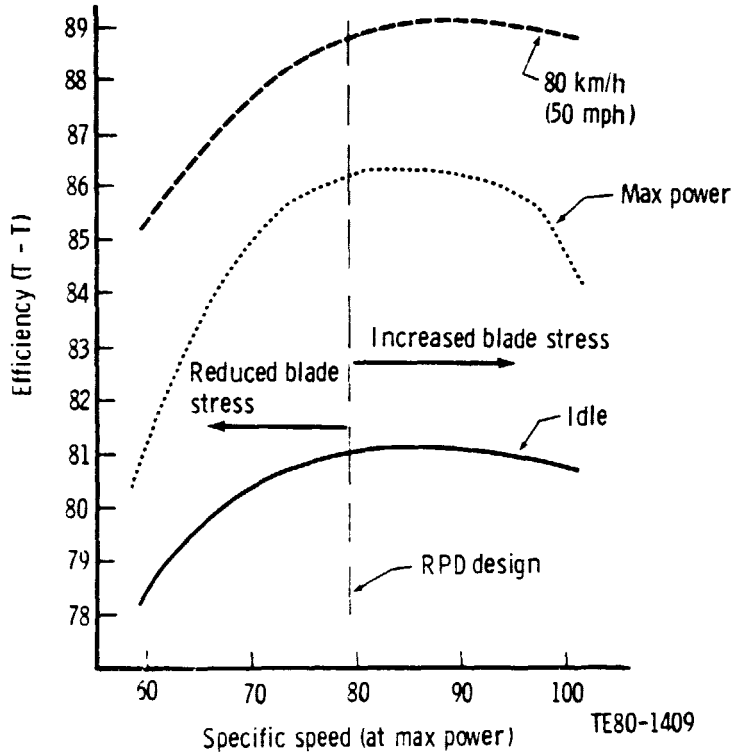

Figure 124. - Effect of Specific Speed on RPD Power Turbine Efficiency.

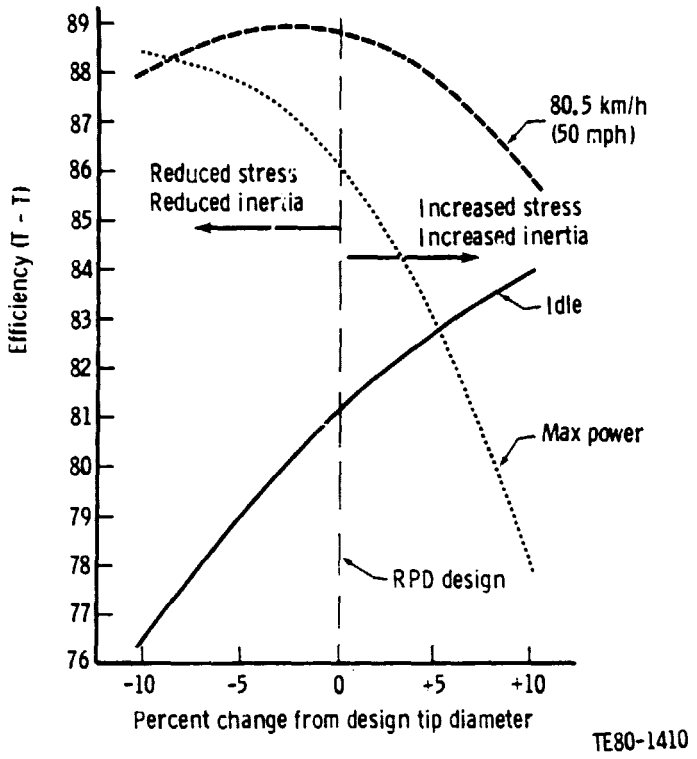

Figure 125. - Effect of Tip Diameter on RPD Power Turbine Efficiency.

Vane Exit Angle

Figure 126 presents the effect of vane exit angle on turbine efficiency. Similar to the gasifier turbine, the angle selection was made toward the hign values to allow higher reaction levels.

Exducer Hub/Tip Radius Ratio

The hub/tip radius ratio of 0.3 for the RPD design is identical to the gasifier. This value provides for high efficiency, as evident in Figure 127 and adequate hub area for dynamic balance.

Exducer Area

Figure 128 illustrates the effect of exducer area on power turbine efficiency. An increase in area over the RPD design would result in higher total-static efficiencies, but would pose higher risk in structural design.

Aerodynamic Performance

The aerodynamic performance of the RPD power turbine has been calculated without the inlet scroll. The efficiency goal for the power turbine is illustrated in Figure 129 as a function of engine road-load power. The trend toward higher efficiency at part power is desirable for the automotive duty cycle.

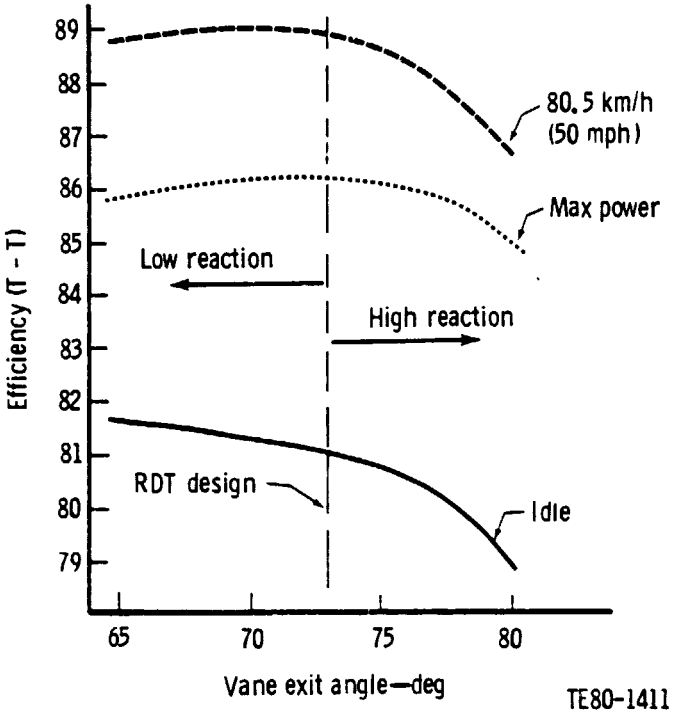

Figure 126. - Effect of Vane Exit Angle on RPD Power Turbine Efficiency.

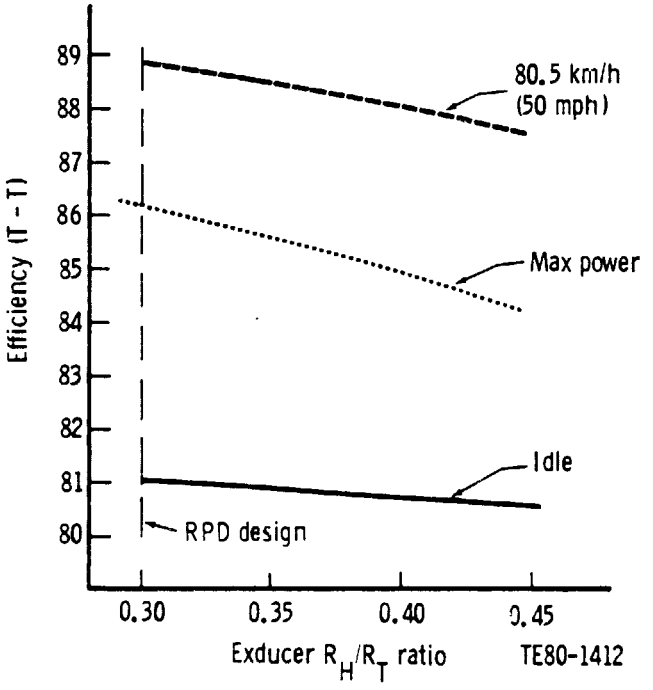

Figure 127. - Effect of Exducer Hub/Tip Radius Ratio on RPD Power Turbine Efficiency.

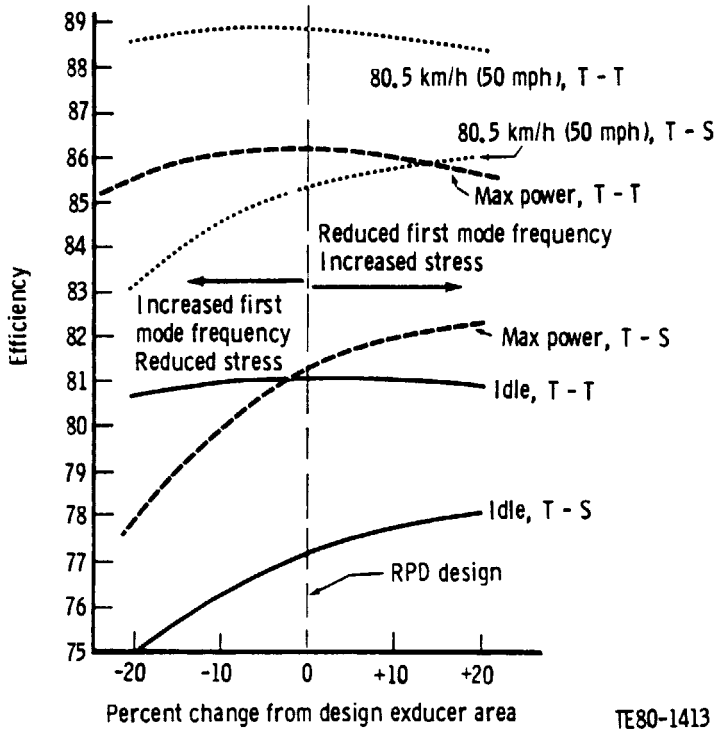

Figure 128. - Effect of Exducer Area on RPD Power Turbine Efficiency.

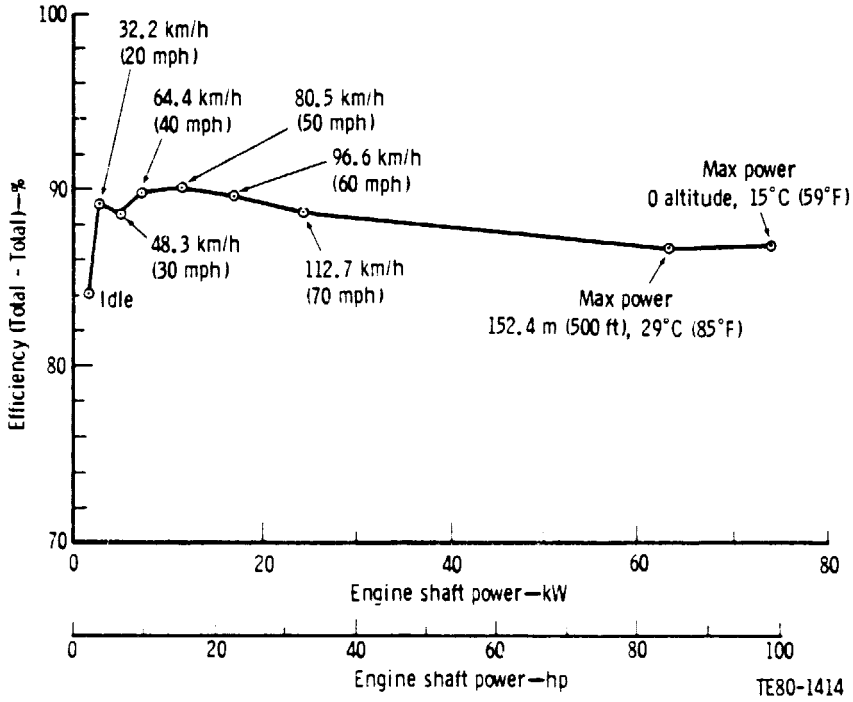

Figure 129. - Efficiency Goal--RPD Power Turbine without Inlet Scroll.

Engine operating points have been superimposed on the torque-speed performance map as illustrated in Figure 130. The majority of the engine operation occurs within the peak efficiency island. Equivalent flow, equivalent work, efficiency, exit swirl, and exit Mach number are illustrated in Figures 131 through 135 as a function of total-to-total expansion ratio.

The preceding turbine performance estimates were calculated through the use of the DDA meanline performance prediction program. This initial effort was followed by a more detailed design analysis using a quasiorthogonal meridional flow analysis. Meridional flow analysis Mach number diagrams for max power (SLS), 80 km/h (50 mph), 48 km/h (30 mph), and idle are presented in Figures 136 through 139.

Scroll Design

The RPD power turbine scroll is similar to the gasifier scroll with regard to design philosophy. However, packaging in the engine compartment more severely constrains the power turbine scroll. In addition, the scroll must accept any flow distortion emanating from the gasifier turbine and interturbine duct.

Scroll cross-sectional shapes at various angular locations are shown in Figure 140. Because of a maximum diameter constraint, the scroll outer diameter does not quite follow an Archimedean spiral. In order to achieve the desired cross-sectional area for the scroll, it was necessary to permit the scroll inner diameter to be less than the vane inlet diameter for 270 deg of the scroll circumference. As with the gasifier scroll, width is circumferentially reduced from the shroud side. The scroll tongue is blended into the nearest vane to minimize flow crossover.

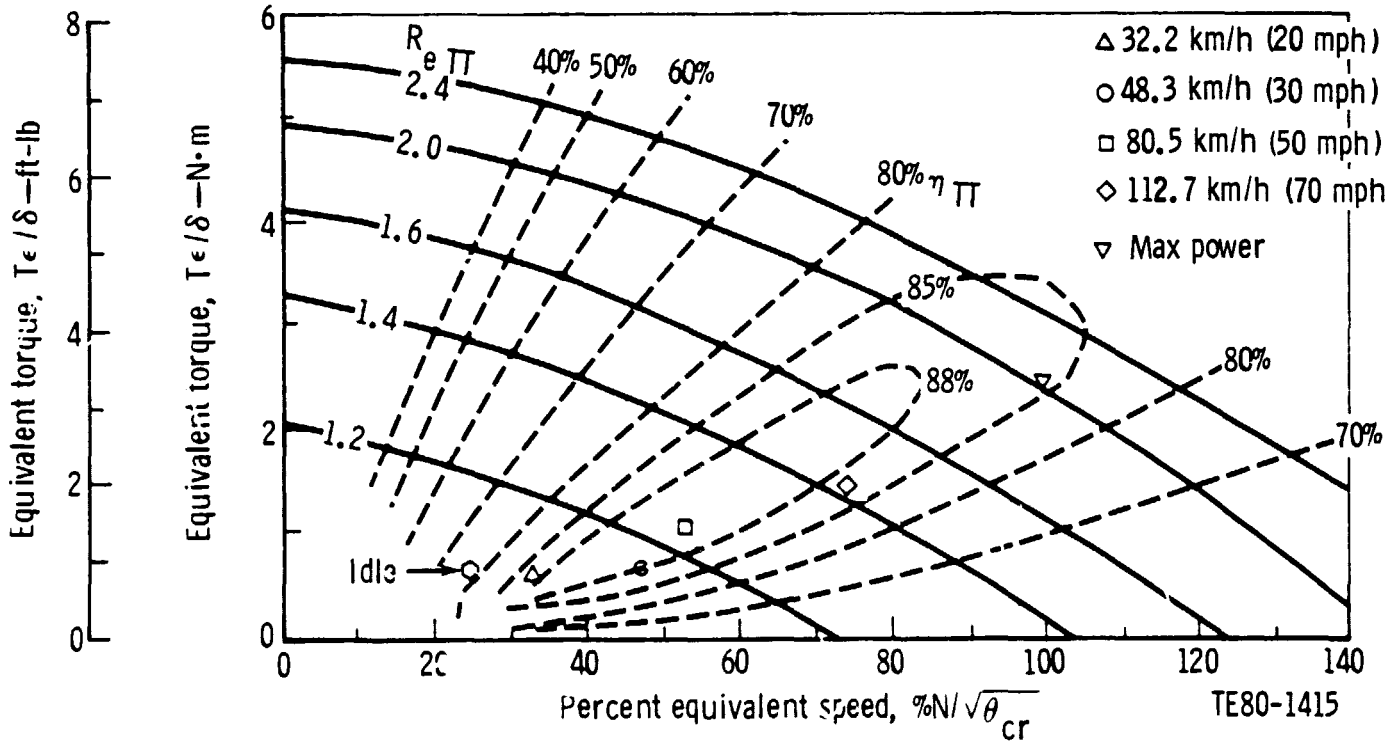

Figure 130. - Predicted Performance Map--RPD Power Turbine without Inlet Scroll.

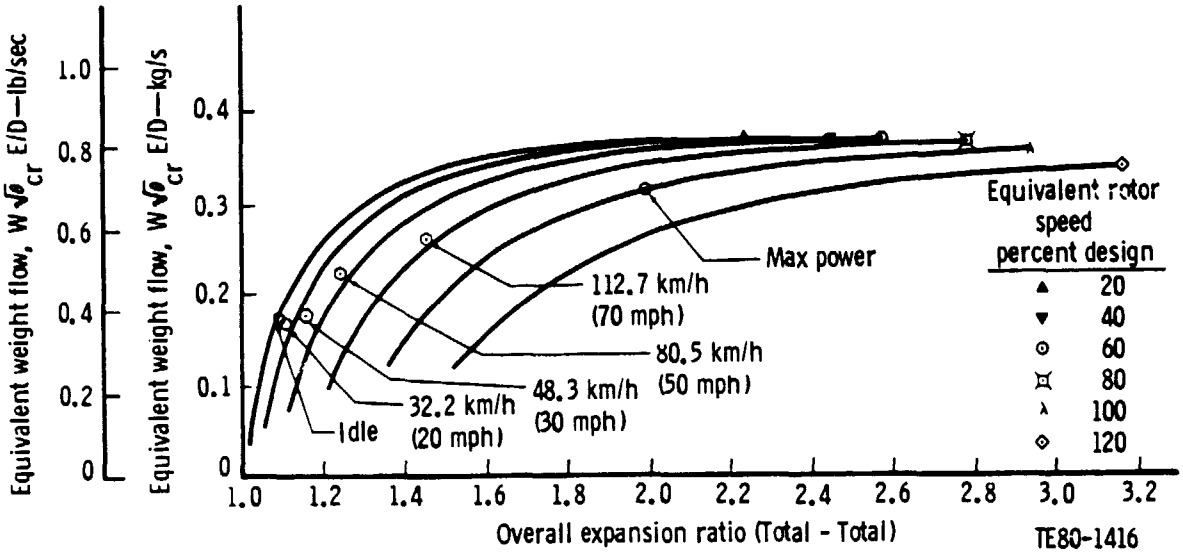

Figure 131. - Predicted Equivalent Flow--RPD Power Turbine.

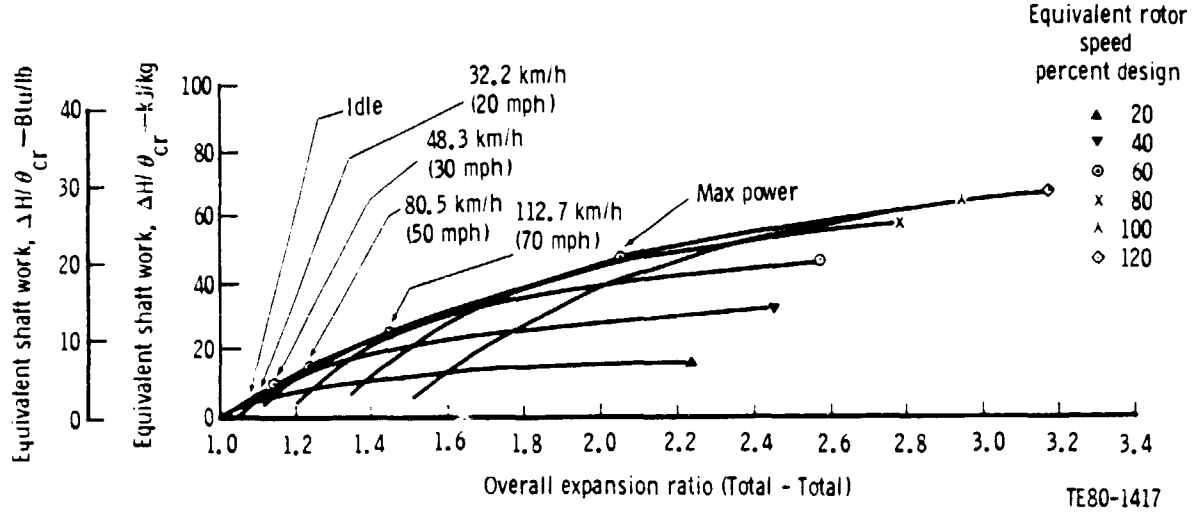

Figure 132. - Predicted Equivalent Work--RPD Power Turbine.

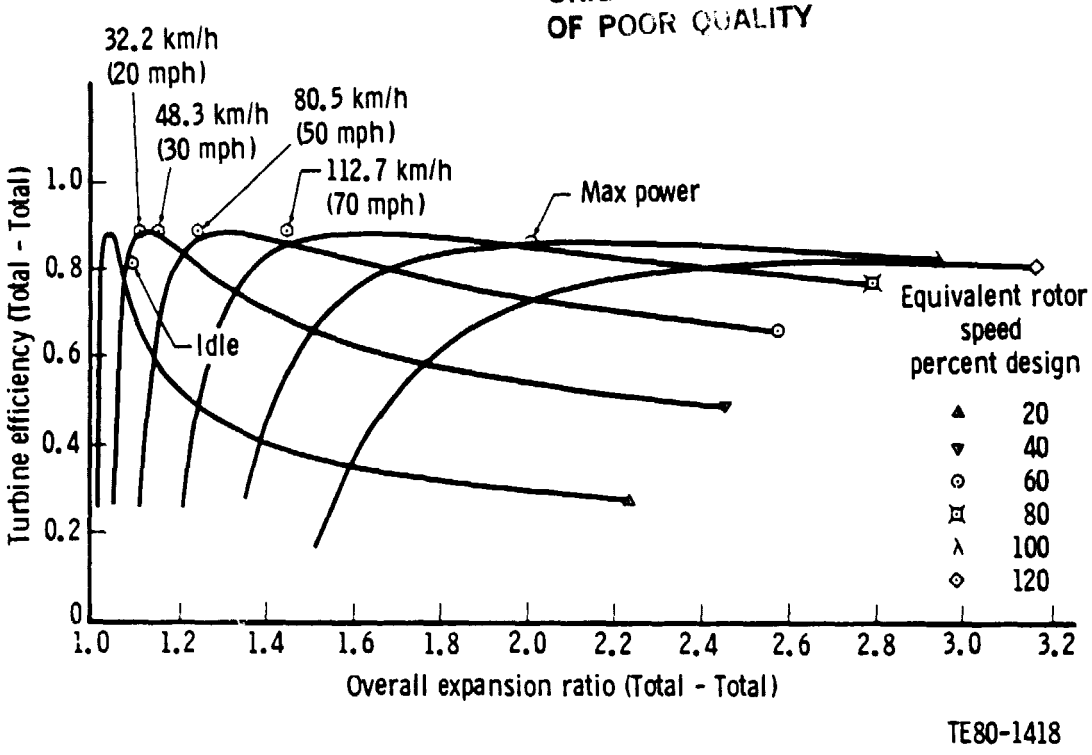

Figure 133. - Predicted Efficiency--RPD Power Turbine.

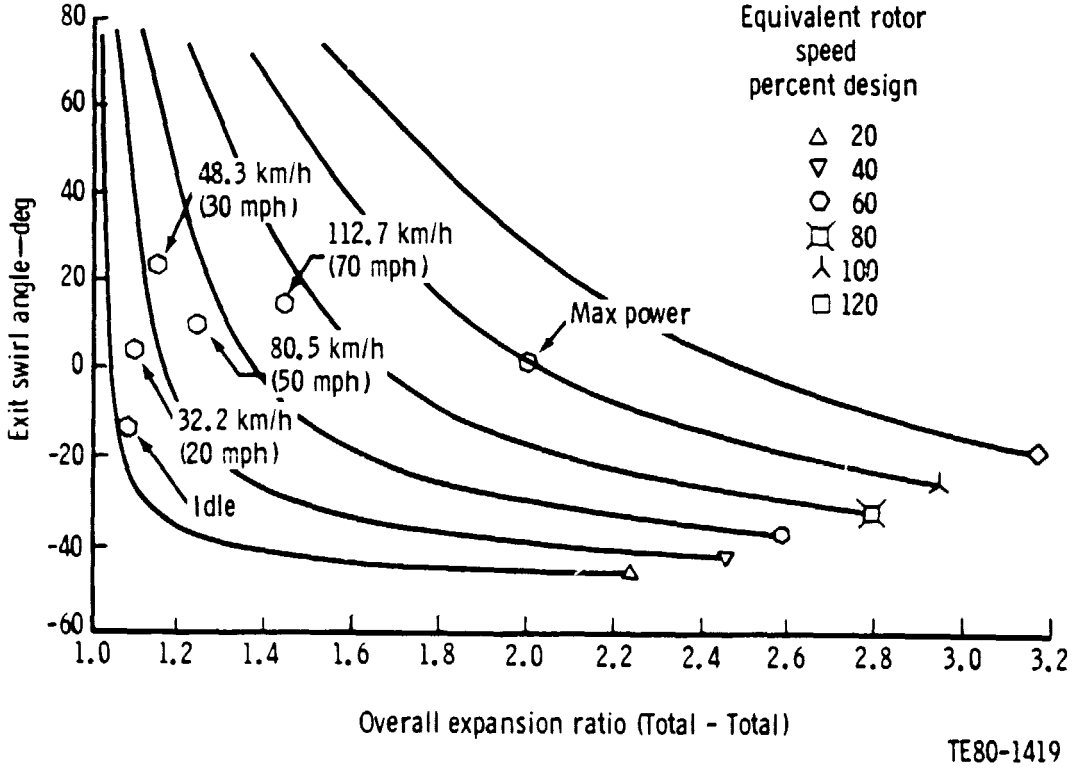

Figure 134. - Predicted Exit Swirl Angle--RPD Power Turbine.

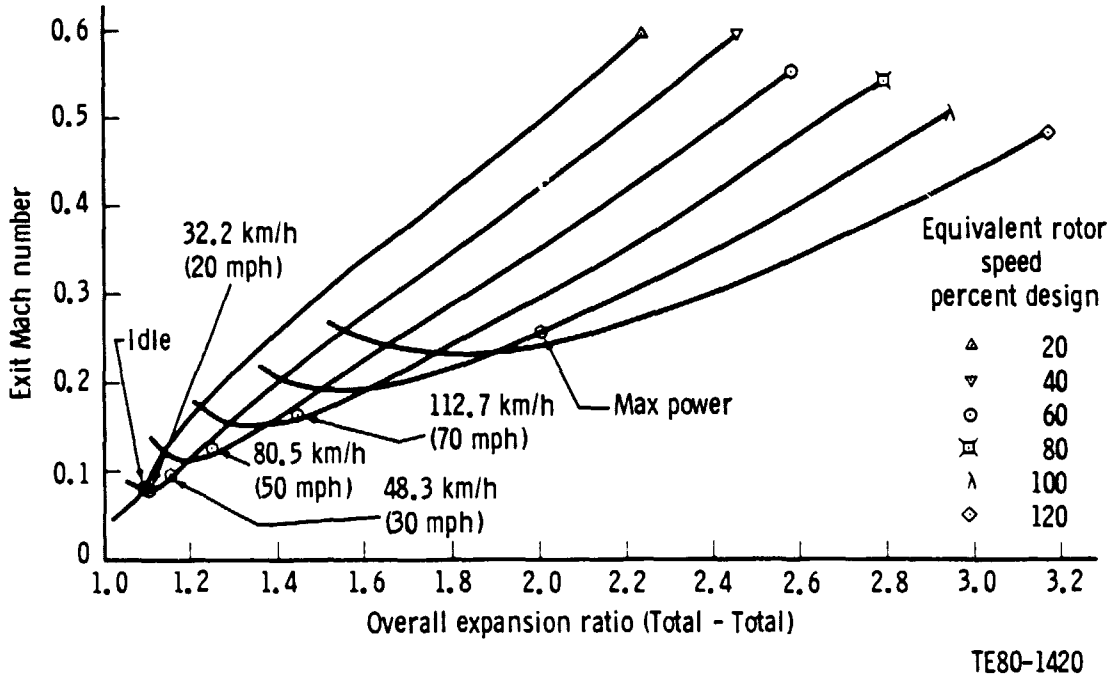

Figure 135. - Predicted Exit Mach Number--RPD Power Turbine.

Through-flow Mach numbers and exit swirl angles for the power turbine scroll are shown in Table XVII. Mach numbers are higher than for the gasifier scroll because of limitations of available space and an acceptable diffusion area ratio of the interturbine duct. The scroll exit angle is circumferentially uniform and varies over the operating range.

Vane Design

The RPD vane is illustrated in Figure 141. Designed for low cost and ceramic construction, the vane exhibits a trailing edge diameter of 0.762 mm (0.030 in.), a leading edge diameter of 5.08 mm (0.20 in.) and a true chord of 31.04 mm (1.222 in.). The vane number of 20 results in a solidity, based on the true chord, of 1.26, a throat width of 7.4 mm (0.2912 in.), and a trailing edge blockage of 9.34%.

The vane design is symmetrical to offer cost reduction in mass production assembly. Cost reduction would occur through not requiring the vanes to be assembled into wall slots with a particular orientation. The symmetrical design exhibited essentially the same aerodynamic characteristics as the cambered version.

Endwall contouring has been incorporated to improve aerodynamic loading of the vane. The favorable effect of meridional contouring on suction surface velocity is evident in Figure 142. Contouring provides a 20% reduction in vane profile loss. Boundary layer displacement thickness and adiabatic form factor for each surface of the RPD vane are illustrated in Figure 143 and 144.

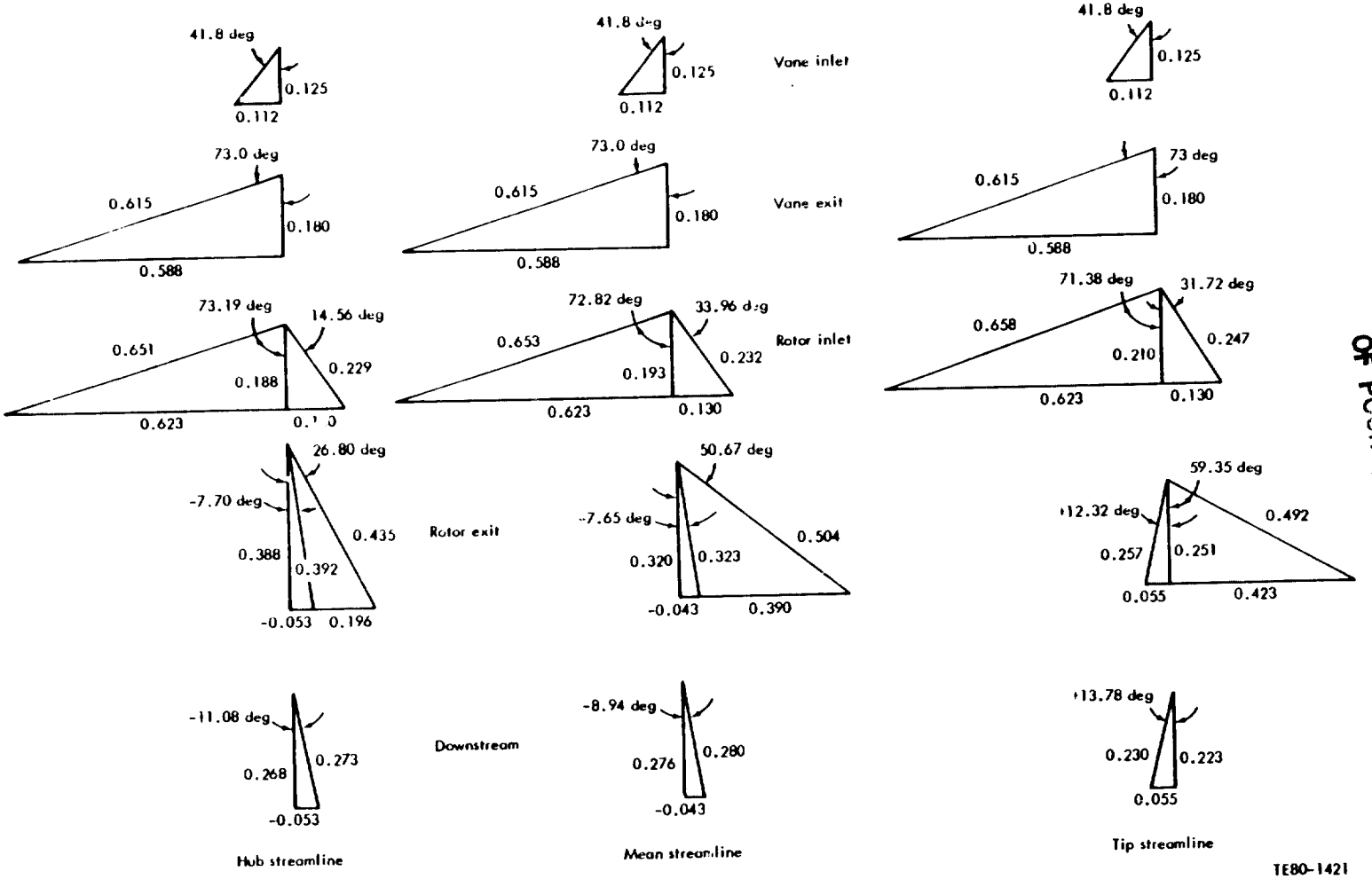

Figure 136. - Design Mach Number Designs--Maximum Power (SLS)--
RPD Power Turbine.

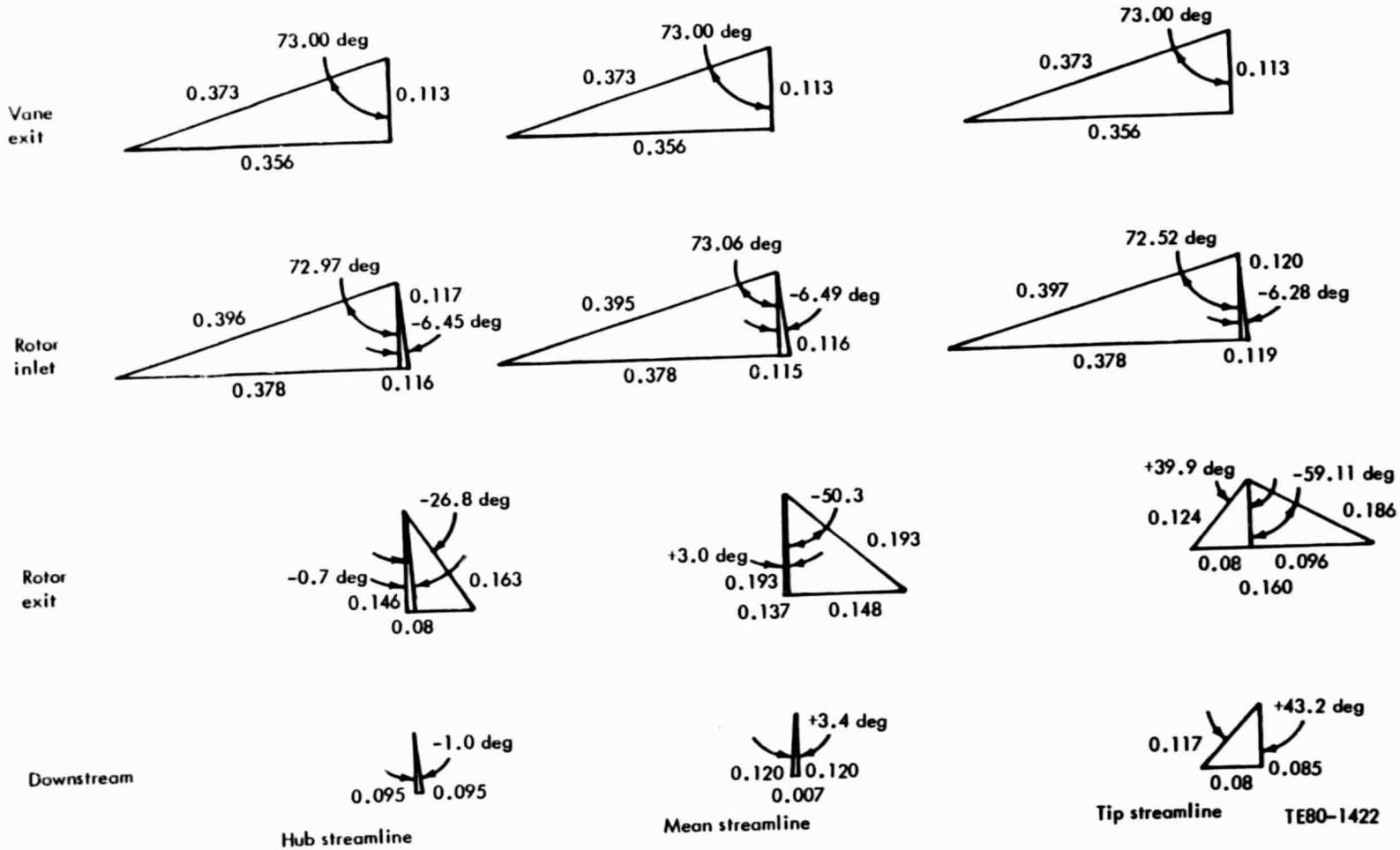

Figure 137. - Design Mach Number Designs--80 km/h (50 mph)--RPD Power Turbine.

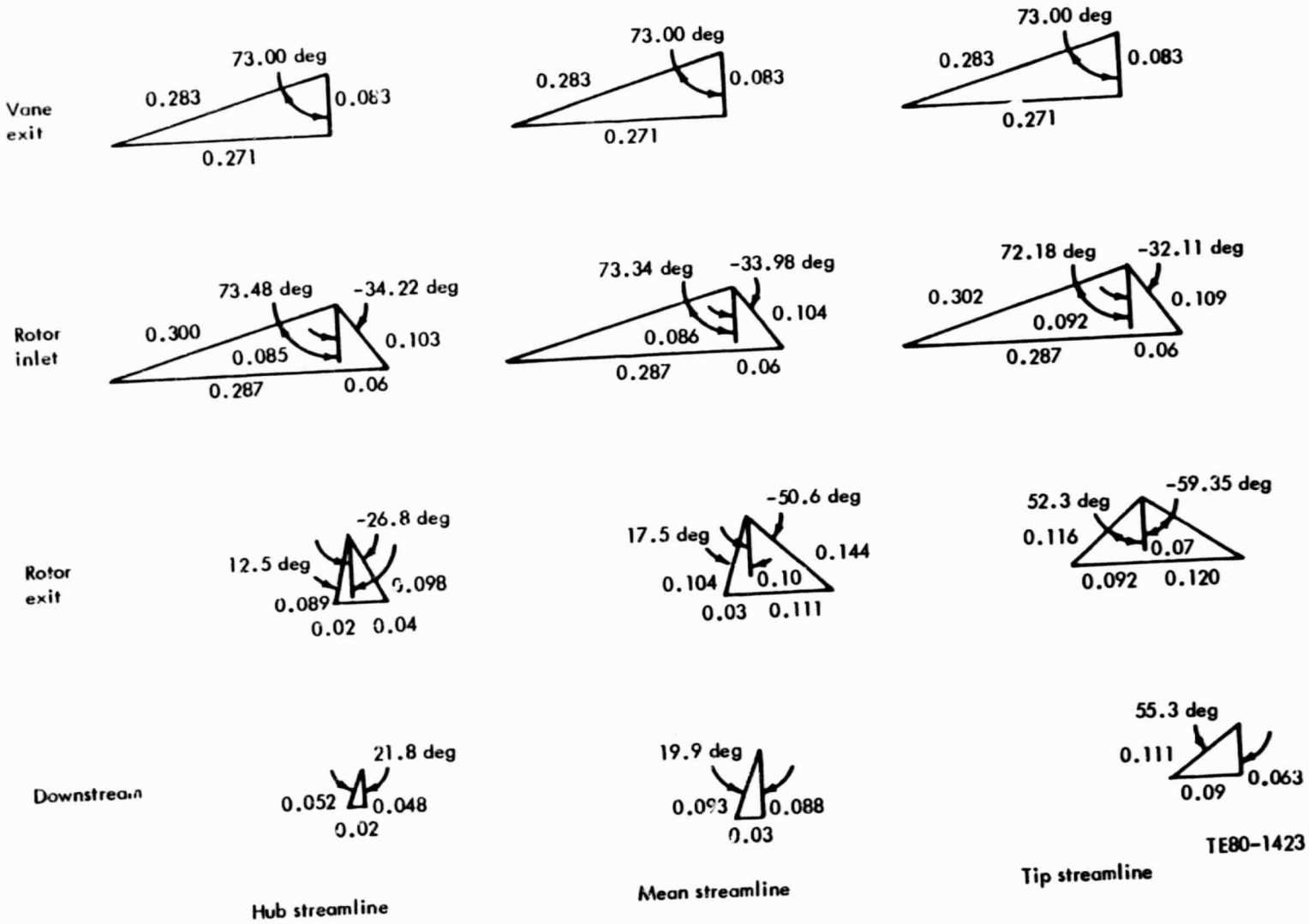

Figure 138. - Design Mach Number Designs--48 km/h (30 mph)--KPD Power Turbine.

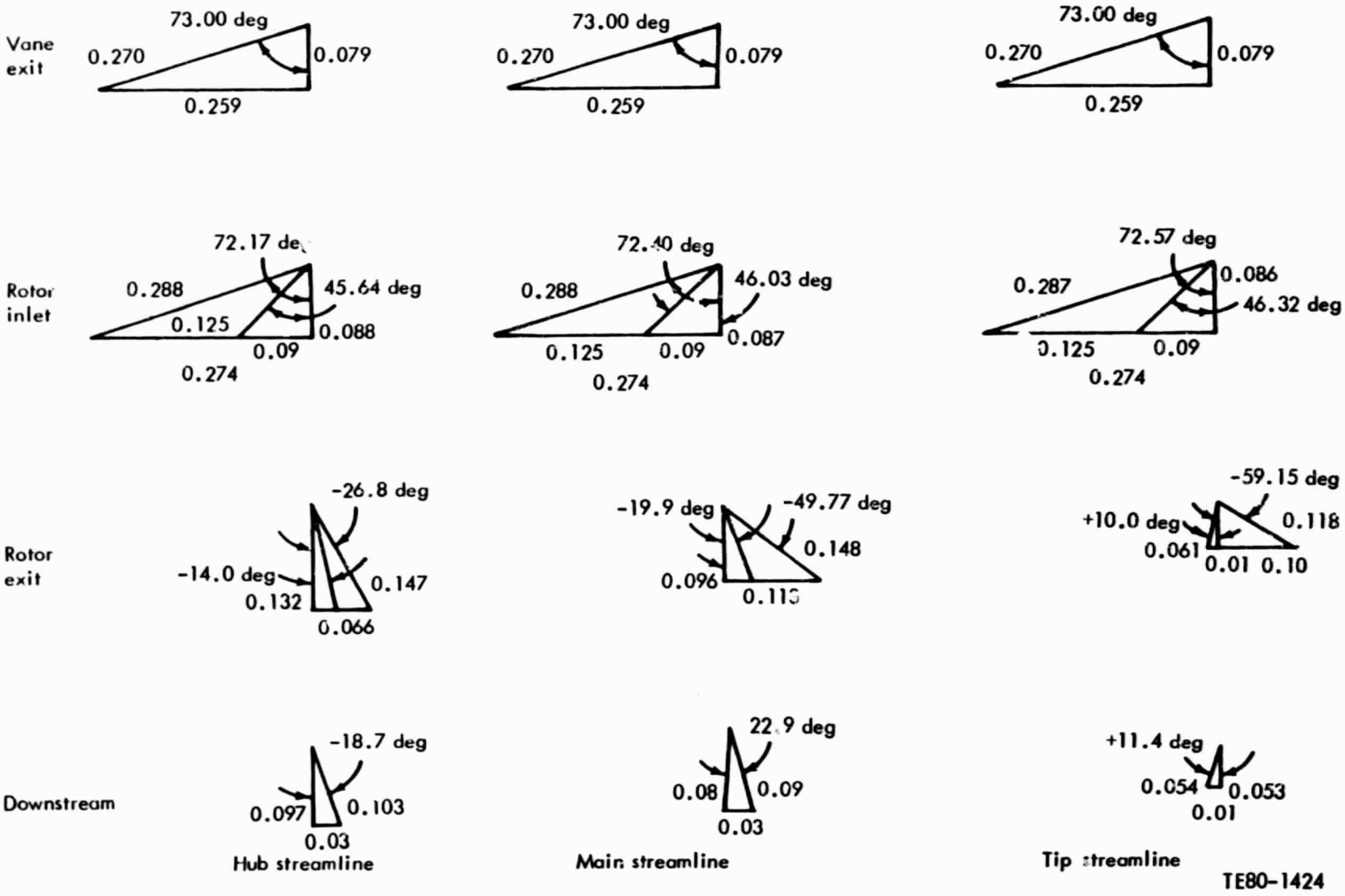

Figure 139. - Design Mach Number Designs--Idle--RPD Power Turbine.

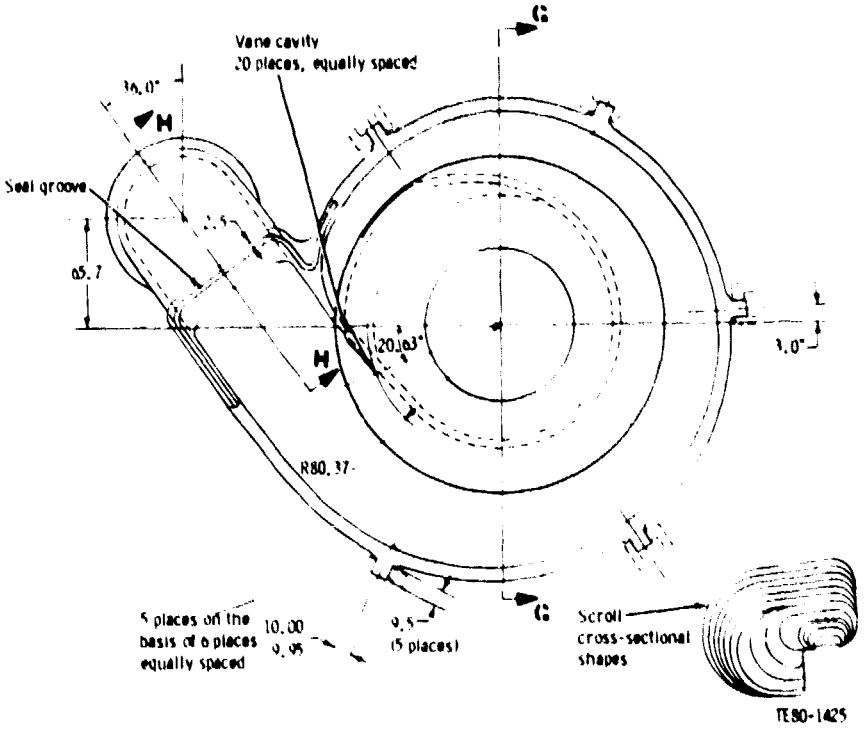

Figure 140. - RPD Power Turbine Scroll.

Design features
- Symmetrical design
- Endwall contouring
- Ceramic construction

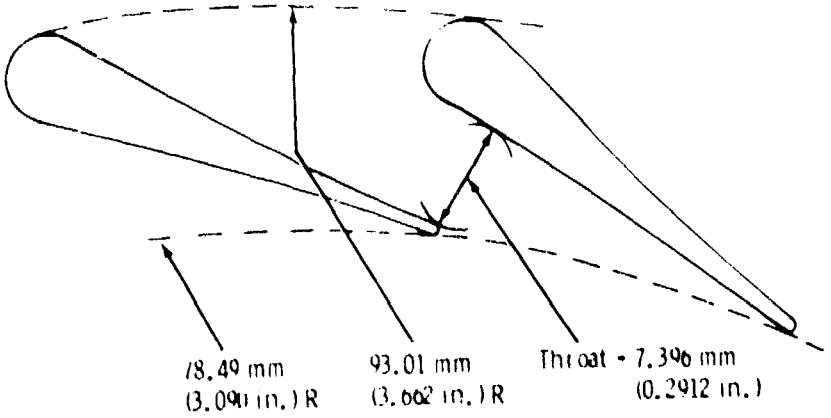

Figure 141. - RPD Power Turbine Vane.

Figure 142. - Effect of Endwall Contouring on Surface Velocity Distribution--RPD Power Turbine Vane.

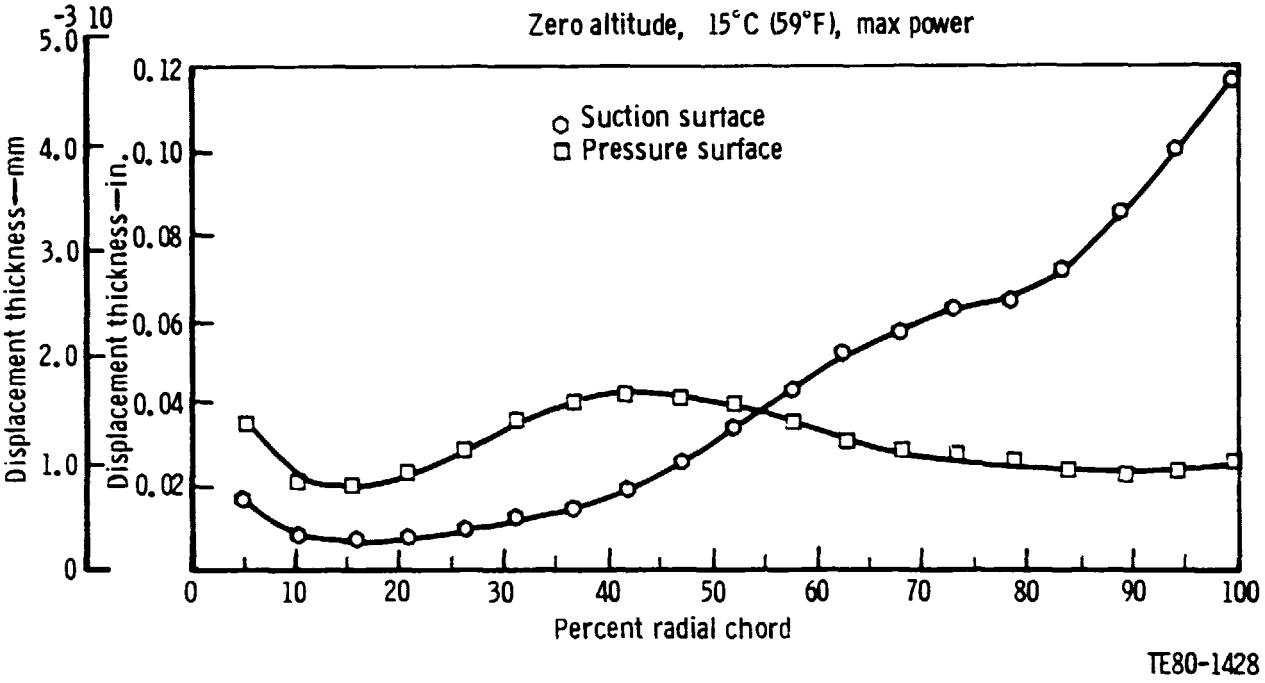

Figure 143. - Boundary Layer Displacement Thickness--RPD Power Turbine Vane.

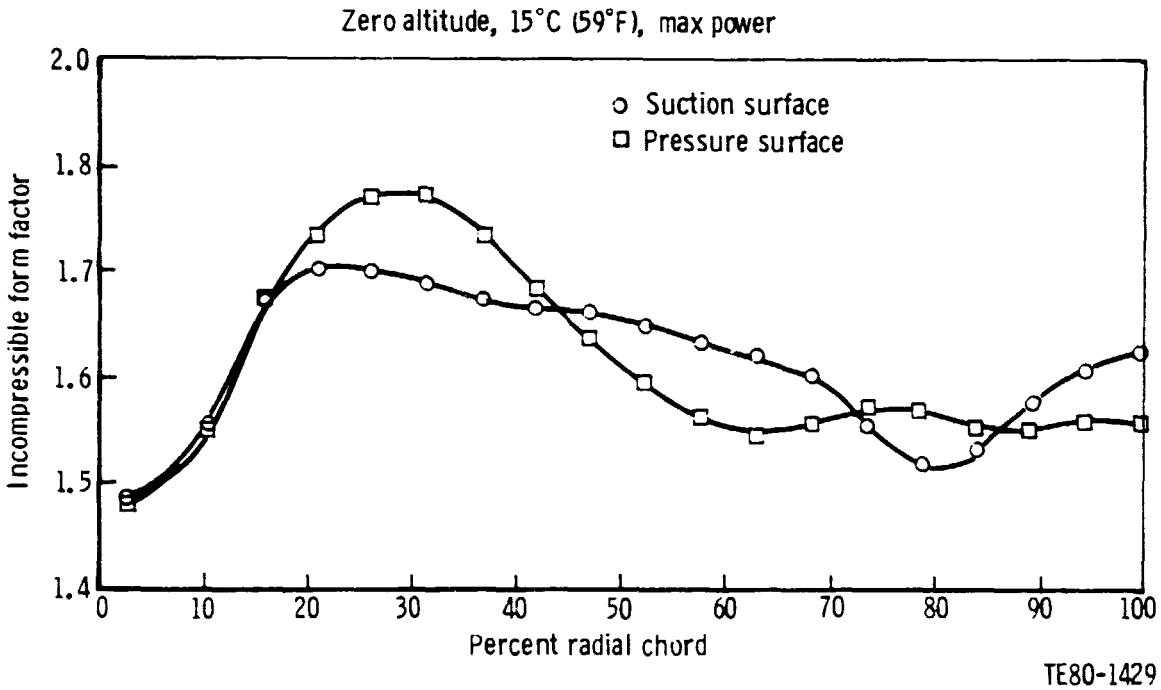

Figure 144. - Boundary Layer Form Factor--RPD Power Turbine Vane.

TABLE XVII. POWER TURBINE SCROLL PERFORMANCE

Operating condition	Through-flow Mach No.	Scroll discharge angle (from radial), deg
Idle	0.079	57
32 km/h (20 mph)	0.075	54
48 km/h (30 mph)	0.079	56
80 km/h (50 mph)	0.102	57
Maximum power	0.144	55

Rotor Design

The rotor has been designed with emphasis on low cost through use of radial blading, low inertia through use of fully scalloped backplate and deeply cut hub, low exit Mach number to minimize exhaust loss, and relatively high maximum power reaction to achieve a broad efficiency band. Consistent with ceramic construction, the minimum blade thickness is 0.762 mm (0.030 in.). The blade thickness distribution is that of an optimum "dog leg." At each axial location, the blade thickness is constant from the tip inward to a specified radius and then follows a logarithmic profile toward the hub. The hub contour was selected to provide balance between blade and hub stress levels.

The blade shape is illustrated by radial section cuts in Figure 145. The rotor throat, trailing edge diameter, and blade angle are presented in Figures 156 through 148, respectively.

Blade-to-blade velocity distributions for hub, mean, and tip (see figure) under SLS maximum power operation are illustrated in Figures 149 through 151. Velocity distributions at 80 km/h (50 mph) are shown in Figures 152 through 154. Idle velocity distributions are presented in Figures 155 through 157.

Rotor exit swirl and Mach number, as calculated from the meridional flow analysis program, are illustrated in Figure 158. The radial variation in turbine total-to-total efficiency is presented in Figure 159.

Power Turbine Exit Diffuser

The power turbine exit diffuser converts the dynamic head of the turbine discharge into static pressure and directs the flow at the regenerator face. Figure 160 shows the diffuser in cross section.

A diffuser area ratio of 1.5 was based on design guidelines for conical diffusers and the available length for diffusion. Because of the orientation of the regenerator with the power turbine, it was necessary to bend the diffuser 30 deg near the power turbine exit. Diffuser cross section was kept circular. Extension of the flow field to the regenerator face produces a football-shaped footprint across the face of the regenerator. Discussion of the importance of this footprint on regenerator performance is presented in Section VII.

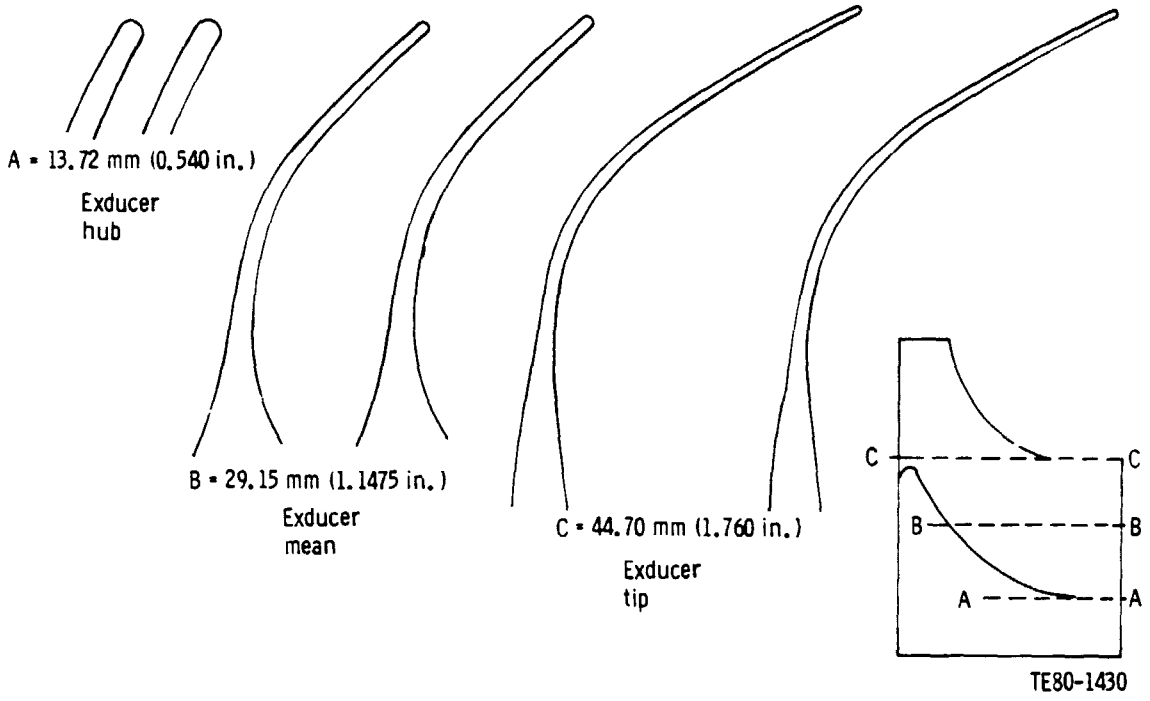

Figure 145. - RPD Power Turbine Rotor Airfoil Sections.

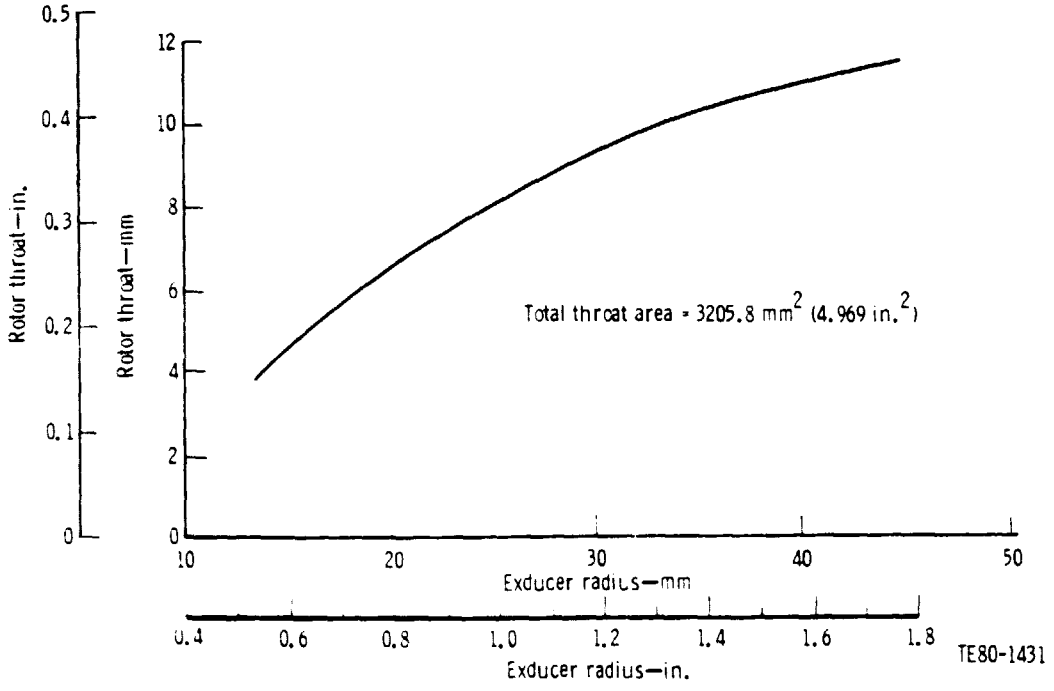

Figure 146. - RPD Power Turbine Rotor Throat.

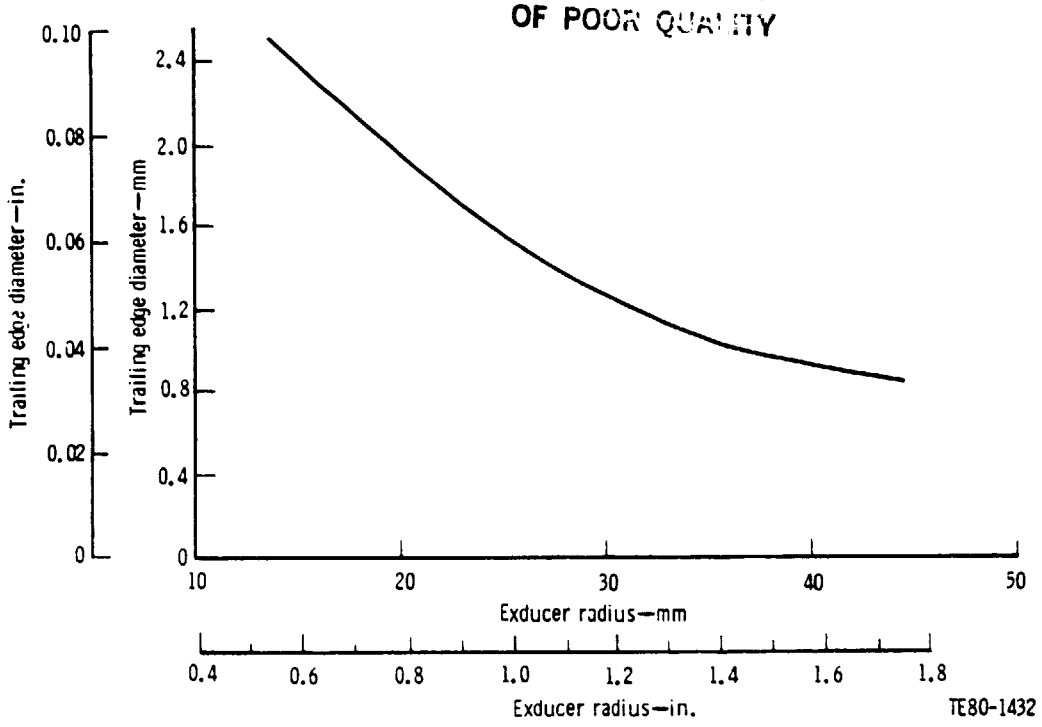

Figure 147. - RPD Power Turbine Rotor Trailing Edge Diameter.

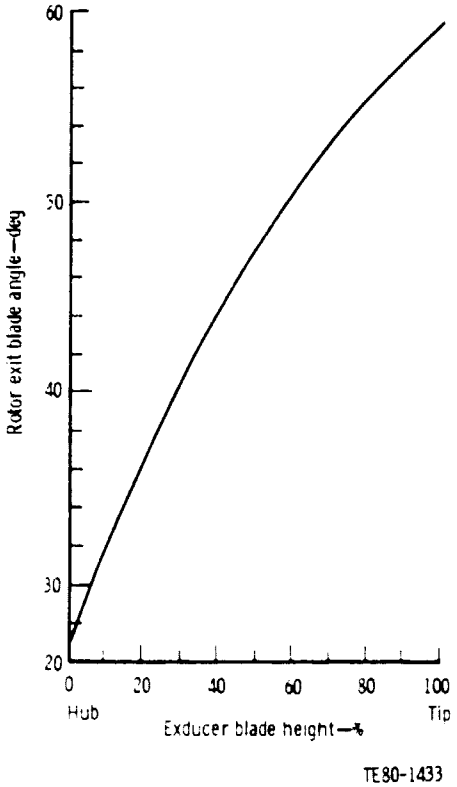

Figure 148. - RPD Power Turbine Rotor Exit Blade Angle.

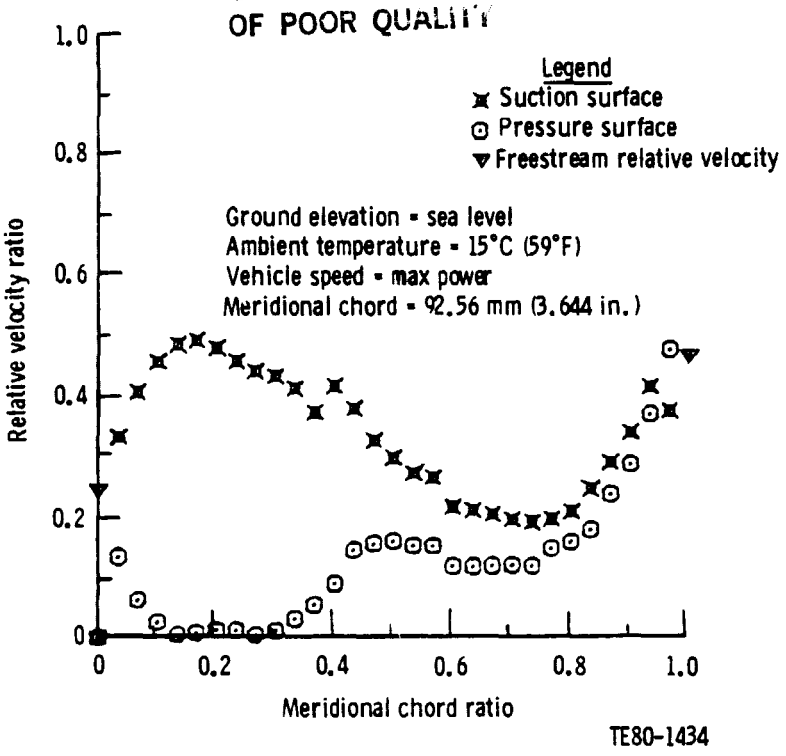

Figure 149. - RPD Power Turbine Rotor Hub Velocity Distribution--Maximum Power.

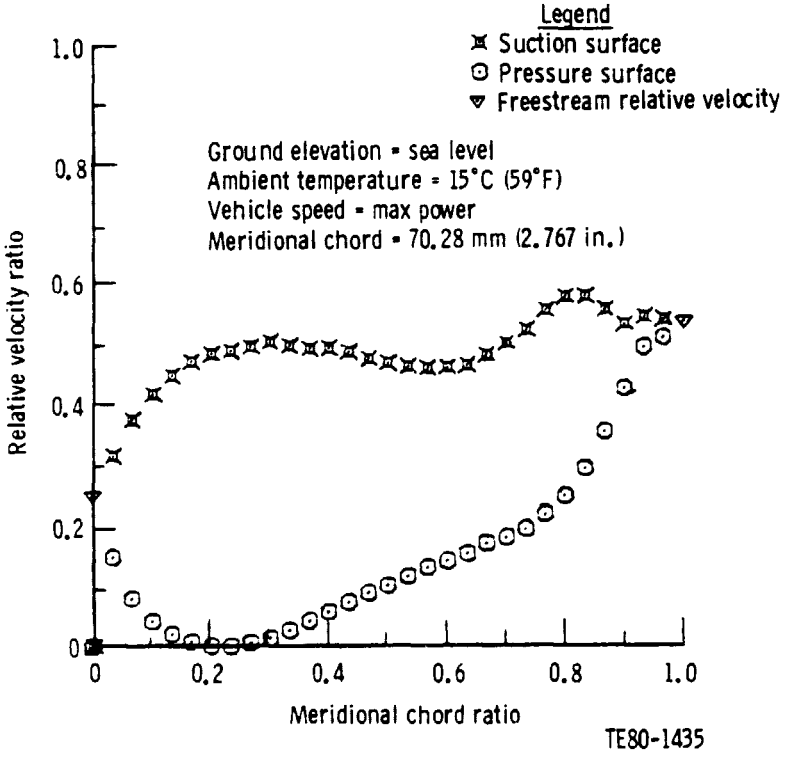

Figure 150. - RPD Power Turbine Rotor Mean Velocity Distribution--Maximum Power.

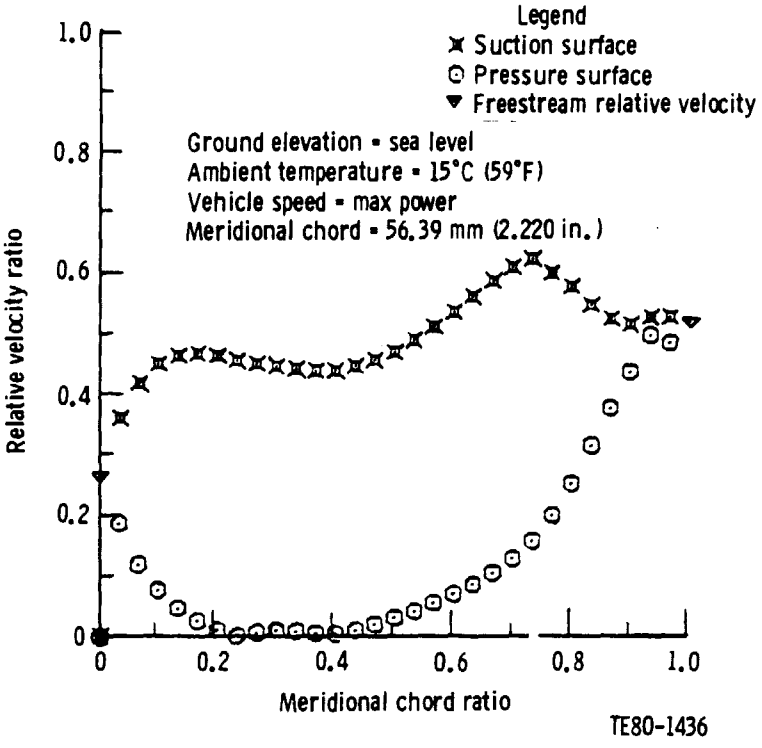

Figure 151. - RPD Power Turbine Rotor Tip Velocity Distribution--Maximum Power.

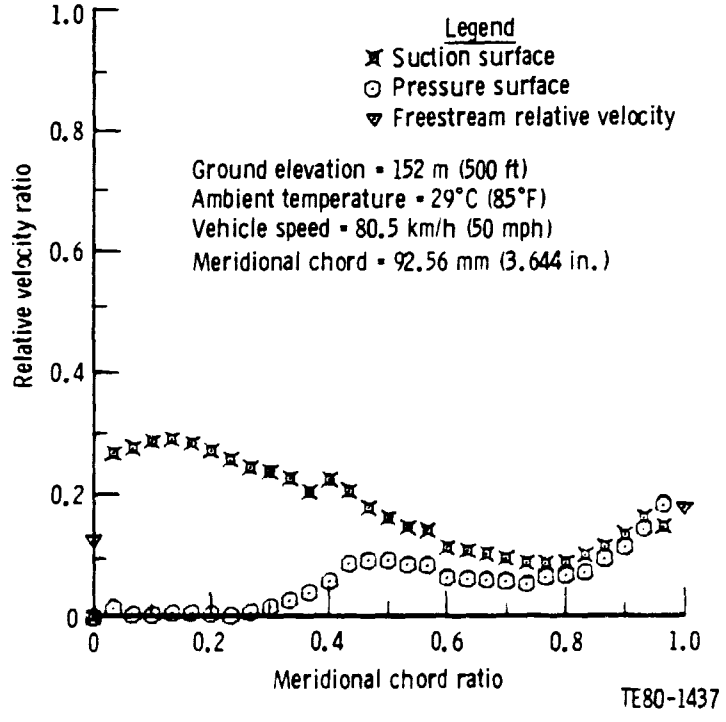

Figure 152. - RPD Power Turbine Rotor Hub Velocity Distribution--92.6 km/h (50 mph).

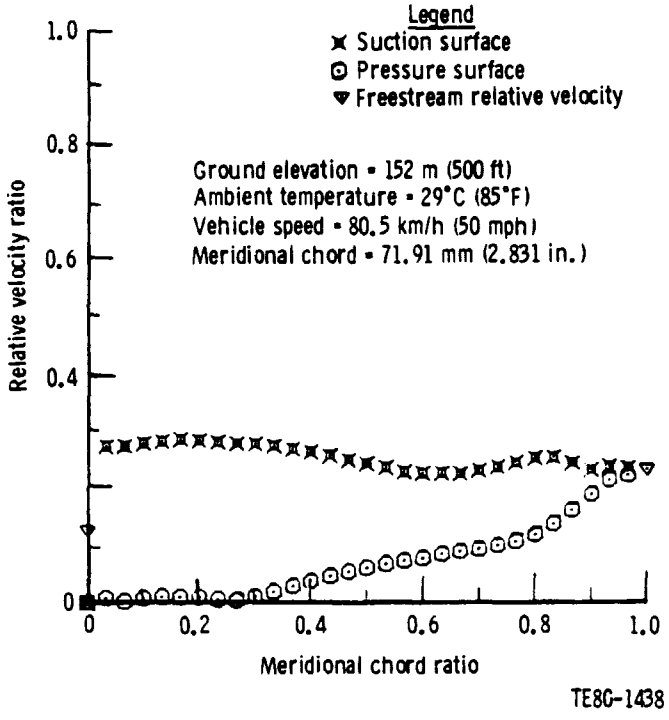

Figure 153. - RPD Power Turbine Rotor Mean Velocity Distribution--92.6 km/h (50 mph).

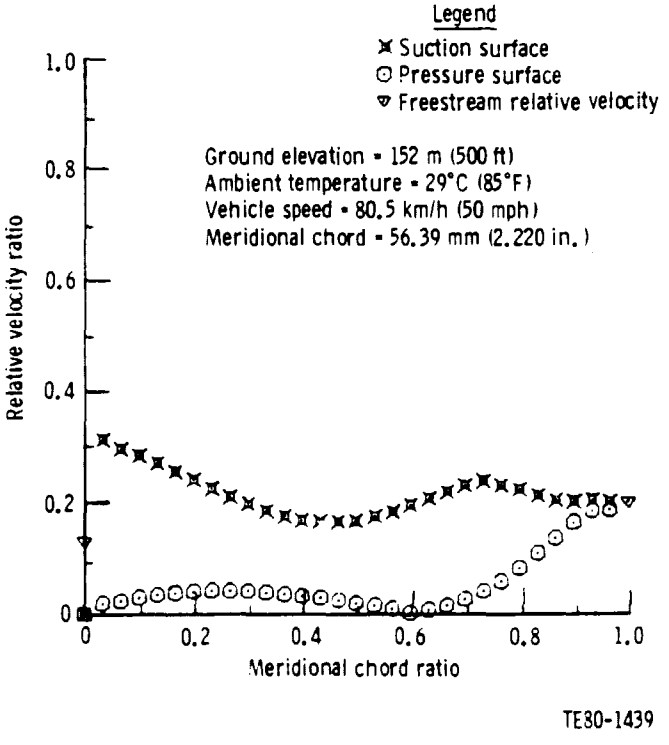

Figure 154. - RPD Power Turbine Rotor Tip Velocity Distribution--92.6 km/h (50 mph).

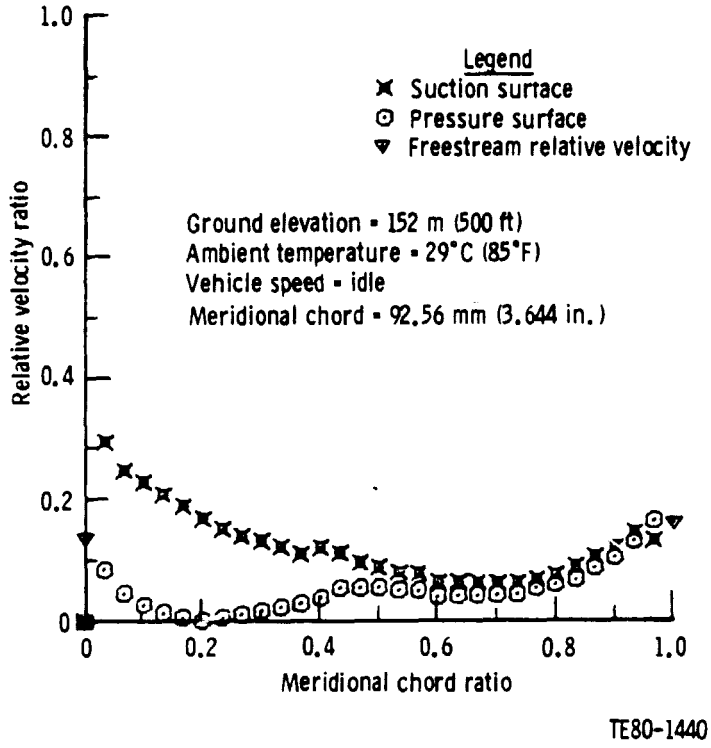

Figure 155. - RPD Power Turbine Rotor Hub Velocity Distribution--Idle.

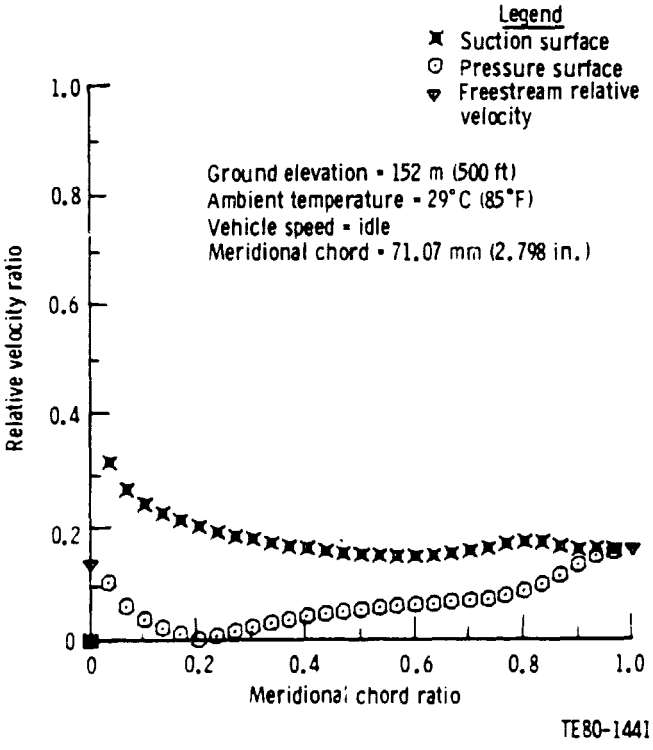

Figure 156. - RPD Power Turbine Rotor Mean Velocity Distribution--Idle.

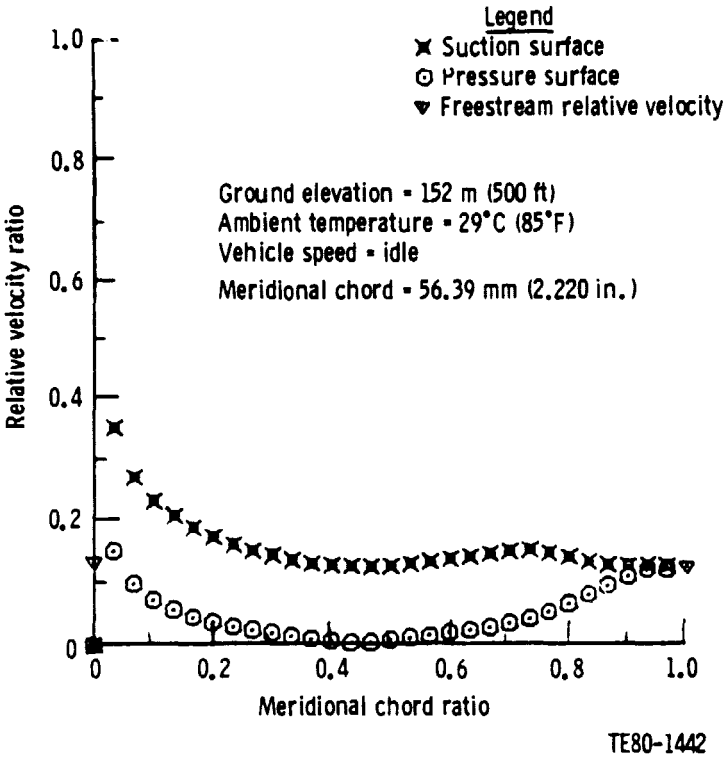

Figure 157. - RPD Power Turbine Rotor Tip Velocity Distribution--idle.

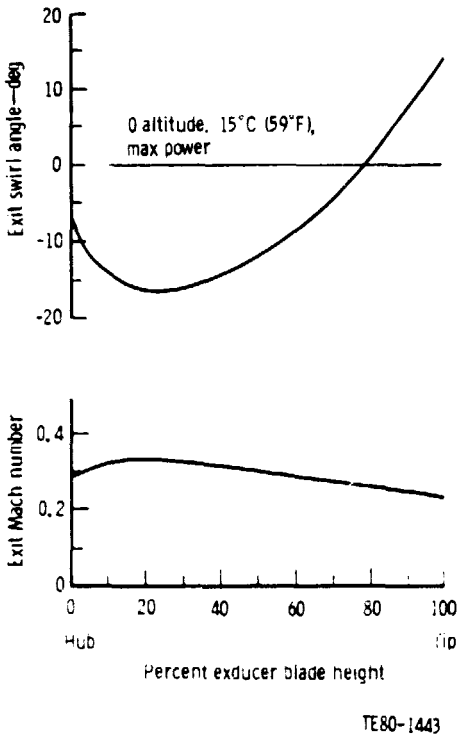

Figure 158. - Predicted Radial Distribution of Exit Swirl and Mach Number--RPD Power Turbine.

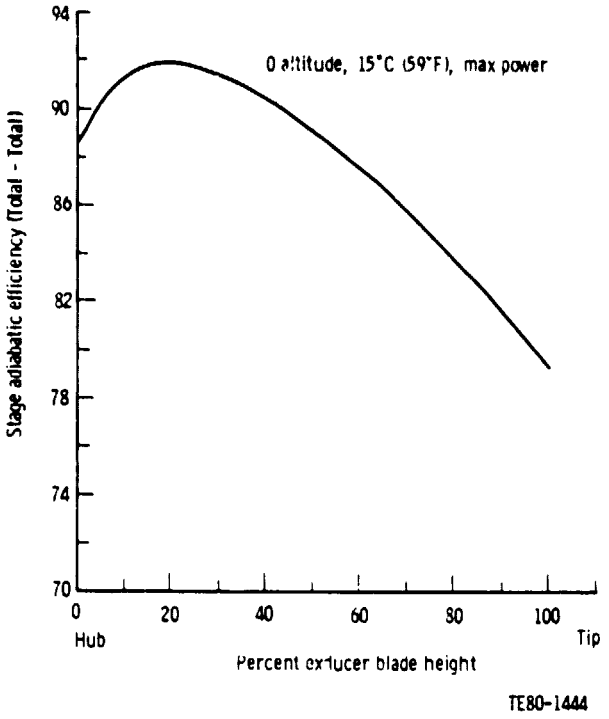

Figure 159. - Predicted Radial Distribution of Stage Efficiency--RPD Power Turbine.

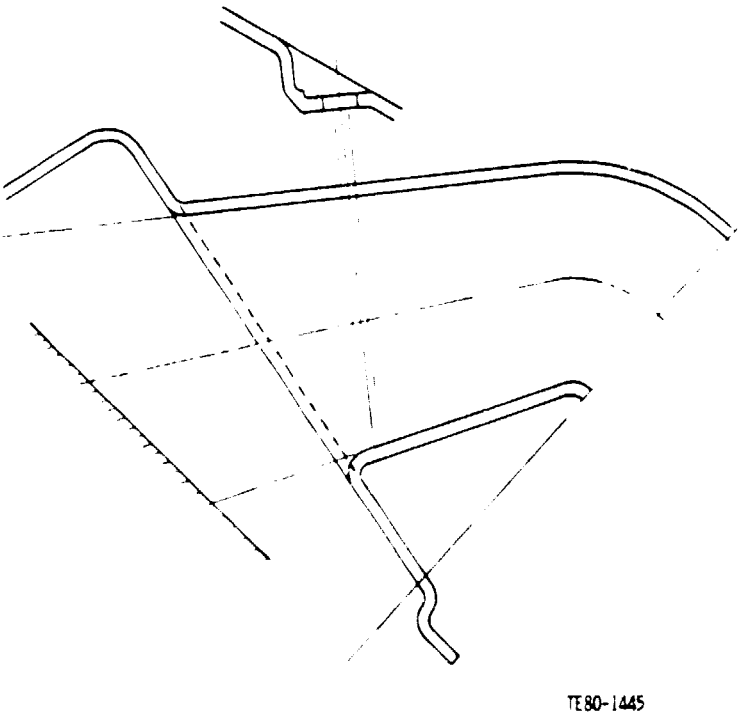

Figure 160. - Power Turbine Exit Diffuser.

Performance of the power turbine exit diffuser has been estimated and is a strong function of diffuser inlet Mach number and swirl. Table XVIII summarizes the diffuser loss for five engine operating conditions.

TABLE XVIII. POWER TURBINE EXIT DIFFUSER PERFORMANCE

Operating condition	Turbine exit MN	Swirl	ΔP/P, %
Idle	0.071	- 9.9	1.06
32 km/h (20 mph)	0.076	+ 4.1	1.13
48 km/h (30 mph)	0.092	+23.0	1.37
80 km/h (50 mph)	0.117	+ 9.2	1.74
Maximum power	0.269	- 2.0	3.86

Mod I Power Turbine Design

Similar to the gasifier turbine, one of the more important design criteria for the Mod I power turbine is flow-path commonality with the RPD configuration. This design criteria is important to allow interchangeability of metallic and ceramic hardware.

The Mod I engine cycle requirements for the power turbine at the maximum power SLS condition are:

Inlet temperature, °C (°F)	883 (1621)
Inlet pressure, kPa (psia)	188.2 (27.30)
Fuel/air ratio	0.0110
Equivalent flow, $W\sqrt{\theta}_{cr}\,\epsilon/\delta$ = kg/s (lbm/sec)	0.350 (0.772)
Equivalent work, $\Delta h/\theta_{cr}$, kJ/kg (Btu/lbm)	36.03 (15.49)
Equivalent speed, $N/\sqrt{\theta}_{cr}$, rpm	27,500
Expansion ratio (Total - Total)	1.706
Efficiency without inlet scroll	84.7

Flow-Path Selection

The preliminary flow path for the Mod I power turbine is illustrated in Figure 161. Because of reduced work level, the maximum power speed for the Mod I power turbine has been reduced to 54,390 rpm. This speed change from the RPD design has been achieved through a relatively minor change in the reduction geartrain. With the exception of vane height change and rotor shroud trim, the Mod I and RPD flow paths are identical. Operating at the SLS maximum power condition, the turbine exhibits a tip speed of 422 m/s (1384 ft/sec), an aerodynamic loading parameter (U/C - Tip Speed/Isentropic Spouting Velocity) of 0.729 and a specific speed of 80. Turbine parameters for several engine operating points under road-load conditions are presented in Table XIX. The Mod I turbine power is 40% less than the RPD. The Mod I equivalent flow is 9.2% higher than the RPD turbine. As a result of the speed change, aerodynamic parameters are quite similar to the RPD design. In order to provide a favorable exit swirl variation, the Mod I turbine rotor blade angle has been reduced (from axial) by approximately 4 deg.

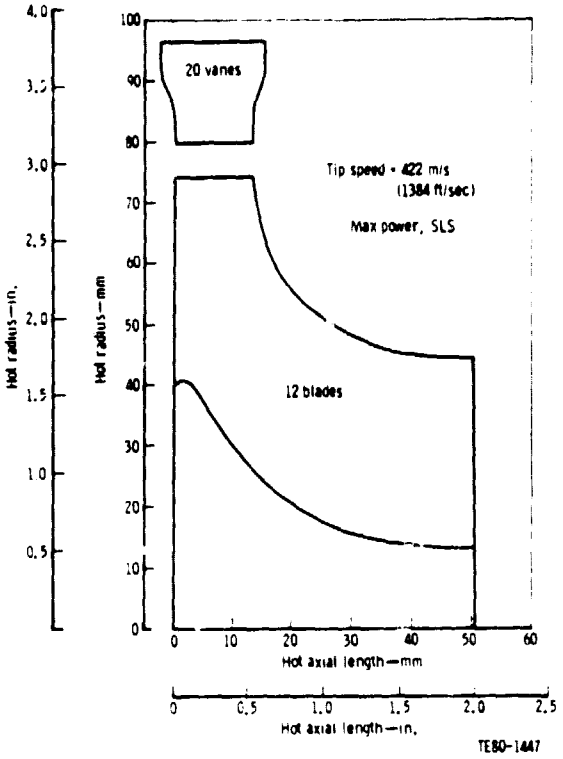

Figure 161. - Mod I Power Turbine Flow Path (Preliminary).

TABLE XIX. MOD I POWER TURBINE PARAMETERS FOR VARIOUS ENGINE OPERATING POINTS (PRELIMINARY)

Speed, km/s (mph)	Idle	32 (20)	48 (30)	80 (50)	102 (70)	Max* power	Max power** (SL)
Turbine power, kW (hp)	1.64 (2.20)	2.50 (3.35)	4.11 (5.51)	8.91 (11.95)	21.13 (28.33)	39.19 (52.55)	44.75 (60.02)
Inlet temperature, °C (°F)	713 (1315)	937 (1718)	977 (1790)	939 (1723)	904 (1659)	889 (1628)	883 (1621)
Equivalent flow, kg/s (lbm/sec)	0.192 (0.424)	0.201 (0.442)	0.211 (0.465)	0.270 (0.595)	0.319 (0.703)	0.327 (0.721)	0.350 (0.772)
Equivalent work, kJ/kg (Btu/lbm)	4.47 (1.92)	5.82 (2.50)	8.68 (3.73)	13.68 (5.88)	23.66 (10.17)	34.17 (14.69)	36.03 (15.49)
Equivalent speed, %	24.8	30.6	45.2	52.1	74.0	99.8	100
Expansion ratio (T-T)	1.075	1.090	1.127	1.212	1.398	1.657	1.706
U/C	0.481	0.542	0.681	0.622	0.674	0.748	0.729
Mean reaction	0.344	0.387	0.500	0.450	0.500	0.576	0.562
N_s	54.5	60.5	72.6	68.9	75.3	84.4	83.6
N_{RE}	32,300	26,400	27,500	40,000	57,800	76,300	83,500
Swirl angle, deg	-17.2	-10.7	7.3	-3.0	0.6	5.9	2.4
$M_{N_{exit}}$	0.090	0.093	0.99	0.136	0.184	0.233	0.247

*Ambient temperature: 29°C (85°F), altitude: 152 m (500 ft).
**Ambient temperature: 15°C (59°F), altitude: sea level.

Aerodynamic Performance

The efficiency goal for the Mod I power turbine without inlet scroll is illustrated in Figure 162. Efficiency levels are on the order of 2 percentage points lower than the RPD power turbine. Work is continuing toward finalizing the Mod I power turbine design. Velocity diagrams and blade-to-blade velocity distributions for selected operating points will be generated during next period.

Scroll Design

The flow path for the Mod I power turbine scroll is the same as the RPD engine. Mechanically, the Mod I scroll is fabricated from metal, whereas the RPD scroll is ceramic. The ceramic scroll is assembled with a circumferential flange at the maximum diameter of the scroll. A rope seal is employed at this flange to minimize flow leakage. In the Mod I engine this joint will be welded to eliminate leakage.

Vane Design

The vane design for the Mod I power turbine is identical to the RPD engine. In order to satisfy Mod I cycle requirements, the vane height must be increased by 21.2%. In the case of the power turbine, a vane reset to open the throat is a viable alternate design.

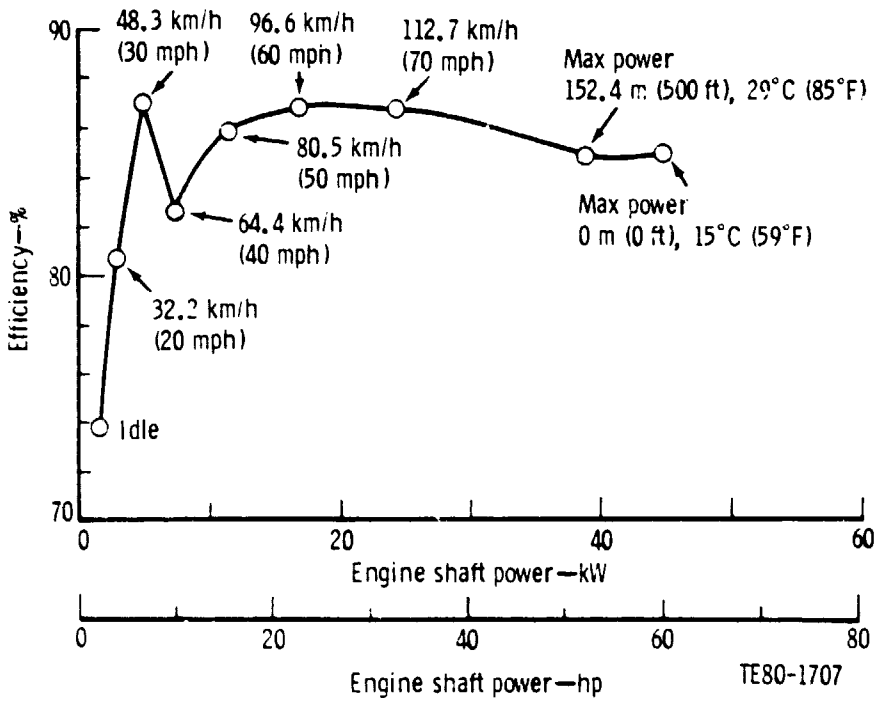

Figure 162. - Efficiency Goal--Mod I Power Turbine without Inlet Scroll.

Rotor Design

As previously mentioned, the power turbine rotor throat was increased (reduced blade angle) to provide favorable exit swirl angles over the operating range. In addition, the same type of modifications to blade thickness distribution as was used on the gasifier turbine were employed for the power turbine wheel. This change in thickness provided sufficient increase in inducer stiffness to avoid the requirement for a partial backplate.

Approximate blade-to-blade velocity distributions based on quasiorthogonal meridional flow analysis are presented in Figures 163 through 165. These preliminary Mod I distributions were generated for the SLS maximum power design point.

During the next reporting period, the Mod I rotor design will be finalized, and master charts for engine hardware will be generated. Experimental data from the turbine development program will be incorporated into the final Mod I power turbine design.

Power Turbine Exit Diffuser

The power turbine exit diffuser for the Mod I engine is exactly the same as the RPD engine except that the Mod I diffuser will be fabricated from metal. Area ratio and geometric shape are the same.

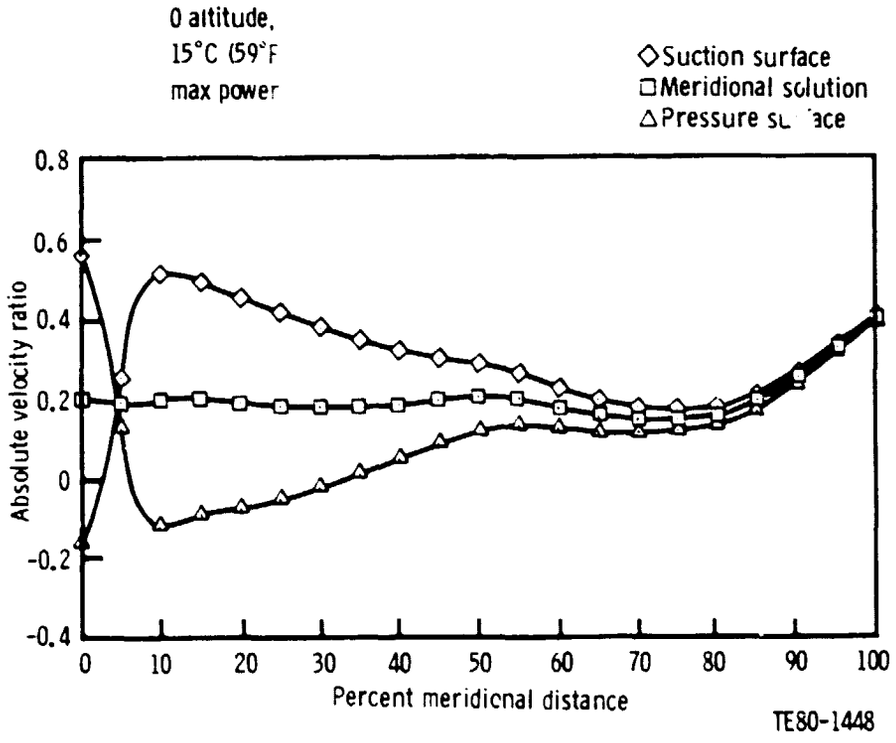

Figure 163. - Approximate Hub Velocity Distribution--Mod I Power Turbine.

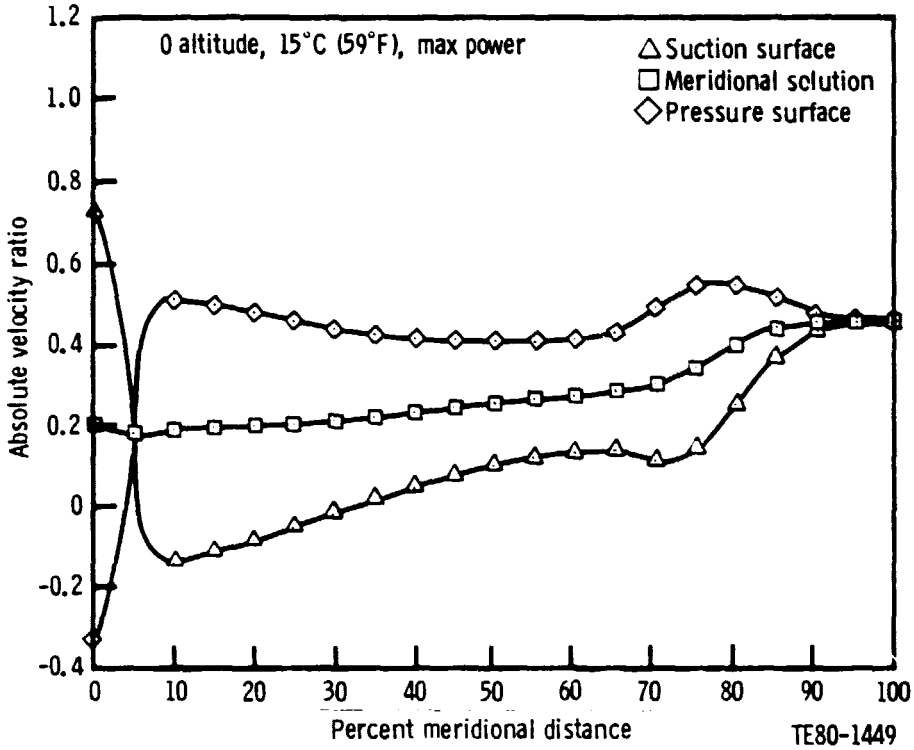

Figure 164. - Approximate Mean Velocity Distribution--Mod I Power Turbine.

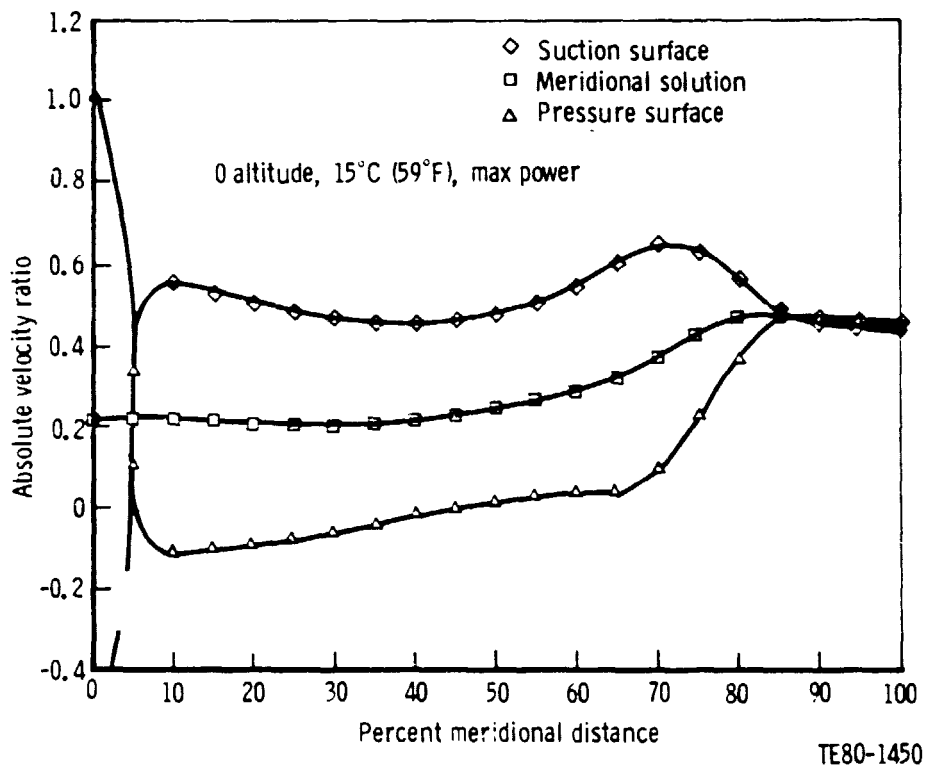

Figure 165. - Approximate Tip Velocity Distribution--Mod I Power Turbine.

Power Turbine Aerodynamic Development

The power turbine rig basic configuration is shown in Figure 166. This rig is similar to the gasifier turbine rig because of the interchangeable features that permit conversion from the gasifier turbine rig on the test facility by using the same shaft and module.

Activity for this period consisted of layout design of the basic rig. Instrumentation locations are similar to those defined in the gasifier turbine rig so as to provide good correlation. Because of the larger size of the power turbine, the clearance adjustments have been simplified. Four tiebolts support the shroud for clearance adjustments to prevent the shroud from moving away from the wheel in the direction of the pressure forces. Other structural support controls movement in the opposite direction and provides the concentricity control.

The power turbine rig uses the loose-vane concept, which reflects the engine design, and the contoured endwalls are part of the basic configuration rather than an alternate design for test purposes. The rig is shown with a cylindrical exhaust diffuser; a subsequent design will define a divergent diffuser. The fiberglass inlet scroll insert is constructed over a removable wood form. Aluminum bulkheads are spaced around the scroll and are used to position it in a pressure casing similar to the gasifier turbine rig. This feature allows replacement of the scroll as an insert to study changes in configuration. Plans call for a flow simulator to be attached to the inlet, which will provide flow profiles into the scroll similar to those obtained from flowpipe model testing of the interturbine duct.

5.2 POWER TURBINE MECHANICAL DEVELOPMENT

RPD

Scroll Design

The power turbine scroll forms the gas flow path from the gasifier turbine exit, via the interturbine duct, to the power turbine rotor. The cylindrical inlet section mates with the outer shroud of the gasifier turbine and is designed to diffuse and turn the gas exiting the gasifier. A constant velocity involute distributes the gas uniformly to the radial inflow turbine rotor inlet. The rotor blade tip shroud is integral with the power turbine scroll, thus forming the flow path through the rotor.

The RPD power turbine scroll design is presented in Figure 167. As shown, the scroll that forms the gas flow path is a three-piece assembly composed of the scroll-forward, scroll-aft, and backplate. The general contour of the forward and aft scrolls was determined from a preliminary two-dimensional stress and deflection analysis, which assumes an axisymmetric shape. A detailed explanation of the method of analysis is covered in Section 4.2. The three-dimensional finite element model, which takes into account the changing cross section, will either verify the design or define necessary changes to ensure structural integrity. Based on the two-dimensional analysis the most critical operating condition for the scroll is the cold fire-up to maximum power transient condition.

The three-piece construction was selected primarily because it simplified the assembly of the vanes into forward and aft scroll assembly. The split line between the aft scroll and the backplate was located outboard of the rotor diameter. This allows the scroll and vane assembly to be installed with the rotor in place.

Also shown in Figure 167 is the scroll cross-key mounting arrangement. The scroll has five mounting lugs located around the outer circumference. Two mounting rings that bolt to the engine block have machined slots to accept the scroll lugs. This design allows for differential thermal radial growth between the ceramic scroll and the steel mounting rings while holding a close tolerance on the scroll lateral motion. Control of the scroll lateral motion is critical in order to maintain shroud to rotor tip clearance. Several joint design review meetings between DDA and Carborundum were held to discuss the scroll functional design features and their impact with respect to slip casting and mandrel coating. The resulting design gives consideration to the manufacturing processes. Carborundum plans to investigate both the slip casting and mandrel coating techniques in its process development program. The selected scroll material is alpha silicon carbide, with a peak operating temperature of 1220°C (2230°F).

Rotor Dynamics

The RPD power turbine rotor was analyzed to predict rotor responses and bearing dynamic loads resulting from simulated rotor unbalances. The turbine was assumed to have a 0.0254-mm (0.001-in.) eccentricity of the center of gravity from the axis of rotation, resulting in an unbalance value of 0.000123 N·m (0.00109 lb-in.). The maximum response level in the steady-state operating speed range is 0.0762 mm (0.003 in.) at the turbine blade rip. If a squeeze film damper is employed at the turbine end (front) bearing support, a 50% reduction in response is achieved at the first mode resonance, which occurs in the transient speed range. The maximum dynamic loads computed are 62.3 N (14 lbf) and 133.4 N (30 lbf) at the front and aft bearings, respectively.

In conjunction with rearrangement studies of the engine, two optional configurations of the power turbine rotor were analyzed. The power turbine rotor was rearranged so that the turbine outlet was at the shaft side of the wheel (see Figures 168 and 169). The exit hub-tip radius ratio was increased to provide radial space for the rotor support bearing. Hub-to-tip ratios of 0.5 (Figure 168) and 0.6 (Figure 169) were studied to minimize turbine overhang. The weights, inertia, and other pertinent parameters for both Figures 168 and 169 are listed in Table XX. The modes for both rigid (infinite stiffness) and formal supports were calculated. Results show that the first bending mode appears in the operating speed range. Critical speed sensitivity studies of the front mount spring rate for both configurations indicate that a rate of 7500 lbm/in. at the front bearing reduces the pitching mode (mode 1) below the idle speed. However, the first bending mode (mode 2) has only a 19% speed margin above the maximum continuous speed for Configuration A and 18%, speed margin for Configuration B. The results are summarized in Table XXI. These two configurations are unacceptable because of the reduced margin.

ORIGINAL PAGE IS
OF POOR QUALITY

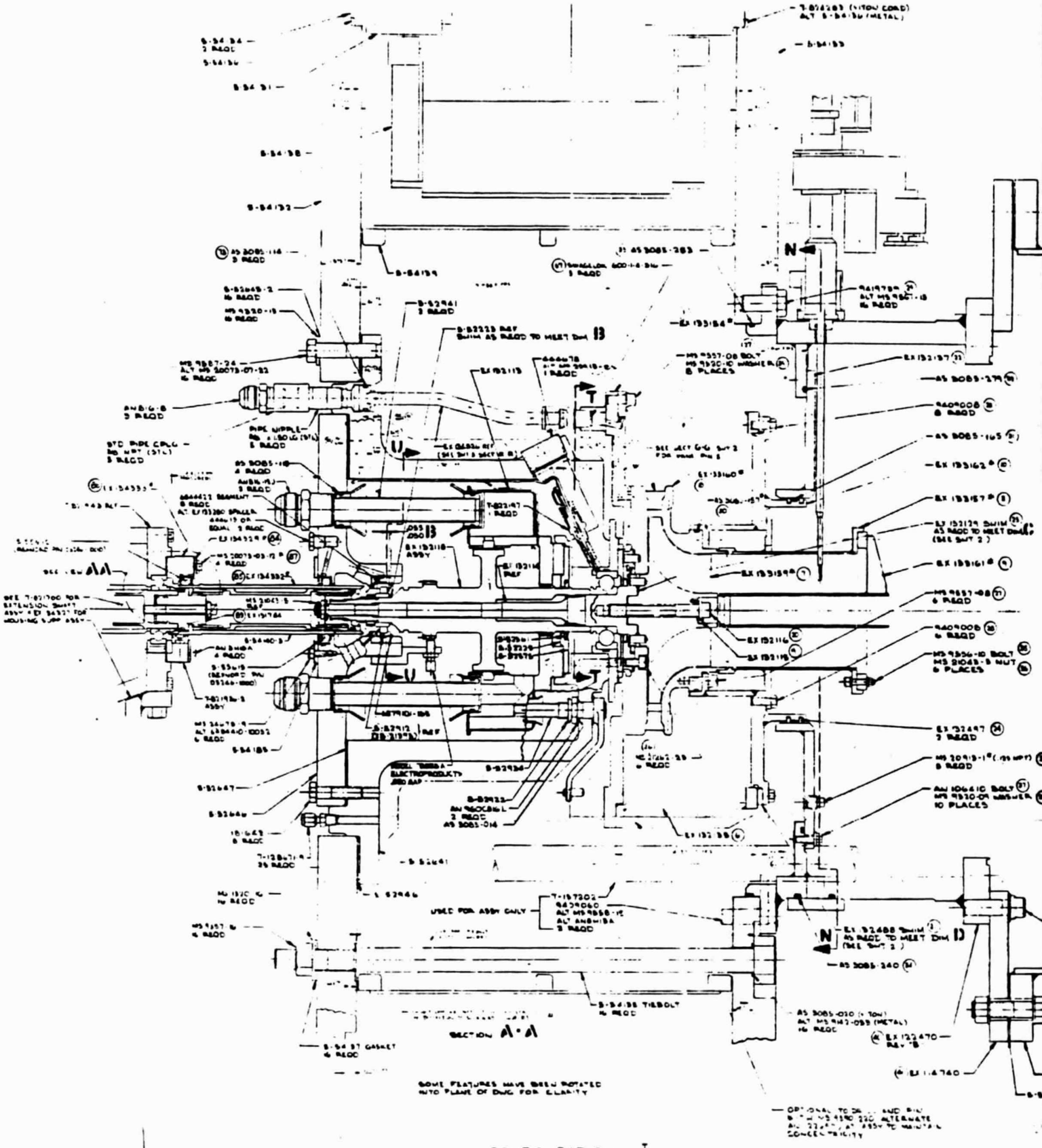

CONFIGURATION I
(WITH CYL DIFFUSER + NO SCROLL)

FOLDOUT FRAME

Figure 166. - AGT-100 Pow

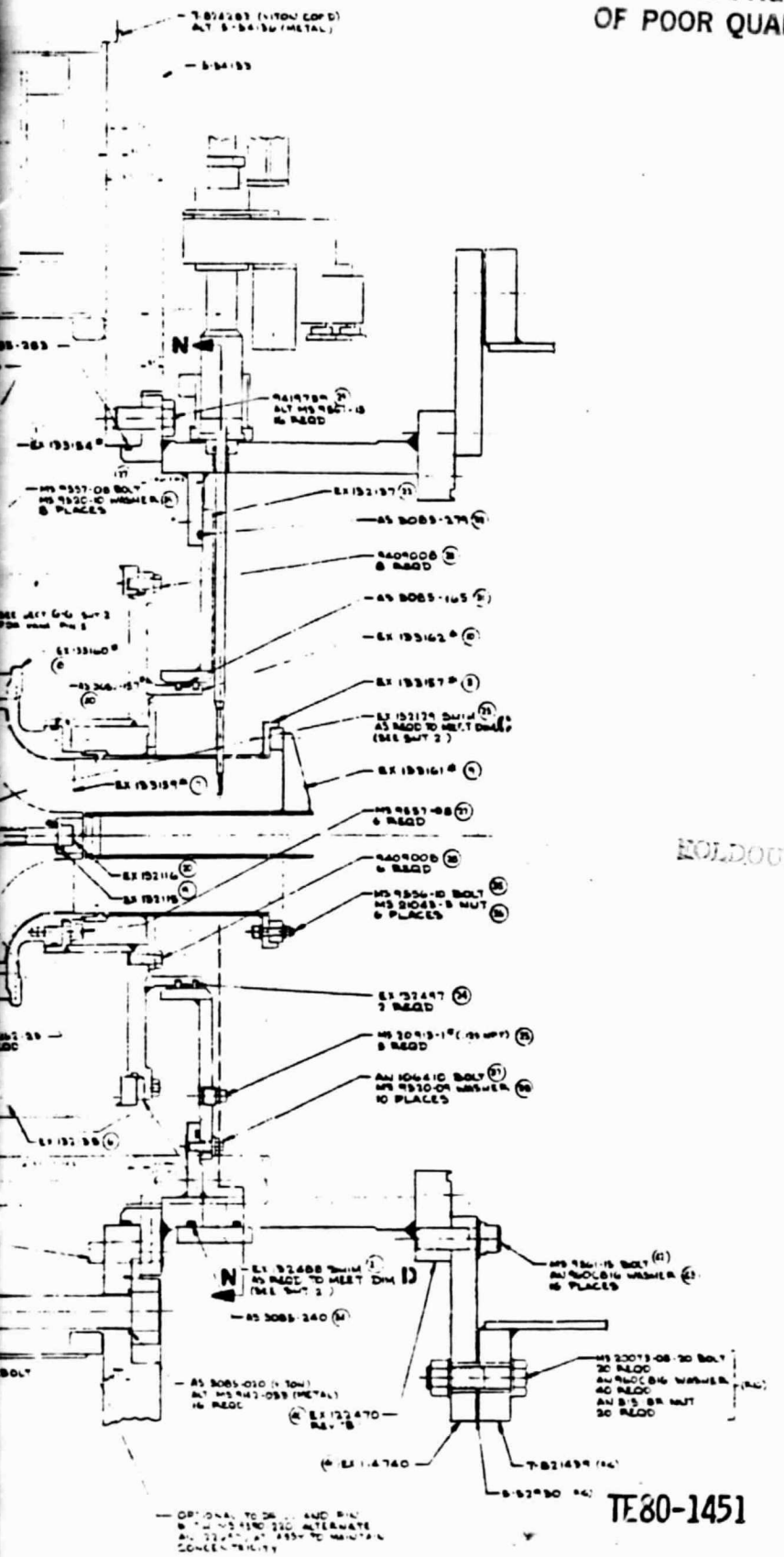

Figure 166. - AGT-100 Power Turbine Rig.

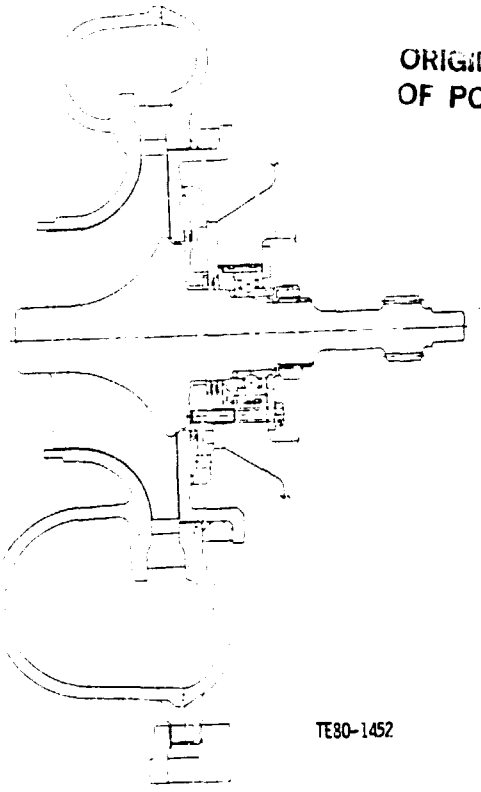

Figure 167. - AGT-100 Power Turbine Cross Section.

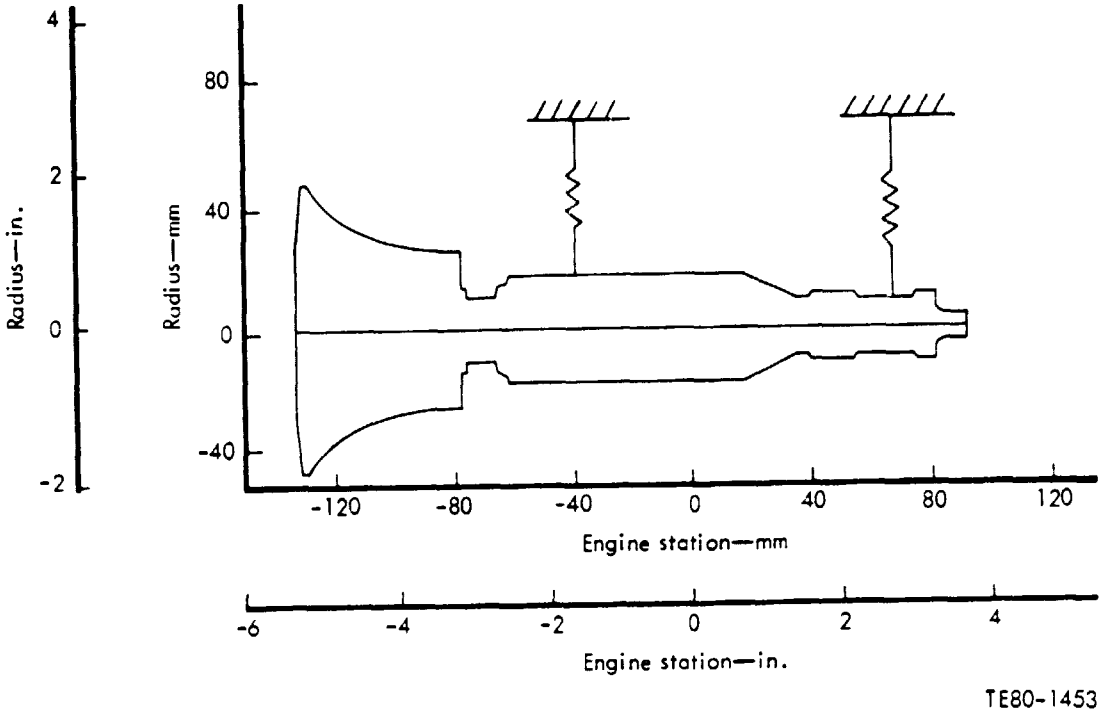

Figure 168. - AGT-100 Power Turbine Rotor (Configuration A) System Geometric Representation.

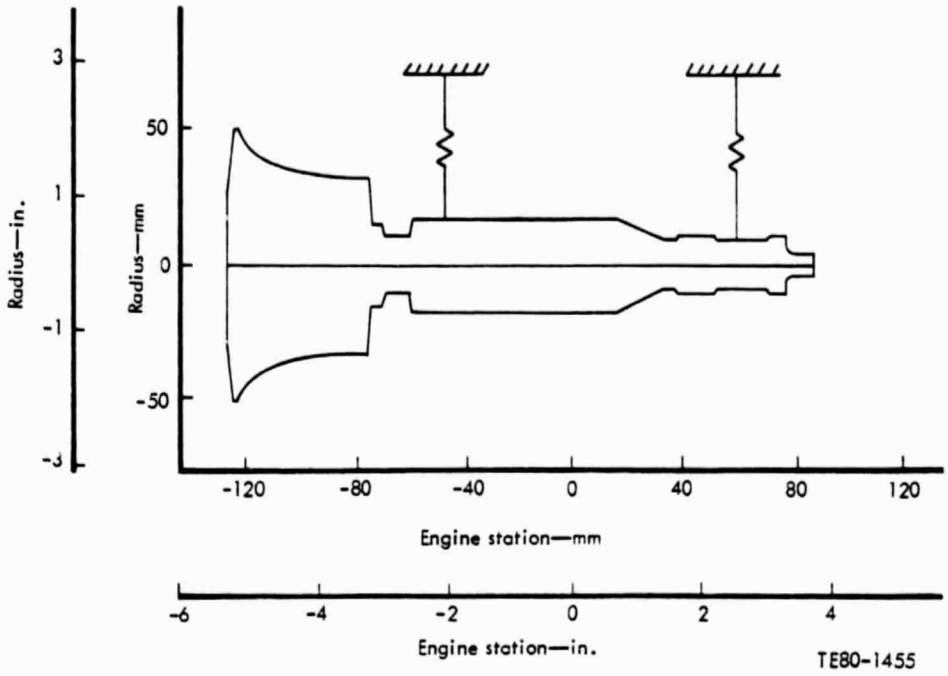

Figure 169. - AGT-100 Power Turbine Rotor (Configuration B) System Geometric Representation.

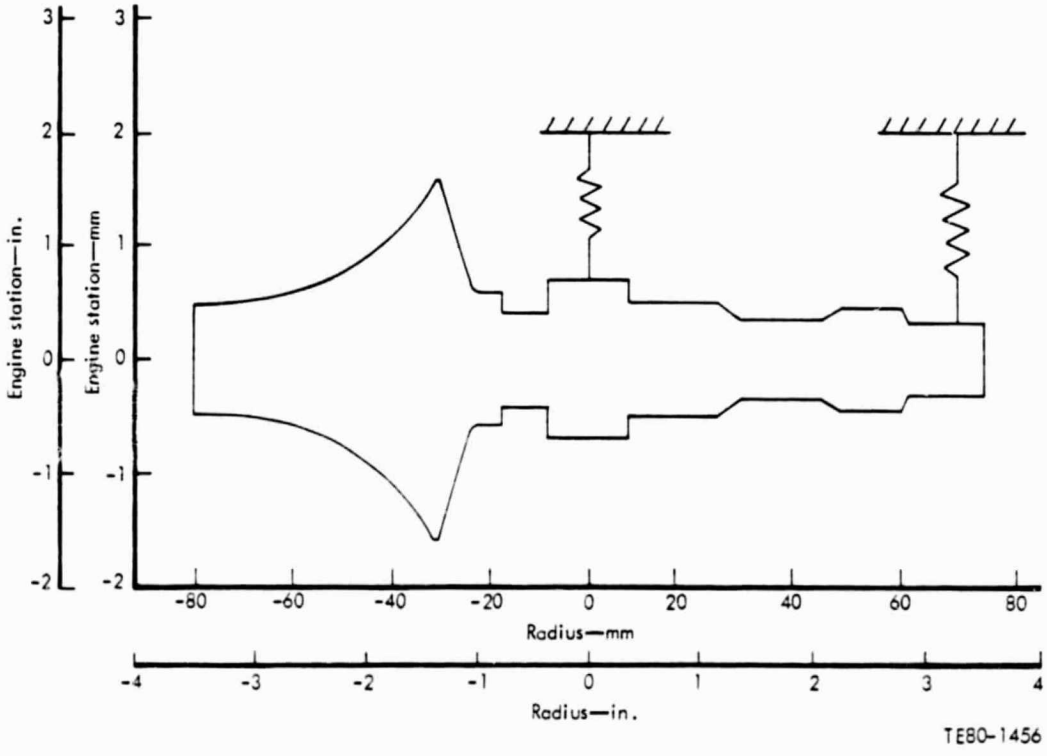

Figure 170. - AGT Power Turbine Rotor for a New Gearbox System Geometric Representation.

TABLE XX. POWER TURBINE MECHANICAL PARAMETERS FOR CONFIGURATIONS A AND B

	Figure 168 (Configuration A)	Figure 169 (Configuration B)
Hub/tip radius	0.5	0.6
Weights		
Turbine, kg (lbm)	0.723 (1.593)	0.867 (1.911)
Shaft, kg (lbm)	0.761 (1.678)	0.803 (1.771)
Inertias (roll)		
Turbine, $kg \cdot m^2$ ($lbm-in.^2$)	0.000495 (1.693)	0.000593 (2.027)
Shaft, $kg \cdot m^2$ ($lbm-in.^2$)	0.000983 (0.336)	0.000111 (0.378)
Turbine overhang beyond front bearing, mm (in.)	76.15 (2.998)	57.27 (2.247)
Bearing span length, mm (in.)	107.19 (4.22)	121.92 (4.80)
Bearing bore diameter, mm (in.)	29.97 (1.18)	29.97 (1.18)
Coupling OD, mm (in.)	21.59 (0.85)	21.59 (0.85)

TABLE XXI. SUMMARY OF POWER TURBINE CRITICAL SPEED ANALYSIS

	Figure 168 (Configuration A)	Figure 169 (Configuration B)
Rigid support		
Mode 1	37,962 cpm (56%)	39,564 cpm (58%)
Normal support*		
Mode 1	28,352 cpm (42%)	30,249 cpm (44%)
Mode 2	110,224 cpm (162%)	102,618 cpm (151%)
Mass isolator**		
Mode 1	6,997 cpm (10.2%)	7,226 cpm (10.6%)
Mode 2	81,199 cpm (119%)	79,932 cpm (118%)

*Mount spring rates assumed to be 52.5 MN/m (300,000 lbf/in.).
**Front mount rate 1.312 MN/m (7,500 lbf/in.). Rear mount rates assumed to be 52.5 MN/m (300,000 lbf/in.).

After the new gearbox was designed, the modified power turbine rotor shown in Figure 170 was analyzed. The critical speed analysis indicated that one critical speed occurred at 61% of the operating speed range (18 to 100% of 68,000 rpm) for a normally supported rotor. When a controlled spring rate (isolator) of 0.875 MN/m (5,000 lbf/in.) is used at the turbine end bearing, the turbine rigid body mode is eliminated from the operating speed range. The mode shapes for this configuration are shown in Figure 171.

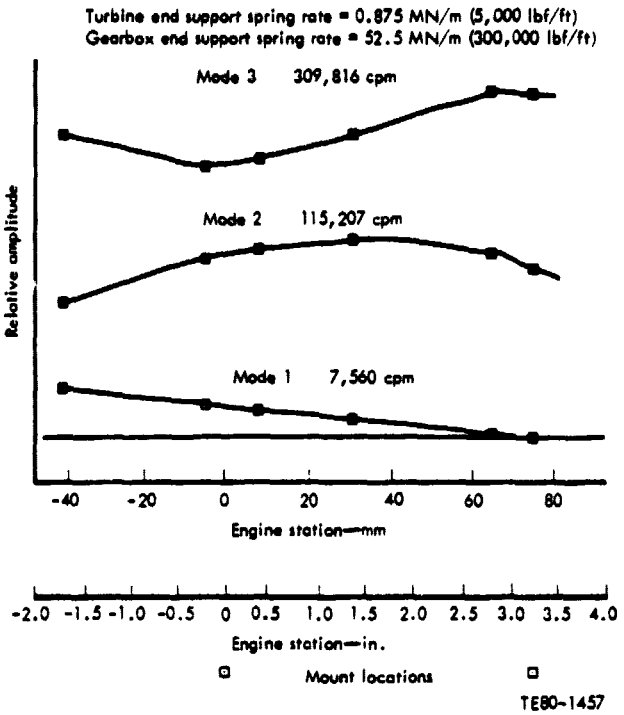

Figure 171. - AGT Power Turbine Rotor for a New Gearbox.

Preliminary calculations of the rotor response to various maneuver's loads were performed using three different conditions: 1.5 rad/s turn, 3g's static load, and 6 g/0.05 s half sine shock pulse. The areas of interest were the turbine tip, piston seal, and pinion gear mesh clearances. The results indicated that the critical area was the turbine tip clearance at the trailing edge. Calculations were made for three different isolator radial clearances, results of which are shown in Table XXII. As can be seen, smaller responses occur at smaller clearances. However, sufficient radial deflection must be available so that the rotor can have the isolated rate during the passage through critical speeds excited by normal unbalances. This trade-off will be investigated further.

TABLE XXII. THE BLADE TIP RESPONSE AT TRAILING EDGE RESULTING FROM THREE DIFFERENT MANEUVER'S LOADS

Isolator radial clearance	0.0508 mm (2 mils)	0.0762 mm (3 mils)	0.1778 mm (7 mils)
1.5 rad/sec gyro, mm (mils)	0.1346 (5.30)	0.1930 (7.60)	0.1935 (7.62)
3g static load, mm (mils)	0.1085 (4.27)	0.1085 (4.27)	0.1085 (4.27)
6 g/0.05 s half sine shock, mm (mils)	0.1135 (4.47)	0.1648 (6.49)	0.1943 (7.65)

Additional calculations are presently being made to assess the effects of power extraction on the power turbine frequencies and response to unbalance.

Mod I

The Mod I design incorporates metal flow-path components--both rotating and static--which will allow engine development testing prior to the delivery of ceramic components. Commonality between RPD and Mod I designs will be maintained whenever possible.

Rotor Mechanical

The design of the Mod I power turbine rotor has been initiated. The blade thickness distribution is being selected to raise the inducer bending mode frequency. Initial review of the latest design iteration indicates that the desired increase in frequency has been accomplished. The rsults of initial heat transfer and stress analysis also show more than adequate stress-rupture life (in excess of 50,000 h), which is primarily a result of the significantly reduced tip speed (454 m/s (1384 ft/sec)) of the Mod I power turbine.

5.3 CERAMIC POWER TURBINE ROTOR

Much of the work done this period on the ceramic gasifier rotor is also relevant to the power turbine. Refer to Section 4.3 of this report.

Revised Two-Dimensional Analysis Results

The two-dimensional finite element model of both turbines was revised to reflect the power transfer configuration, the addition of balance stock, the effects of gas recirculation from backface pumping, and the new joint configuration. The steady-state maximum power results are shown in Figure 172.

Transient schedules, shown in Figure 173, were used to examine non-steady-state conditions. The results are shown in Figure 174. Calculation of the power turbine rotors probability of survival using Weibull material parameters indicate a minimum point is reached at 38-s elapsed time.

Transient analysis results relating material strength to design probability of survival were given in Section 4.3, but the plot is repeated here for convenience (Figure 175).

Power Turbine Dynamic Analyses

Preliminary analyses have been performed on the power turbine blade. Figures 176 and 177 present speed-frequency relationships for silicon carbide and silicon nitride materials. The potentially most troublesome mode (inducer bending) clears fourth engine order in both cases and thus satisfies one of the design criteria.

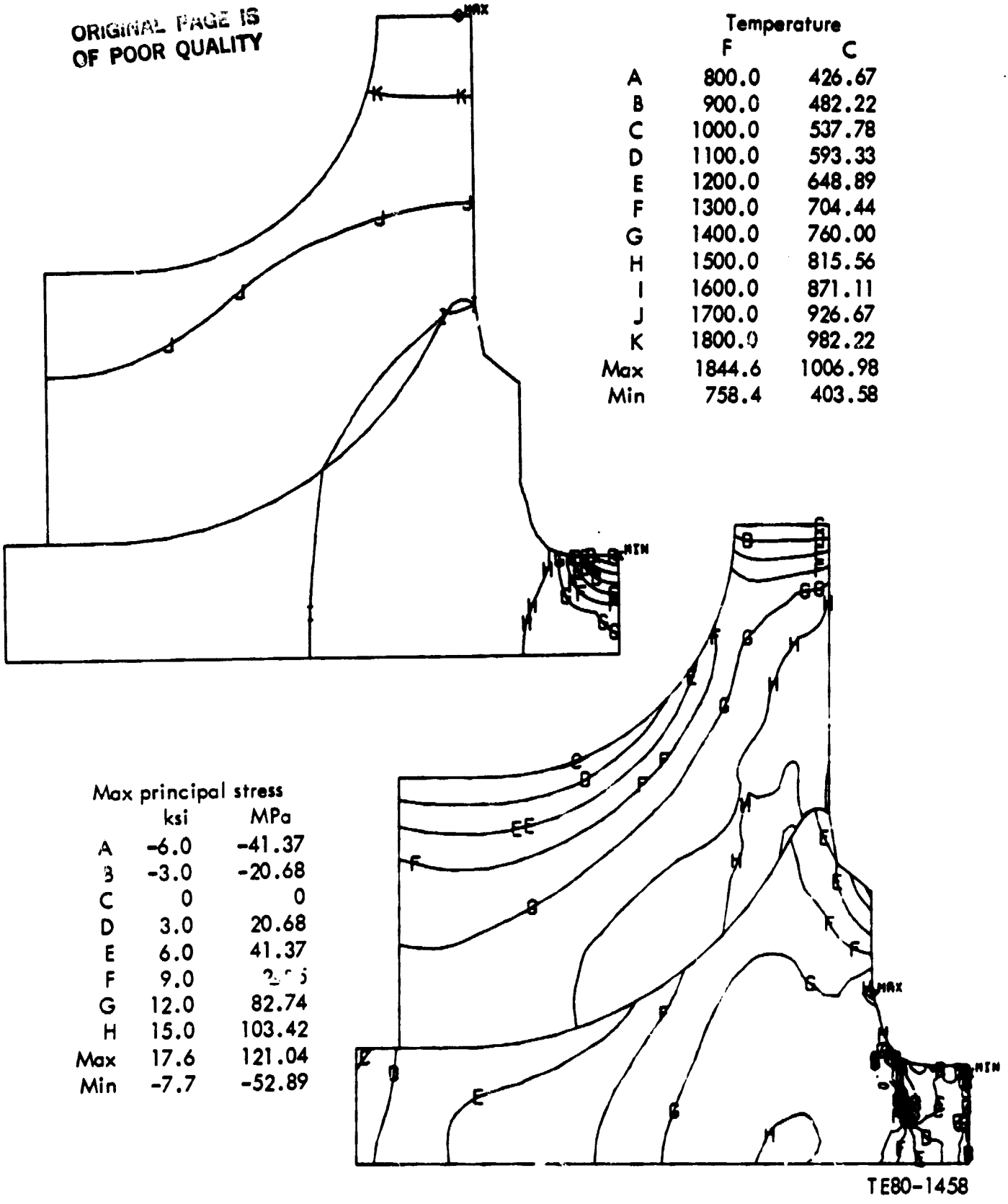

	Temperature F	C
A	800.0	426.67
B	900.0	482.22
C	1000.0	537.78
D	1100.0	593.33
E	1200.0	648.89
F	1300.0	704.44
G	1400.0	760.00
H	1500.0	815.56
I	1600.0	871.11
J	1700.0	926.67
K	1800.0	982.22
Max	1844.6	1006.98
Min	758.4	403.58

Max principal stress	ksi	MPa
A	-6.0	-41.37
B	-3.0	-20.68
C	0	0
D	3.0	20.68
E	6.0	41.37
F	9.0	[illegible]
G	12.0	82.74
H	15.0	103.42
Max	17.6	121.04
Min	-7.7	-52.89

Figure 172. - AGT Power Turbine--Steady-State Maximum Power Analysis Results.

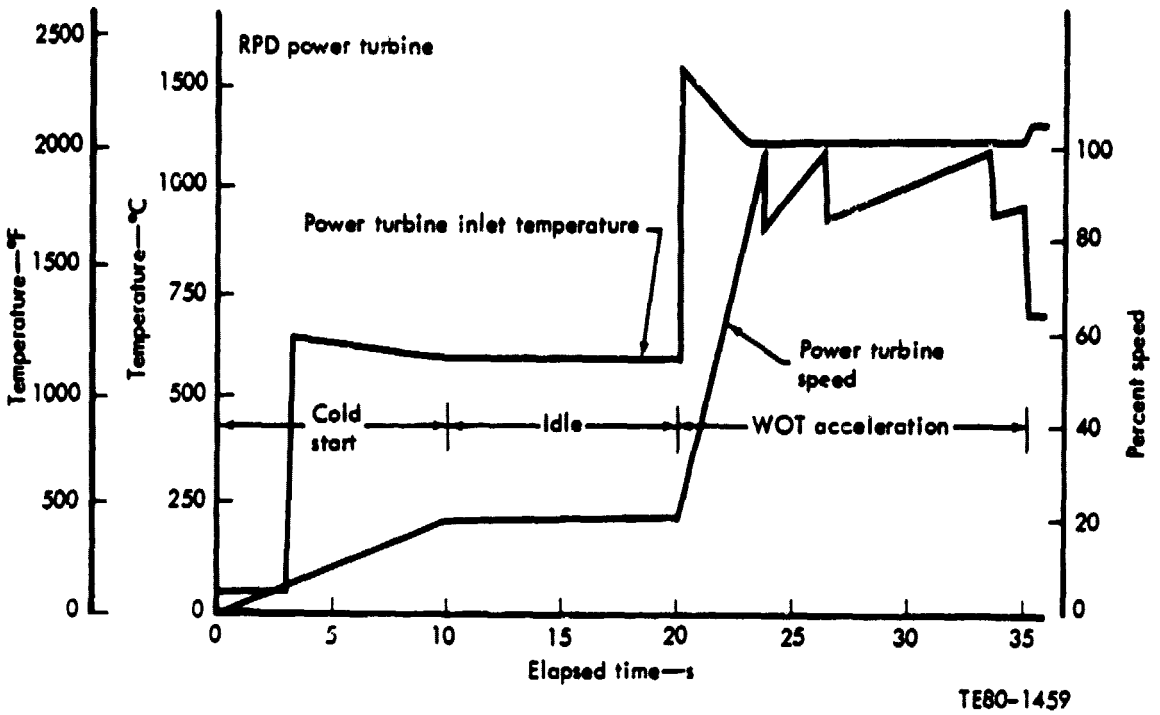

Figure 173. - AGT-100 Cold Start to Maximum Transient.

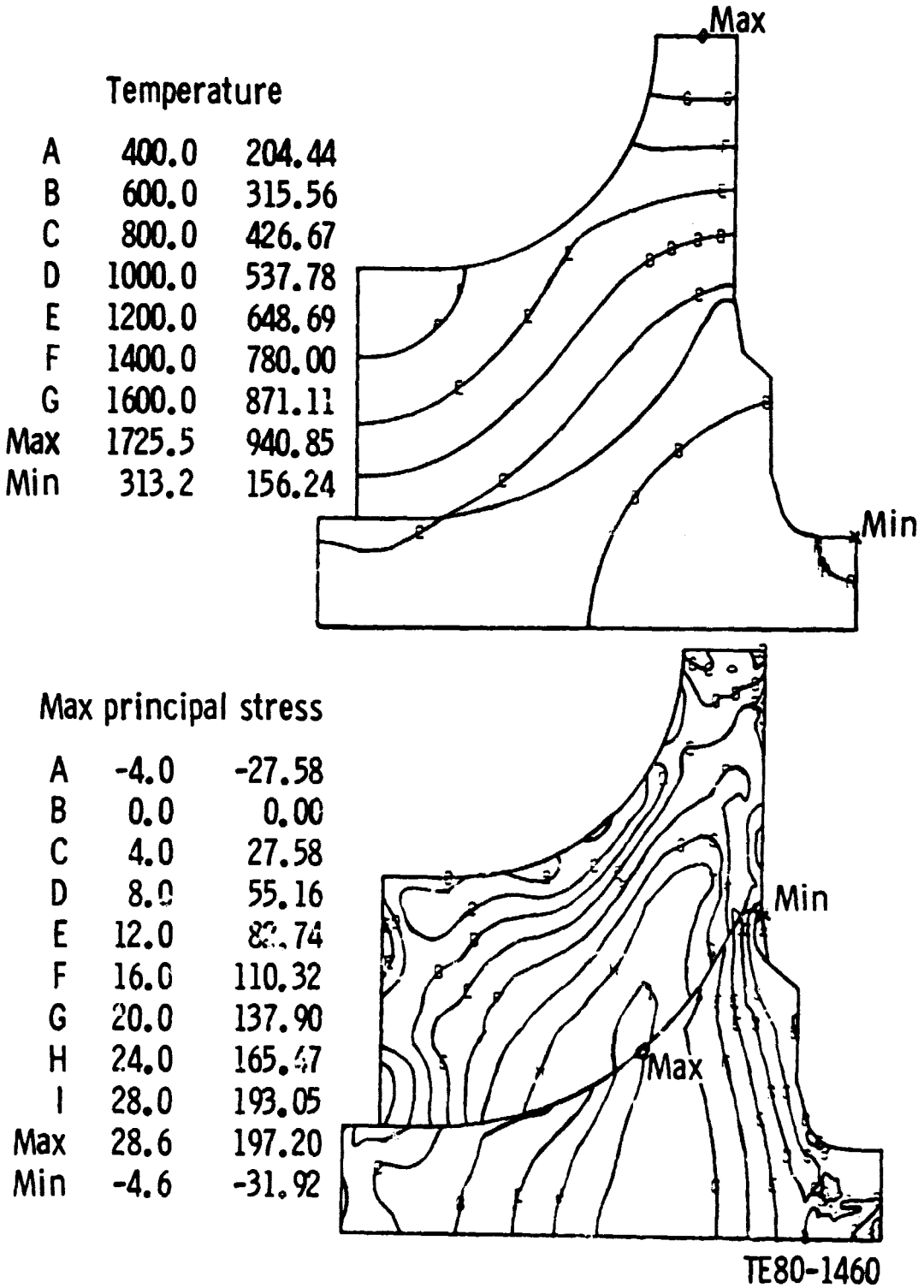

Figure 174. - Ceramic Power Turbine Maximum Transient Results.

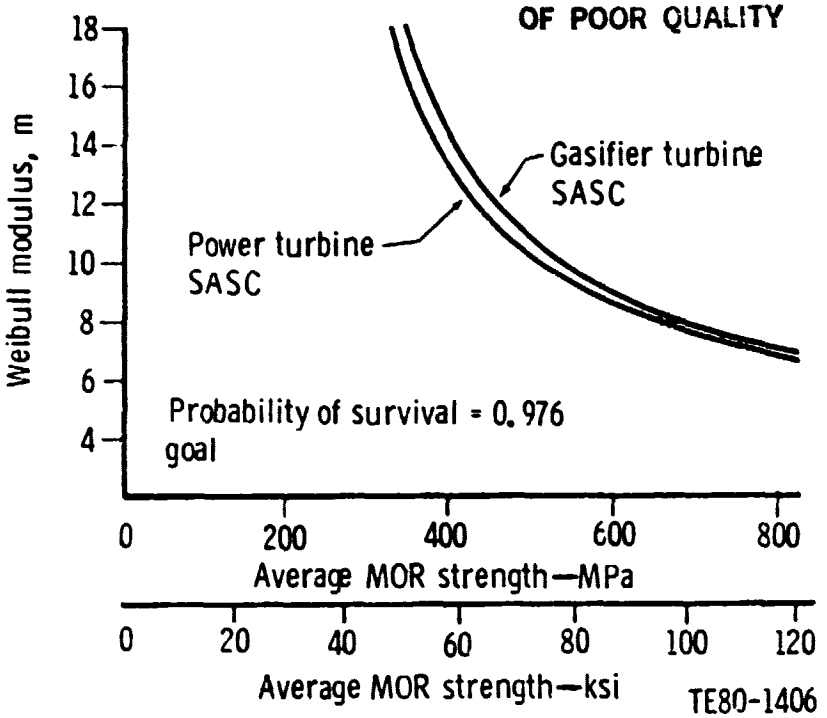

Figure 175. - Material Strength Requirements for Ceramic Turbines.

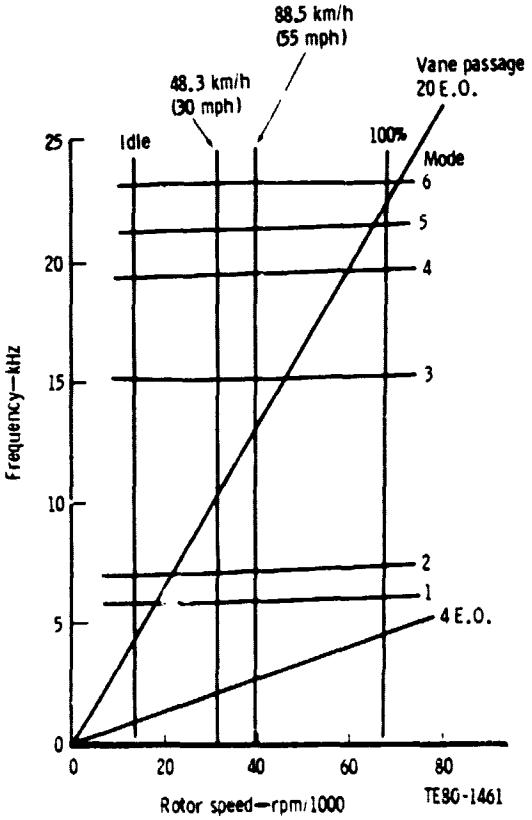

Figure 176. - Preliminary Frequency--Speed Interference Diagram--SiC Power Turbine.

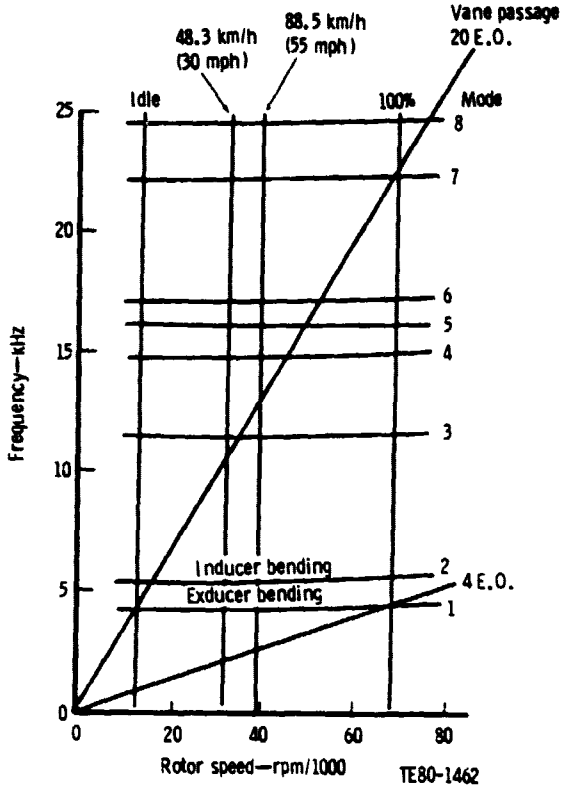

Figure 177. - Preliminary Frequency--Speed Interference Diagram--Si_3N_4 Power Turbine.

6.1 RPD

The design of the combustor for the AGT-100 RPD has closely followed the design of previous DDA low-emission combustors. The fuel and a portion of the inlet air are combined in a swirling mixture within a prechamber. The fuel is vaporized within the prechamber because of the high temperature of the prechamber walls and the inlet air. When the fuel and air leave the prechamber, they enter the main burning zone in a highly premixed and prevaporized condition.

To keep the exhaust emissions below a specified level, the burning zone temperature must be carefully controlled to stay within narrow limits. This control is accomplished by adjusting the division of primary and dilution zone air through the use of variable geometry.

At idle, sufficient air is admitted into the prechamber through a fixed swirler to maintain the proper combustion zone temperature. As the fuel flow rate is increased above idle, the variable geometry must be moved to introduce more air into the fuel preparation zone. This is accomplished by uncovering a swirler that allows air to feed into the prechamber, combining with the air entering the prechamber through the axial swirler.

As the variable geometry is opened further, the flow area can become a significant portion of the flow area through the prechamber, especially when a large diameter centerbody is used with the prechamber as it is in the AGT-100 RPD design. When these areas become similar, the total flow through the prechamber is less than that which would be expected for the open areas of both the swirlers. This flow reduction, which can be accounted for by reducing the value of flow coefficient for the swirler openings, must be known before the prechamber can be properly sized.

Aerodynamic Design

The RPD combustor conditions for steady state operation are given in Table XXIII. The last column of this table lists the total effective area required for the combustor if it is to operate at the design pressure drop of 2.5%. The prechamber diameter was sized to permit sufficient flow through the swirler for a given movement of the variable geometry.

TABLE XXIII. AGT-100 RPD COMBUSTOR CONDITIONS AT 152.4 m (500 ft), 29°C (85°F)

Mod I

	W_A, kg/s (lbm/sec)	BIT, °C (°F)	BIP, kPa (psia)	F/A	F_1	W_F, kg/h (lbm/hr)	BOT, °C (°F)	Total effective area mm^2 ($in.^2$)
Max power	0.289 (0.638)	727 (1341)	416.44 (60.4)	0.0106	0.0219 (0.448)	10.98 (24.2)	1080 (1976)	1665 (2.58)
80 km/h (50 mph)	0.156 (0.345)	839 (1543)	227.54 (33.0)	0.0073	0.0229 (0.468)	4.13 (9.1)	1080 (1976)	1735 (2.69)
32 km/h (20 mph)	0.105 (0.231)	854 (1570)	166.17 (24.1)	0.0052	0.0212 (0.432)	1.95 (4.3)	1025 (1877)	1606 (2.49)
Idle	0.111 (0.245)	616 (1140)	158.59 (23.0)	0.0038	0.0219 (0.426)	1.54 (3.4)	749 (1380)	1581 (2.45)

The values of discharge coefficient, which were determined from prechamber experiments (described later in this section), were used for the swirlers. An iterative solution was followed to arrive at the proper combination of prechamber diameter, swirler opening area, annulus area, and centerbody diameter.

A determination of the required dilution zone area can be made after a primary zone flame temperature has been selected for each operating point. This flame temperature can theoretically be as high as 1649°C (3000°F) without producing excessive emissions. For the AGT-100, RPD combustor, however, this temperature has been limited to values consistent with previous DDA low emission experience.

The flame temperature can be used with the condition of Table XXIII to determine what portion of this total airflow should pass into the primary zone and take part in the combustion process. The total effective area shown in Table XXIII is required to operate at the design pressure drop of 2.5%. Multiplying this area by the percent primary flow determines the required primary zone area. At idle and low speed, the actual primary zone area, which is made up of the swirler area and the leakage area under the variable geometry band, is larger than the ideal primary zone area. As a result, the total combustor area must be increased to maintain the proper percent primary flow, and therefore, the combustor pressure drop will decrease at vehicle speeds below 24 km/h (15 mph). The dilution zone area is found by subtracting the primary zone effective area from the total combustor effective area. Figure 178 presents curves of total, primary, and dilution effective area as a function of vehicle operating speed.

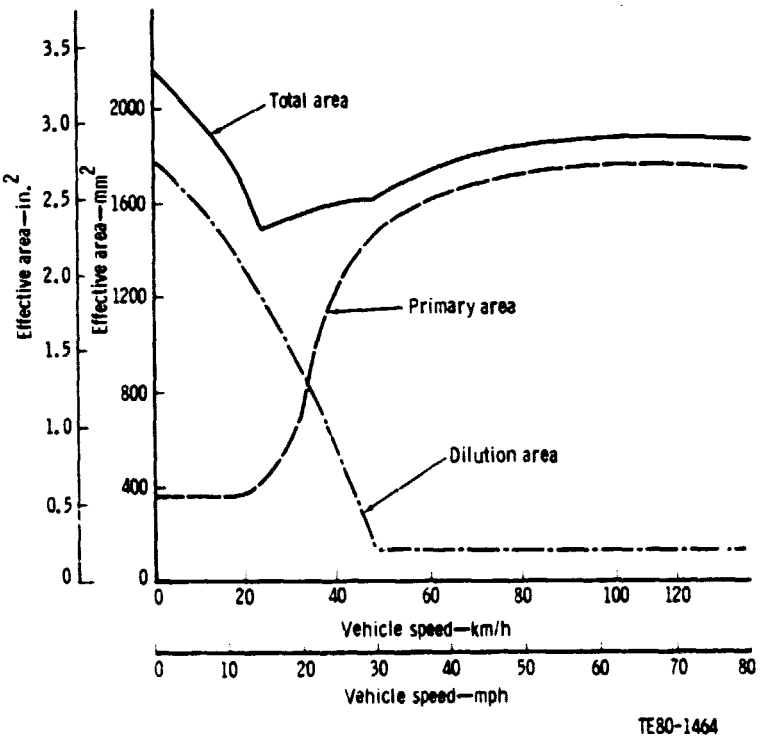

Figure 178. - Variation with Vehicle Speed of AGT-100 Combustor Areas.

The relation between dilution effective area and variable geometry movement is shown in Figure 179. This relationship is the most ideal variation possible and would result in a nearly constant pressure drop over the operating cycle at speeds above 24 km/h (15 mph). It is necessary to select an actual dilution hole shape that will follow as closely as possible the ideal relationship of effective area versus variable geometry.

Several dilution hole configurations were considered. Each configuration produced a slightly different total area for any given flow split to the primary zone. Since the total area changed, the combustor pressure drop also changed, and it was necessary to evaluate the resulting pressure drop for the various configurations. Three dilution hole options are shown in Figure 180. Option 1 represents the simplest shape to fabricate. Option 4 represents a configuration that would maintain a reasonably constant pressure drop, and option 7 represents the maximum amount of contouring that would seem feasible for a ceramic liner. The pressure drops for options 1 and 7 are also shown in Figure 180 as a function of vehicle speed.

Option 7 offers a slightly more uniform pressure drop; however, the difference between the two configurations is of little significance and, therefore, the simple shape of option 1 was selected. The final relationship for the RPD combustor between total effective area, variable geometry position, and primary zone flow split is shown in Figure 181.

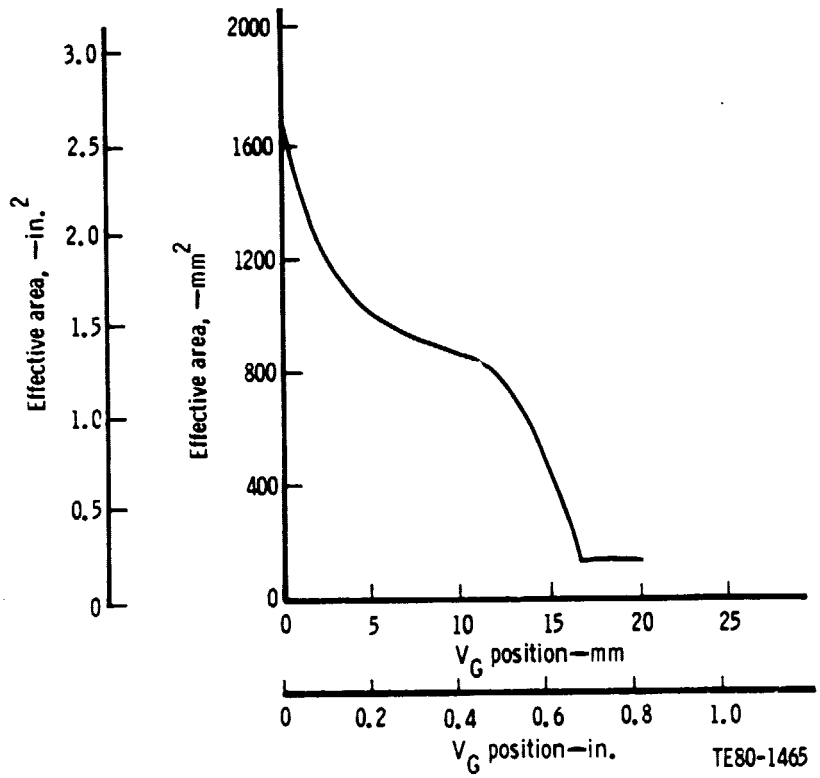

Figure 179. - Ideal Variation of Dilution Area for AGT-100 RPD Combustor with Variable Geometry Position.

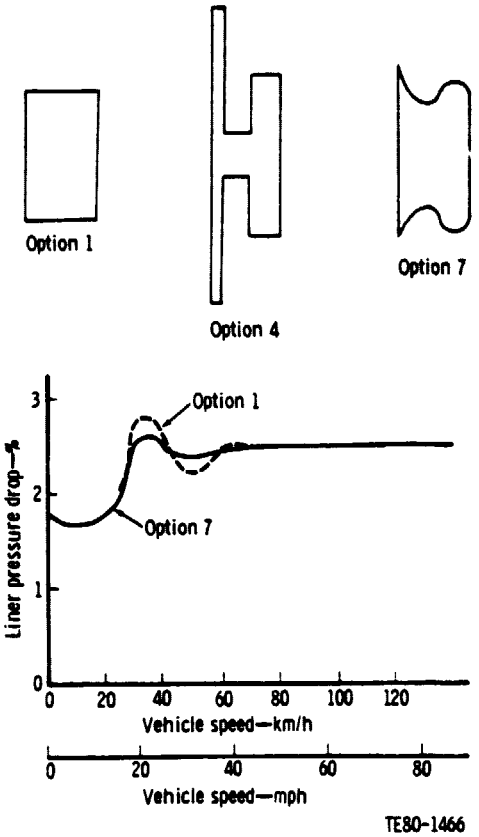

Figure 180. - Dilution Hole Geometry and Its Effect on Liner Pressure Drop.

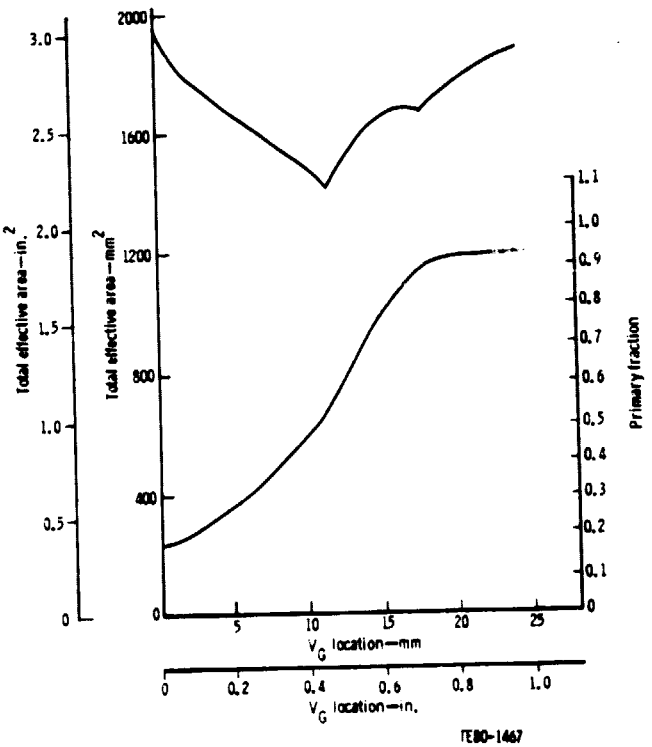

Figure 181. - AGT-100 RPD Combustor Total Area and Percent Primary Flow for Dilution Option 1.

Analytical Analysis

A computer program has been developed by DDA to analyze swirling, reacting turbulent flow in axisymmetric combustors. The program is entitled COSMIC (Computation of Swirl/Mixing in Combustors) (ref. 4), and it can be used to predict velocities, pressures, temperatures, species concentrations, and turbulence quantities throughout the region of interest.

The COSMIC computer program was first used to predict the flow field to determine the appearance of the flow in a combustor whose performance had previously been determined. Two conditions were analyzed--idle and maximum power. For the idle point, all of the primary zone air was assumed to enter through the axial swirler at the beginning of the prechamber. The predicted streamlines for this condition are shown in Figure 182. The large recirculating zone enclosed by the "zero" streamline begins almost immediately downstream of the axial swirler and extends beyond the exit of the combustor. Approximately 23% of the flow recirculates in this zone. The dilution holes are not shown in this figure and were not included in the computer analysis. The leading edges of the dilution slots were located at about 241 mm (9.5 in.) from the prechamber axial swirler. The computer analysis indicates that the dilution hole location might have allowed some dilution air to recirculate to the primary zone.

When the operating conditions are changed from idle to maximum power, the variable geometry is moved to decrease the dilution slot area and to expose an increased area at the prechamber. Figure 183 shows the flow streamlines at the maximum power condition. The recirculation zone now begins at the end of the centerbody and is completed before reaching the dilution holes. In addition, only 8% of the flow is involved in the recirculating flow. The combustor included a trip (orifice) located at the exit of the prechamber; however, this geometric flow blockage was not included in the computer analysis shown here.

The flow field within the AGT-100 RPD combustor was also analyzed using the COSMIC computer program. The program was modified to include the proper contour at the exit of the combustor, the spherical end on the prechamber centerbody and the prechamber trip. The analysis was made at idle, 32 km/h (20 mph), 96 km/h (60 mph), and max power. The resulting streamlines for the idle condition are shown in Figure 184. Two differences can be noted between this flow field and that for the first configuration. First, a recirculation zone can now be seen in the corner of the main chamber. This zone has been observed both analytically and experimentally in other combustors, and its existence is related to the angle of the combustor dome wall and the angle of swirl. Above 70% of the total flow is involved in this zone. Second, the center recirculation zone is slightly larger and contains more flow than the first configuration. The center zone recirculates almost 35% of the flow, about 1.5 times that of the first combustor.

The flow streamlines shown in Figure 185 are for a vehicle speed of 96 km/h (60 mph), and the results are similar to other speeds. At this speed, the recirculation zones appear to be established well within the length of the combustor.

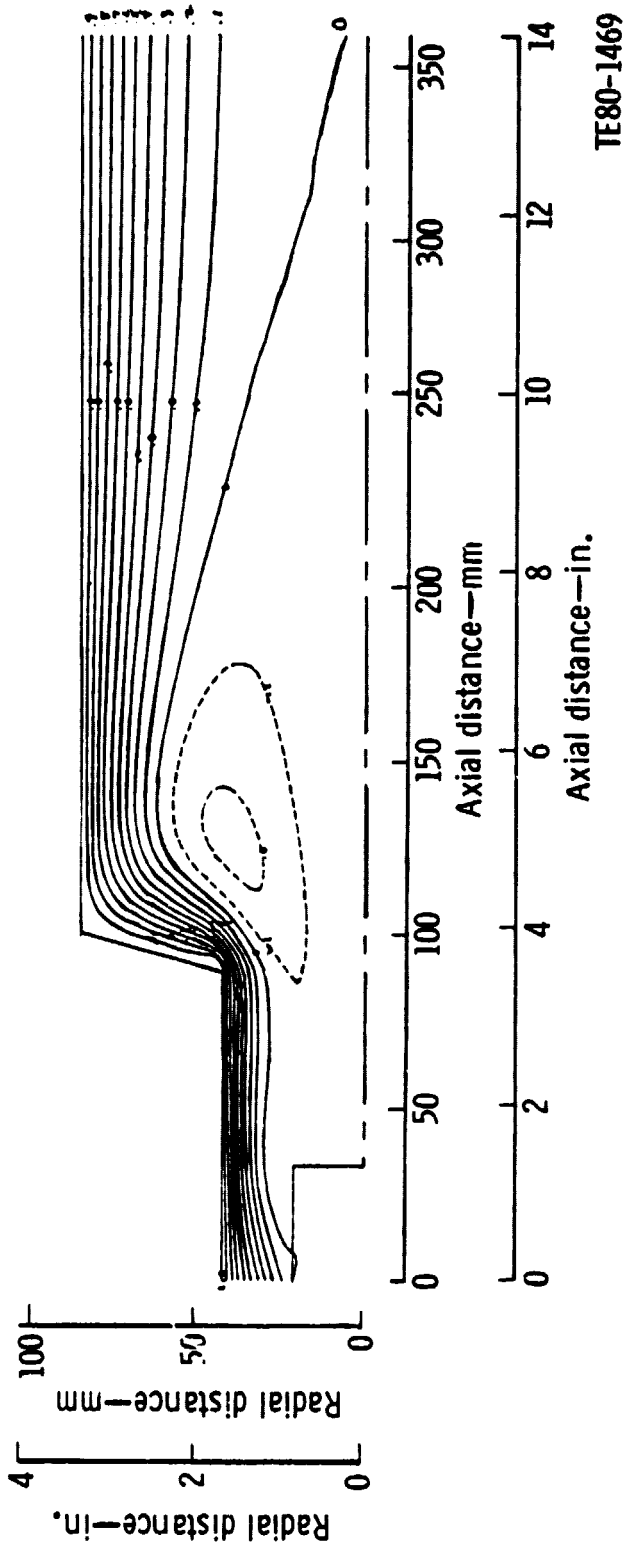

Figure 182. - Idle Point Streamlines for Prior Combustor.

ORIGINAL PAGE IS
OF POOR QUALITY

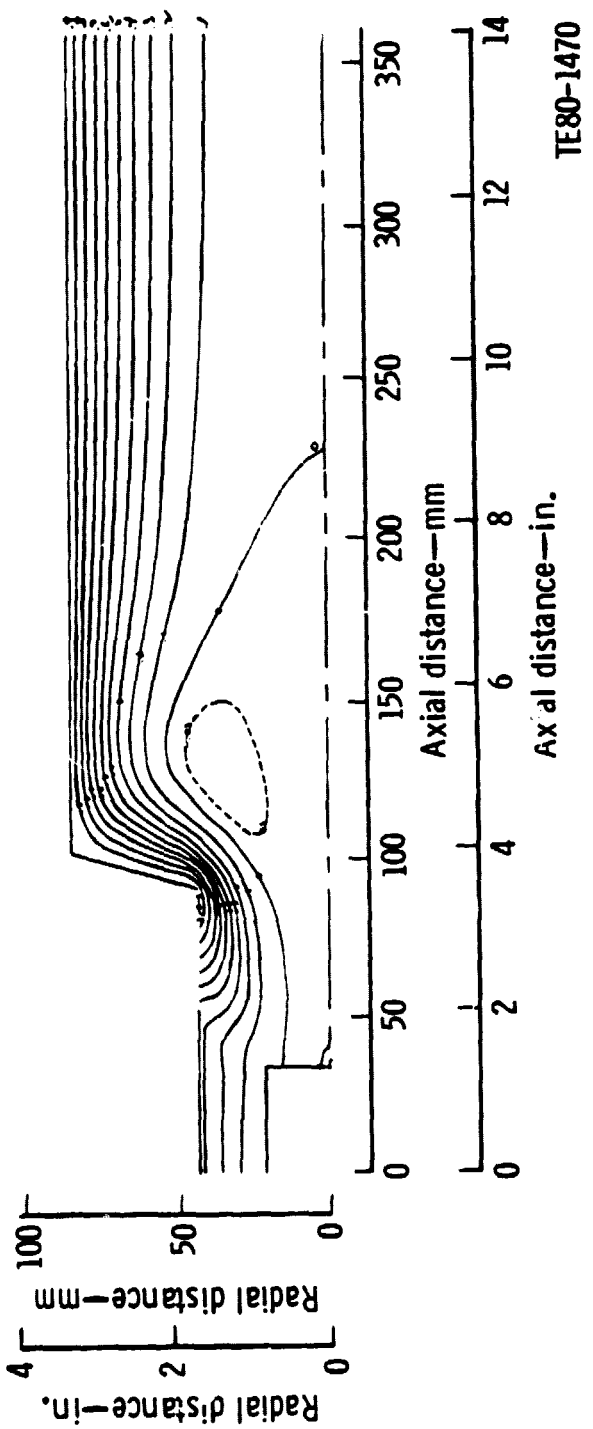

Figure 183. - Maximum Power Point Streamlines for Prior Combustor.

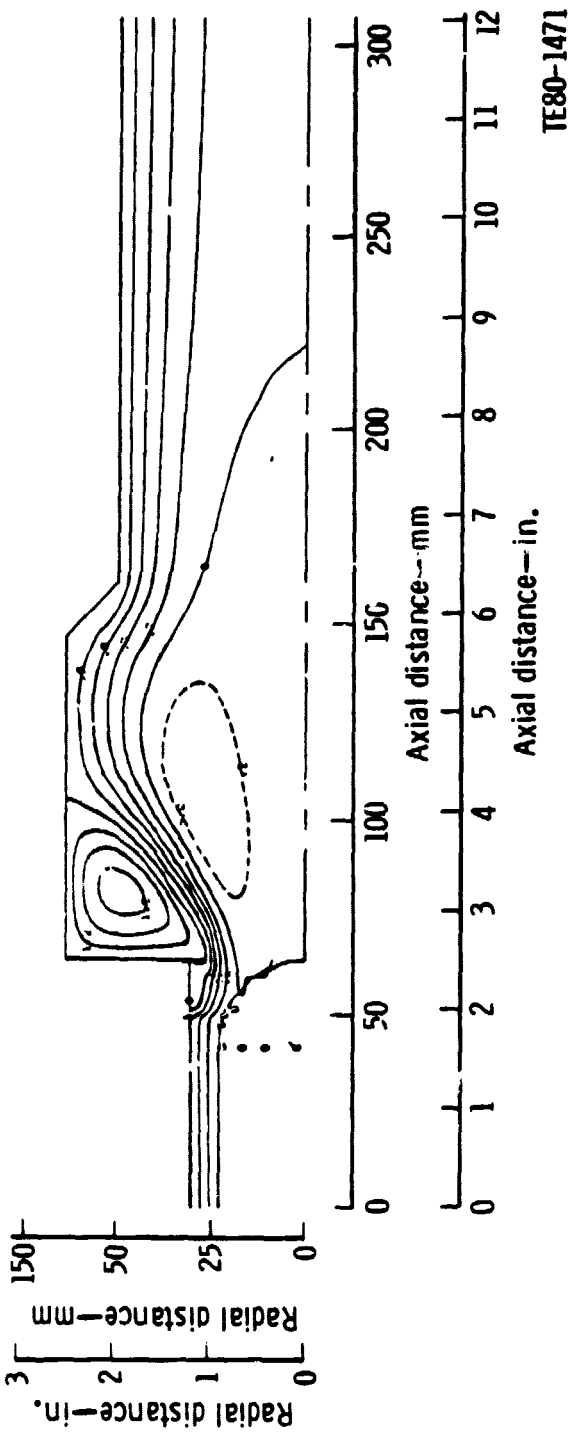

Figure 184. - AGT-100 Flow Streamlines at Idle.

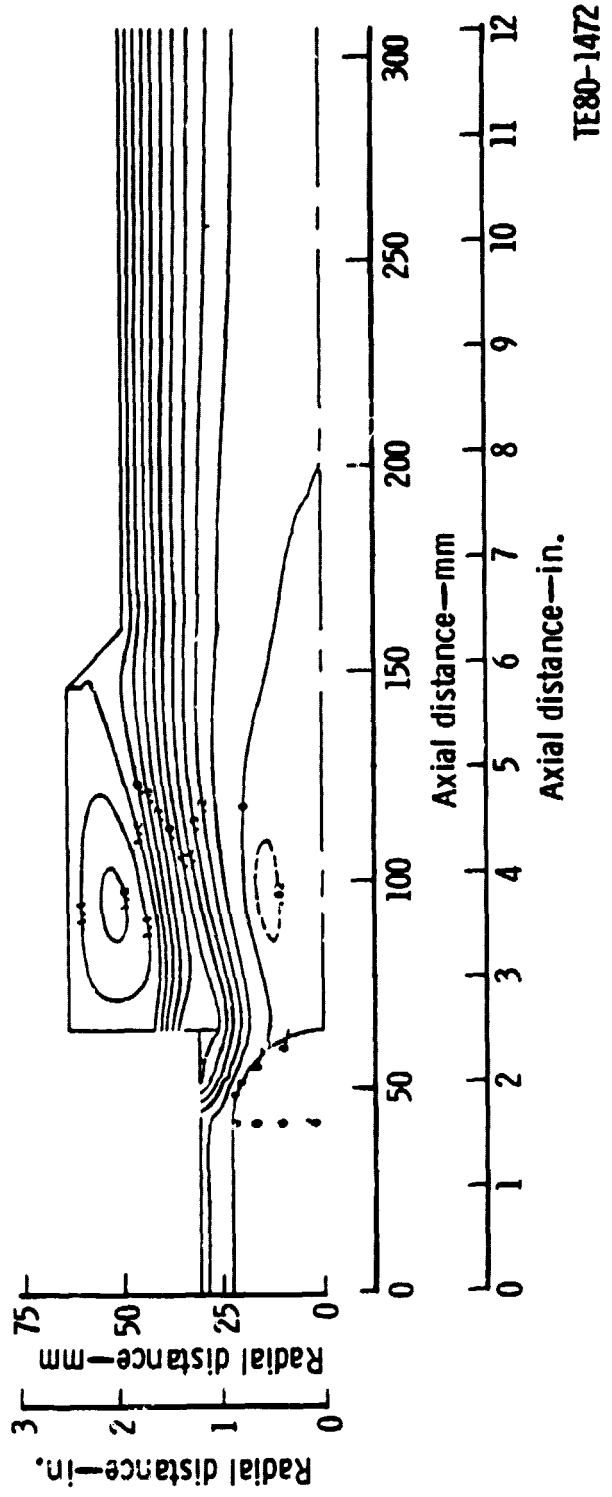

Figure 185. - AGT-100 Combustor--96 km/h (60 mph) Flow Streamlines.

At this time, there has not been sufficient correlation between actual combustion experiments and COSMIC predictions to understand the total significance of these results. It would intuitively seem that larger recirculation zones would improve stability and reduce CO, whereas NO_x might increase because of the increased residence times. The ultimate value of the COSMIC results, however, is in predicting trends. Should an experimental test produce promising results, the COSMIC program can be applied to determine what aerodynamic change resulted. Additional experimental modifications can first be evaluated by a COSMIC analysis at greatly reduced cost to determine whether the desired aerodynamic change is enhanced by the particular modification.

The COSMIC computer analysis was also performed on the RPD combustor at the conditions corresponding to a vehicle speed of 32 km/h (20 mph) for a matrix of conditions to determine the effect of trip height, axial swirl angle, and dome wall angle on the internal flow field. The general appearance of the flow was the same regardless of the height of the trip used. The quantity of flow in the outer corner recirculation zone, however, increased significantly with the size of the trip. A similar effect was noted by increasing the axial swirler angle by 5 deg. The general appearance of the flow field looked the same for both angles, but the outer corner recirculation zone was smaller and contained less mass when the swirl angle was increased from 75 to 80 deg. When the dome wall was angled toward the exit of the combustor, the outer corner recirculation zone initially remained unchanged. However, as the angle was increased further, the corner zone abruptly disappeared, and the center recirculation zone volume was enlarged. The minimum dome angle necessary to eliminate the outer corner recirculation zone was less for an 80-deg axial swirler than for 75 deg.

Figure 186 compares the baseline combustor with 75-deg axial swirler angle and straight dome wall to the modified design with 60-deg axial swirler and 30-deg dome angle. It should be pointed out that no evidence exists to indicate that one of these flow patterns is more desirable than the other. The main purpose of this analysis was to determine whether changes in internal flow field were easily achieved with changes in geometry, and to determine which geometric variables were the most significant.

Heat Transfer and Stress Analysis

To evaluate the stresses and probabilities of survival of the ceramic combustor components, a finite element model of the RPD combustor was developed. A representative section through the ceramic barrel and cover of the model is shown in Figure 187. Also shown is a 45-deg segment of the barrel model (viewed from inside the combustor) and a 45-deg segment of the cover model (viewed from above). The particular barrel segment depicted shows half of a dilution hole and the pilot burner hole. The other barrel segments have a regular mesh in place of the burner hole as described by the section view.

A heat transfer analysis was performed on the combustor at the conditions corresponding to a vehicle speed of 96 km/h (60 mph). The COSMIC computer program was used to generate the internal flow field and to define the velocities and temperatures used as the boundary conditions for this analysis.

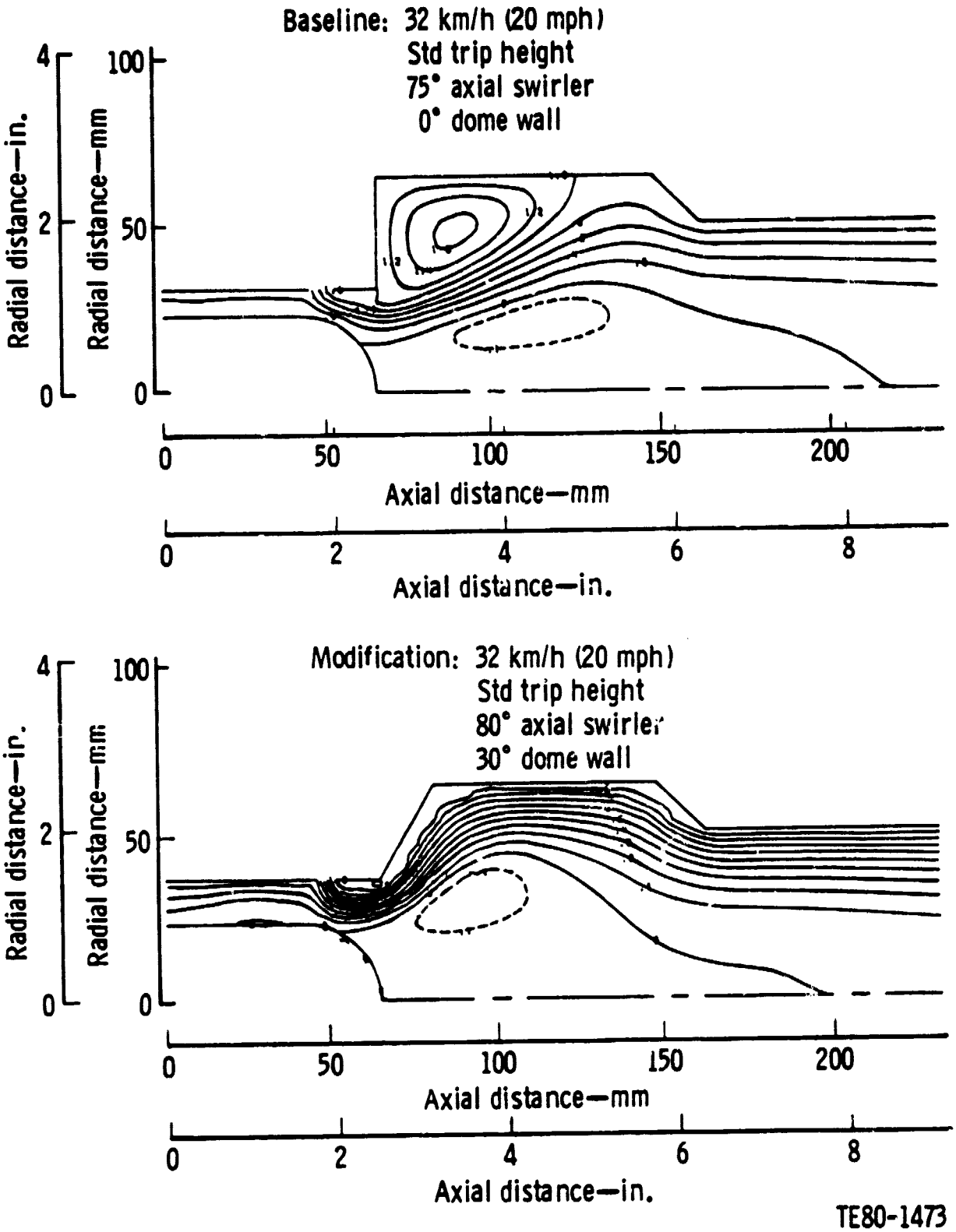

Figure 186. - Comparison of Internal Flow Fields for Two AGT-100 RPD Combustor Concepts.

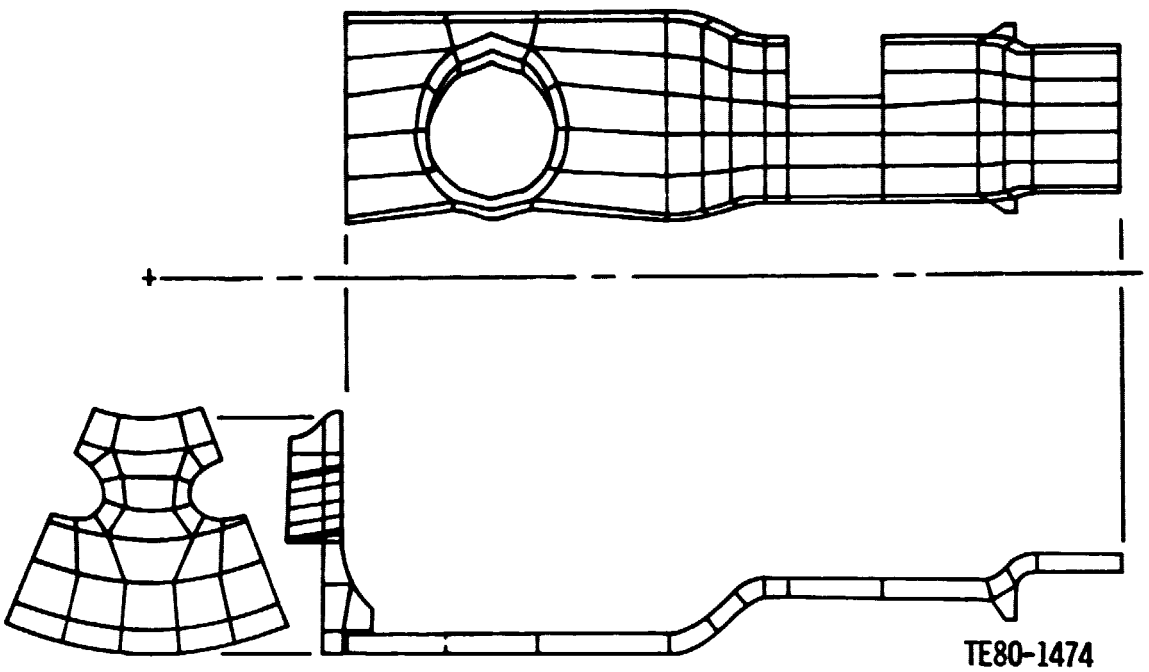

Figure 187. - Representative Section Through Ceramic Combustor Barrel and Cover.

The combustor temperatures predicted by the heat transfer analysis were relatively low and quite uniform. The maximum temperature on the cover plate (dome) was 1041°C (1906°F) and was located near the outer diameter, whereas the minimum temperature of 1037°C (1888°F) was located near the prechamber exit. The maximum temperature on the cylindrical portion of the combustor was 1170°C (2138°F) and was located at the exit; the minimum was 1020°C (1886°F) located about 1.3 mm (0.5 in.) below the front edge of the cylinder.

These temperatures were then used as boundary conditions for a stress analysis of the steady state, 92 km/h (60 mph) condition. An analysis of the cover plate (dome) was not made because the thermal gradients were obviously too low to produce any significant stresses. In the cylindrical portion of the combustor, the computer analysis predicted low stresses with the maximum stress being approximately 10 MPa (1.45 ksi). This level would yield a probability of failure of about 10^{-12}.

A typical cold start transient cycle was also defined to evaluate the heat transfer and stress analysis of the RPD combustor during transient conditions. The assumed cycle was similar to one that had been used for the gasifier turbine analysis. In this cycle, the engine is started from ambient conditions and accelerated to idle in 10 seconds. Idle speed is maintained for an additional 10 seconds followed by a 15 seconds full-power acceleration. The 35 second cycle was divided into nine increments of time and a COSMIC analysis of the flow and temperature fields was made at each of the nine conditions. These COSMIC results were used as step inputs into a transient heat transfer analysis of the ceramic combustor. A stress analysis will be made at whatever point(s) during the cycle the thermal gradients appear to be the most severe.

Mechanical Design

A drawing of the RPD combustor is shown in Figure 188*. The components that make up the total combustion system are summarized below.

- o Continuous flame pilot fuel chamber
- o Starting fuel nozzle
- o Wall film fuel injection
- o Prechamber
- o Variable geometry
- o Ceramic liner

The following description presents the combustor mechanical features, in the order in which the particular component functions during an engine light-off, start, and run cycle. The engine light-off is initiated in the pilot fuel chamber, which is located on the side of the main combustion liner. Atomized fuel is ignited as it enters through the pilot fuel nozzle and mixes with air entering through the swirler surrounding the nozzle tip. The pilot flame burns continuously during all engine operations. The pilot combustion products enter the main combustion liner in a tangential direction because the pilot chamber centerline is not radial to the main combustion liner. A flame sensor sends a signal to open the starter fuel nozzle valve after a flame is detected.

*Modified to delete certain patent-sensitive items.

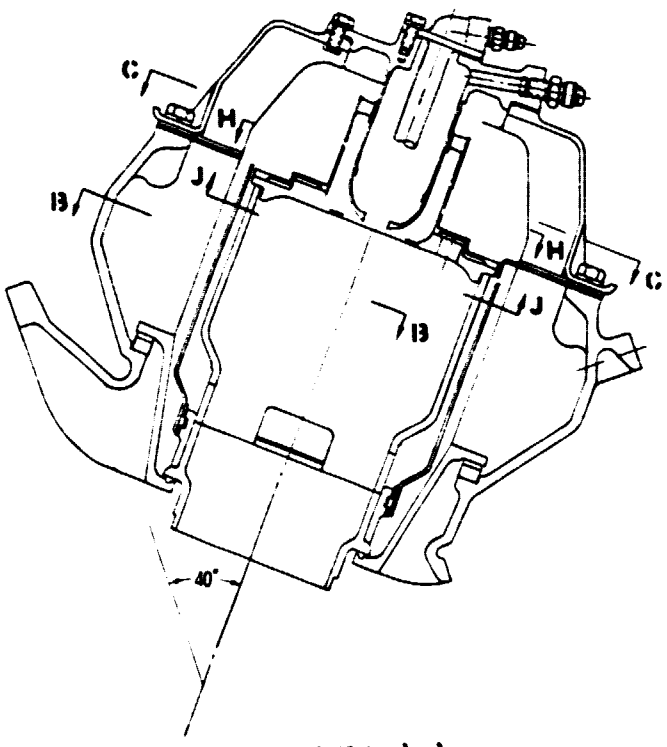

Figure 188. - RPD Combustor Layout (Modified to Delete Certain Patent-Sensitive Items).

The starter fuel nozzle is located on the burner centerline inside the prechamber centerbody. Compressor discharge pressure (CDP) air, which flows through the centerbody and surrounds the nozzle to prevent coking, discharges through nozzle swirler vanes. Fuel from the starter nozzle is ignited by the pilot flame, and the starting nozzle provides a diffusion flame during the start and warmup process. The starter fuel accelerates the engine to near idle speed until the burner inlet temperature (BIT) has increased sufficiently to permit operation of the main fuel system. After the main fuel system begins operation, the starter fuel shuts off and remains off during the remainder of the engine operation.

The prechamber and variable geometry components which are exposed to combustor inlet air temperature of 1023°C (1875°F) are made of Hastelloy X material. The liner dilution sliding band, which is exposed to the 1288°C (2350°F) burner out temperature is made of sintered alpha silicon carbide (S-SiC).

Above idle speed, the main fuel is supplied from a manifold around the prechamber. The manifold is air-cooled and is located downstream of the swirler. The prechamber was sized to be long enough to provide sufficient area for fuel vaporization but short enough to prevent high residence times, which could cause preignition. The velocity of the fuel/air mixture within the prechamber is maintained appreciably above the flame speed to prevent combustion from occurring within the prechamber itself.

As the engine speed increases above idle, more primary zone flow and thus more flow area is required to maintain the desired flame temperature. This is accomplished by a control signal to the variable geometry actuator shaft, which lifts the variable geometry mechanism toward the top of the combustor. Initially, the supply port to the swirler is uncovered which allows more flow to pass into the prechamber to mix with the vaporizing fuel. When the variable geometry linkage is lifted to open this prechamber port, the dilution air port is closed since the two bands are linked together. The design is such that the dilution air is nearly closed for most operating conditions above idle. The ignition of the premixed fuel/air ratio takes place at the prechamber exit inside the liner.

The liner material, which will be exposed to maximum peak temperature of 1455°C (2650°F), is sintered alpha silicon carbide. The ceramic liner consists of three components: the dome, the body, and the exit flange. The dome is basically a flat machined disk which forms the top of the combustor. The body is a cylinder with 5-mm (0.2-in.) walls and has cut-outs for the dilution air ports and the pilot fuel chamber. The flange, located at the combustor exit, rests on an additional ceramic structure, which is located between the combustor and the engine block.

A seal at the exit flange prevents high-pressure air from bypassing the combustor. A normal force must be maintained on this seal under all operating conditions. Because there is a three-to-one difference in thermal expansion between the ceramic liner and the cast iron block, they cannot be rigidly attached. Therefore, the liner positioning and sealing force in the vertical direction is provided by spring loading, which accommodates the differential thermal growth. The liner lateral loads are reacted by radial stops, which extend from the burner housing block/cover flange.

6.2 MOD I DESIGN

The Mod I combustor conditions for steady-state operation are given in Table XXIV. The last column of this table lists the total area required for the combustor to operate at 2.5% pressure drop. The procedure followed in designing the Mod I combustor was very similar to that followed for the RPD. The axial swirler was kept identical to the RPD. The flow factors for the Mod I conditions are less than the flow factors for the RPD conditions. Therefore, less flow area is required to maintain the same pressure drop. Because of this situation the prechamber diameters are slightly less for the Mod I combustor than they were for the RPD.

TABLE XXIV. AGT-100 MOD I COMBUSTOR CONDITIONS AT 152.4 m (500 ft), 29°C (85°F)

	Mod I							
	W_A, kg/s (lbm/sec)	BIT, °C (°F)	BIP, kPa (psia)	F/A	F_1	W_F, kg/h (lbm/hr)	BOT, °C (°F)	Total effective area, mm² (in.²)
Max power	0.289 (0.638)	727 (1341)	416.44 (60.4)	0.0106	0.0219 (0.448)	10.98 (24.2)	1080 (1976)	1665 (2.58)
80 km/h (50 mph)	0.156 (0.345)	839 (1543)	227.54 (33.0)	0.0073	0.0229 (0.468)	4.13 (9.1)	1080 (1976)	1735 (2.69)
32 km/h (20 mph)	0.105 (0.231)	854 (1570)	166.17 (24.1)	0.0052	0.0212 (0.432)	1.95 (4.3)	1025 (1877)	1606 (2.49)
Idle	0.111 (0.245)	616 (1140)	158.59 (23.0)	0.0038	0.0219 (0.426)	1.54 (3.4)	749 (1380)	1581 (2.45)

The maximum burner outlet temperature for the Mod I combustor is 1071°C (1976°F). The flame temperature necessary to maintain low emissions was assumed to be constant at 1204°C (2200°F). This temperature and the conditions of Table XXIV were used to define the required dilution area. The variation in dilution area was best met by using triangular dilution holes rather than the rectangular openings used for the RPD. The final Mod I combustor design is shown in Figure 189.

No ceramic material was used in the Mod I design. Instead, Lamilloy®* was used for the main body and pilot flame tube. A one-dimensional heat transfer analysis was conducted to determine the proper Lamilloy® configuration. A three ply composite with a flow coefficient of approximately 0.004 was chosen for use in the main body. For the smaller diameter pilot flame tube, a two-ply structure was chosen with a flow coefficient of 0.013. The dome area and the exit cylindrical portion of the Mod I combustor are exposed to high temperatures but are difficult to cool because of their design and location. It may be necessary to add a ceramic coating on both of these areas to provide additional thermal protection.

Combustor Rig

A new combustor test rig as shown in Figure 190 was designed for the AGT-100 test program. This rig has the capability of operating at the actual high inlet and exit temperatures of the AGT-100 engine cycle. It incorporates the

*Lamilloy® is a registered trademark of the General Motors Corporation.

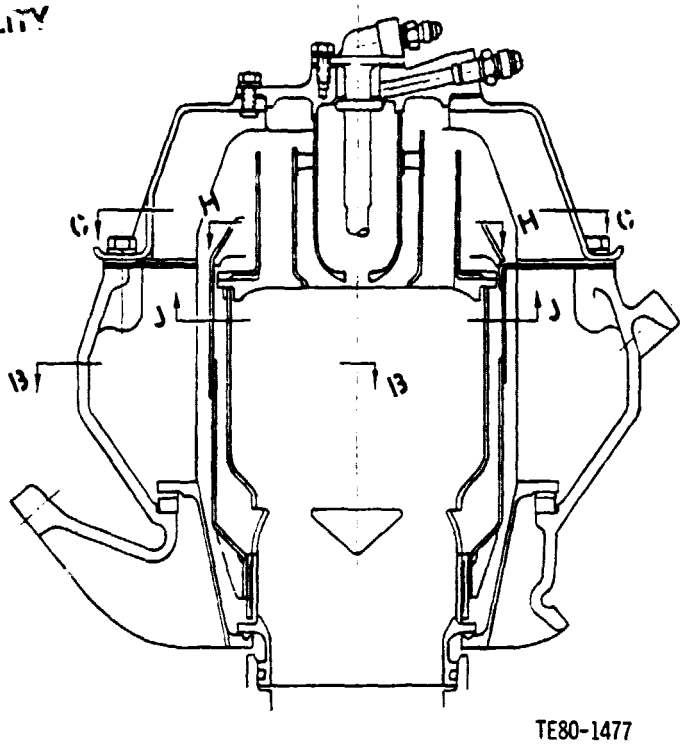

Figure 189. - Mod I Combustor Layout.

engine flow path, insulating features, and combustor orientation and can control the variable geometry in the same manner as it will be controlled on the engine. The engine fuel delivery and ignition systems will also be incorporated on the rig. Because of the higher combustor exit temperature, much of the discharge section has been water cooled to allow use of conventional materials. Instrumentation for this higher temperature rig will be designed specifically for this application. Previous DDA experience has shown that water-cooled gas sampling probes perform satisfactorily at burner exit temperature levels that will be encountered in testing the AGT-100 combustors and that temperature and pressure probes should be fabricated from thoriated platinum.

Features of the combustor instrumentation are as follows:

- o Combustor exit temperature will be obtained from four radial rakes, each having four single-element closed junction thermocouples made from platinum-rhodium alloy. The thermocouples are located at radial positions that are in the center of four equal-area sectors.
- o The exit total pressure is measured by a single element located on each of the four radial rakes. The four pressure taps will be connected to a single manifold external to the rig.
- o The gas sampling probes consist of four additional radial rakes, each having sampling openings located in equal area zones across the exit flow path. The gas sampling rakes are water cooled, and gas samples at the four radial depths are combined into a single, water-cooled manifold within each rake. An external manifold is used to collect the samples from the four rakes.

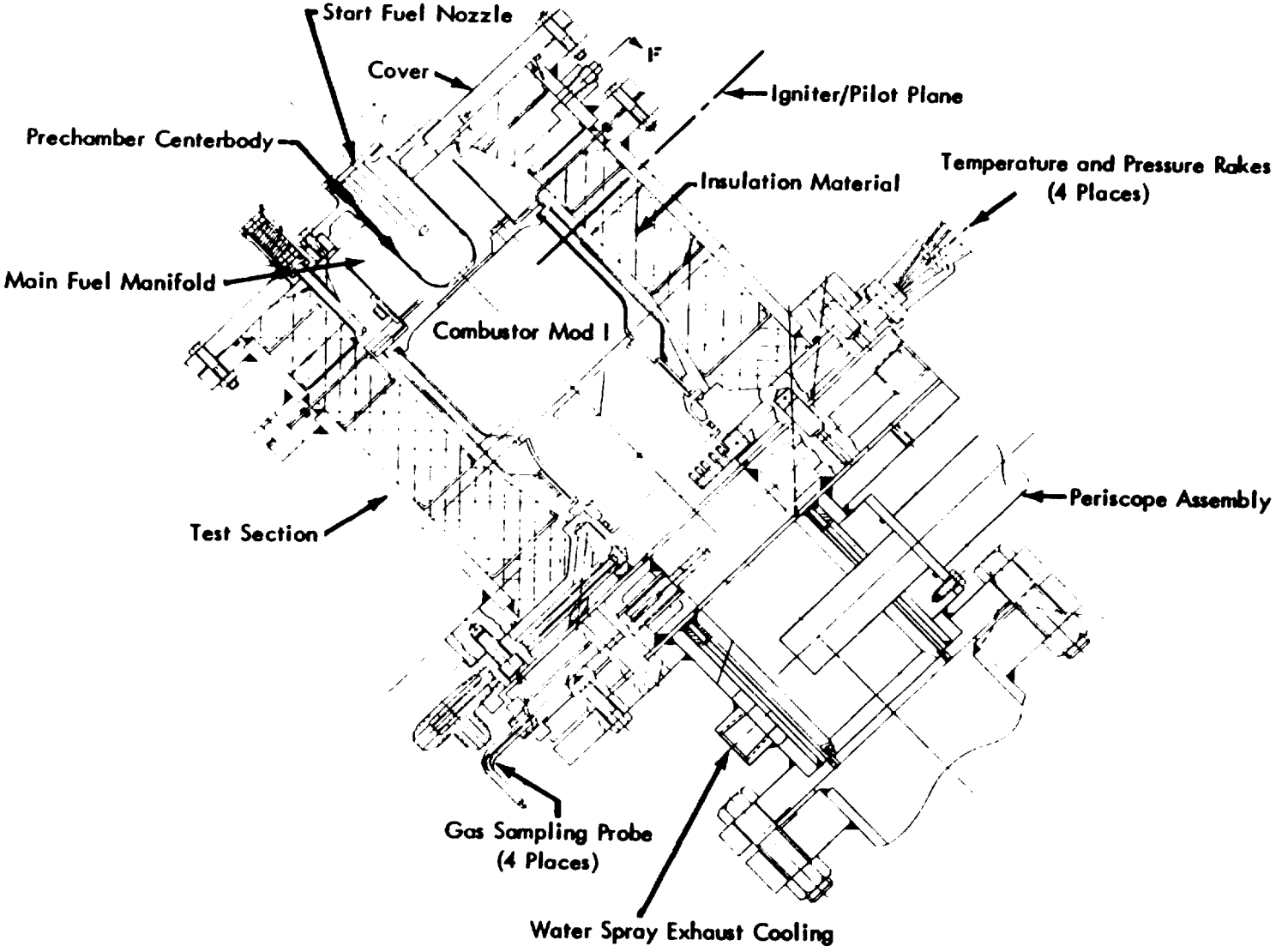

Figure 190. - Combustion Rig Layout.

- o Inlet temperature and pressure instrumentaton bosses are positioned at several locations along the flow path from the air preheaters to the inlet to the combustor rig. Four thermocouples and four inlet static pressure taps will be positioned immediately upstream of the combustor section for monitoring the inlet test conditions.

Prechamber Test

An experimental investigation was conducted to determine the flow characteristics of a typical prechamber. A prechamber model, which included an axial and a variable area radial swirler and also made use of two different diameter centerbodies to change the annulus area, was constructed. A schematic of the test setup is shown in Figure 191, and a photograph of the prechamber is shown in Figure 192. Initially, the prechamber was replaced with a known diameter orifice. Sufficient data were recorded to determine that the orifice discharge coefficient was 0.599, thereby verifying the accuracy of the experimental instrumentation.

The first series of tests with the prechamber flow model revealed several interesting results. The flow angle exiting the prechamber annulus was found to vary considerably with radial location and quite significantly with radial swirler opening. It was also found that that exit flow angle was constant at any particular radial position for any given radial swirler opening regardless of pressure drop (and hence airflow through the prechamber).

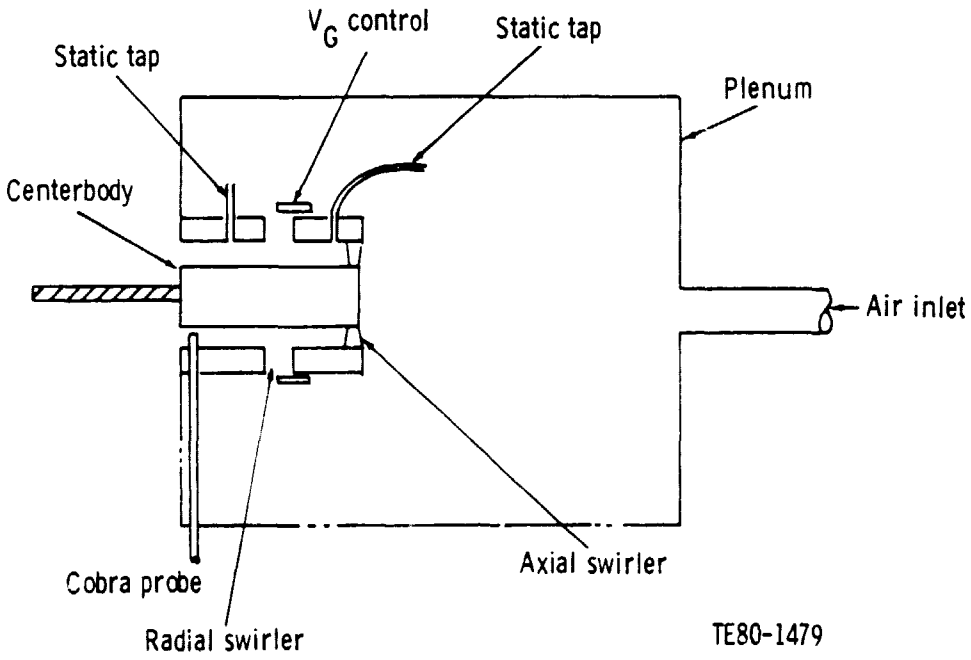

Figure 191. - Prechamber Test Setup.

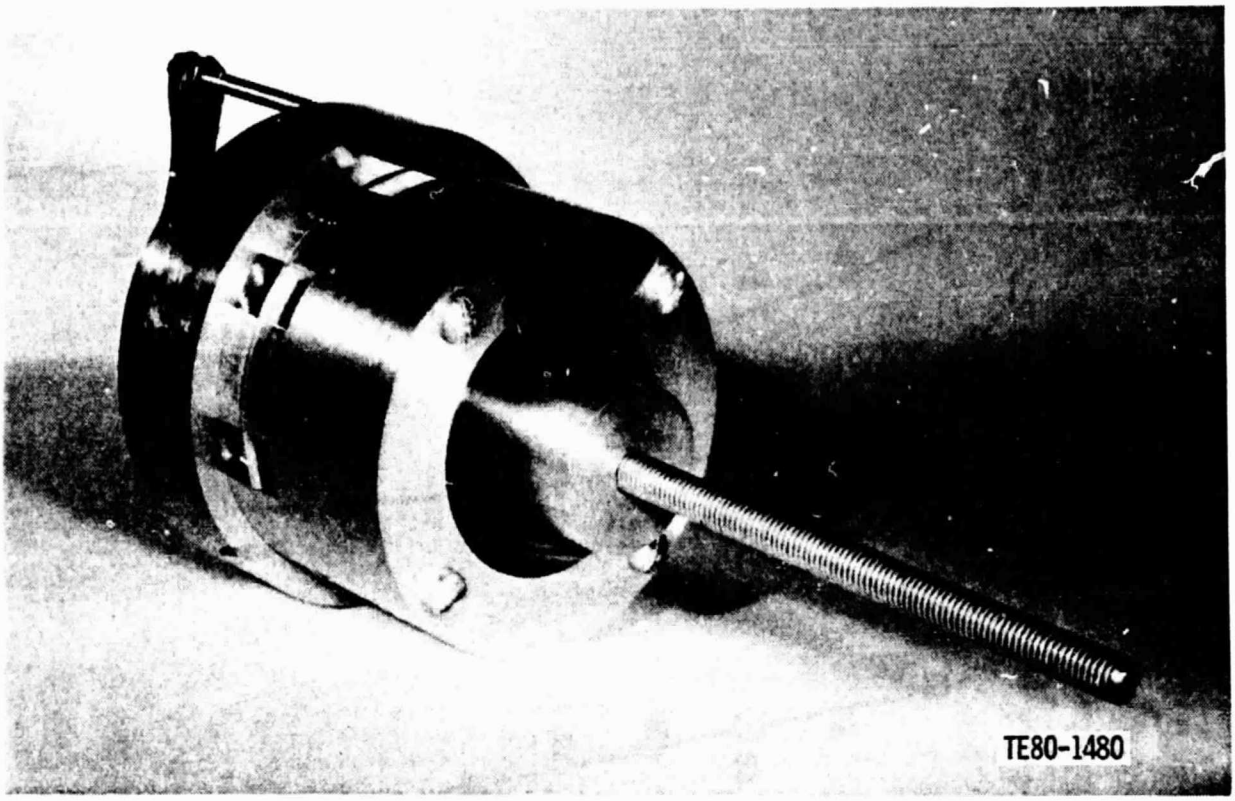

Figure 192. - Prechamber Flow Model with Centerbody.

Another series of tests was performed to determine in what manner the total flow through the prechamber changed and whether the flow through the axial swirler was decreased as the radial swirler area was increased. Both the large and small diameter centerbodies were used to determine the effect of annulus flow area. The angle of the flow exiting the annulus area when the radial swirler was closed was somewhat more axial for the smaller annulus area. However, the change in exit flow angle, which occurred when the radial swirler was opened, was very similar for the two different annulus areas.

The total flow through the prechamber was found to increase proportional to the increase in radial swirler area until the radial swirler area became about 75% of the area in the annulus between the centerbody and the prechamber ID. Beyond that point, the total flow increased much more slowly with radial swirler opening. As the radial swirler flow area was increased, the flow through the axial swirler decreased; however, the apparent C_d for the swirler did not decrease much more than the apparent C_d for the radial swirler.

Figure 193 compares the results for the two different centerbodies. The ratio of radial swirler area to annulus area is probably not the optimum correlating parameter, and the effect of axial swirler angle has not been included. However, the data can be readily used to size the AGT-100 combustors more accurately, and to ensure that the required pressure drop will be obtained.

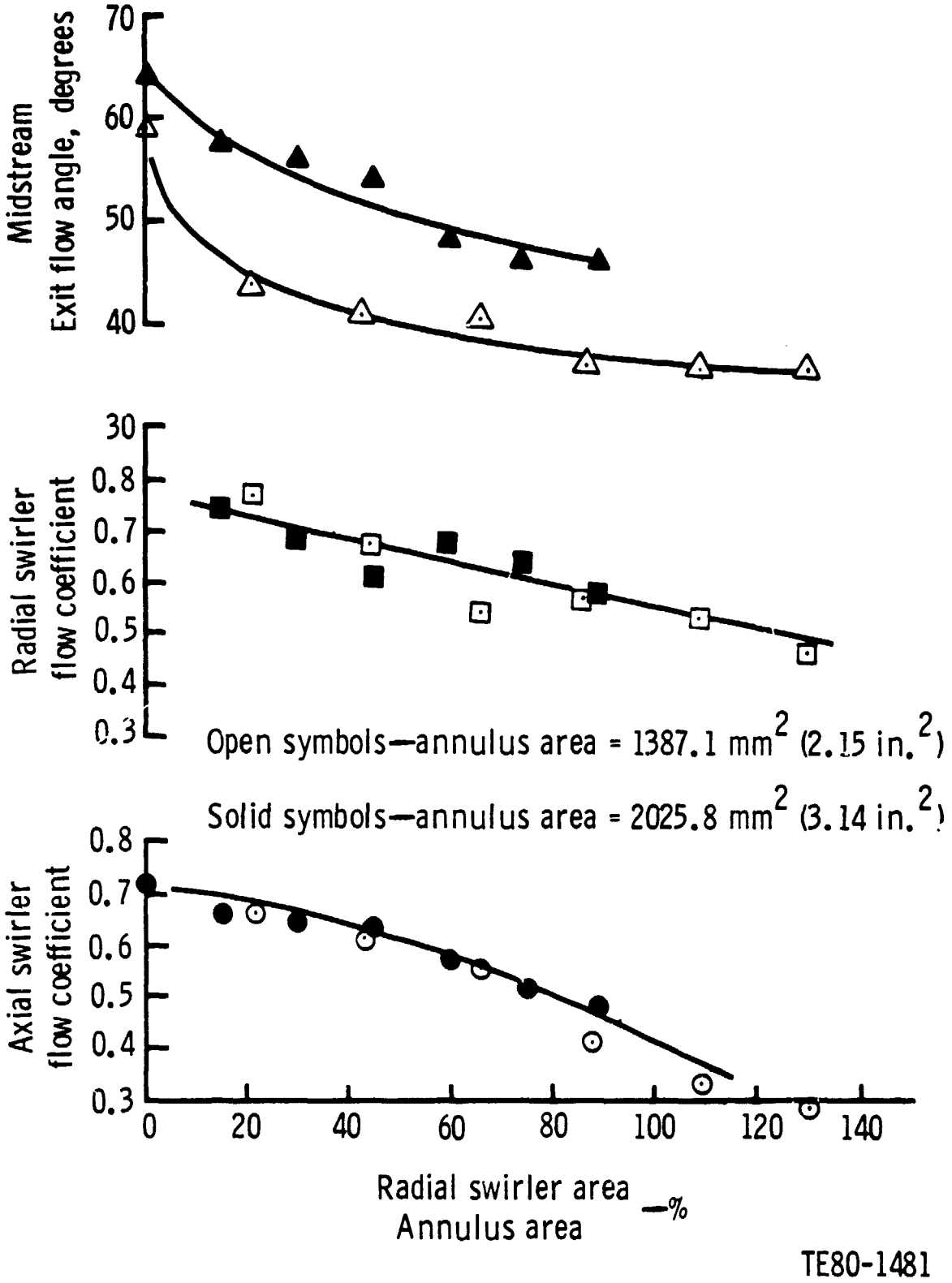

Figure 193. - Prechamber Flow Characteristics--Effect of Radial Swirler and Annulus Area.

7.1 RPD

The general arrangement and principal features of the RPD regenerator system are illustrated in Figure 194. The illustration is an excerpt from the design layout, which is essentially completed. A description of the major components and related, in-progress thermal analyses follows.

Regenerator Disk and Gear Assembly

General Description

The regenerator will be driven by a geartrain from the gasifier turbine rotor and, at 100% rotor speed, turn at 23.58 rpm. The disk will have an OD of 467.4 mm (18.4 in.), a thickness of 74.7 mm (2.94 in.), and an effective core frontal area of about 0.131 m^2 (203 $in.^2$). The Corning Glass Works' aluminum silicate T14-20 matrix configuration (sinusoidal triangle) was selected as the baseline configuration for disk performance and structural calculations, although other matrices will be studied and possibly developed. The T14-20 matrix has a surface area-to-volume ratio of about 54.1 cm^2/cm^3 (1650 ft^2/ft^3). Corning's aluminum silicate disks are currently limited to an operational temperature of 1100°C (2012°F), but 1200°C (2192°F) disks are being developed. This uprating is considered essential to the AGT-100 regenerator in order to provide an adequate operational temperature margin. Although the AGT-100 regenerator inlet temperature will be controlled to a 1066°C (1950°F) limit, that is an average value; higher localized temperatures will occur, particularly during engine accelerations.

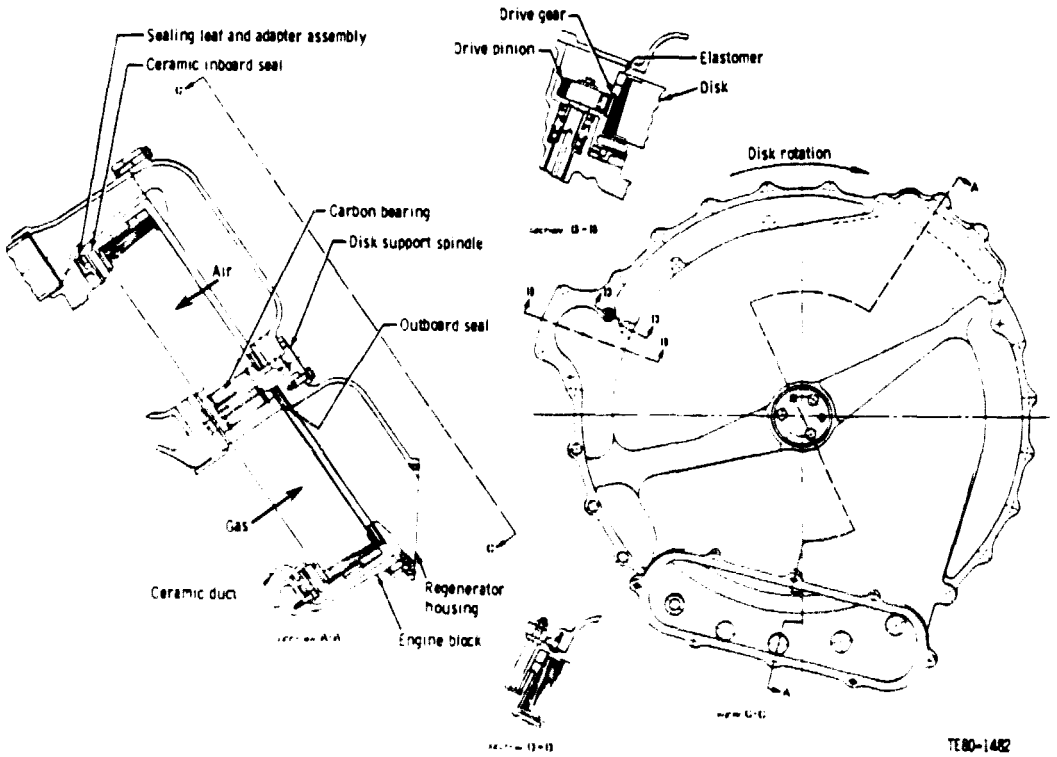

Figure 194. - AGT-100 RPD Regenerator System.

The regenerator disk will be rim driven and center supported by a spindle mounted on the outer enclosure, or housing, of the regenerator cavity. The disk drive and support system is an adaptation of the one performing satisfactorily in the Ceramic Applications to Turbine Engine (CATE) program. As in the CATE, a solid ceramic hub fused into the disk will distribute the hub reaction loads into the matrix and provide a precision pilot for a carbon hub bearing. The bearing is designed with a modified spherical OD surface to accommodate slight tilting of the disk as the disk reacts to axial excursions of the face seals. The disk will be driven with a ring gear that is attached to the outboard ("cold") side of the disk rim with a heat-resistant elastomer. As shown in Figure 194, Section B-B, the adapter between the gear and elastomer will be made the full width of the disk rim to protect the rim from handling damage. The gear and adapter will be made of carbon steel, with suitable coatings to provide resistance to oxidation and tooth wear. The elastomer will be a room-temperature-vulcanizing (RTV) rubber that, to date, has functioned satisfactorily in the CATE regenerator system. Because of the insulating effect of the compressor discharge air and the disk rim, the temperatures of the gear, adapter, and elastomer are not expected to exceed 275°C (528°F).

Figure 194, Section D-D, illustrates a feature that will be incorporated in the regenerator system to facilitate assembly. Because the disk and gear assembly will be hub mounted on the regenerator housing, it must be preassembled with the housing (i.e., placed on the hub spindle) before it is installed in the engine block. Since the hub spindle is canted 35 deg downward in the engine, the disk and gear assembly must also be axially secured to the housing during its installation and removal. The stop shown in Figure 194 will provide the necessary control of the disk and gear assembly during its installation or removal. (As the disk and gear assembly is seated in its operational position, it will be shifted out of contact with the stop, as illustrated.)

Disk Thermal Analysis

A thermal analysis of the regenerator disk has been partially completed. The analysis is used to predict the thermal gradients that will occur in the disk during various operational conditions; these gradients, in conjunction with the associated mechanical and pneumatic loads, provide a basis for computing disk stresses. (The analysis is also used to compute regenerator performance or "effectiveness".) To date, disk temperatures have been computed for the following three operational conditions:

- o 100% engine speed (disk RPM of 23.58) on a 29.4°C (85°F) day at 152.4 m (500 ft) above sea level
- o 48.3 km/h (30 mph) car speed (disk RPM of 11.79), at above ambient conditions
- o Engine idling (disk RPM of 11.79), at above ambient conditions

The effects of variations in the inlet gas flow distribution were also examined; these included, for the 100% engine speed condition, both the "best" and "worst" conceivable distributions--completely uniform flow versus an extreme velocity gradient. The latter distribution was based upon the assumption that the gas leaving the power turbine exhaust duct would not be diffused but would rather impinge upon the regenerator disk in a elliptical spot corresponding to a projection of the conical diffusing section of the duct. (Further informa-

tion about the duct is presented later in this section of the report.) Figure 195 illustrates, in a radial section of the disk, the effect of these two assumed gas flow conditions upon disk temperatures. The effect of the resultant thermal gradients upon matrix stresses has not yet been computed.

Further heat transfer computations also remain to be done, including a disk thermal analysis of the "most likely" flow distribution. Also, the effect of maximum engine accelerations upon disk temperatures and stresses will be an important part of the study.

Inboard (Hot) Side Disk Seal Assembly

General Description

This seal assembly will consist of two separate components: first, the member that will interface with the disk, comprised of a ceramic platform (substrate) and the rubbing wearface material and, second, a static sealing leaf assembly of heat resistant alloys that will be sandwiched between the ceramic platform and the engine block. (Refer to Figure 195, Section A-A.)

The initial candidate for the ceramic seal platform will be a one-piece structure of lithium aluminum silicate (LAS) produced by the Corning Glass Works. This material was selected because of its very low coefficient of thermal expansion and low thermal conductivity; the former characteristic is desirable for minimal seal warpage, whereas the latter will provide some thermal protection for the static sealing leaves that are pressure-loaded against the platform. The insulating characteristic of the LAS ceramic was considered in the selection of the initial platform thickness.

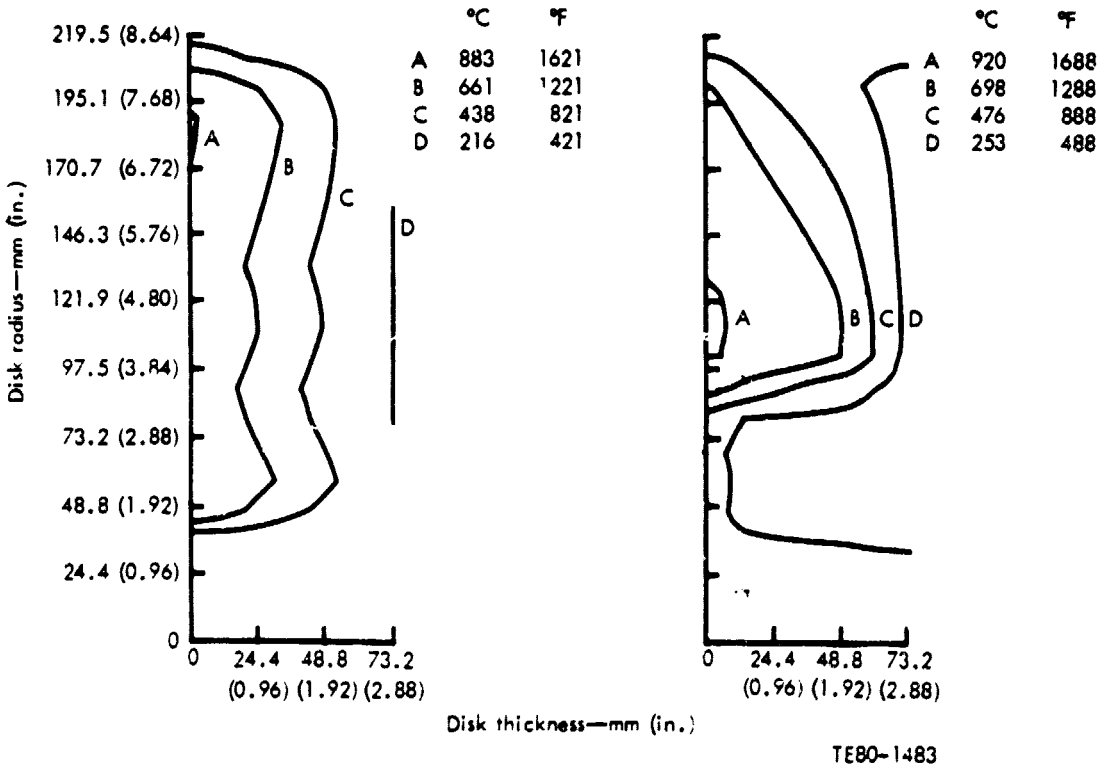

Figure 195. - The Effect of Inlet Gas Flow Distribution Upon Regenerator Disk Temperatures at 100% Engine Speed (Uniform Flow at Left, Extremely Distorted Flow at Right).

The ceramic seal wearface material presents a dual development task: first, finding a material with a satisfactory wear rate over the operating temperature range 621°C (1150°F) to 1066°C (1950°F) and, second, developing a method for attaching the wearface material to the ceramic substrate. One particularly important characteristic that will influence the method of attaching a wearface material to the LAS substrate will be its coefficient of thermal expansion; although Figure 194 depicts bonding, a mechanical interface joint may be necessary to accommodate thermal growth mismatch.

Specimens of LAS ceramic were ordered for laboratory test evaluation of candidate seal wearface materials now under development at DDA. These specimens, 6.3 x 25.4 x 38.1 mm (0.25 x 1.0 x 1.5 in.) in size, will be used to screen the wearface materials from the standpoint of bonding techniques, rubbing friction, and wear characteristics over the full range of engine operational temperatures. The results of the work with these specimens, scheduled for delivery shortly after the close of this reporting period, will then be applied to full-scale ceramic seals for hot test rig evaluation.

Thermal Analysis

An enlarged cross-sectional view of the inboard seal rim and adjacent parts is shown in Figure 196. A three-dimensional, finite element model of the negative half of the seal crossarm and adjacent components was prepared for the analysis, as shown in Figure 197. It is toward this half of the crossarm that the regenerator disk rotates from the exhaust gas cavity, and the region of the inboard seal assembly that will reach the highest operational temperatures. The crossarm model was divided into eight sections of 44 elements per section, one of which (section 4) is shown in Figure 198. The metal sealing leaves were not included in the three-dimensional model but were analyzed separately, using the results from the finite element analysis to define the thermal boundaries. Figure 199 shows the two-dimensional model that was made for the rim section of the seal, where the leaves are again excluded.

Figure 200 presents some of the highest temperatures computed for the crossarm and sealing leaf adapter at four operational conditions. The temperature calculations included radiation effects.

The maximum computed temperatures for the crossarm sealing leaves and cooling air baffle, based on operational Condition 1 listed in Figure 200, are presented in Figure 201. The only seal rim temperatures computed to date are presented in Figure 202.

Conclusions that can be drawn from the portion of the thermal analysis completed to date follow:

- In the crossarm area, the radiation heat transfer across the air gap separating the ceramic seal and the static sealing leaf adapter is greater than the convective heat transfer resulting from either the 0.5 or 1.0% cooling airflow rate at the 48.3 km/h (30 mph) condition.

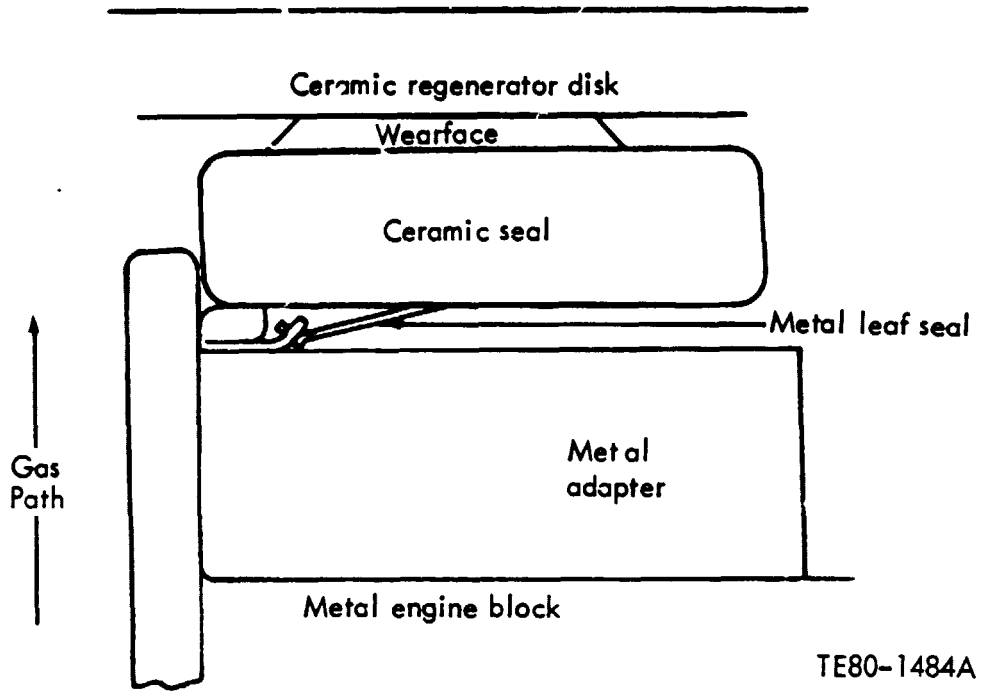

Figure 196. - Cross Section of Seal at Rim of Regenerator.

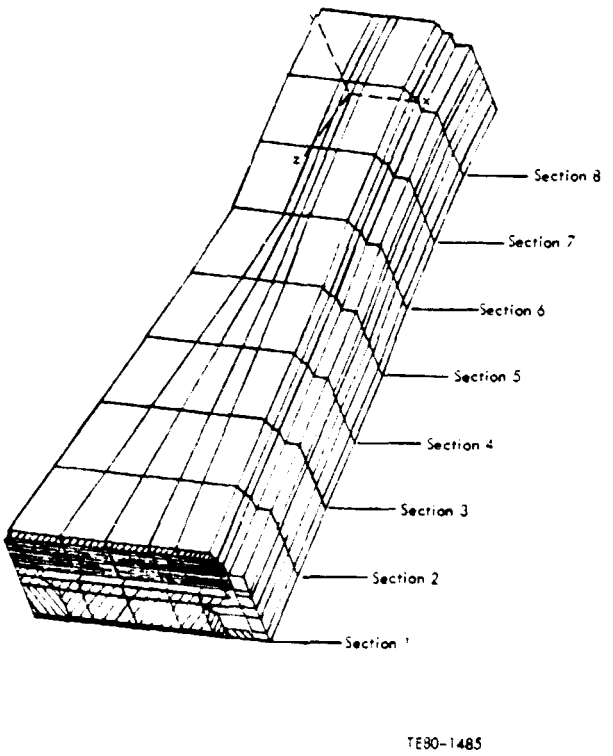

Figure 197. - Three-Dimensional Finite Element Analysis of Regenerator Seal.

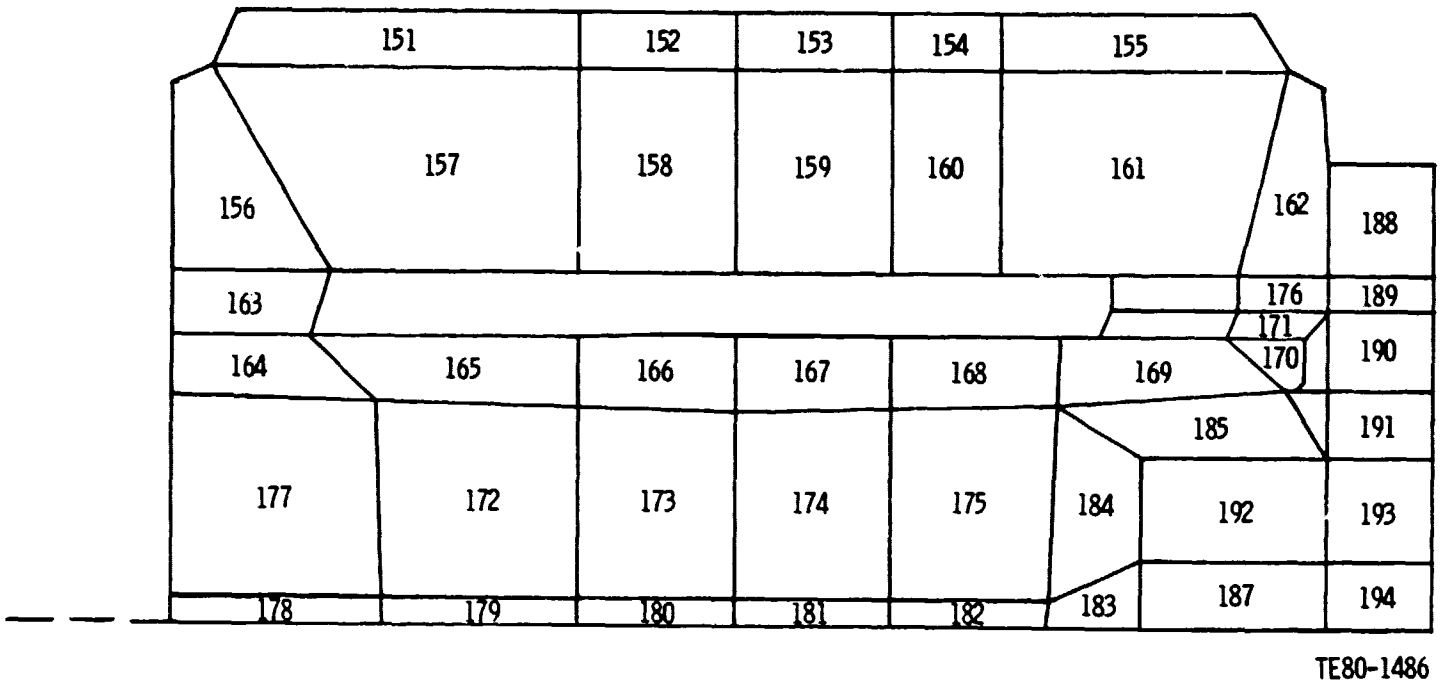

Figure 198. - Three-Dimensional Finite Element Analysis of Section 4 Crossarm.

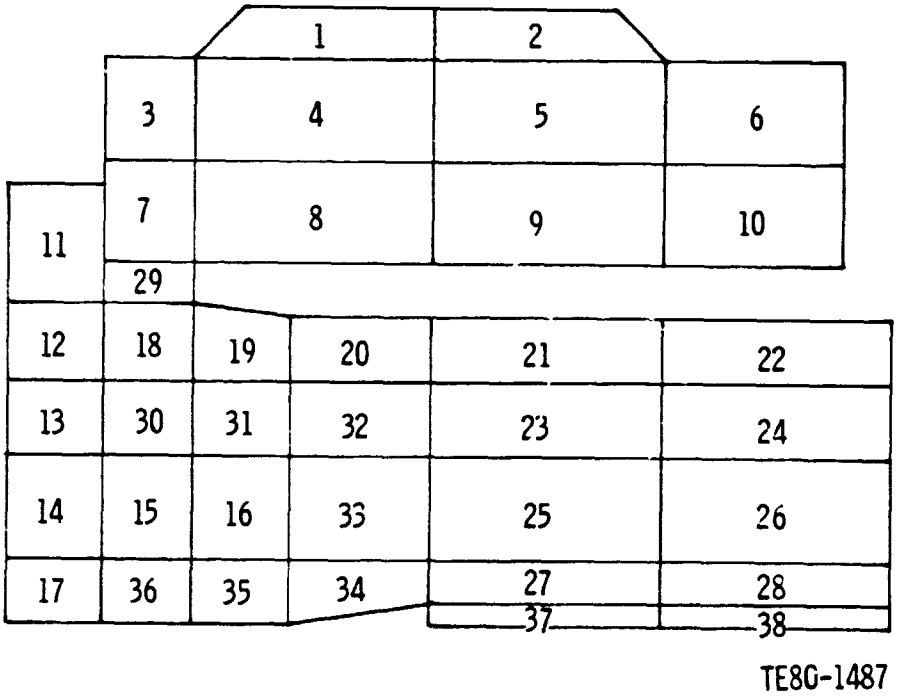

Figure 199. - Two-Dimensional Model for Regenerator Seal Rim Section.

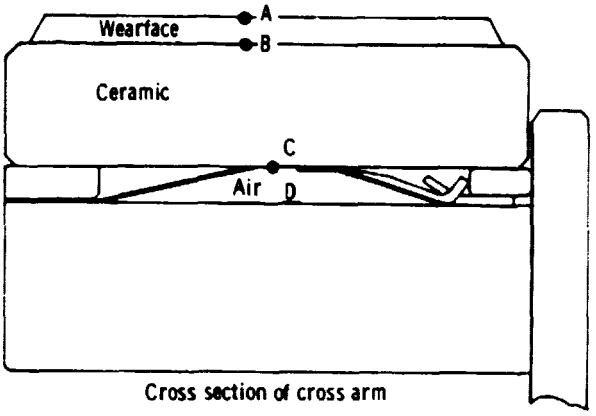

Cross section of cross arm

Temperatures—°C (°F)

Location	Condition			
	1	2	3	4
A—Wearface surface	1038.9 (1902)	1037.8 (1900)	1038.9 (1902)	906.7 (1664)
B—Wearface/ceramic interface	1016.7 (1862)	1012.8 (1855)	1025.6 (1878)	892.8 (1639)
C—Coolant surface of ceramic	876.7 (1610)	854.4 (1570)	881.7 (1619)	800 (1472)
D—Coolant surface of metal	911.7 (1313)	698.9 (1290)	712.2 (1314)	636.1 (1177)

Condition	Description
1	48.3 km/h (30 mph), 0.5% cooling air, 0% of wearface gone
2	48.3 km/h (30 mph), 1.0% cooling air, 0% of wearface gone
3	48.3 km/h (30 mph), 0.5% cooling air, 50% of wearface gone
4	Max power, 0.5% cooling air, 0% of wearface gone

TE80-1488A

Figure 200. - Summary of Temperatures Calculated for the Regenerator Crossarm.

- o The 48.3 km/h (30 mph) condition produces higher temperatures and gradients in the regenerator seals than the maximum-power condition.
- o A change in the thickness of the wearface material from 2.5 to 1.3 mm (0.10 to 0.05 in.) results in little change in the temperature level or the thermal gradients in the ceramic seal.
- o The temperature distribution in the regenerator disk greatly affects the temperature distribution that will result in the ceramic seal.
- o The static sealing leaf temperatures appear to marginally satisfactory. (This tentative conclusion remains to be substantiated by stress calculations and, finally, hot rig testing.)

Outboard (Cold) Side Disk Seal Assembly

Because the outboard seal assembly operational conditions (temperatures and pressure loads) will differ little from those in the IGT engine and CATE regenerator systems, the seal technology developed in those engine programs is directly transferable to the AGT-100. However, simplification of the sealing leaves is planned because of the reduced axial compliancy that will be required in the AGT-100. Whereas the IGT seal was designed to accommodate the

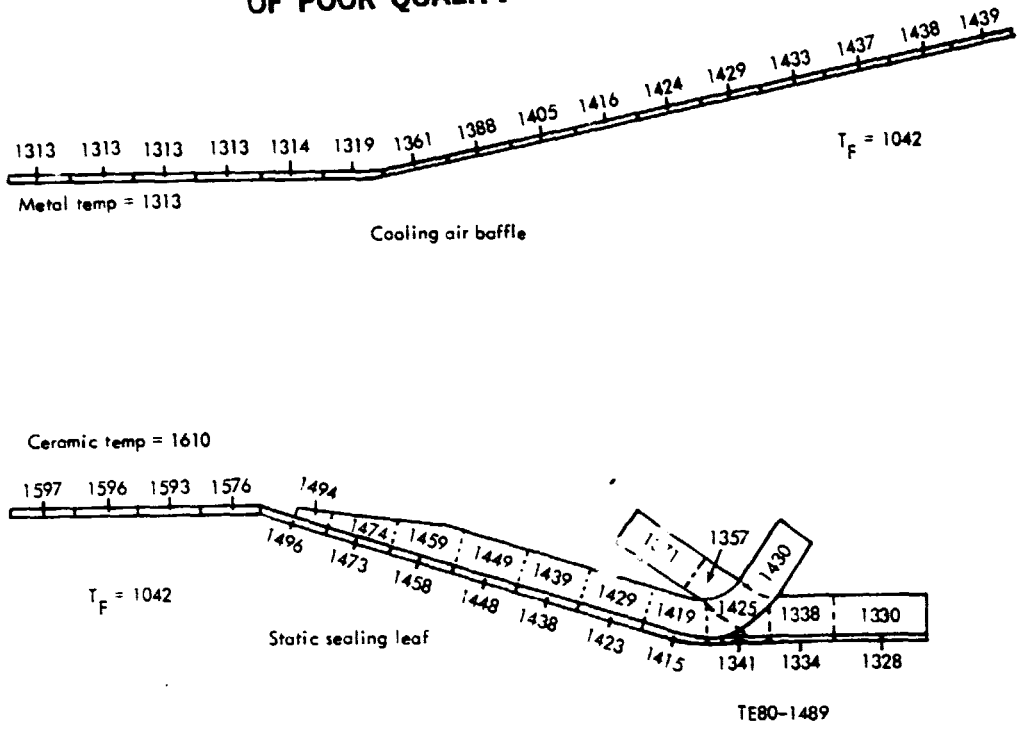

Figure 201. - Regenerator Crossarm Metal Leaf Seal Temperatures at 48 km/h (30 mph), 0.5% Cooling Air.

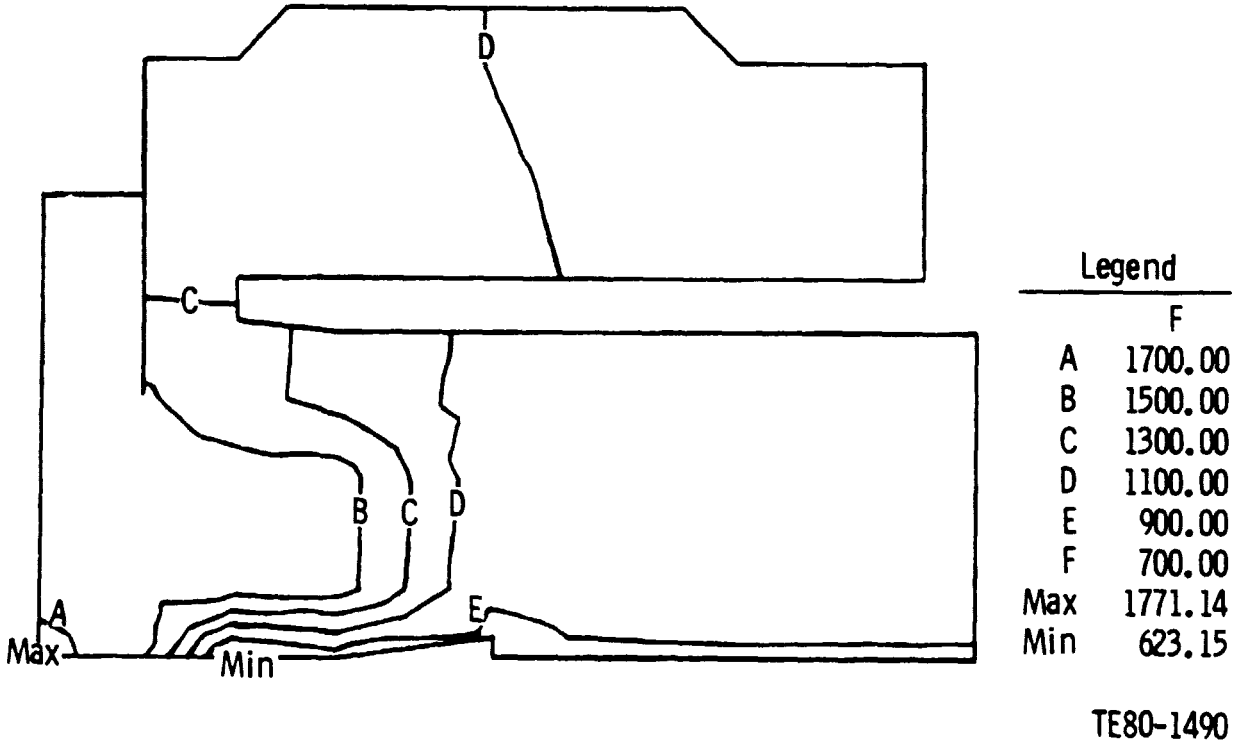

Figure 202. - Regenerator Seal Rim Temperatures at 48 km/h (30 mpn).

considerable thermal "dishing" that occurs in a metal regenerator disk, the superior dimensional stability of a ceramic regenerator (particularly one made of aluminum silicate) greatly reduces the need for axial compliancy in the seal. (The CATE seal is an adaptation of the IGT engine seal.) As in the IGT engine and CATE regenerator systems, the regenerator disk will be pressure loaded toward the outboard seal, which minimizes the axial compliancy required in the outboard sealing leaves.

Regenerator Ducting and Flow Distribution

The regenerator housing has two basic functions: first, it serves as a support structure for the regenerator disk and outboard seal and, second, the principal portions of the ducts for the compressed inlet air and the exhaust gas are an integral part of the housing. (Refer to Figure 194.) During the development of the regenerator system, it is anticipated that refinements will be required in the duct configurations selected for integration into the first housing castings. The primary basis for the refinements, if needed, will be the test results from a cold flow distribution rig; verification of the refinements will then be made with the regenerator hot test rig. These two rigs are described later in this section.

Flow distribution through the hot and cold side of the regenerator has a significant effect upon thermal effectiveness, disk pressure drop, and engine fuel economy. In the design process, care must be taken to minimize flow nonuniformities and to match the hot and cold side distributions. Based on extensive DDA experience in the design and testing of regenerator feed systems on the IGT engine, the AGT-100 configuration is being designed to ensure matched radial distribution of the flow on the air and gas sides.

A sectional view of the regenerator inlet air ducting is illustrated in Figure 194, Section A-A (upper half). It will have an entry of circular cross section (left side of illustration) at the exit of the compressor wrap-around scroll. Across the rim of the regenerator, the ducting cross section will make a smooth transition to a rectangular shape. The duct will then turn 90% over the outboard corner of the regenerator rim and discharge the air parallel to the crossarm, across the disk face. The transition from a circular-to-rectangular cross section will be accomplished at constant area, which will minimize the 90-deg turn loss and spread the flow across the regenerator face. At maximum power, the discharge Mach number from the rectangular duct will be 0.06.

The regenerated air will flow to the combustor through a 58 mm^2 (9 $in.^2$) opening. The area of this opening is limited by the block configuration and insulation requirements and may influence the flow distribution through the disk.

The regenerator inlet gas duct is illustrated in Figure 203. In it, the gas discharged from the power turbine will flow through a circular cross section, 1.5 area-ratio diffuser, and be directed at the regenerator face. An extension of this conical diffuser forms an oval-shaped "footprint" on the regenerator disk, which extends across the radius of the disk face, as shown in Figure 203. This pattern should produce a favorable match with the cold side distribution and result in high thermal effectiveness. The discharge Mach number from the diffuser at maximum power will be 0.175.

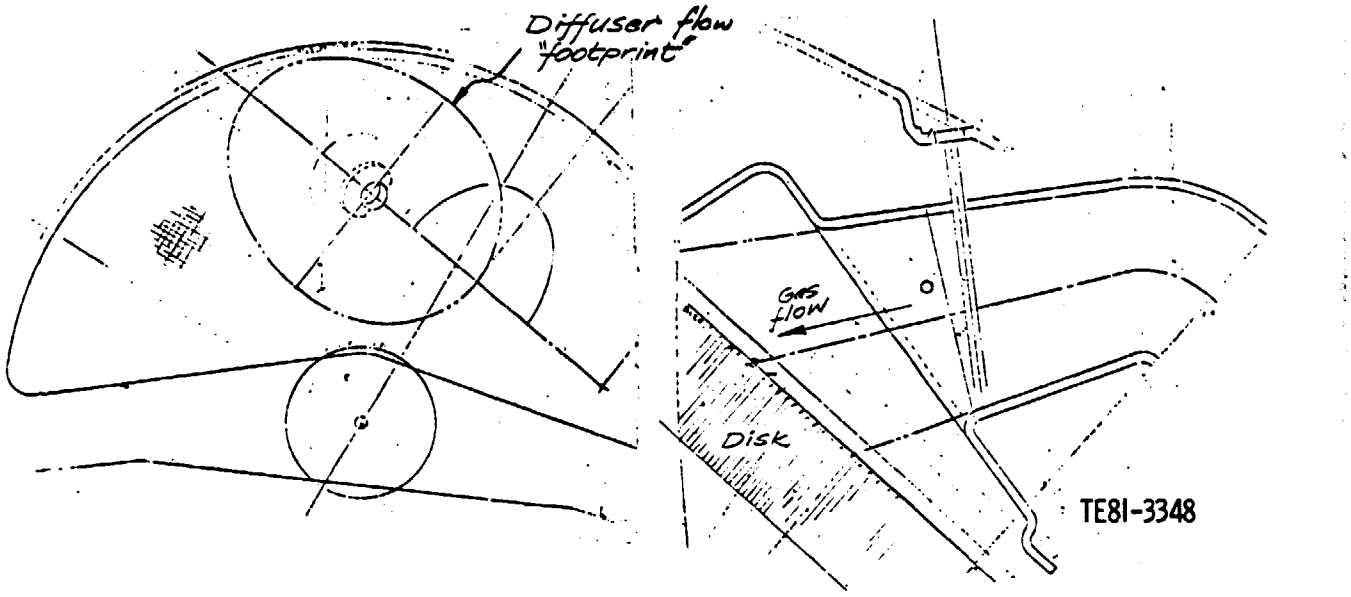

Figure 203. - Regenerator Inlet Gas Duct (From Power Turbine).

As the gas discharges from the regenerator disk, it will enter the regenerator housing (refer to Figure 194) and be ducted into the vehicle's exhaust system through a 193-cm^2 (30-$in.^2$) port. The volume of the discharge system and the smooth transition from the regenerator exit should produce minimal back-pressure. The discharge Mach number at the exhaust port at maximum power will be 0.06.

7.2 MOD I

Engine Parts Design and Fabrication

The design for the RPD regenerator system also forms the basis for the design of both the regenerator hot test rig and the Mod I engine regenerator system, with one exception. Because of the time that will be required to develop ceramic seal wearface coatings and techniques for attaching the coatings, an interim metal-platform seal will be designed and procured to help ensure on-schedule hot rig and Mod I engine testing. To a large extent, the design of this seal will be based upon the CATE configuration, which was designed for operation at regenerator inlet temperatures up to 982°C (1800°F).

Rig Design, Fabrication, and Test

Hot Test Rig

The rig design consists of two units: a hot loop and a working section. The hot loop, shown in Figure 204, contains an air-measuring section and a burner that heats the air passing to the ceramic regenerator disk to simulate the flows and temperatures exiting from the AGT-100 power turbine. The working section, shown in Figure 205, contains the ceramic disk and seal assemblies

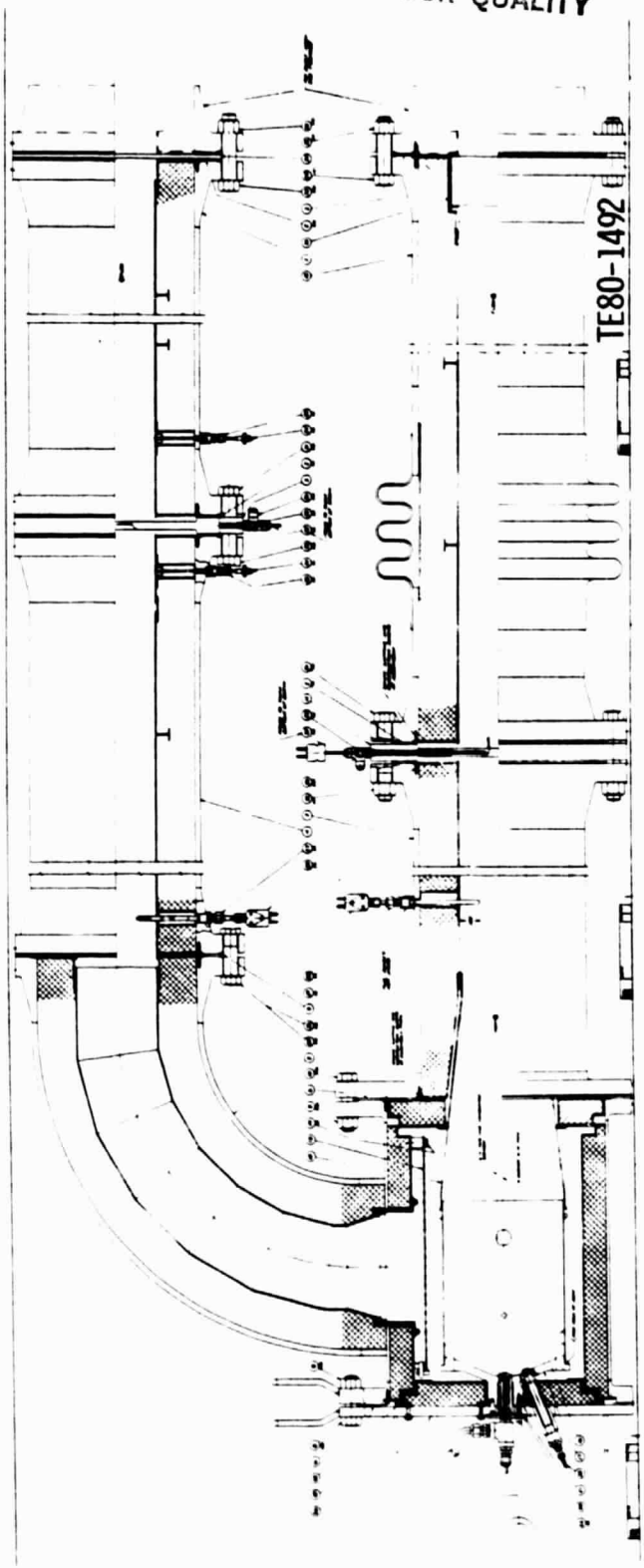

Figure 204. - Regenerator Hot Test Rig--Hot Loop Section.

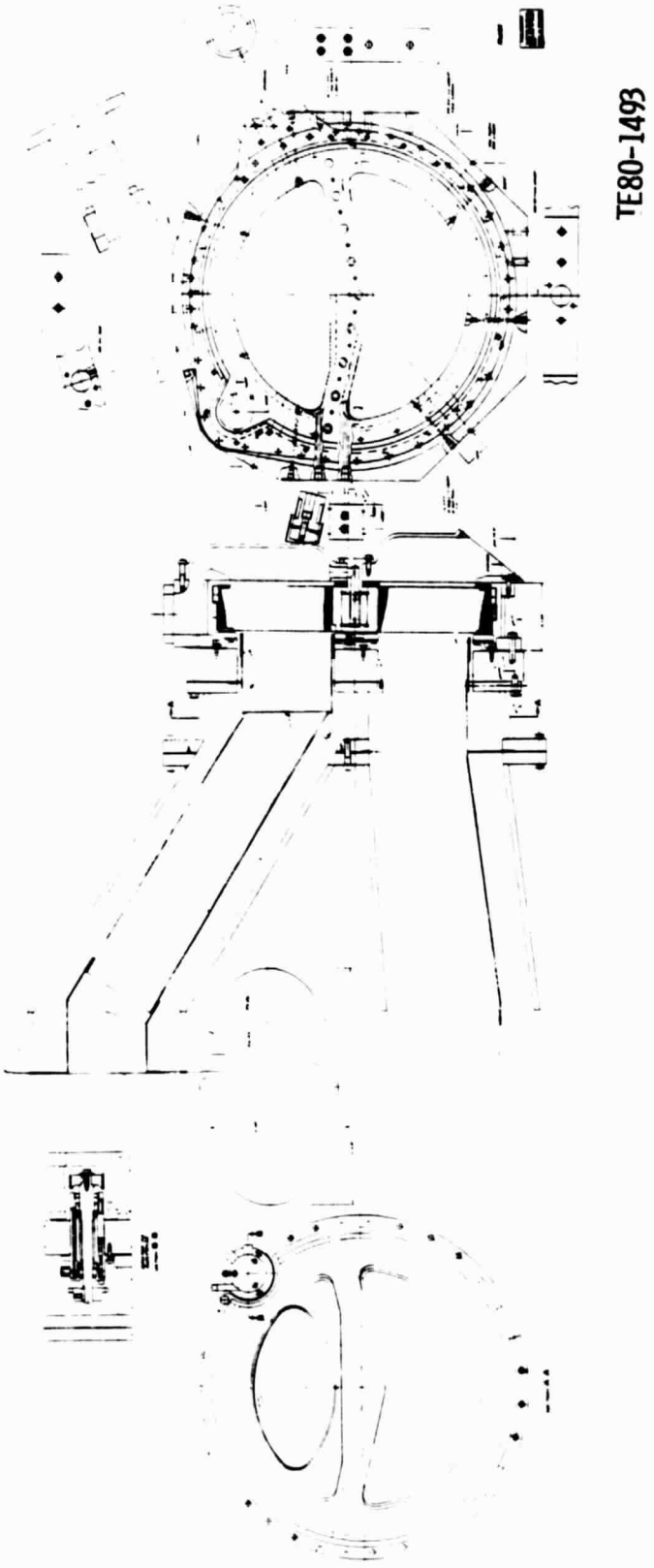

Figure 205. - Regenerator Hot Test Rig--Working Section.

and a variable speed drive mechanism to duplicate the proper disk speed for each engine operational condition. An existing shop air system will supply heated air to the working section and hot loop to duplicate engine compressor airflows and temperatures.

The status of the rig design and fabrication follows:

Hot Loop

- o Released for fabrication to the DDA shop.
- o All material is on order with 20% received.
- o The fabrication of the liner assemblies has started.

Working Section

- o All detailed drawings are completed and through checking; checking corrections are in process.
- o The assembly drawing corrections are nearly complete.

Test Cell Adaptations

- o The test cell conversion has begun.

Cold FLow Distribution Rig

It is important to match the air and gas flow distribution to achieve high regenerator thermal effectiveness. Therefore, a cold flow regenerator flow distribution rig is being designed. This rig will be fabricated and used to study and optimize radial flow distribution. The rig will use ambient temperature air but will simulate both Reynolds and Mach numbers in order to ensure the proper influence of back pressure on flow distribution. Flow field measurements will be used to modify the rig as necessary to establish the most efficient configuration.

Design layouts of the flow distribution rigs are in progress. For flow simulation purposes, the regenerator and its interconnecting duct work have been separated into two distinct flow rigs. One rig will simulate the air side as shown in Figure 206; the other will simulate the gas side of the regenerator as shown in Figure 207. The air side rig will be pressurized with shop air, and the flow conditions will be established to match the engine Mach and Reynolds numbers. The best match of Mach and Reynolds numbers for the gas side will require operation at subambient pressure, and this rig is being designed to operate from a steam ejector vacuum source. Instrumentation is being provided to measure:

- o Flow rate
- o Temperature
- o System pressure
- o Pressure drop across the regenerator disk
- o Velocity survey at the regenerator discharge face

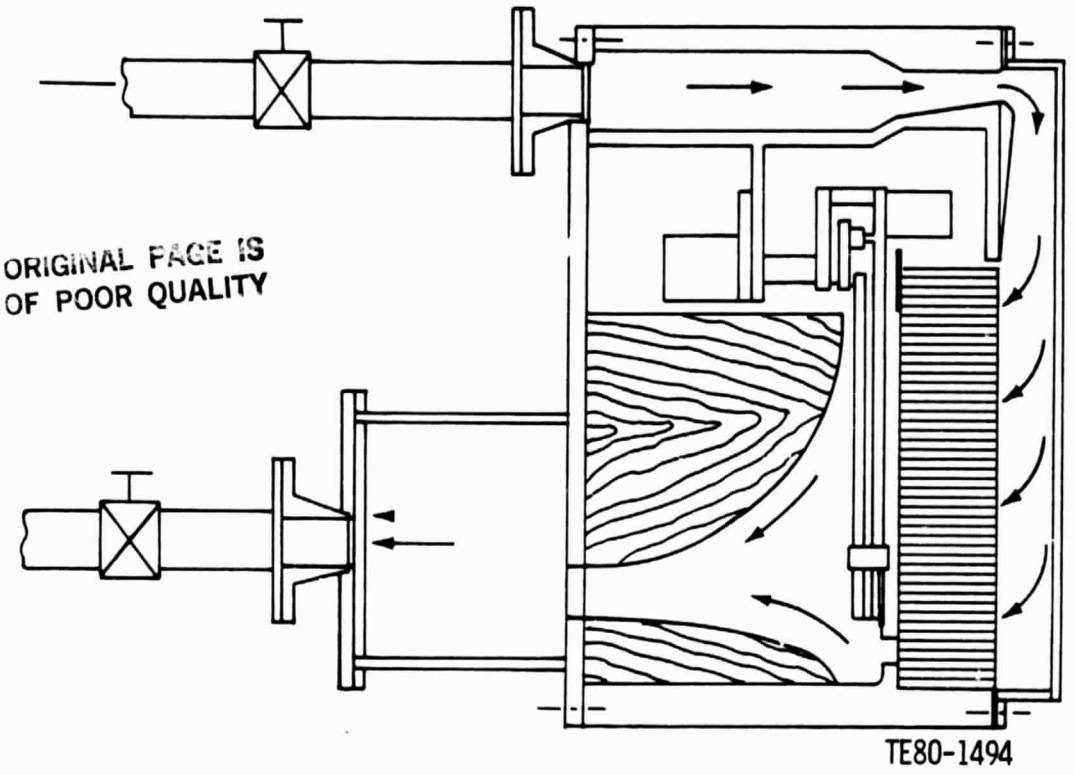

Figure 206. - Regenerator Flow Distribution Rig--Air Inlet S ‹e.

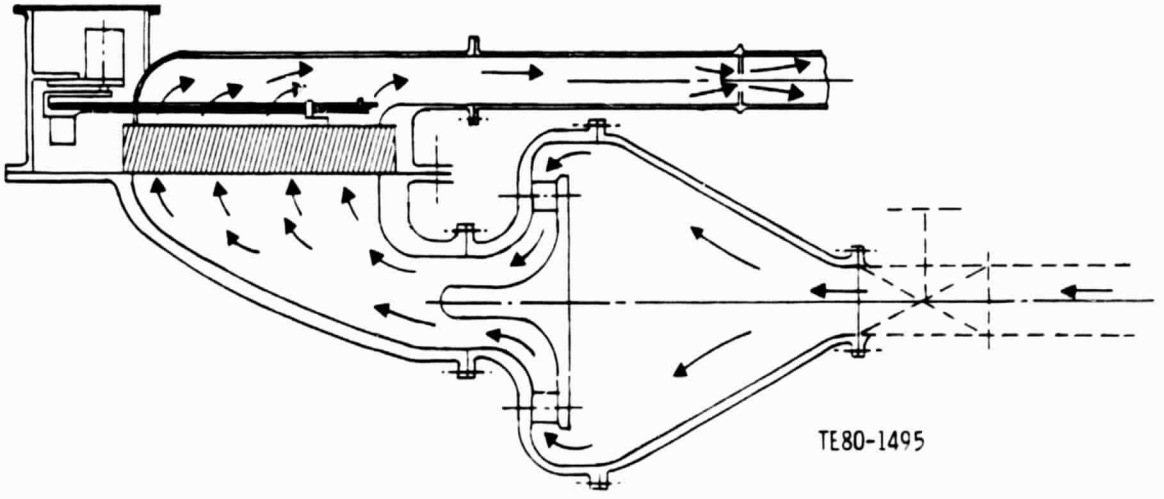

Figure 207. - Regenerator Flow Distribution Rig--Gas Inlet Side.

Flow distribution will be measured with a hot wire probe. Geometric modeling of both the approach and discharge plenums will be facilitated with plenum inserts; these will permit inexpensive modifications as the plenum flow-path geometry is optimized. The rigs will be constructed of steel, wood, and fiberglass.

Regenerator Core Rig

The objective of this rig and associated tests is to develop experimental methods to assess the effects of thermal exposure on the strength and time to crack propagation, or fracture, of AS matrix, which can be related to disk performance in the engine.

The regenerator core evaluation effort consists of three major test items:

1. Disk variability
2. High-temperature exposure
3. Engine simulation

A rig has been built and methods developed to evaluate core samples for these effects.

Engine Simulation Test

Three approaches were considered before selecting low-cycle fatigue (LCF) testing as the best experimental method available in terms of data return. The first approach compared the MOR of the as-received matrix with the thermally exposed MOR. Two disks were tested using this technique. The change in MOR was well below statistically significant levels both for the mean and regression coefficients (ref. 5). This might be expected since the thermal range is caused by the growth of high thermal expansion mullite grains in the alumino-silicate structure and the internal stress caused by this reaction may be significant only at elevated temperatures.

The second approach compared MOR versus temperature for the as-received and thermally exposed materials up to the maximum temperature anticipated in engine use. The method is simple but has a drawback in that it implicitly assumes that the duration of the applied stress is not an important variable. Studies have clearly established that glass, glass ceramics, and some polycrystalline ceramics will fail under long term stresses well below the short time scale stress to fracture (ref. 6, 7, 8). This effect has been shown to be a result of accelerated chemical attack at the tip of the crack resulting from environmental agents; water vapor and oxygen have been identified as two of the agents.

It is clear from the discussion of results in the reference papers that long time scale stresses will play an important part in the ultimate life of the automotive ceramic regenerator. What is not clear is how to apply four point bending data, even taken at elevated temperatures, to the typical acceleration-deceleration cycle for the vehicular turbine. In this case, the temperature level and distribution, the water vapor, and oxygen levels are all varying in a way that is very hard to analyze and relate to steady-state laboratory testing.

Accordingly, a third approach was adopted where a gas burner facility was designed to simulate an idle-maximum acceleration-idle service cycle and thus serves as a transient LCF model. Similitude in inlet gas temperature, flow rate, and rate of temperature change is achieved, and similarity in gas chemistry, with the exception of SO_2-SO_3 level, is maintained by preheating the burner air. The supply of water vapor to the crack tip depends on the gas chemistry and temperature and the ceramic temperature (absorption). The effect on the material depends on the thermally induced stress in the ceramic. Hence, the acceleration branch of the transient cycle achieves complete small-scale similitude with the engine. There are differences, however, in the overall disk stresses, in the mechanically induced and burner pattern factor stress, and in the cyclic counterflow effects.

Results

The gas burner facility used for steady-state exposure of 65 x 39 x 75 mm (2.55 x 1.55 x 2.970 in.) ceramic specimens was modified by adding a two-function electronic cycle control/timer/cycle counter and a variable supply of cooling air that can be injected and thoroughly mixed with the burner gas stream. Figure 208 is a section of the water jacketed burner exit plenum and transition section, and the short, low-mass test section with the sample between two fine wire Pt/Pt-Rh-shielded thermocouples. The quench air supply parameters--pressure, maximum flow rate, time rate of addition to the gas stream, and period--are controlled by the electrical and pneumatic controls indicated. The time rate of addition is controlled by the pressure level and rate of air bleed through the throttling valve downstream of the bonnet of the pneumatically controlled valve. The two important rates of change in gas temperature were 1167°C (2100°F) at the acceleration branch onset and 333°C/s (600°F/sec) at the deceleration branch onset of shock, these rates are achieved by alternately increasing the gas temperature level and adjusting the cooling air parameters until the inlet and outlet thermocouples gave the correct levels and rates of change at the simulated engine rated flow.

Approximately 2000 rig cycles and 800 cycles for the first thermal exposure sample have been run. The instrumentation, control, and burner operation are satisfactory to this point. Reproducibility of the cycle is good, and analog time-temperature recording is accurate enough for control and monitoring during cycle accumulation.

The detection of thermal fatigue cracks is initially being done by 30 and 150X microscopic inspection. Fluorescent particle detection methods are currently being tested for this purpose.

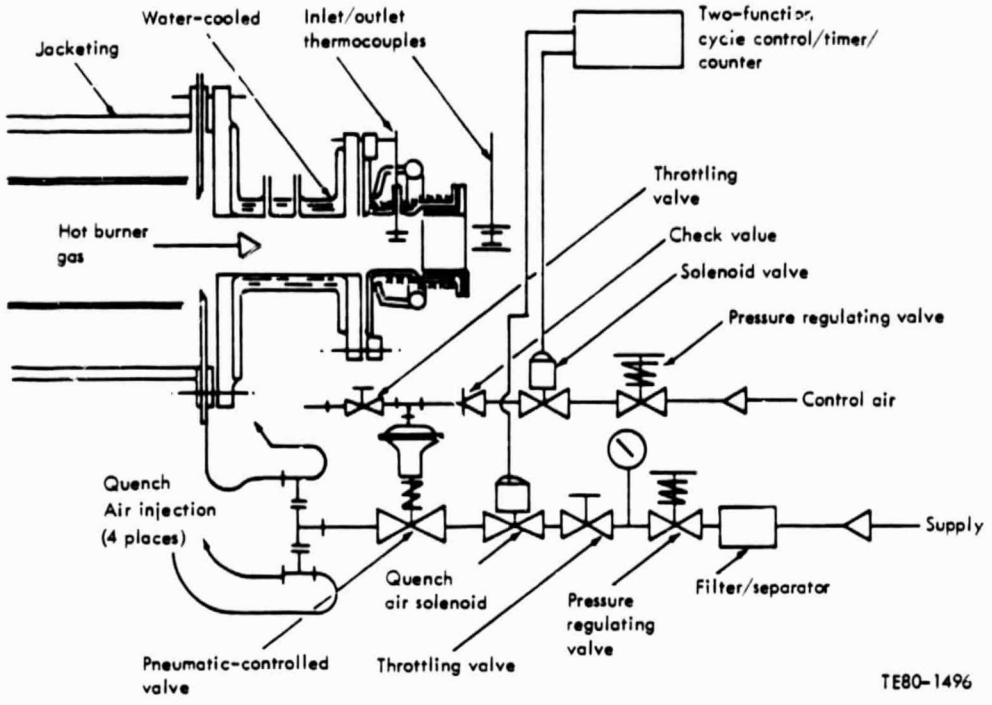

Figure 208. - Regenerator Material Thermal Cycle Test Rig.

VIII. SECONDARY SYSTEMS

8.1 BLOCK/INSULATION

The engine block is the primary structural component of the engine. It is an iron casting that houses the regenerator disk, the combustor, the gearbox, the gasifier turbine assembly, and the power turbine assembly. The compressor assembly bolts to the block at the gasifier turbine flange. The exterior shape of the block is irregular. This is the result of design trade-offs between the shapes of the components it houses (which essentially define the gas flow path), the insulation thickness requirements for reduced heat rejection, and the interior dimensions of the Pontiac Phoenix engine compartment.

The current block evolved from the original block layout design for a variable geometry engine. That concept was for a modular design. The block would only have housed the gasifier turbine and the power turbine and provided bolt flanges for the gearbox, combustor and regenerator. As the design progressed, space problems required the incorporation of the combustor, regenerator, and gearbox into the block casting. The advantages of this design are reduced block weight and elimination of potential split line leak paths.

The current engine block layout design is the result of general arrangement studies initiated to satisfy installation requirements and also provide additional insulation to reduce engine thermal heat loss. The major revisions include:

- o Change in center distance between turbine rotors, distance between gasifier and power turbine flange shortened 35 mm (1.5 in.)
- o Reduction gear case shortened 50.8 mm (2.0 in.)
- o The combustor/block angular position changed.

An important function of the block is to provide surfaces for insulation to minimize heat loss. To meet this requirement the exterior of the block will be essentially contoured to the interior of the engine compartment in order to maximize the available space for insulation. This design will be used in both the RPD and Mod I engines.

A detailed description of the block is shown in Figures 209 through 211 with the salient features identified. The overall size of the block is 711 x 635 x 609 mm (28 x 25 x 24 in.). Figure 209 is a view looking into the gearbox housing and shows true views of the gearbox cover flange and the power turbine mounting flange. Figure 210 shows a true view of the gasifier turbine mounting flange, and the regenerator cover mounting flange is shown in true view in Figure 211. The nominal wall thickness is 5.6 mm (0.220 in.), which is within acceptable casting practice.

Ductile Ni-Resist type D-58 alloy has been selected as a low-risk block material for the development engine test program. Based on the Allison GT 404/505 industrial gas turbine experience the AGT-100 block temperature in the regenerator crossarm area could be in the 730°C (1350°F) range. Ni-Resist is recommended for service up to 815°C (1500°F). It has a high thermal shock resistance and responds to a stabilization heat treatment to prevent growth and warpage during service. Therefore, the use of this material will result in the

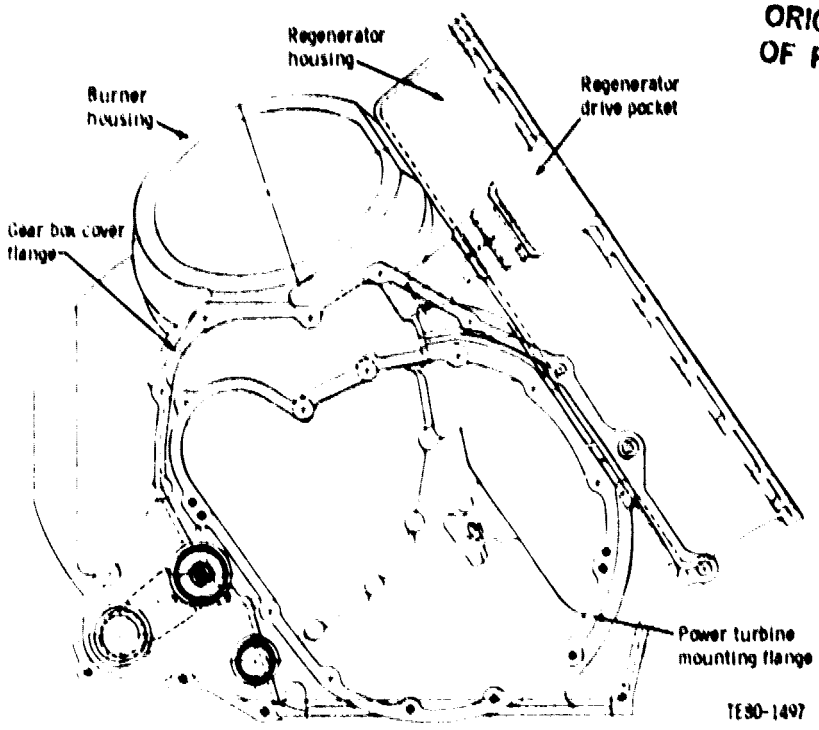

Figure 209. - AGT-100 Engine Block--View Into Gearbox Housing.

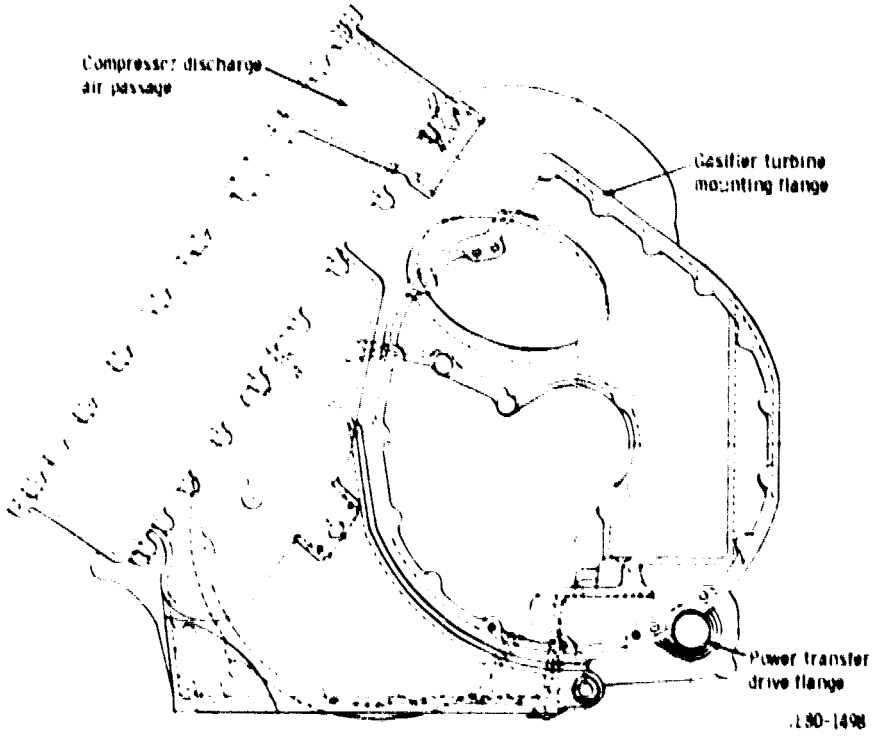

Figure 210. - AGT-100 Engine Block--View Into Gasifier Turbine Flange.

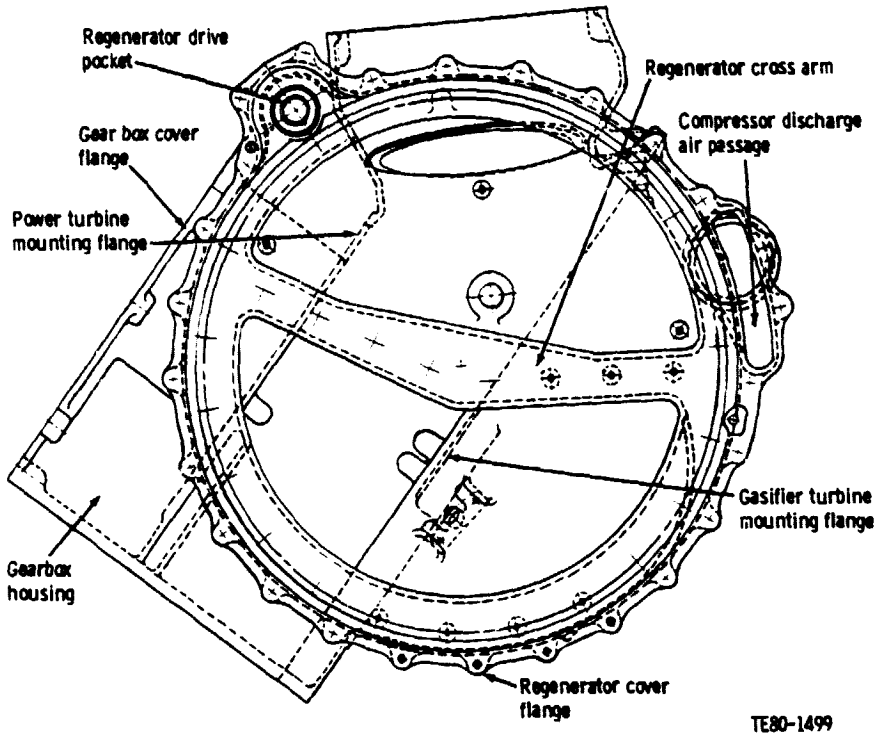

Figure 211. - AGT-100 Engine Block--View Into Regenerator Housing.

lowest risk of block failure during development testing. The RPD material selection will be made based on measured block temperatures during engine development testing.

The detailed design of the block must be structurally sound at all operating temperatures. In terms of block wall temperature, minimum block thermal distortion requires that the wall temperatures be nearly uniform and within the material allowable creep limits. This has been accomplished in the design by eliminating buried internal walls. All walls have a heat sink, either air or oil. The wall temperature is then controlled by the type and amount of insulation between the ceramic scrolls, which are essentially at flow path temperature, and the block. The design, therefore, is a compromise between structural stability and minimum heat rejection.

Preliminary heat rejection analyses were made from the original block layout drawing. Based on this study, the heat rejection goal for the fixed geometry engine was established. Figure 212 presents this goal in terms of percent of fuel energy versus percent power. This is the heat loss that is included in the engine performance calculations for the fixed geometry engine. This engine is essentially a constant temperature engine, and fuel input reduces as power reduces. Therefore, the heat rejection as a percent of fuel energy is greater at the lower power conditions.

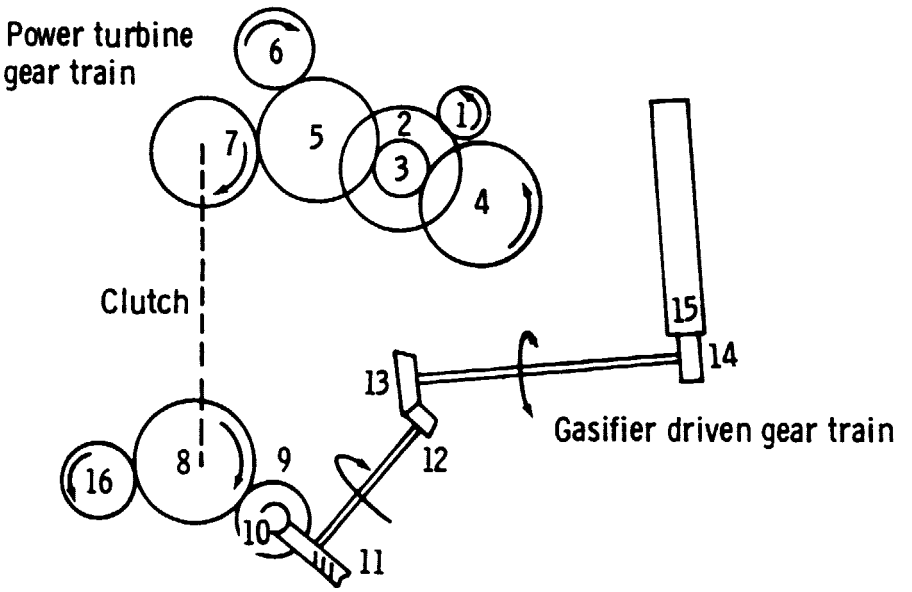

Gear	Function	Teeth	Module	Helix angle	100% rpm
1	Power turbine	20	1.25	20°R	54,390
2		75	1.25	20°L	14,504
3		18	1.75	17°L	14,504
4	Output	76	1.75	17°R	3,435
5		79	1.75	17°R	3,304
6	Accessory drive	68	1.75	17°R	3,839
7		46	1.75	17°L	5,675
8		65	1.75	22.6976°L	5,675
9		32	1.75	22.6976°R	11,528
10		1	2.00	84.30136°R	11,528
11		26	2.00	5.69864°R	443
12		16	1.5875	35°L	443
13		33	1.5875	35°R	215
14		43	1.25	0	215
15	Regenerator	392	1.75	0	23.6
16	Power transfer	32	1.75	22.6976°R	11,528

Figure 213. - AGT-100 Mod I Gearbox Schematic.

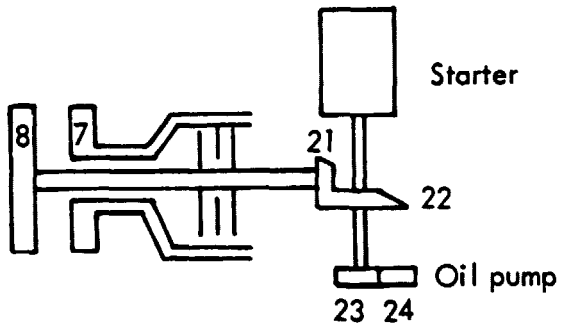

TE80-1685

Gear	Function	Teeth	Module	Helix angle	RPM
21		21	2.54	0°	5675
22		42	2.54	0°	2838
23	Oil pump	7	4.233	0°	2838
24		7	4.233	0°	2838

Figure 214. - Starter Gear Train Schematic.

TABLE XXV. GENERAL GEAR TRAIN ARRANGEMENT

Gear	Width mm (in.)	Material	
1	15 (0.59)	9310	
2	40 (1.57)	9310	Semi recess action
*3	20 (0.79)	8620	
4	18 (0.67)	8620	
5	12 (0.47)	8620	
6	11 (0.43)	8620	
7	11 (0.43)	8620	
8	11 (0.43)	8620	
9	11 (0.43)	8620	
10	---	8620	Full recess action
11	10 (0.39)	SAE 65 Bronze	
12	12.7 (0.50)	8620	
13	12.7 (0.50)	8620	
**14	22 (0.87)	1144	Full recess action
15	26 (1.02)	Harrison Div	
16	12 (0.47)	8620	
21	10 (0.39)	8620	
22	10 (0.39)	8620	
23	25.4 (1.00)	Sintered iron	
24	25.4 (1.00)	Sintered iron	

*Enlarged pinion--spread centers 3-4 & 3-5, 0-90.
**Spread centers 0.39 cold.

conservative pitch line speeds and will be lubricated by oil splash. However, the power turbine bearings and gear mesh will have individual jets directed between the inner race and separator of the bearings, and into the power turbine pinion teeth as they move into mesh. The worm mesh will be positively lubricated because of the relatively high sliding velocities and wear tendencies inherent in gears of this type. Positive oiling is also directed to the regenerator pinion bearing because of its isolated position and the adjacent hot metal components.

Compressor discharge air is bled from the regenerator cavity in the block and directed between the close contact ring seals immediately next to the power turbine back plate, to create a relatively cool barrier of high pressure air, and prevent the leakage of hot flow-path gases into the gearbox.

A double seal is also provided at the regenerator pinion shaft to avoid the possibility of extensive regenerator damage resulting from oil leaks in this area. Although a favorable pressure differential will normally exist at this location to prevent oil leaks, studies have shown that abnormal events can occur and induce oil leaks to the outside. A low clearance carbon ring seal is used to contain regenerator air, and a rubber lip seal to contain gearbox oil, with an overboard vent provided between the seals.

The power transfer clutch between gears 7 and 8 is a hydraulically controlled disk design, which turns at a maximum speed of 5,675 rpm. Clutch parameters are described in Table XXVI. Cooling oil will be scheduled as a function of control oil pressure, so that parasitic losses resulting from clutch pumping are reduced during periods when heat rejection is low. Pertinent design criteria for the clutch are shown in Figures 215 through 217.

TABLE XXVI. AGT-100 POWER TRANSFER CLUTCH

No. of friction surfaces	10
Max lockup torque, N·m (lbf-in.)	77.5 (686)
Max control oil pressure, kPa (psi)	482.6 (70)
Piston OD, mm (in.)	0.14 (3.5)
Piston ID, mm (in.)	0.07 (1.72)
Piston area, mm^2 ($in.^2$)	4709.7 (7.3)
Friction surface OD, mm (in.)	0.13 (3.3)
Friction surface ID, mm (in.)	0.09 (2.34)
Friction surface area, mm^2 ($in.^2$)	2741.9 (4.25)
Normal return spring force, N (lbf)	333.6 (75)
Max unit pressure on friction surfaces, kPa (psi)	710.2 (103)
Max continuous heat rej/disk area ($hp/in.^2$)	(0.24)

The single element engine oil pump and regulating valve are mounted externally for easier servicing, beneath the starter motor. The unit will operate at speeds between 1419 and 2838 rpm with capacity to provide 1170.3 kg/s (43 lbm/min) engine oil flow at pressures between 482.6 and 551.6 kPa (70 and 80 psi) as shown in Figure 218. The pump design is patterned after Pontiac practice and uses existing components from this reciprocating engines.

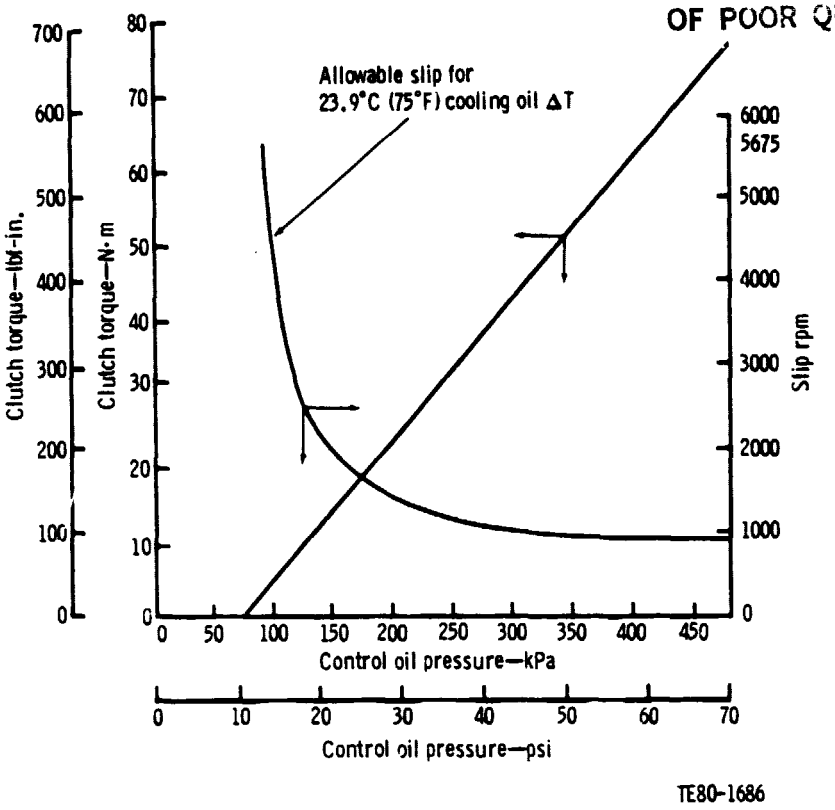

Figure 215. - AGT-100 Power Transfer Clutch Torque.

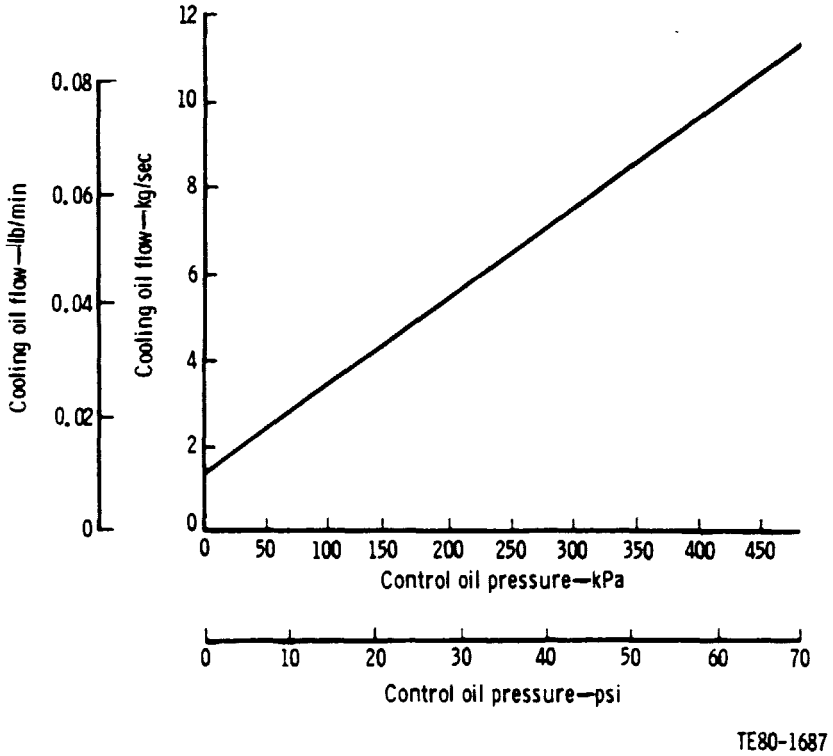

Figure 216. - AGT-100 Power Transfer Clutch Cooling Oil Flow.

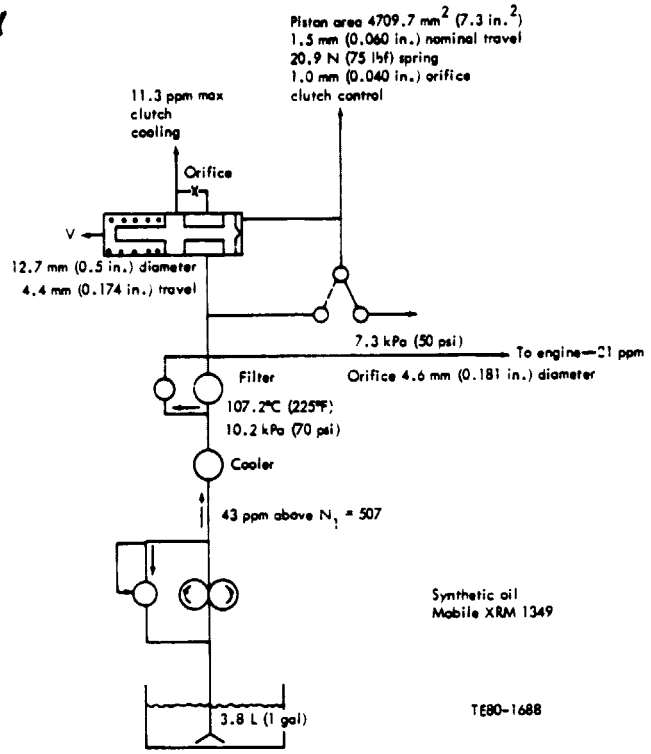

Figure 217. - AGT-100 Oil System Schematic.

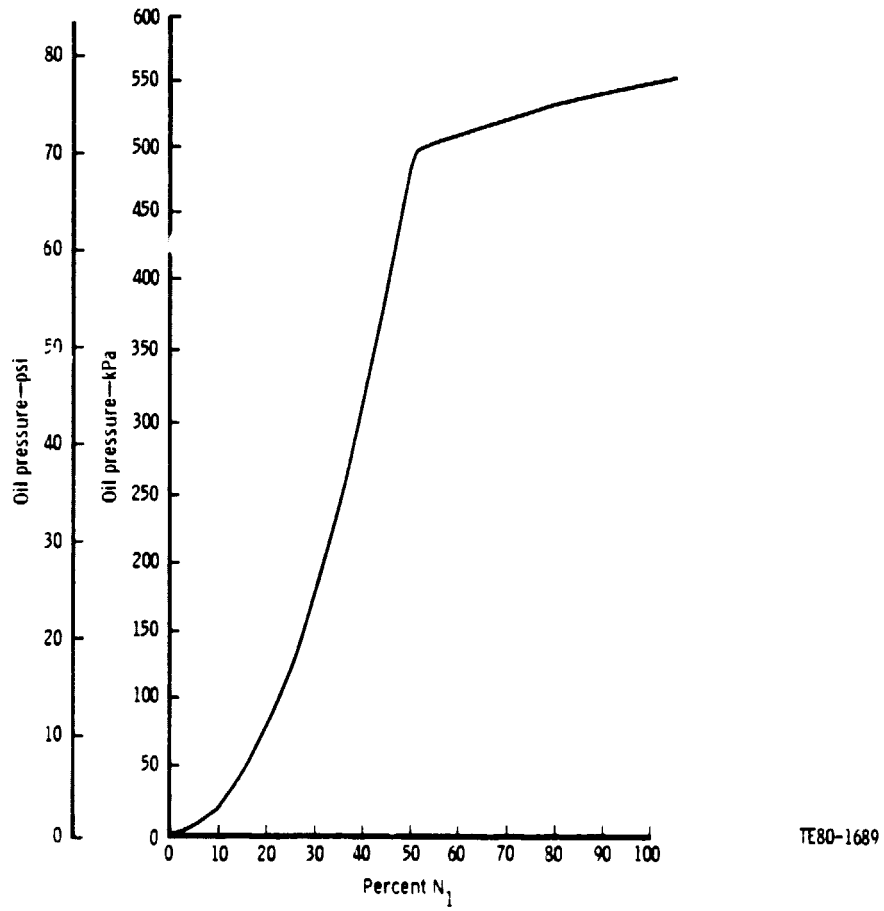

Figure 218. - AGT-100 Oil Pressure vs Percent N_1.

8.3 ROTOR BEARINGS

The No. 1 bearing runs at a speed rating of 1.29×10^6 DN. The No. 2 bearing runs at a speed rating of 2.58×10^6 DN. The material for the No. 1 and No. 2 bearings is SAE 52100 and M50, respectively. Predicted low-pressure bearing lives are 4528 h for the No. 1 and 3000 h for the No. 2 bearing. Studies are underway to identify the degree of thermal soakback during shutdown.

Both critical speed and unbalance response analysis were performed on the compressor rig configuration of the gasifier rotor. To avoid critical speeds in the operating range both bearings are mounted on mass isolaters. Spring rates are 3,327, 409.2 N/m (19,000 lbf/in.) for the No. 1 and 10,507,608 N/m (60,000 lbf/in.) for the No. 2 bearing. An oil squeeze film is incorporated in the No. 1 bearing mount to reduce the responsive amplitude of the transient modes resulting from out of phase unbalance.

Vibration stiffness analysis is being conducted for the engine version of the gasifier rotor including the power transfer shafting to ensure that shaft frequencies and bearing mounting spring rates are compatible with the operational requirements of the engine.

The power turbine rotor is mounted on two rolling element bearings. The bearing adjacent to the rotor is a split inner ball bearing (No. 3). It is the same bearing used for the gasifier rotor; the other is a roller bearing (No. 4). The No. 3 bearing carries both radial and thermal load, whereas the No. 4 carries radial load only. The speed ratings for the No. 3 and No. 4 bearings are 2.05×10^6 DN and 1.02×10^6 DN, respectively. The material for the No. 3 and No. 4 bearings is M50 and SAE 52100, respectively. Predicted low-pressure lives are 1780 h for the No. 3 bearing and 730,000 h for the No. 4 bearing.

8.4 SECONDARY AIRFLOW SYSTEM AND THRUST BALANCE

The secondary airflow system for the AGT-100 engine is concerned with minimizing leakage flow, isolating bearing compartments from hot gas, and determining thrust balance loading to ensure proper selection of bearing size.

The secondary airflow system analysis is performed using an in-house-generated computer program that models the gas path pressures as flow sources and sinks and the possible leakage areas as resistances to flow. These resistances are linked by a series of chambers where pressure level is calculated. Solution is obtained for a given operating condition when the system is balanced such that, for each calculated chamber, the flows entering and leaving are equal. Figure 219 identifies the AGT 100 system resistance (squares) and calculated pressures (circles). Calculated flows and pressures are presented in Table XXVII.

Thrust balance is computed by summing the forward and aft pressure x area and momentum loads that act upon the rotating components. Calculated thrust loads are summarized in Figure 220.

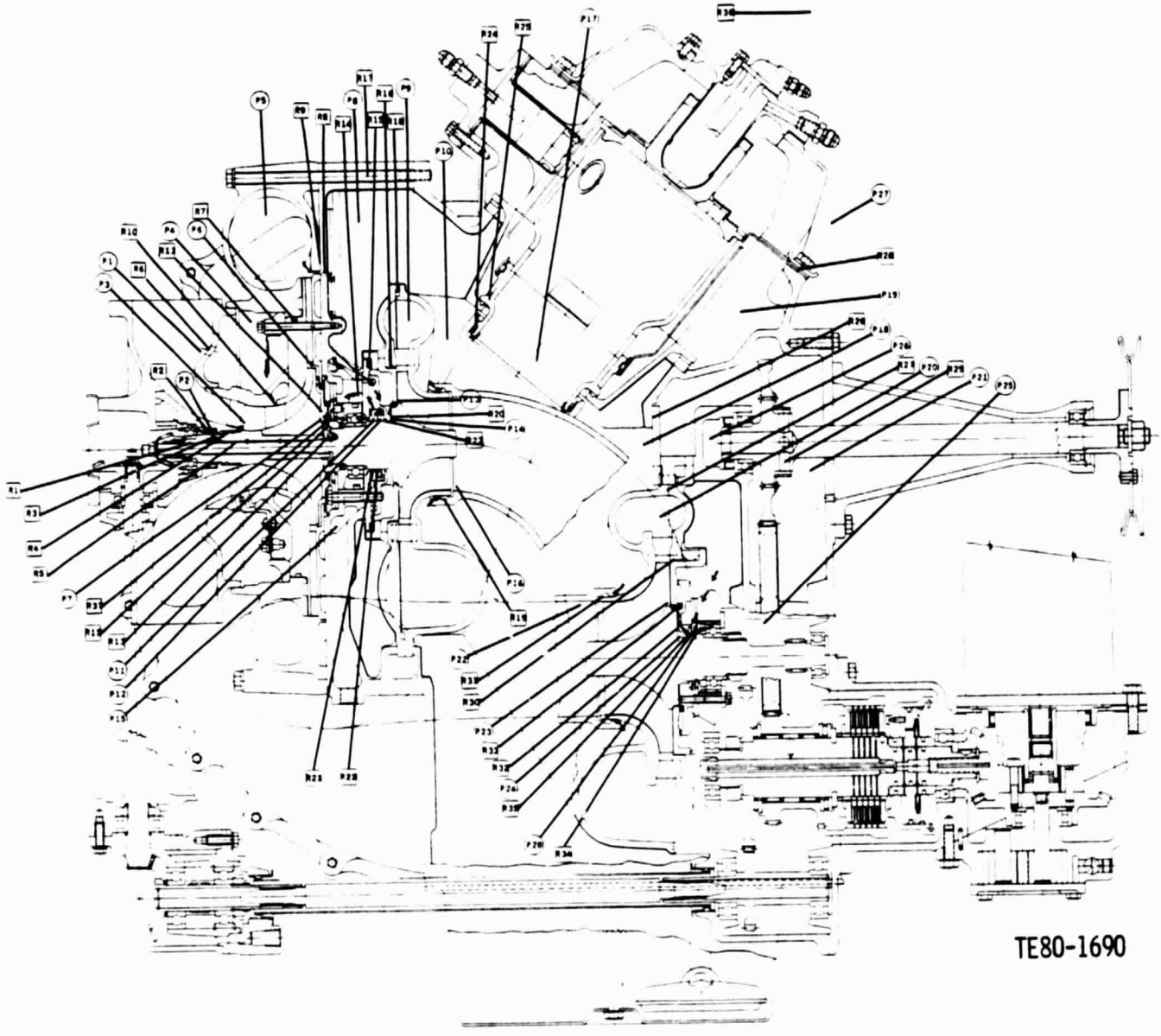

Figure 219. - Basic Engine Schematic.

RESTRICTION AND LEAKAGE DATA
(FLOW IN PERCENT OF COMPRESSOR INLET FLOW)

RESTRICTION NO.	DESCRIPTION	AREA Sq CM	AREA Sq IN	MAX POWER	80 KM/H (50 MPH)	48 KM/H (30 MPH)	32 KM/H (20 MPH)	IDLE
R1	SHAFT GAP	[illegible]	[illegible]	[illegible]	[illegible]	[illegible]	[illegible]	[illegible]
R2	FRONT COMP SHAFT SHAFT HOLE	.102	(.0158)	0.08	0.11	0.09	0.11	[illegible]
R3	FWD BC RING SEAL	.008	(.0013)	0.06	0.10	0.07	0.10	0.07
R4	FRONT COMP RING SEAL	.008	(.0013)	0.06	0.10	0.07	0.11	[illegible]
R5	SHAFT GAP	.257	(.0399)	0.12	0.21	0.16	0.22	[illegible]
R6	BLEED SLOT-INLET	----	------	1.59	10.18	----	----	----
R7	COMPRESSOR SCROLL RING SEAL	0.0	(0.0)	0.0	0.0	0.0	0.0	[illegible]
R8	FRONT GT RING SEAL FEED	.203	(.0314)	0.46	0.45	0.44	0.45	[illegible]
R9	FLANGE GAP	0.0	(0.0)	0.0	0.0	0.0	0.0	0.0
R10	COMP SHROUD BLD SLOT	----	------	1.59	10.18		----	
R11	PUMPING - REAR COMP	---	------	0.10	0.33	0.18	0.39	0.20
R12	COMP STUB SHAFT HOLE	.258	(.040)	0.12	0.21	0.18	0.22	0.15
R13	SHAFT FEED SLOTS	.290	(.045)	0.12	0.21	0.18	0.22	0.15
R14	SEAL BALANCE CHANNEL	.290	(.045)	0.13	0.04	0.12	0.03	[illegible]
R15	LOWER GT BACKFACE RING SEAL	0.0	(0.0)	0.0	0.0	0.0	0.0	0.0
R16	GT BACKFACE "E" SEAL	0.0	(0.0)	0.0	0.0	0.0	0.0	0.0
R17	FLANGE GAP	.052	(.008)	0.27	0.27	0.27	0.28	[illegible]
R18	GT SCROLL FLANGE GAP	0.0	(0.0)	0.0	0.0	0.0	0.0	0.0
R19	GT EXIT JOINT	.064	(.0099)	0.04	0.01	0.03	0.01	0.00
R20	PUMPING - REAR GT SEAL RECIRCULATION			0.22 1.11	0.24 1.14	0.24 1.24	0.24 1.20	0.24 1.07
R21	CENTER BC - APT RING SEAL	.015	(.0023)	0.11	0.17	0.13	0.18	0.12
R22	CENTER GT RING SEAL	.015	(.0023)	0.24	0.22	0.25	0.21	0.19
R23	GT RING SEAL	.015	(.0023)	0.22	0.24	0.24	0.24	0.20
R24	BURNER DISCHARGE JOINT	.077	(.0119)	0.73	0.68	0.69	0.68	0.75
R25	BURNER/BLOCK JOINT	0.0	(0.0)	0.0	0.0	0.0	0.0	0.0
R26	PLENUM/GEARBOX FLANGE	0.0	(0.0)	0.0	0.0	0.0	0.0	0.0
R27	PT SCROLL FLANGE GAP	0.0	(0.0)	0.0	0.0	0.0	0.0	0.0
R28	BURNER COVER FLANGE	.038	(.0013)	0.11	0.09	0.10	0.09	[illegible]
R29	DEOILER	----	------	0.55	0.75	0.65	0.76	0.56
R30	PT BACKFACE "E" SEAL	0.0	(0.0)	0.0	0.0	0.0	0.0	0.0
R31	PT EXIT JOINT	.081	(.0126)	0.42	0.40	0.43	0.42	[illegible]
R32	PUMPING - REAR PT SEAL RECIRCULATION			0.29 0.91	0.31 0.44	0.33 0.62	0.31 0.35	0.26 0.41
R33	LOWER PT BACKFACE RING SEAL	0.0	(0.0)	0.0	0.0	0.0	0.0	0.0
R34	REAR BC RING SEAL	.015	(.0023)	0.29	0.31	0.33	0.31	0.25
R35	PT RING SEAL	.015	(.0023)	0.29	0.31	0.32	0.31	0.26
R36	OVERBOARD LEAKAGE(EST)			1.2	1.45	1.62	1.58	1.3[illegible]
R37	REAR COMP RING SEAL	.014	(.0021)	0.09	0.16	0.12	0.17	0.11

PRESSURES - KPA (PSIA)

CHAMBER NO.	MAX POWER	80 KM/H (50 MPH)	48 KM/H (30 MPH)
P1	101.3 (14.7[illegible])	99.5 (14.43)	99.5 (14.4
P2	192.6 (27.93)	139.[illegible] (19.99)	1[illegible].4 (18.[illegible]
P3	96.2 (13.95)	96.3 (13.96)	96.3 (13.9
P4	100.9 (14.63)	99.3 (14.40)	99.3 (14.4
P5	452.2 (65.56)	175.9 (25.97)	152.2 (22.0
P6	319.3 (46.31)	166.6 (23.32)	131.5 (19.0
P7	194.1 (28.15)	139.8 (19.53)	118.9 (16.9
P8	229.7 (33.31)	126.4 (18.04)	114.6 (16.6
P9	438.4 (63.56)	179.6 (26.08)	147.3 (21.3
P10	229.7 (33.31)	126.1 (18.[illegible])	114.6 (16.6
P11	194.4 (28.19)	139.7 (19.56)	118.8 (16.[illegible]
P12	407.5 (59.[illegible])	174.2 (25.26)	143.6 (20.8
P13	269.7 (39.12)	133.9 (19.42)	12[illegible].6 (17.4
P14	216.3 (31.37)	123.5 (17.92)	114.2 (16.5
P15	101.3 (14.7[illegible])	99.5 (14.43)	99.5 (14.4
P16	227.5 (32.99)	126.1 (18.00)	115.1 (16.6
P17	438.4 (63.56)	179.8 (26.08)	147.3 (21.3
P18	229.7 (33.31)	126.4 (18.09)	114.8 (16.6
P19	448.7 (65.[illegible])	184.[illegible] (26.69)	15[illegible].9 (21.6
P20	229.0 (33.22)	126.3 (18.32)	116.2 (16.8
P21	229.7 (33.31)	126.4 (18.[illegible])	114.6 (16.6
P22	102.7 (14.89)	101.4 (14.71)	101.3 (14.7
P23	126.9 (18.41)	104.7 (15.19)	102.9 (14.9
P24	98.6 (14.30)	92.8 (14.16)	97.4 (14.1
P25	[illegible].3 (14.7[illegible])	99.5 (14.43)	99.5 (14.4
P26	101.3 (14.70)	99.5 (14.43)	99.5 (14.4
P27	101.3 (14.7[illegible])	99.5 (14.43)	99.5 (14.4
P28	438.4 (63.58)	165.9 (14.43)	144.2 (22.0

FOLDOUT FRAME

TABLE XXVII. LEAKAGE DIRECTIONS

PRESSURES - KPA (PSIA)

MAX POWER	80 KM/H (50 MPH)	48 KM/H (30 MPH)	32 KM/H (20 MPH)	IDLE
91.3 (14.7)	99.5 (14.43)	99.5 (14.43)	99.5 (14.43)	99.5 (14.43)
182.6 (27.73)	139.- (20.99)	112.4 (16.31)	116.4 (16.89)	112.4 (16.30)
96.2 (13.95)	96.3 (13.66)	96.3 (13.66)	96.3 (13.66)	96.3 (13.66)
99.9 (14.63)	99.3 (14.40)	99.3 (14.40)	99.3 (14.40)	99.3 (14.40)
182.2 (69.55)	175.9 (25.97)	152.2 (22.08)	144.2 (20.92)	147.3 (21.36)
129.3 (48.51)	166.5 (23.32)	131.5 (19.06)	124.8 (18.07)	122.4 (18.46)
96.1 (28.15)	134.8 (19.53)	110.9 (16.05)	110.7 (16.06)	113.2 (16.42)
129.7 (33.31)	124.4 (18.04)	114.6 (16.62)	111.4 (16.16)	110.5 (16.03)
168.4 (63.56)	179.8 (26.08)	147.3 (21.37)	139.8 (20.25)	144.1 (20.90)
129.7 (33.31)	124.1 (18.0-)	114.6 (16.62)	111.4 (16.16)	110.5 (16.03)
108.4 (28.13)	134.7 (19.54)	114.6 (16.07)	114.9 (16.96)	113.2 (16.42)
197.5 (59.11)	174.2 (25.26)	143.6 (20.83)	137.4 (19.93)	139.3 (20.21)
150.7 (39.12)	133.9 (19.42)	120.4 (17.47)	114.3 (16.87)	114.7 (16.63)
126.3 (31.37)	123.5 (17.92)	114.2 (16.56)	110.2 (15.98)	108.7 (15.76)
91.3 (14.7)	99.5 (14.43)	99.5 (14.43)	99.69 (14.43)	99.5 (14.43)
127.5 (32.99)	124.1 (18.00)	115.1 (16.69)	111.8 (16.18)	109.3 (15.85)
168.4 (63.56)	179.8 (26.08)	147.3 (21.37)	139.8 (20.25)	144.1 (20.90)
129.7 (33.31)	124.4 (18.04)	114.6 (16.62)	111.4 (16.16)	110.5 (16.03)
188.7 (65.26)	166.9 (24.69)	152.9 (21.88)	142.9 (20 73)	146.0 (21.17)
129.0 (33.22)	124.3 (18.02)	114.2 (16.86)	111.9 (16.06)	110.2 (15.95)
129.7 (33.31)	124.4 (18.04)	114.6 (16.62)	111.4 (16.16)	110.5 (16.03)
142.7 (19.69)	101.4 (14.71)	101.3 (14.70)	100.5 (14.58)	100.1 (14.52)
106.9 (18.61)	104.7 (15.19)	102.9 (14.92)	102.0 (14.79)	101.6 (14.73)
98.6 (14.30)	92.8 (14.16)	97.4 (14.13)	99.8 (14.44)	100.8 (14.62)
91.3 (14.7)	99.5 (14.43)	99.5 (14.43)	99.5 (14.43)	99.5 (14.43)
91.3 (14.73)	99.5 (14.43)	99.5 (14.43)	99.5 (14.43)	99.5 (14.43)
91.3 (14.7)	99.5 (14.43)	99.5 (14.43)	99.5 (14.43)	99.5 (14.43)
168.4 (63.56)	165.9 (24.43)	144.2 (22.58)	144.2 (20.92)	147.3 (21.36)

AIR TEMPERATURES - DEG F (DEG R)

	MAX POWER	80 KM/H (50 MPH)	48 KM/H (30 MPH)	32 KM/H (20 MPH)	IDLE
CIT	289 (5209)	303 (5469)	303 (5469)	303 (5469)	303 (5469)
-	- - -	- - -	- - -	- - -	- - -
CIT	289 (5209)	303 (5469)	303 (5469)	303 (5469)	303 (5469)
-	- - -	- - -	- - -	- - -	- - -
CIT	473 (852)	376 (676)	351 (632)	348 (626)	351 (632)
CIT	473 (852)	376 (676)	351 (632)	348 (626)	351 (632)
-	- - -	- - -	- - -	- - -	- - -
MIX	1297 (2336)	1362 (2452)	1346 (2423)	1234 (2222)	833 (1500)
EOT	1561 (2810)	1499 (2698)	1466 (2702)	1313 (2364)	911 (1640)
MIX	1297 (2336)	1362 (2452)	1346 (2423)	1234 (2222)	833 (1500)
-	- - -	- - -	- - -	- - -	- - -
-	- - -	- - -	- - -	- - -	- - -
GT-EOT	1561 (2810)	1499 (2698)	1466 (2702)	1313 (2364)	911 (1640)
-	- - -	- - -	- - -	- - -	- - -
EC	515 (927)	396 (713)	342 (616)	372 (670)	378 (680)
GT-EOT	1383 (2489)	1403 (2525)	1381 (2486)	1255 (2259)	849 (1567)
EOT	1561 (2810)	1499 (2698)	1466 (2702)	1313 (2364)	911 (1640)
MIX	1297 (2336)	1362 (2452)	1346 (2423)	1234 (2222)	833 (1500)
EIT	1144 (2066)	1296 (2337)	1298 (2337)	1191 (2144)	817 (1471)
GT-EOT	1383 (2489)	1403 (2525)	1381 (2486)	1255 (2259)	849 (1567)
MIX	1297 (2336)	1362 (2452)	1346 (2423)	1234 (2222)	833 (1500)
PT-EOT	1193 (2148)	1339 (2410)	1339 (2410)	1228 (2210)	843 (1518)
-	- - -	- - -	- - -	- - -	- - -
-	- - -	- - -	- - -	- - -	- - -
EC	515 (927)	396 (713)	342 (616)	372 (670)	378 (680)
CIT	289 (5209)	303 (5469)	303 (5469)	303 (5469)	303 (5469)
CIT	289 (5209)	303 (5469)	303 (5469)	303 (5469)	303 (5469)
-	- - -	- - -	- - -	- - -	- - -

Thrust Load
Equivalent to Mean Load - Newton (Lbf)

LOAD DESCRIPTION	MAX POWER		80 KM/H (50 MPH)		48 KM/H (30 MPH)		32 KM/H (20 MPH)		IDLE	
COMPRESSOR										
FA	-1856	(-417)	-1669	(-375)	-1166	(-262)	-1131	(-254)	-1159	(-260)
MVX	-46	(-10)	-39	(-9)	-33	(-7)	-33	(-7)	-34	(-8)
FB1	-33	(-7)	-30	(-7)	-32	(-7)	-32	(-7)	-32	(-7)
FB2	-28	(-6)	-25	(-6)	-28	(-6)	-27	(-6)	-28	(-6)
FC1	+1687	(+379)	+1513	(+340)	+1078	(+242)	+1036	(+233)	+1063	(+239)
FC2	+1013	(+228)	+913	(+205)	+611	(+137)	+578	(+130)	+603	(+136)
TOTAL COMPRESSOR LOAD	+317	(+71)	+271	(+61)	-11	(-3)	-94	(-21)	-223	(-50)
GASIFIER TURBINE										
FE	+1039	(+234)	+1476	(+332)	+1153	(+259)	+1116	(+251)	+1113	(+250)
MVX	+64	(+14)	+59	(+13)	+34	(+8)	+32	(+7)	+33	(+7)
FDB	-1227	(-276)	-1027	(-231)	-752	(-169)	-796	(-179)	-793	(-178)
FDA	-605	(-136)	-511	(-115)	-376	(-84)	-401	(-90)	-397	(-89)
FF	+77	(+17)	+42	(+9)	+42	(+9)	+39	(+9)	+36	(+8)
TOTAL GASIFIER TURBINE LOAD	+348	(+78)	+139	(+31)	+101	(+23)	+90	(+20)	+85	(+19)
POWER TRANS	-36	(-8)	-27	(-6)	-30	(-7)	-22	(-5)	-3	(-1)
TOTAL GASIFIER LOAD	+429	(+96)	+193	(+43)	+76	(+16)	+68	(+15)	+118	(+26)
POWER TURBINE										
FF	-2267	(-510)	-1766	(-397)	-1736	(-391)	-1726	(-388)	-1692	(-380)
MVX	-76	(-16)	-52	(-12)	-37	(-8)	-35	(-8)	-36	(-8)
FJ	+1797	(+404)	+1369	(+308)	+1276	(+287)	+1244	(+280)	+1236	(+278)
FK	+521	(+117)	+434	(+97)	+423	(+95)	+419	(+94)	+419	(+94)
FG	-57	(-13)	-57	(-13)	-57	(-13)	-57	(-13)	-57	(-13)
FL	+109	(+25)	+108	(+24)	+108	(+24)	+106	(+24)	+107	(+24)
METER	-330	(-74)	-277	(-62)	-139	(-31)	-136	(-31)	-141	(-32)
TOTAL POWER TURBINE LOAD	+237	(+53)	+251	(+56)	+134	(+30)	+115	(+26)	+136	(+31)

Compressor Thrust Load

F_A - Inducer and shroud load (compressor)
MV_{XC} - Inlet momentum
F_B - Shaft centerline to inducer hub (includes seal load)
F_{C_1} - Compressor rear face, tip to break
F_{C_2} - Compressor rear face from break to seal

Gasifier Turbine Thrust Load

F_{D_B} - Load from rotor tip to rotor web
F_{D_A} - Load from rotor web to seal
F_E - Shroud and inducer load
MV_{XGT} - Inducer momentum load
F_F - Load from inducer hub to centerline of gasifier turbine

Power Turbine Thrust Load

MV_{XPT} - Power turbine inducer momentum
F_J - Load on rear face of turbine from rotor tip radius to web radius
F_K - Load on rear face of turbine from web radius to seal radius
F_G - Load from inducer hub radius to turbine centerline
F_L - Load from seal radius to turbine centerline

H80-1691

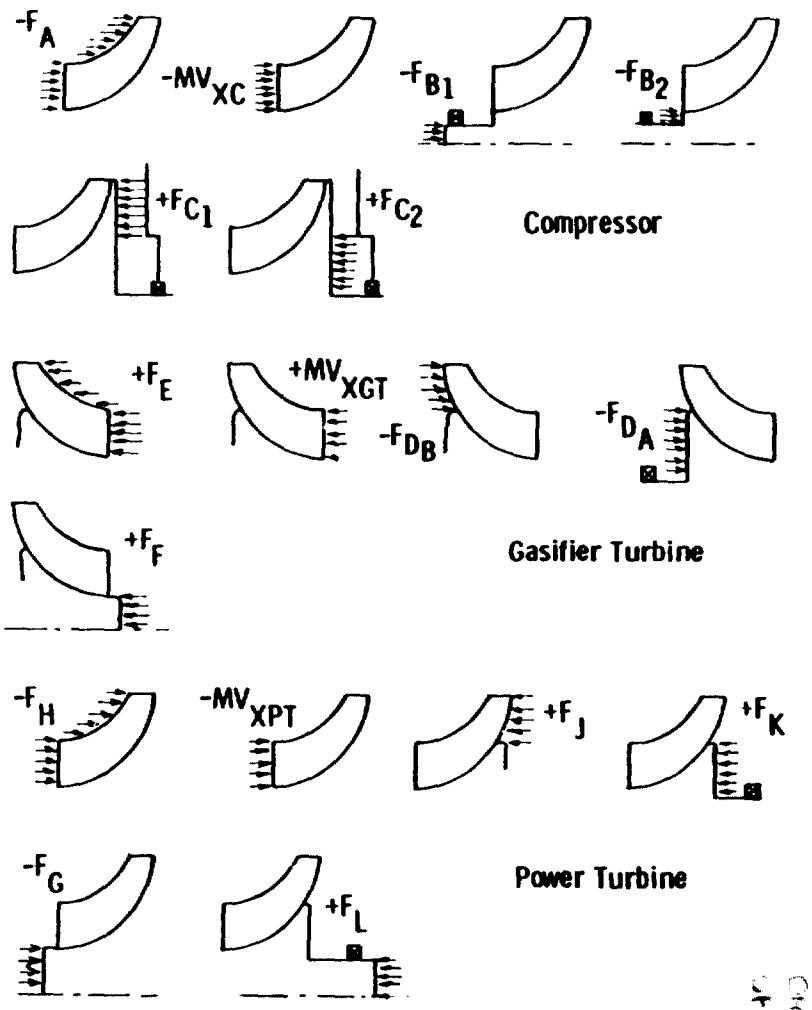

Figure 220. - Thrust Balance.

IX. MATERIALS DEVELOPMENT

9.1 MATERIALS DEVELOPMENT--DDA

Design Support

Reference Powertrain Design

Approximately 90% of the materials have been selected for the RPD. Special projects have been initiated for more material data (low-cycle fatigue) for the aluminum impeller and to develop a bonding technique for the ceramic rotor to a steel shaft.

Mod I

Approximately 70% of the materials have been selected for Mod I (see Table XXVIII). Some of the materials in the high-temperature areas of the combustor are still being reviewed for oxidation resistance, availability, and cost.

TABLE XXVIII. MOD I MATERIALS LIST

Carbon Steel:
- SAE 1144

Low Alloy Steels:

SAE 4140	SAE 9310
SAE 4340	SAE 52100
SAE 8620	M-50

Corrosion and Heat Resistant Steels:

AISI 409	Inconel X750
AISI 410	Inco 718
AISI 430	L 605
Inco 903	HA 188
IN 100	Mar-M 246

Aluminum Alloys:
- SAE 335 (Type C355)
- SAE 326 (Type 319)

Cast Iron:
- GM-13M (SAE G-3000)

A special investigation was conducted to determine if the LCF properties of the aluminum impeller could be increased by peening or prestressing. Peening parameters were established, stress gradients were measured on wrought samples, and test bars were machined and peened for LCF testing. One test specimen was cycled 20 times, 0 to 0.41% strain, at 121°C (250°F). X-ray diffraction evaluation of the specimen after testing showed the compressive surface stresses from peening were retained. This indicates a potential improvement in LCF life by peening.

Gasifier Turbine Wheel Replicas

Two types of molding fixtures have been prepared to permit the reproduction of gasifier turbine wheel replicas. These molds and wheel replicas are being used by the ceramic vendors to produce laboratory samples for ceramic evaluations. The first mold produced is shown in Figures 221 and 222. This mold was made from a partially finished metal rig wheel that did not have the backface profile machined. It served to produce only the blade and flow-path contours for preliminary ceramic evaluations. The inserts were made of RTV664 silicon rubber supported in a REN plastics RP3215-1 casing. A small number of wheels of urathane rubber were produced from this mold.

After machining of the rig wheel backface, another mold using an aluminum backplate and a casing employing a revised method of holding the inserts was constructed. Turbine wheel replicas made from thermoset 600 epoxy resin with thermoset No. 13 hardener were produced. This mold and its product are shown in Figure 223. This method of reproduction allows the ceramic vendors to obtain gasifier turbine wheel replicas from DDA, which are suitable for ceramic wheel evaluation at an earlier time in the program schedule for a small cost. The wheel used as a master was obtained from the gasifier turbine aerodynamic development rig program. This wheel has a material allowance on the blade tip to permit recontouring after aerodynamic development test evaluations.

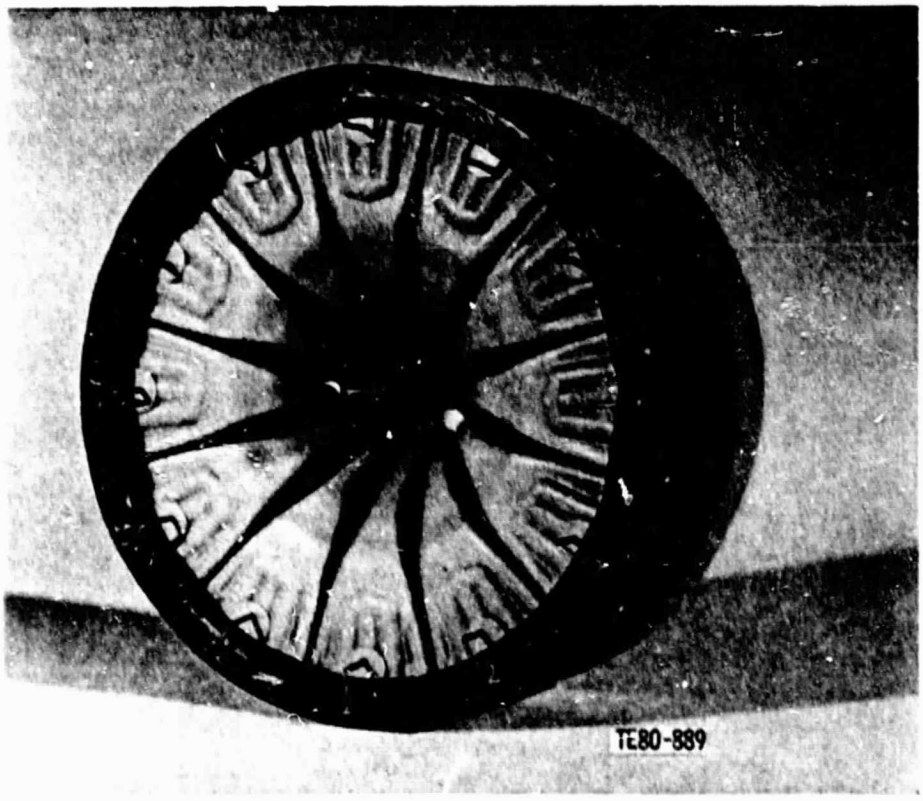

Figure 221. - Assembled Gasifier Turbine Wheel Mold.

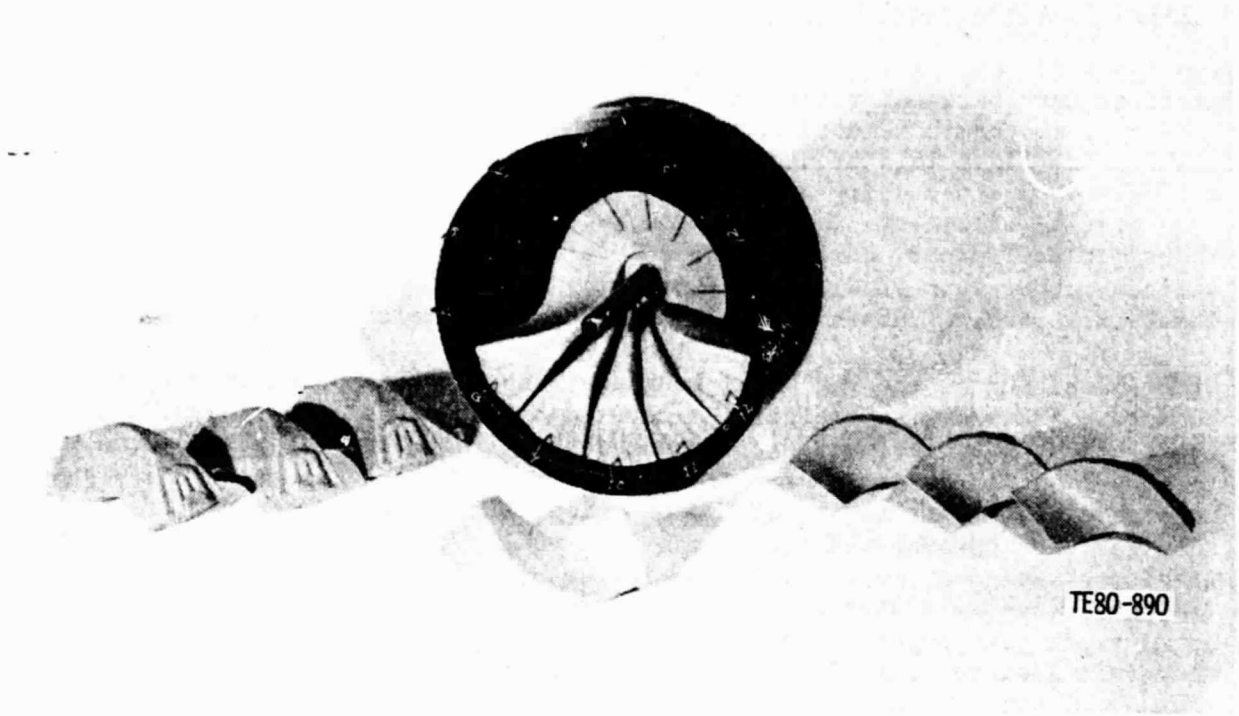

Figure 222. - Disassembled Gasifier Turbine Wheel Mold.

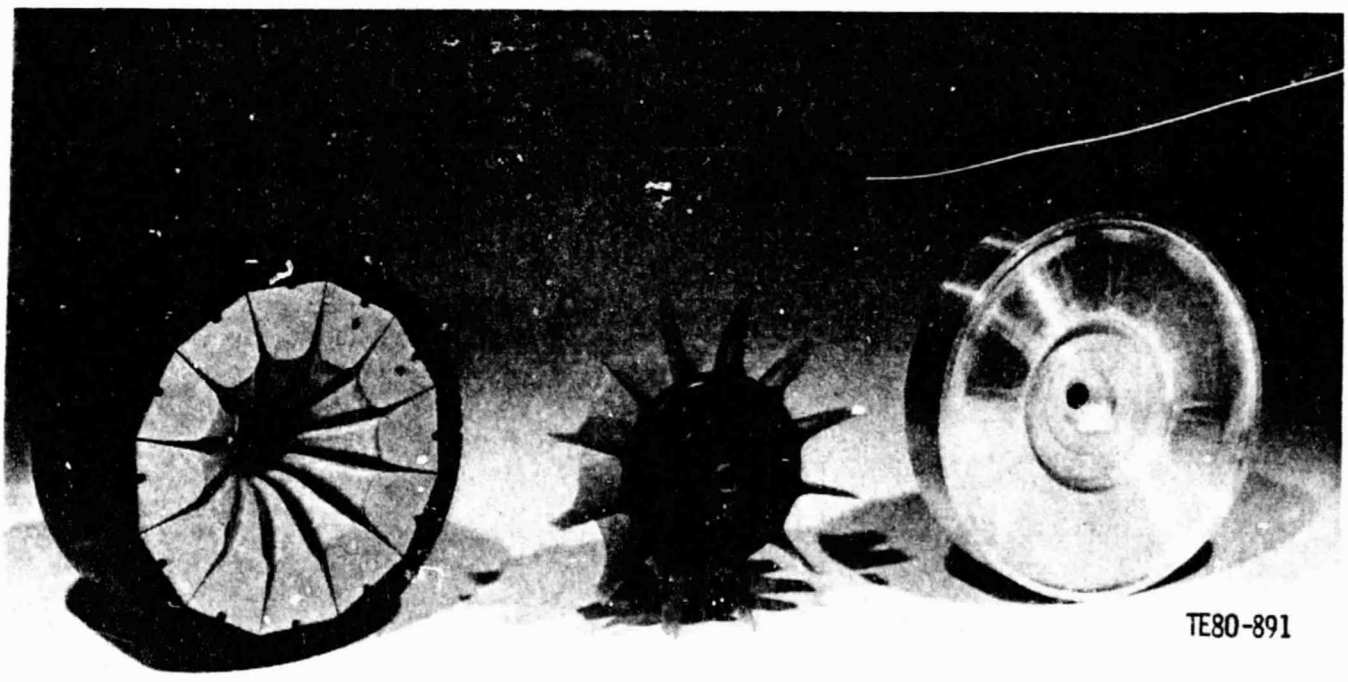

Figure 223. - Mold and Turbine Wheel Epoxy Castings.

9.2 MATERIALS DEVELOPMENT--SUPPLIERS

The Alpha Silicon Carbide Division, Carborundum Company is the primary source of AGT structural ceramic components. Its role is to both supply initial silicon carbide prototype components needed to support the test/development activity and to develop ceramic forming methods for ultimate production use. In addition, there is a mutual effort to further develop design procedures and ceramic nondestructive evaluation (NDE) techniques.

Of the currently configured AGT-100 components, the gasifier rotor is the most highly stressed and, without question, the most difficult component to fabricate. Immediate effort, therefore, was concentrated on adapting compatible processing techniques to this shape. Since a ceramic rotor is common to both the DDA and AiResearch engine configurations, the major portion of this initial work, which focused on a generalized shape, has been jointly sponsored. A detailed description of the approach/progress will appear under a separate cover, and only a brief summary of the effort will be presented here. Initial work specifically related to the DDA rotor configuration along with that associated with the scroll will also be summarized here.

Unique Effort

Rotor Fabrication

Based on initial design analysis the reaction-bonded type of silicon carbide material appears to be compatible with the operational requirements of the AGT-100 gasifier rotor. Furthermore, the minimal amount of dimensional change that occurs during the processing of this type of material makes it very attractive for use in complex shapes like the rotor. Therefore, the application of reaction-bonded silicon carbide has received considerable attention. Emphasis has been placed on three green body techniques--green machining, thixotropic casting, and transfer molding.

Green Machining

Preliminary work to establish the feasibility of ultrasonically machining green bodies of both reaction-bonded and sintered alpha silicon carbide materials have been completed. The primary concern was whether this technique was capable of forming blades without breakage.

Cast copper tooling was produced from a turbocharger rotor similar in size and shape to the Mod I gasifier rotor. This tooling was fitted to a small 200-W Sheffield Cavitron machine. Initial studies were confined to warm-molded reaction-bonded silicon carbide, both in the as-molded and baked conditions, and to isopressed alpha silicon carbide.

While machining rates were relatively low for both the as-molded and baked reaction-bonded materials, a thin blade-like structure could be produced free of cracks as shown in Figure 224. Similar results were achieved with isopressed alpha silicon carbide. In all cases, some small pitting was found in the top surface of the billets near the cavities and to a lesser extent within the cavities. This presumably was caused by improper flushing of the abrasive slurry and could be corrected.

TE80-1692

Figure 224. - Small Ultrasonic Machining Tools and Green-Machined Reaction-Bonded SiC Materials.

The method of using a solid ultrasonic tool is thought to be too slow to be economically viable. A more efficient approach would be to use a hollow tool. Consequently, a set of hollow tools has been produced from the turbocharger pattern previously used. Figure 225 shows the cast tools. In addition, solid tools for finish cutting have also been produced. Additional machining trials using these tools will be conducted during the next reporting period.

Thixotropic Casting

The objective of this effort was to adopt a thixotropic casting technique for producing complex shapes of reaction-bonded silicon carbide to the AGT-100 gasifier rotor. Initial efforts concentrated on casting a small turbocharge rotor. This effort yielded a completely siliconized rotor with stub shaft as shown in Figure 226. The shaft was attached green and bonded during siliconization.

Subsequently, plastic replicas of the Mod I gasifier rotor were supplied to Carborundum. After adding material to increase blade thickness by abc .25 mm (10 mils), several rubber molds were produced. After numerous trial castings, a completely siliconized rotor as shown in Figure 227 was successfully fabricated. Visual appearance of the rotor was excellent, and no density variations could be discerned radiographically. Dye penetrant inspection revealed a through crack at the tip of one blade and a small porous section in another blade. Bulk density was measured to be 2.97 g/cm^3 (185 lbm/ft^3).

Figure 225. - DDA Truck Turbocharger and Cast Ultrasonic Machining Tools.

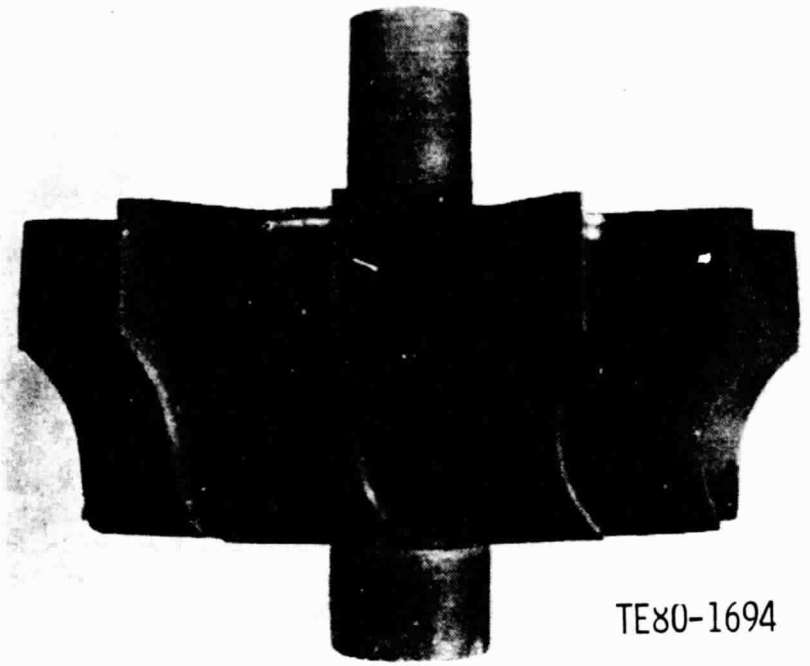

Figure 226. - Thixotropic Cast Reaction-Bonded SiC DDA Truck Turbocharger Rotor with Shaft Extension.

Figure 227. - Thixotropic Cast Reaction-Bonded SiC Gasifier Rotor.

Transfer Molding

The objective of this effort was to assess the feasibility of adopting a transfer-molding process developed for vanes under the CATE program to the fabrication of a solid one-piece rotor. A small Carborundum rotor injection tool was modified for molding studies. Initial attempts to produce sound green components with the standard vane mix, unfortunately, were not successful since molded rotors were severely cracked. Consequently, this initial effort was terminated. A second attempt will be made, however, as soon as an injection-molding tool for alpha SiC becomes available.

Stationary Components

A number of different forming techniques including slip casting, mandrel coating, and injection molding, have been considered for fabrication of larger stationary components. Slip casting has been selected as the primary fabrication method, and initial components will be produced accordingly. However, the slip casting method imposes a significant restriction on design flexibility. Conequently, other methods with greater shape capability are being pursued in parallel. The following sections summarize this work.

Mandrel Coating

In the mandrel-coating technique, silicon carbide grain dispersed in a liquid resin is applied to a foam mandrel of complex shape. Any number of application methods, including brushing, dipping, and spraying can be used. The mandrel is then removed by solvent leaching, melting, or thermal decomposition depending on the foam and powder binder system being used. The free-standing shape is then fired to final density.

Both reaction-bonded and sintered alpha silicon carbide shapes can be produced by this coating technique. Figures 228 and 229 are examples of parts of both methods. The internal surfaces accurately replicate the shape of the mandrel.

The sintered alpha SiC test parts were made by a brush-painting technique, and after sintering, internal cracks following the brushing directions were noted in X-ray inspection. Spray coating and dipping are currently being developed.

Reaction-bonded SiC, mandrel-coated parts have been more successful relative to cracking, but it has become obvious that the coating's binder must not react with the mandrel material if good surface finishes are desired. The first parts made used the relatively coarse mix composition, which was also used for thixotropic casting. Since the thixotropic casting mixes have been progressively made finer, there has been no adverse effect on coating ability.

Component Fabrication Status

Combustor

Tooling for the combustor body, gasifier scroll, and gasifier backplate have been designed. An aluminum pattern for the combustor body has been received as shown in Figure 230. A plaster mold made from this pattern is shown in Figure 231. Patterns for the remaining two components are on order.

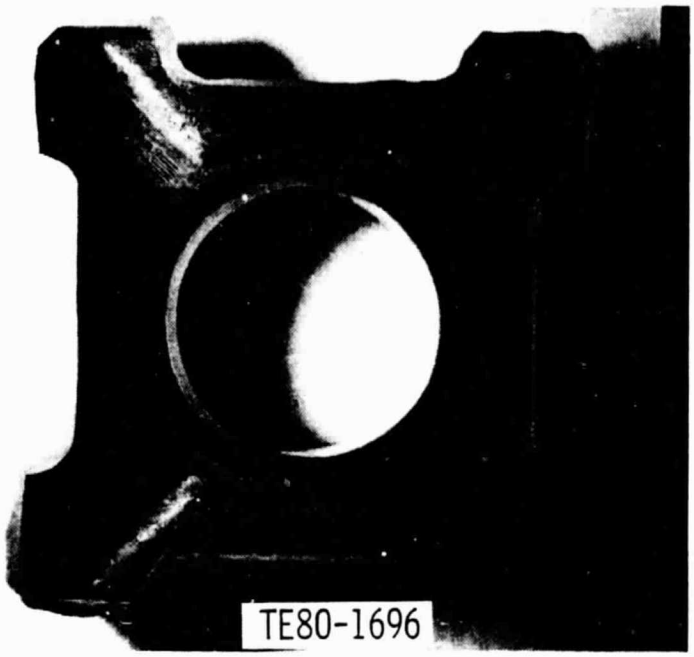

Figure 228. - Sintered Alpha SiC Test Piece Made by Mandrel Coating Process.

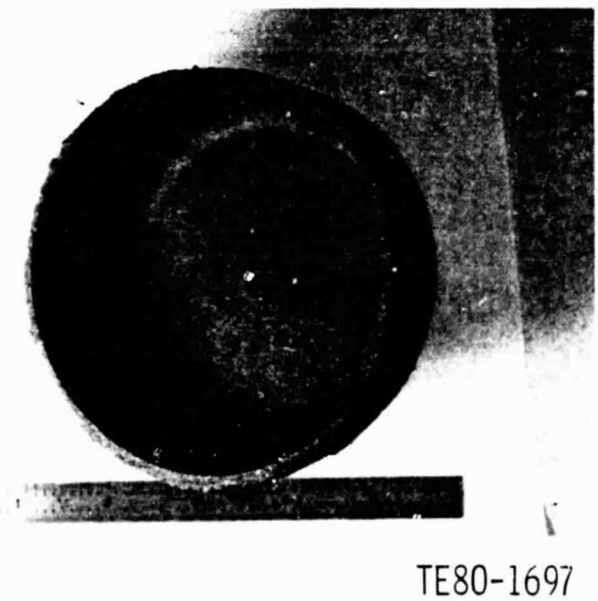

Figure 229. - Coarse-Grained Reaction-Bonded SiC Test Piece Made by Mandrel-Coating Process.

Figure 230. - Combustor Pattern for Slip Casting Plaster Mold Fabrication.

Figure 231. - Plaster Slip Casting Mold for Combustor.

Backplate

The current backplate is a two-piece design. The outer section has been selected as the component upon which to develop injection-matching methodology as applied to larger shapes. Currently a tool has been designed and ordered. Delivery is expected early in the next reporting period.

Gasifier Rotor

Injection-Molded Alpha Silicon Carbide

Injection molding is the primary fabrication method for producing solid one-piece alpha SiC gasifier rotor. Consequently full-scale tooling has been designed and ordered. Delivery is expected early in the next reporting period.

Common Effort - CBO

The common work activity currently being sponsored at the Carborundum Company may be classified into four major areas: rotor fabrication, NDE, physical and mechanical properties of silicon carbide, and machining. Emphasis has been focused on the first three areas and particularly on rotor fabrication.

The following sections summarize the work completed to date.

- o Rotor Fabrication
  Presently the temporary binder system used in injection molding of silicon carbide bodies cannot be removed from sections greater than about one inch in thickness without producing extensive cracking. The objectives of this activity are to (1) examine alternate techniques for binder removal and (2) investigate other fabrication approaches based on joining rotor segments by appropriate binding techniques.

  To expedite fabrication, an existing tool originally used to fabricate stylized rotors under an earlier program was modified to produce a bell-like shape simulating a rotor hub without blading. This shape was to be used to evaluate alternate binder removal procedures. In addition, tool inserts were also made so that three segments, shell, core, and back plate could be produced. These pieces would subsequently be bonded together to form a complete simulated hub. Figure 232 shows schematically the segments both individually and as assembled.

  In addition to extended versions of the standard baking cycle, vacuum baking and plasma baking have been investigated. Solid one-piece hubs free of visual defects were used in these studies. Results to date show that crack-free bodies could not be obtained by any of the procedures examined. It should be noted, however, that the simulated hub is considerably greater in thickness than the AGT 100 gasifier rotor. With proper tool design it may yet prove feasible to use the existing binder system for the gasifier.

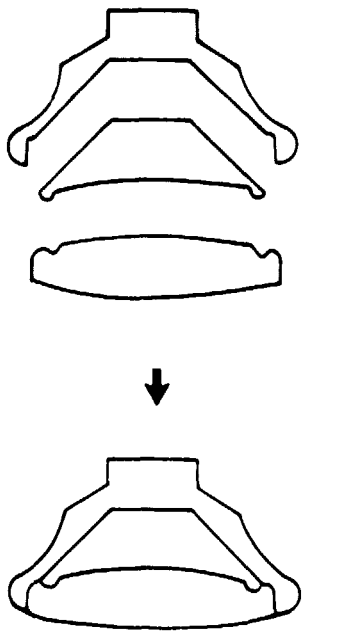

Figure 232. - Injection-Molded Alpha Silicon Carbide Segments Used in Rotor Fabrication Studies.

Two basic approaches to produce integral rotors from segments were investigated. In the first, the outer shell was filled with either a sinterable powder which was subsequently hot press bonded, or a silicon carbide/carbon mix which was reaction sintered. In the former case densities as high as 2.97 gm/cc have been achieved. However, distortion and/or cracking of the shell remains a problem. In the latter case densities of 2.96 gm/cc were attained if reaction sintering was followed by hot pressing. Again distortion and cracking of the shell occurred. Also, the thermal expansion mismatch presented an added difficulty. While good bonding to the shell could be attained with either filler, adequate bonding was not consistently achieved.

The second approach consisted of bonding together fired and densified segments by any of several techniques including hot pressing and brazing. Of the techniques and variations evaluated, a hot pressing procedure using an extrudable alpha SiC mix as a joining medium proved to be the most successful. Densities consistently greater than 3.13 gm/cc were realized for the final assembly. Grain growth across the joint interface was observed by optical microscopy. In MOR tests, base material or joint material failure occurred in many instances rather than joint failure.

Bonding or joining of segments is not the most desirable rotor fabrication procedure owing to the difficulty associated with nondestructively assessing joint quality. However, it may be an acceptable method to facilitate early development and testing of prototype rotors. Clearly, a major effort must continue under the unique program to establish fabrication procedures for a single piece rotor.

o Nondestructive Evaluation

The nondestructive evaluation effort is directed toward establishing and defining techniques to detect strength-limiting flaws. The approach is to introduce known flaws into the ceramic and evaluate techniques for detecting them. Two flaw inducing methods are described here--seeding to introduce foreign matter or voids in the material during processing, and inducing hardness indentations on the surface, which tends to produce cracks at the base of the indentation.

The seeding and fabrication of large (125-250 μm) and intermediate (50-125 μm) size void disks of all thicknesses have been completed. The fabrication of disks with large (125-250 μm) carbon inclusions was completed. NDE will follow for these specimens. The fabrication of disks with B_4C inclusions is in progress.

An evaluation of Knoop-flawed as-fired SiC specimens has been completed by Prof. R. L. Thomas of Wayne State University by using the SPAM technique. An argon laser beam was used with a chopping frequency of 1 kHz. The focal spot size was 10 μm. The laser beam scanned in the X-direction while the sample was translated in the Y-direction. The intrinsic defects on the as-fired SiC surface made characterization of the Knoop indentations very difficult. The SPAM traces, however, show good resolution and reproducibility and display the characteristic defect features of these surfaces.

An evaluation of Knoop-flawed SiC disks was also completed by Sonoscan, Incorporated. In these initial tests, the indentation damaged zone was not removed. Flaw sizes ranged from 90 to 160 microns.

All Knoop flaws were detected by SLAM, using dark field imaging mode. A general increase in the detectability of the indents was observed with increasing flaw size.

The 1 kg indents exhibit image contrast similar to the background structure, and imaging from several insonification angles was needed to distinguish them from the background.

Future SLAM work will involve examination of internal voids, carbon, and boron carbide inclusions, as well as complex shape examination.

o Baseline Mechanical Properties

The baseline properties data for alpha silicon carbide manufactured by different processing techniques have been evaluated and the results are given in Tables XXIX and XXX.

In all cases, the specimen cross section was 1/8" x 1/4" and a total of 30 specimens were tested per each baseline data.

It should be noted that the strength data obtained for injection molded specimens were obtained for as-furnaced surface condition. For the case of cold pressed and slip cast material, the surfaces were machined by using 180 grit diamond wheel. The test bars were annealed for 2 hours in argon atmosphere prior to flexural test.

TABLE XXIX. STRENGTH DATA FOR INJECTION MOLDED ALPHA SiC

4-Point Bend; 1.5" Outer Span; 0.5" Inner Span

	Material	Average Strength (10^3 psi)	Standard Deviation (10^3 psi)	Weibull Modulus (m)	Charact. Strength (10^3 psi)	Low Strength (10^3 psi)	High Strength (10^3 psi)
25°C 77°F Data	As-Received	54.49	13.07	4.98	64.70	37.26	83.41
1200°C 2192°C Data	Annealed	61.52	11.05	5.76	66.19	40.56	78.62
	Annealed	57.46	10.31	5.97	61.85	35.28	76.92

TABLE XXX. ROOM TEMPERATURE [25°C (77°F)] STRENGTH DATA FOR COLD PRESSED AND SLIP CAST ALPHA SiC

4-Point Bend; 1.5" Outer Span; 0.75" Inner Span

Material	Average Strength (10^3 psi)	Standard Deviation (10^3 psi)	Weibull Modulus (m)	Charact. Strength (10^3 psi)	Low Strength (10^3 psi)	High Strength (10^3 psi)
Cold Pressed	48.05	6.25	8.42	50.78	36.24	59.62
Slip Cast	54.46	11.39	4.84	59.40	29.22	72.79

X. CONTROLS

The control effort is divided between Delco Electronics Division and DDA. Delco's responsibility is the electronic control unit; DDA has responsibility for the overall control system and for all components other than the electronic control.

10.1 DELCO ELECTRONICS

Engineering efforts on the AGT-100 control have concentrated in three main areas: 1) updating information on the latest engine configuration and performance predictions, 2) defining the interface sensors and actuators, and 3) defining key areas of the control system specification in which Delco experience could be used to establish design requirements.

Initial activities have led to the following Delco work definition:

- o Information on environmental limits and electrical characteristics of current microprocessor designs for automobile applications
- o An initial mechanization diagram showing in detail the major components and interconnection of the control electronics based on the latest interface
- o Initial design data on a test simulator having the desired automatic and manual input features

General test requirements for functional testing and key qualification tests (Vibration, Electromagnetic Interference, etc) have been established. It has been decided that any control test simulator (or monitor) will have means to manually control or to input selected control parameters (such as IGV angle, gasifier speed command, TOT command, and fuel flow). This manual input feature would be used during initial engine tests to map or limit engine parameters.

10.2 DETROIT DIESEL ALLISON

DDA efforts during the initial control design period concentrated in three main areas: 1) hardware definition of key sensors, actuators, fuel system, and interface, 2) control mode definition, and 3) development of required digital simulations of control-engine-vehicle and related analysis techniques.

Hardware Definition

Performance requirements and physical characteristics of the control electronics and individual components are being developed to produce detailed specifications for each part. A general interface definition and selection of key requirements for sensors, fuel system components, and variable geometry actuators has resulted. These areas are discussed in the following paragraphs.

Interface

Interface of the electronic control unit (ECU) with the selected sensors, actuators, engine, and vehicle is shown in the implementation diagram of Figure 233. The ECU contains all necessary power conditioning, signal conditioning, output devices, and microprocessor components. Outputs are driven directly by the ECU except for high-current items such as the starter and ignition. A separate relay panel for these components is planned.

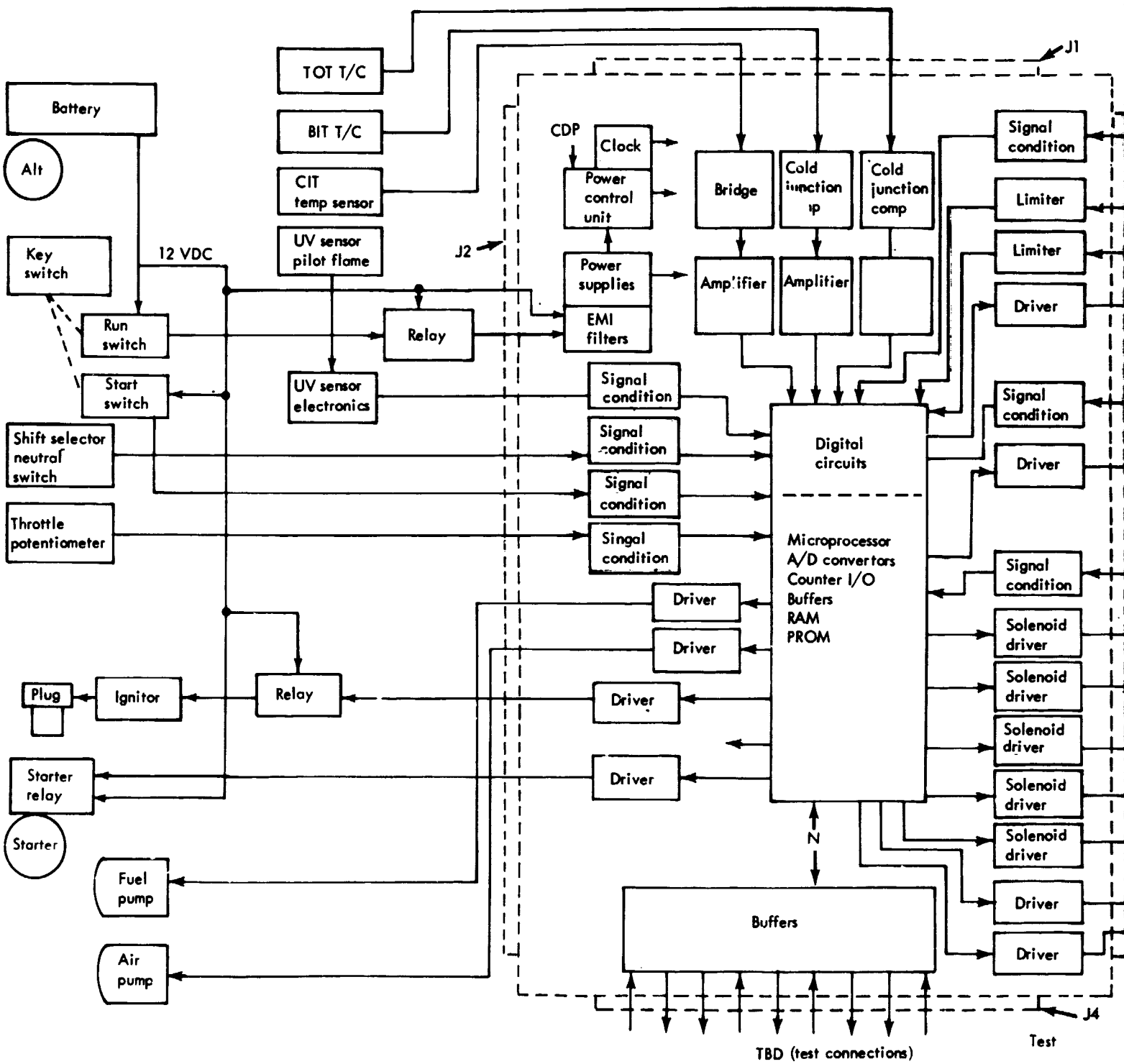

Figure

FOLDOUT FRAME

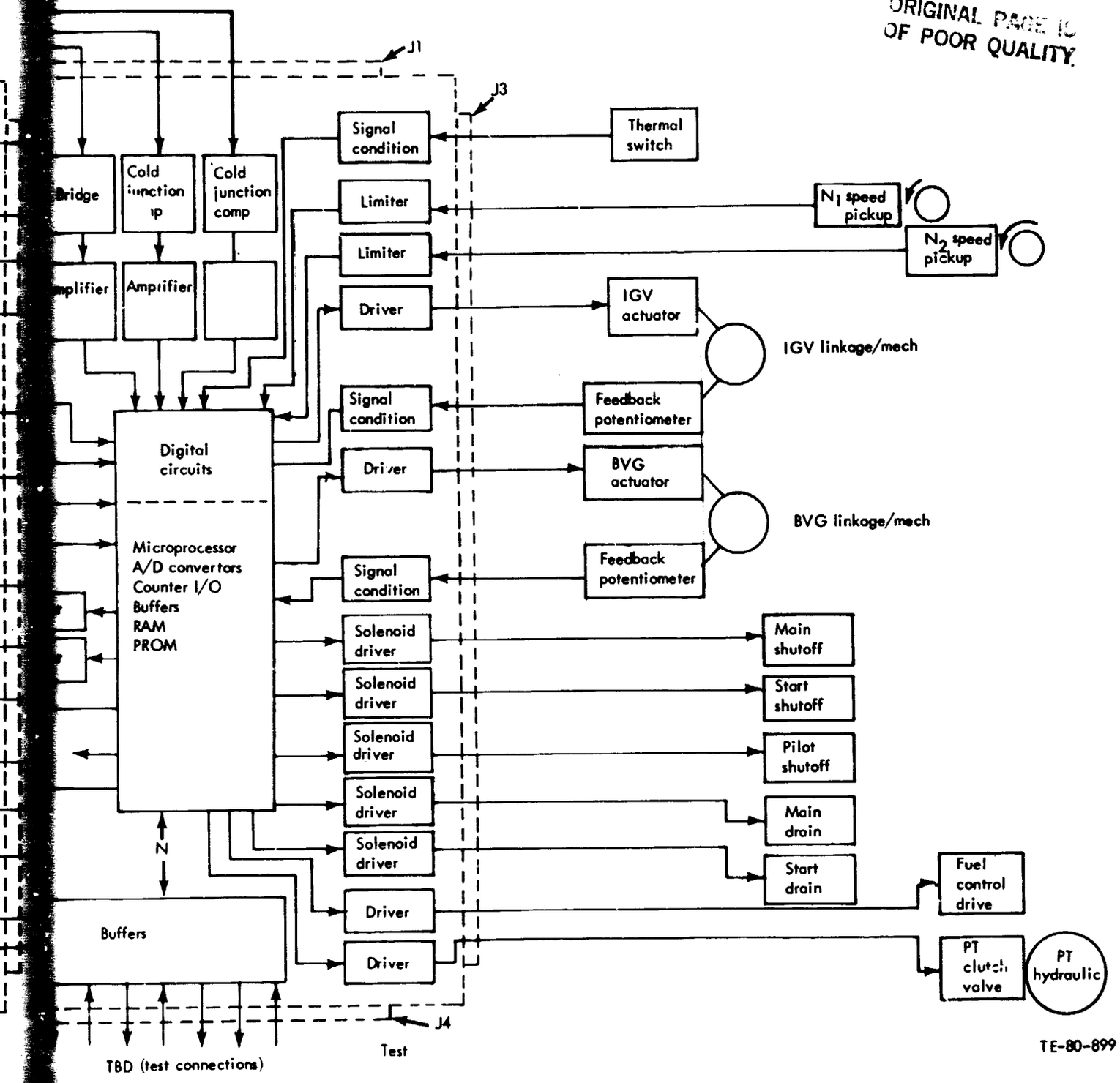

Figure 233. - AGT-100 Control Implementation Diagram.

Sensors

Functional requirements have been defined for the following key sensors:

- o Turbine output temperature (TOT) thermocouples
- o Burner inlet temperature (BIT) thermocouple
- o Compressor inlet temperature (CIT) temperature sensors
- o Pilot flame sensor
- o Exhaust gas temperature sensor
- o Gasifier (N_1) speed sensor
- o Power turbine (N_2) speed sensor

Detailed design has started on the first two and the last two items. Table XXXI summarizes the key sensors selected.

TABLE XXXI. KEY SENSOR CHARACTERISTICS

Sensor	Type	Number	Location	Key parameters
TOT thermocouple	Platinel II	1, dual junction	Turbine outlet duct	1065°C (1950°F) avg
BIT thermocouple	Platinel II	1, dual junction	Regenerator cold side output	1010°C (1850°F) avg
CIT temperature sensor	Temperature--sensitive resistor	2	Air inlet housing	±2°C (3.6°F) accuracy
Pilot flame sensor	Ultraviolet sensor	1	Pilot nozzle assembly	0.25-s response time
Exhaust gas temperature sensor	Bimetallic temperature switch	1	Exhaust duct	Activate 593°C (1100°F)
Gasifier speed sensor	Magnetic pickup	1	Power transfer clutch gearbox	100% N_1 6150 Hz
Power turbine speed sensor	Magnetic pickup	1	Power transfer clutch gearbox	100% N_2 4350 Hz

Fuel System

The AGT-100 fuel system configuration is shown in Figure 234 and is described as follows:

Shutoff Solenoids

The engine has a three-manifold fuel system--pilot, start, and main. Each manifold is controlled by a separate ON-OFF solenoid shutoff valve. The solenoids are normally OFF (closed) and are energized as required during starting and normal running. In the event of power failure or at shutdown, the solenoids will be closed to provide fuel shutoff. The pilot manifold is on during all operation with a minimum flow of 0.11 kg/h (0.25 lbm/hr). Starting is accomplished using the start nozzle until the burner is warm enough to support combustion by wall-film vaporization, at which time the main nozzle is activated and the start nozzle fuel flow subsequently turned off. "Turn-on" sequencing of all three manifolds can thus be achieved using the three shutoff solenoids.

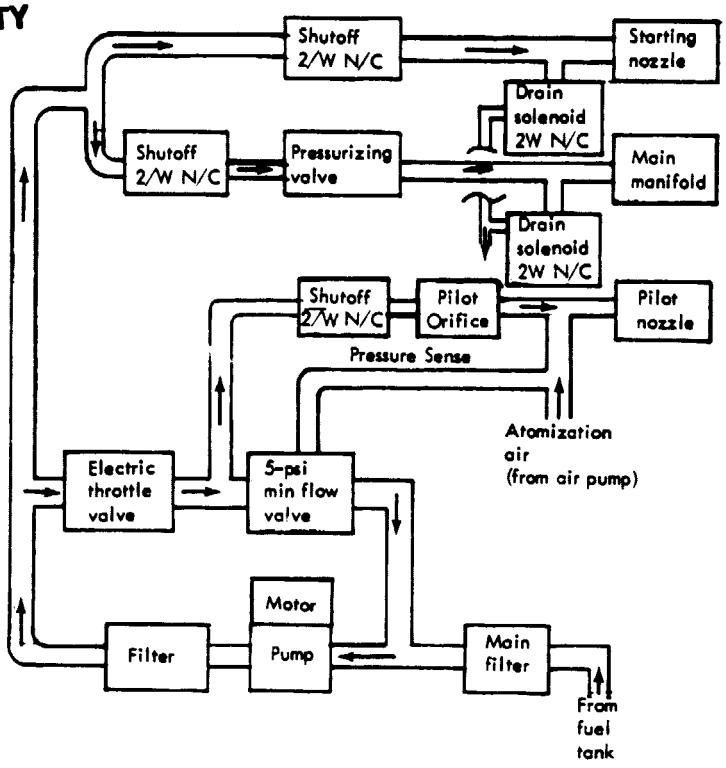

TE-80-896

Figure 234. - AGT-100 Fuel System.

Drain Solenoids

Manifold drain solenoid valves are used in the main and start manifolds to allow purging of the nozzles when shutdown occurs. This prevents coking or excess emissions. The normally closed solenoid valves are located very close to the nozzles to minimize the lengths of manifold to be drained and subsequently refilled. Each solenoid is momentarily turned on either at shutdown (main drain) or after use (start drain). The pilot nozzle does not require a drain valve since the atomizing air provides forward purging of fuel at shutdown.

Pressurizing Valve

The pressurizing valve in the main manifold ensures that the main manifold will not completely rob the start nozzle and cause flameout. This is essentially a diverter or flow divider valve performing the normal function typical of operating with dual manifolds. When the regulated fuel flow/pressure is decreased to cause a pressure drop of less than 68.9 kPa (10 psi) across the pressurizing valve, the valve closes, stopping fuel to the main. Thus, by dropping upstream system pressure to less than 68.9 kPa (10 psi) above compressor discharge pressure (CDP), the main can be decreased to zero flow.

Pilot Flow--Minimum Flow Valve

Pilot nozzle fuel flow is controlled to a constant rate by a minimum flow valve. This is also a pressurizing valve, located in the bypass return line, that is varied in setting by CDP. The purpose of this valve is to maintain a pressure 34.5 kPa (5 psi) greater than pilot nozzle air pressure to provide the constant flow source for the pilot nozzle. The minimum flow valve is similar to a conventional bypass valve concept except that it is controlling the pressure drop across the pilot orifice rather than a metering valve. By being in the bypass line, it is not critical on leakages in that it has high flow (pump flow) when regulating the 0.11 kg/h (0.25 lbm/hr) minimum flow to the pilot nozzle.

Air Pump

The pilot nozzle is an air-assist configuration. Atomizing air is supplied by an air pump driven by an electric motor. The air pump is preferred over direct atomization of fuel using a high-pressure fuel pump since the high-pressure system requires a very small orifice that is susceptible to contamination, coking, and varnish buildup. The air-assist method eliminates this disadvantage. A positive displacement air pump will be used to boost the compressor discharge air pressure by an additional 34.5 kPa (5 psi). Two different types of DC motor driven air pumps, a diaphragm type and a vane type, were ordered for evaluation. A test program has been planned to evaluate pressure pulse effects, motor speed versus flow characteristics, and endurance (durability) capabilities.

Start Nozzle

The minimum flow valve also controls the minimum flow to the start nozzle. The 34.5 kPa (5 psi) pressure drop is maintained across the pilot orifice (assuming the electric throttle valve is full open). An additional 34.5 kPa (5 psi) drop is maintained across the pilot nozzle by the atomization air pump. Thus, 68.9 kPa (10 psi) appears across the start nozzle. The result is a minimum flow of 2.5 kg/h (5.4 lbm/hr) to the start nozzle (based upon a flow number of 1.7). The start nozzle is not reduced to zero flow at 0 mA to the electric throttle valve.

Electric Throttle Valve--Main Flow

The electric throttle valve is the primary fuel control and modulation valve for all operation at greater than minimum flow. To increase the fuel flow to the engine, the valve closes down in response to an electrical command. The result is a pressure drop increase across the valve causing a higher system pressure and more flow to the burner.

When maximum flow is required, the valve is closed, diverting pump flow to the burner. When in the closed-position, it will allow a through flow of more than 0.11 kg/h (0.25 lbm/hr) to ensure pilot flow.

When minimum flow is desired, the valve is full open, with essentially zero pressure drop across it.

The throttle valve is a single nozzle-flapper servo type. It consists of a double coil torque motor (for failure protection), which positions a flapper valve in front of a fuel supply nozzle. The valve thus sees a high fuel flow rate and is capable of high accuracy at the low flow rate when only the pilot is on. By being in the pump bypass line the throttle valve is not critical on leakage or fuel shutoff.

The electric throttle valve controls pressure, and thus fuel flow, with an accuracy suitable for closed-loop scheduling. For light-off flow, the valve should be sufficiently accurate provided the pilot and start nozzle sizes can be controlled. A trim adjustment can be provided in the ECU, if necessary, to set light-off fuel pressure (flow).

Fuel Pump

The positive-displacement fuel pump is DC motor driven. It sucks the fuel from the fuel tank and pressurizes it for introduction into the combustor. The pump will be started before engine cranking to ensure full battery voltage to the motor and to achieve fast engine start-up. At engine shutdown, the pump will be deenergized.

Fuel Filters

Two fuel filter points are used in the fuel system. The main filter is to protect the fuel pump. It is a serviceable filter to remove the bulk contaminant. The secondary filter is to protect the rest of the system from contamination that might be produced in the event of a pump failure. Additional filtration may be required at certain components for protection from built-in or generated comtaminant.

Actuators

Electromechanical actuators are employed on the AGT-100 to control burner variable geometry (BVG) position and inlet guide vane (IGV) position. In the interests of commonality, a single actuator design is proposed for both applications. An electric motor-driven screw jack was selected as the most suitable for this application. The electric actuator will receive signals from the engine ECU to control the rate, extent, and direction of actuator travel. The electric actuator has a particular advantage in being able to operate off vehicle batteries when the engine is not running (for maintenance reasons) and also ensures that the geometry is in the correct position before engine starting.

Power Transfer Clutch Servo Valve

This valve is used to direct engine oil to the piston of the power transfer clutch and to control cooling oil flow to the plates of the multiple disk clutch when engaged. The valve is operated by a double coil torque motor. The valve itself is a single flapper-double nozzle servo type used to control pressure and flow. It is used in conjunction with the engine ECU, engine oil system, and engine power transfer clutch assembly to modulate oil pressure to the power transfer clutch to obtain partly engaged (slipping) or locked-up operation.

Control Mode Definition

Basic Operation

A block diagram of the control system presently being evaluated is presented in Figure 235. A gas generator speed reference signal (N_1 ref) is calculated as a function of the throttle lever position (T/L). A speed error signal (ϵ N_1) is calculated as the difference between the speed reference and the actual gas generator speed (N_1). A proportional-plus-integral controller operates on the speed error signal to determine the appropriate control current to the power transfer clutch. A power transfer clutch valve positions the clutch plates and adjusts the clutch pressure to obtain the required torque and horsepower transfer to control gasifier speed.

When the percent gas generator speed and percent power turbine speed are equal, the clutch plates are not slipping but turning at equal speed. When that results, the clutch is said to be locked up. If N_1 is below the reference speed, the control reduces clutch pressure to keep the N_1 speed up by allowing a slip speed at the clutch. If N_1 is above the reference speed, the control increases the clutch pressure, which tends to keep the clutch locked up as long as the transmitted torque remains less than the amount required to make the clutch slip. Throttle increases or transmission shifts can cause the clutch to slip.

During locked up operation, the clutch pressure control maintains the locked up condition but has no influence over speed. The control mode presently under examination for locked up speed control closes the inlet guide vanes by an amount proportional to the speed error. The increased IGV angle reduces power thereby controlling speed. The system requires a speed error signal to position the IGV's. The engine speed therefore will run slightly above the reference speed to produce the error signal that will maintain the required IGV angle.

When operating at idle throttle position, the IGV angle is commanded to its closed position to minimize the idle horsepower. The desired IGV angle (IGV_{ref}) is selected by presently undefined logic from the throttle scheduled IGV angle and the locked up IGV control signal. The measured actuator position IGV_{FB} is compared to IGV_{ref}. The error signal is used to control the rate of change of IGV angle.

For maximum operating efficiency, it is desired to run the engine at the highest possible cycle temperatures. Material considerations limit the maximum steady-state TIT to 1288°C (2350°F) and the TOT to 1066°C (1950°F). Because the turbine inlet temperature is too high for practical thermocouple measurement, turbine outlet temperature is used as the control variable. The turbine inlet limitation is observed by calculating the corresponding turbine outlet temperature (TOT_{ref}) as a function of gas generator speed N_1, power turbine speed N_2, and CIT. The control current (i_{WF}) in milliamps, which activates the electric throttle valve, is calculated as a proportional-plus-integral function of the temperature error (ϵ_{TOT}).

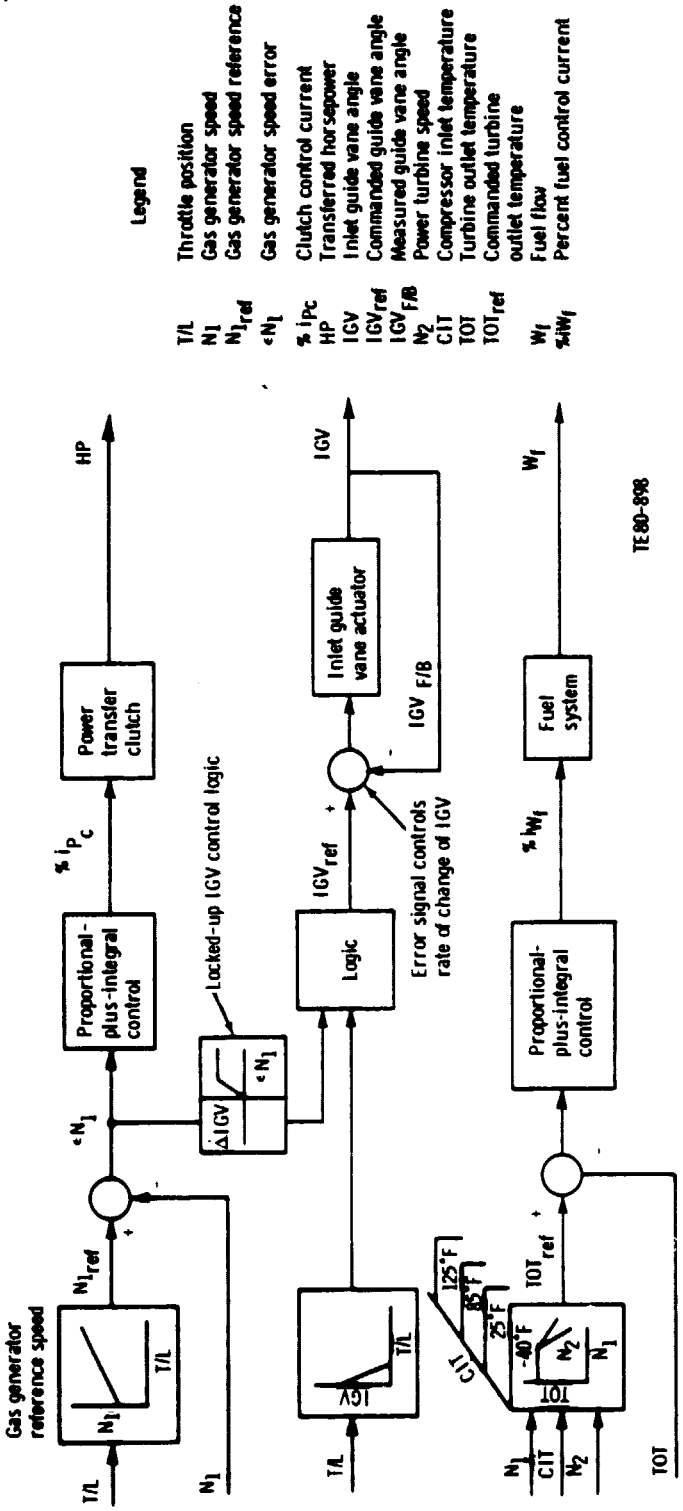

Figure 235. - AGT-100 Control Simulation Block Diagram.

Burner Variable Geometry

The production of CO and NO_x emissions is primarily affected by combustion zone flame temperature (T_f). NO_x levels become excessive as T_f exceeds an upper critical threshold. However, CO emissions exceed required limits when T_f falls below a lower threshold. Consequently, emission requirements can be met only when flame temperature is controlled within an allowable "window." The control shown in Figure 236 is configured to provide this degree of flame temperature control.

Flame temperature control is accomplished by use of a variable geometry combustor. Cooler combustion temperatures result when the primary airflow is highest (less dilution airflow), whereas increased dilution airflow causes combustion (flame) temperatures to rise. A synthesized flame temperature (T_{fs}) is computed (from TIT, BIT, and W_p/W_A) and compared with a desired (minimum emission) level to generate a flame temperature error. This error is used to position the BVG and reduce the temperature error. Temperature error is directly coupled to throttle position through a lead/lag filter. This provides anticipation during vehicle transients and more quickly alters burner geometry to control transient emission levels.

Engine airflow (W_A) is necessary to compute R_T (the residence time) and is synthesized from N_1. TIT (used in the computation of T_{fs}) is not measurable and will be synthesized from TOT. Both BIT and TOT are processed through lead/lag filters to compensate for thermocouple lag.

Simulation

A transient simulation has been developed to assist in the control system design. The simulation includes a thermodynamic cycle match of the AGT-100 engine, which computes engine temperatures, pressures, airflow, and horsepower. Engine gas generator speed is calculated by integrating the gas generator torque unbalance from the cycle match. A vehicle simulation subroutine calculates power turbine speed, transmission characteristics, and vehicle velocity. An electronic control subroutine calculates the power transfer clutch control current, the desired IGV angle, and the fuel flow control current. Three subroutines are provided for computing dynamic calculations for the IGV actuator, the fuel system, and power transfer clutch. A flow diagram of the simulation is shown in Figure 237.

The control subroutine in the simulation calculates the clutch control current from gas generator speed error as described in the control mode definition. A power transfer clutch subroutine calculates clutch position, pressure, torque, and transferred horsepower. If the gas generator speed N_1 exceeds the reference speed, horsepower is transferred to the power turbine to slow down the gas generator. During locked up operation, the horsepower transferred to the power turbine is calculated from the horsepower unbalance on the gas generator, including acceleration effects. This horsepower is limited to the maximum horsepower that can be transmitted by the clutch at the pressure supplied by the control. If this maximum horsepower is exceeded, the clutch again begins to slip.

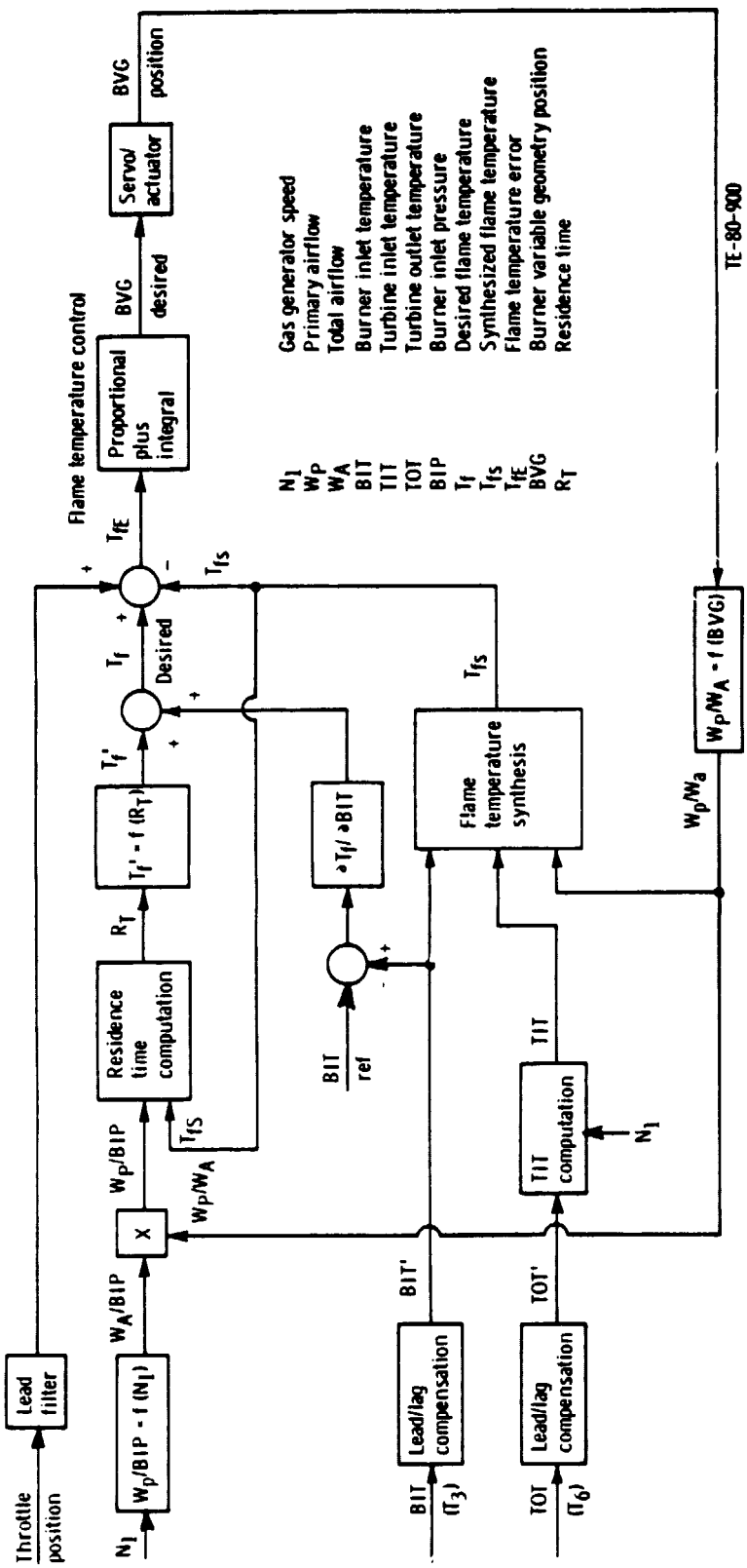

Figure 236. - Burner Variable Geometry Control.

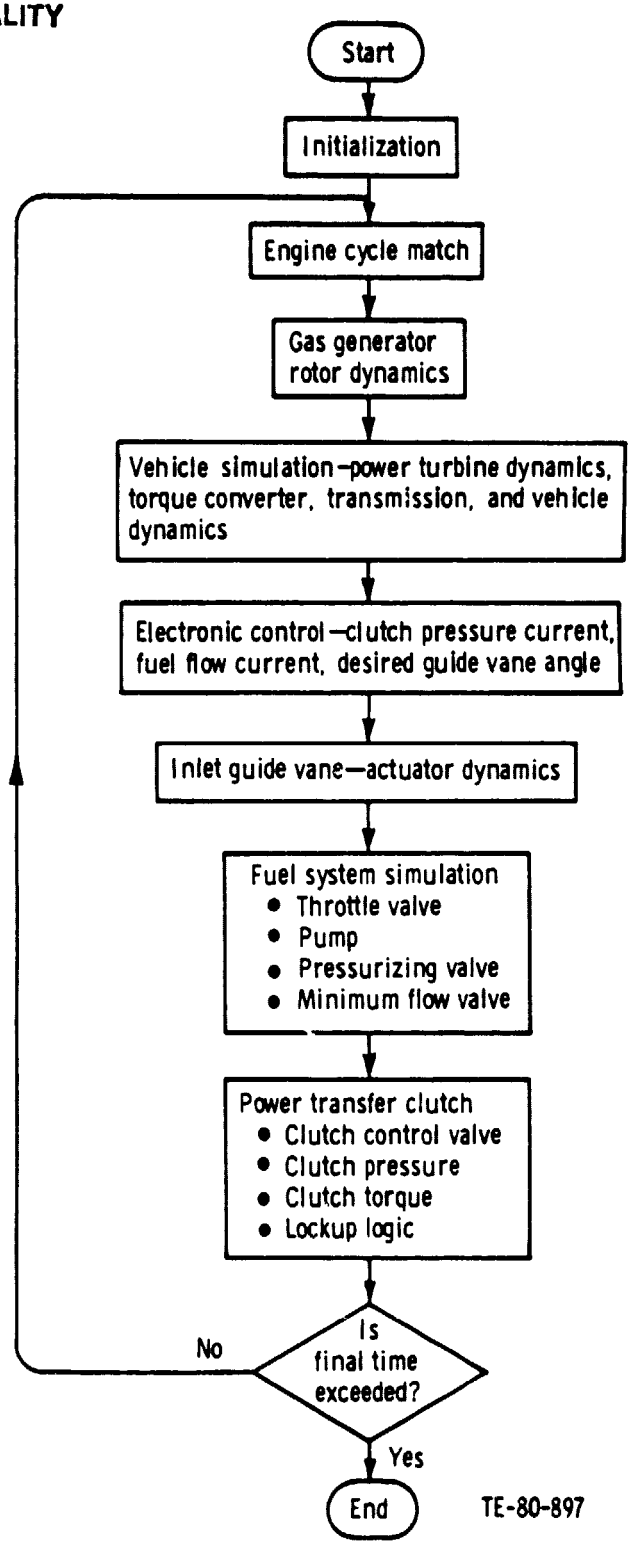

Figure 237. - AGT-100 Transient Simulation Flow Diagram.

The command inlet guide vane angle (IGV_{ref}) is the higher of either the throttle scheduled IGV angle or the gas generator speed error scheduled IGV angle. An inlet guide vane subroutine compares the actual IGV angle to the reference. A control rate up to 200 deg/s is calculated proportional to the IGV angle error.

The engine cycle match program was used to calculate tables of TOT versus gas generator speed (N_1), power turbine speed (N_2), and CIT, while operating at maximum temperature within engine operating limits. These tables are used to look up a reference value (TOT_{ref}) that is compared to the TOT from the cycle match routine from the transient deck. The temperature error signal is operated on by a proportional-plus-integral temperature controller that calculates the percent control current ($\%i_{WF}$) for the fuel control throttling valve. A fuel system subroutine simulates the valve, pump, and pressurizing valve characteristics necessary to calculate fuel flow (W_f).

Additional items will be required in the control system, which will be added to the simulation as they are being evaluated. To improve transient acceleration/deceleration performance, control logic will be added to increase the TOT_{ref} during acceleration transients and decrease it during deceleration transients. It is anticipated that minimum and maximum governors will be required on both N_1 and N_2. Also, dynamic compensation may be required in the temperature control loop to compensate for thermocouple measurement lag.

XI. TRANSMISSION DEVELOPMENT

The transmission selected for use with the AGT-100 two-shaft gas turbine engine is a General Motors front-wheel-drive automatic transaxle transmission shown schematically in Figure 238. The transmission will include a three-element torque converter with torque converter clutch mounted on the engine input centerline. Application of the torque converter clutch provides a direct mechanical drive from input to output. Also mounted on the input centerline is an engine-driven variable displacement pump and a turbine-driven chain drive sprocket. By means of the chain drive, power is transferred to a four-speed range gear set mounted concentric with the output centerline. Full power from the range gear set flows through the sun gear of a single planetary final drive reduction gear and into a concentric differential from which the power is split to the right and left output wheel drive couplings. Unique to the front wheel drive transmissions is that the differential and final drive gears are located within the transmission. The two-planetary gear and clutch arrangement provides four speeds forward and one speed reverse.

Production transmission options designed to cover the applicability of a multitude of spark ignition engines are shown in Table XXXII. Various combinations of these options have been evaluated to determine the effect on the gas turbine powertrain fuel economy and vehicle performance. Table XXXIII presents the transmission data used in optimizing the engine/transmission match for maximum fuel economy at steady state road load over a vehicle speed range from 16 to 96 km/h (10 to 60 mph). Table XXXIV lists the transmission input and output losses used in this study based on GM test data on accessory losses, variable displacement pump data, and the THM125-3 (1980 "X" car transmission) losses. Table XXXV indicates the gear range efficiencies and torque converter capacity used in the fuel economy study.

TABLE XXXII. AGT-100 TRANSMISSION OPTIONS

Torque converter capacity	1.92:1 STR 1.98:1 STR 2.08:1 STR 2.38:1 STR
Chain drive ratios	35/35--1.00:1--direct 37/33--0.892:1--Overdrive 33/37--1.1212:1--Reduction
Final drive ratios	2.842:1 3.333:1

Matching the four speed transmission gear ratios to the AGT-100 engine was made for each gear range to indicate the fuel economy characteristics obtained in each range at steady-state road load from 16 to 110 km/h (10 to 69 mph). Figures 239 and 240 are steady-state performance maps of the AGT-100 RPD engine. Figure 240 is an enlarged segment of the performance map in the 0-17.9 kW (0-24 hp) output range showing the specific fuel consumption characteristic as a function of engine output shaft horsepower for constant percent output shaft speeds. Transmission output shaft horsepower requirements at steady-

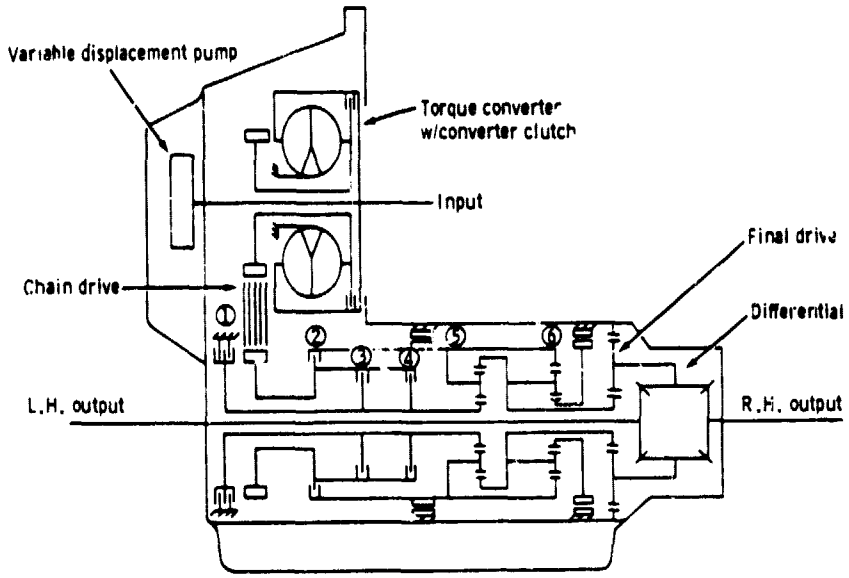

Gear range	Clutch applied	Gear ratio
1	4 & 6	2.921
2	2 & 6	1.567
3	2 & 3	1.000
4	2 & 1	0.704
REV	4 & 5	2.384

Figure 238. - Schematic of Automatic Transaxle Transmission.

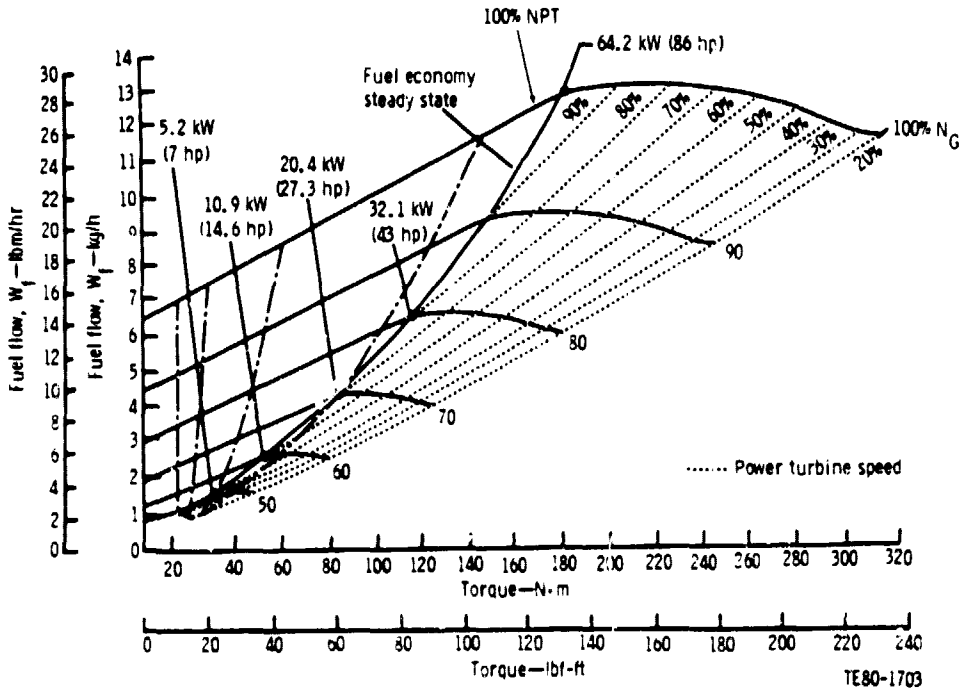

Figure 239. - Steady-State Performance Map with Optimum Fuel Economy Curve.

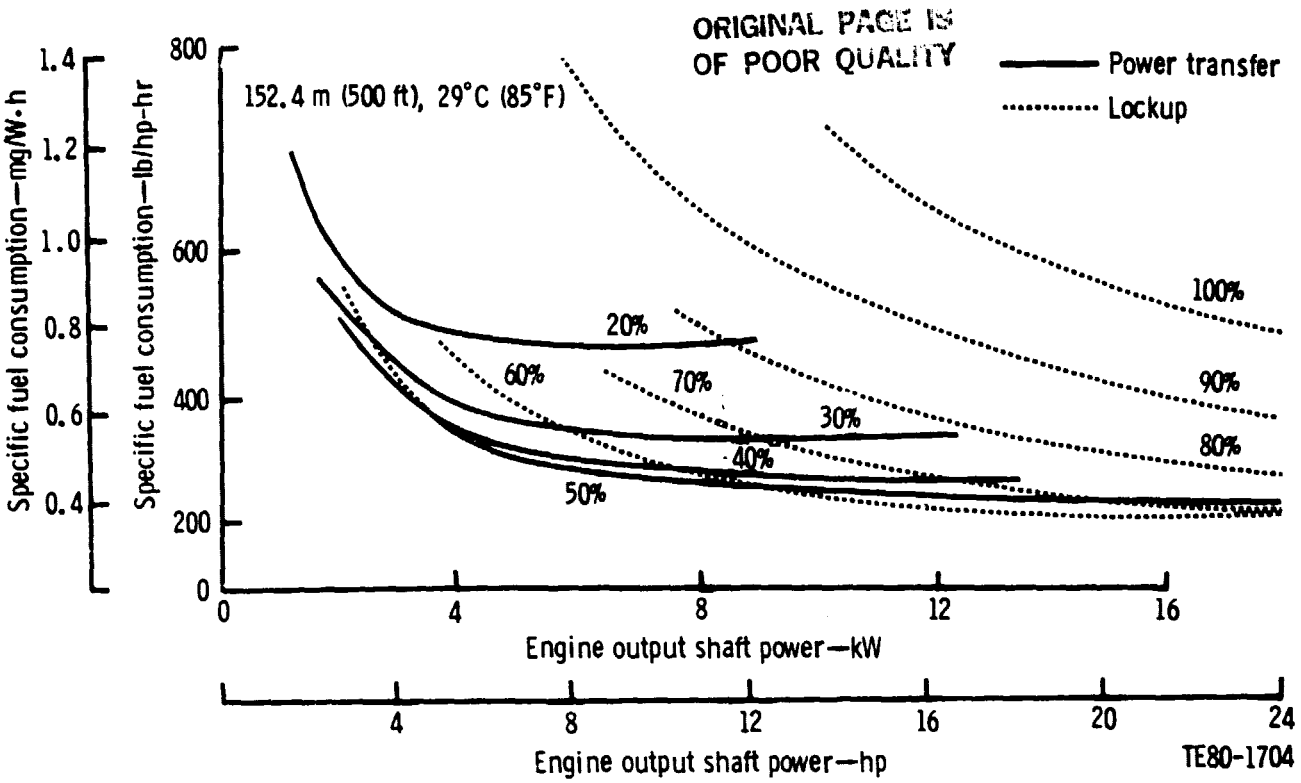

Figure 240. - Steady-State Performance SFC Versus Engine Output.

state road load vary from 0.79 kW at 16 km/h to 14.9 kW at 96 km/h (1.055 hp at 10 mph to 19.96 hp at 60 mph). Transmission operation, which programs the engine to operate in power transfer at minimum engine output shaft speed for selected horsepower ranges results in maximum fuel economy at steady-state road load. Tables XXXVI through XXXIX are detailed analyses for determining the engine horsepower from 16 to 96 km/h (10 to 60 mph) in each gear range. With the aid of Figure 240, the fuel flow and fuel economy can be determined for each segment of vehicle speed in each gear range. Figure 241 shows the result of this analysis for each gear range in which fuel flow is plotted against vehicle speed. Figure 242 is a similar result of this data showing the SFC required to develop steady-state vehicle road-load power from 16 to 96 km/h (10 to 60 mph). Optimization for maximum steady-state road-load fuel economy shows that the best fuel economy is obtained by selecting second-gear operation from 16 to 32 km/h (10 to 20 mph); third gear operation from 32 to 54 km/h (20 to 34 mph) and fourth-gear operation above 54 km/h (34 mph).

TABLE XXXIII. FUEL ECONOMY STUDIES AT STEADY-STATE ROAD-LOAD TRANSMISSION DATA

Net HP_E = 86 hp (without accessories)

N_E at converter pump = 3421 rpm (1.92 STR)

Road load HP_0 at transmission based on 2996# vehicle

Transmission gear ratios 1--2.921
2--1.567
3--1.000
4--0.704

TABLE XXXIII. (CONT)

Chain drive ratio = 1.1212

Final drive ratio = 3.333

Tires 529 rev/km (846 rpm)

$$N/V = \frac{846 \times 3.33}{60} = 46.95$$

$$\text{Max speed } N_{o_{\text{third gear}}} = \frac{3421}{1.1212 \times 1.00} = 3051 \text{ rpm}$$

$$V = \frac{3051}{46.95} = 104 \text{ km/h (65 mph)}$$

$$\text{Max speed } N_{o_{\text{fourth gear}}} = \frac{3421}{1.1212 \times 0.704} = 4334 \text{ rpm}$$

$$V = \frac{4334}{46.95} = 148 \text{ km/h (92.3 mph)}$$

TABLE XXXIV. FUEL ECONOMY STUDIES AT STEADY-STATE ROAD-LOAD TRANSMISSION DATA

Input Losses

N_E into converter pump, rpm	Accessory gear train loss, N·m (lbf-ft)	Variable displacement pump loss, N·m (lbf-ft)
400	2.67 (1.97)	2.71 (2.00)
600	2.49 (1.84)	2.03 (1.50)
1000	2.41 (1.78)	1.49 (1.10)
1500	2.57 (1.90)	1.22 (0.90)
2000	2.79 (2.06)	1.15 (0.85)
2500	3.04 (2.24)	1.08 (0.80)
3000	3.28 (2.42)	1.08 (0.80)
3421	3.49 (2.58)	1.08 (0.80)

N_T turbine speed, rpm	Spin losses, N·m (lbm-ft)
400	2.17 (1.60)
600	2.03 (1.50)
1000	1.90 (1.40)
1500	1.86 (1.37)
2000	1.94 (1.43)
2500	2.03 (1.50)
3000	2.17 (1.60)
3421	2.37 (1.75)

TABLE XXXV. FUEL ECONOMY STUDIES AT STEADY-STATE ROAD-LOAD TRANSMISSION DATA

Gear arrangement efficiency, %	
Chain drive	99
First range	96
Second range	98
Third range	100
Fourth range	98

Torque converter capacity

Speed ratio	K_P	K_T
0	218	0
0.137	220	22
0.333	215	55
0.512	217	92
0.646	235	131
0.697	245	151
0.750	255	175
0.800	267	201
0.877	287	249
0.908	299	271
0.922	315	290
0.931	334	311
0.938	352	330
0.945	381	360
0.963	471	453
0.967	498	482
0.970	525	509

K_P = Pump speed/$\sqrt{\text{Pump torque}}$

K_T = Turbine speed/$\sqrt{\text{Turbine torque}}$

TABLE XXXVI. FUEL ECONOMY STUDY--SECOND-GEAR CONVERTER OPERATION--1.567:1

Vehicle speed, km/h (mph)	Transmission out, kW (hp)	Transmission out speed, rpm	Transmission out torque, N·m (lbf-ft)	Converter SR	Transmission input speed, rpm	Input to engine speed, %	Output spin loss, kW (hp)	Turbine power (gear and chain loss), kW (hp)	Input pump loss, kW (hp)
16 (10)	0.787 (1.055)	469.5	16.0 (11.8)	0.918	899	26.2	0.17 (0.23)	0.988 (1.324)	0.153 (0.205)
24 (15)	1.270 (1.703)	704.3	17.2 (12.7)	0.953	1298	38	0.25 (0.33)	1.563 (2.095)	0.254 (0.341)
32 (20)	1.867 (2.503)	939	19.0 (14.0)	0.975	1692	49.4	0.32 (0.43)	2.255 (3.023)	0.334 (0.448)
48 (30)	3.521 (4.72)	1409	23.8 (17.6)	0.98	2525	73.8	0.53 (0.71)	4.178 (5.60)	0.538 (0.721)
64 (40)	6.056 (8.118)	1878	30.8 (22.7)						
80 (50)	9.74 (13.05)	2348	39.6 (29.2)						
96 (60)	14.89 (19.96)	2817	50.4 (37.2)						

Vehicle speed, km/h (mph)	HP_E into transmission, kW (hp)	Over all transmission efficiency, %	Accessory loss, kW (hp)	HP_E net, kW (hp)	HP_E to total, %	Turbine torque N·m (lbf-ft)	Engine torque N·m (lbf-ft)	SFC mg/Wh (lbm/hp-hr)	Fuel flow, kg/h (lbm/hr)	Fuel economy, km/L (mpg)
16 (10)	1.229 (1.647)	64	0.230 (0.308)	1.46 (1.96)	2.27	11.4 (8.4)	15.4 (11.4)	614.4 (1.01)	0.90 (1.98)	15.2 (36)
24 (15)	1.89 (2.54)	67	0.340 (0.457)	2.24 (3.00)	3.48	12.1 (8.9)	16.4 (12.1)	474.5 (0.78)	1.06 (2.34)	19.2 (45.6)
32 (20)	2.65 (3.55)	71	0.471 (0.631)	3.12 (4.18)	4.86	13.0 (9.6)	17.6 (13.0)	395.4 (0.65)	1.24 (2.72)	22.1 (52.3)
48 (30)	4.80 (6.44)	73	0.803 (1.077)	5.60 (7.51)	8.73	16.1 (11.9)	21.1 (15.6)	547.5 (0.90)	3.07 (6.76)	13.3 (31.5)

TABLE XXXVII. FUEL ECONOMY STUDY--SECOND-GEAR CONVERTER CLUTCH APPLIED--1.567:1

Vehicle speed, km/h (mph)	Transmission out, kW (hp)	Transmission out speed, rpm	Transmission out torque, N·m (lbf-ft)	Converter SR	Transmission input speed, rpm	Input to engine speed, %	Output spin loss, kW (hp)	Turbine power (gear and chain loss), kW (hp)	Input pump loss, kW (hp)
16 (10)	0.787 (1.055)	469.5	16.0 (11.8)	1.0	825	24.1	0.17 (0.23)	0.988 (1.324)	0.152 (0.204)
24 (15)	1.270 (1.703)	704.3	17.2 (12.7)	1.0	1237	36.2	0.25 (0.33)	1.563 (2.095)	0.175 (0.235)
32 (20)	1.867 (2.503)	939	19.0 (14.0)	1.0	1650	48.2	0.32 (0.43)	2.255 (3.023)	0.206 (0.276)
48 (30)	3.54 (4.72)	1409	23.8 (17.6)	1.0	2475	72.3	0.53 (0.71)	4.178 (5.60)	0.281 (0.377)
64 (40)	6.056 (8.118)	1878	30.8 (22.7)						
80 (50)	9.74 (13.05)	2348	39.6 (29.2)						
96 (60)	14.89 (19.96)	2817	50.4 (37.2)						

Vehicle speed, km/h (mph)	HP_E into transmission, kW (hp)	Over all transmission efficiency, %	Accessory loss, kW (hp)	HP_E net, kW (hp)	HP_E to total, %	Turbine torque N·m (lbf-ft)	Engine torque N·m (lbf-ft)	SFC mg/Wh (lbm/hp-hr)	Fuel flow, kg/h (lbm/hr)	Fuel economy, km/L (mpg)
16 (10)	1.140 (1.528)	69	0.212 (0.284)	1.35 (1.81)	2.21	11.4 (8.43)	15.6 (11.5)	656.9 (1.08)	0.89 (1.96)	15.4 (36.3)
24 (15)	1.74 (2.33)	73	0.324 (0.434)	2.06 (2.76)	3.21	12.1 (8.89)	15.9 (11.7)	498.8 (0.82)	1.03 (2.27)	20.0 (47)
32 (20)	2.46 (3.30)	76	0.459 (0.615)	2.92 (3.92)	4.55	13.0 (9.62)	16.9 (12.5)	407.5 (0.67)	1.19 (2.62)	23.0 (54.2)
48 (30)	4.46 (5.98)	79	0.79 (1.06)	5.24 (7.03)	8.17	16.1 (11.9)	20.2 (14.9)	547.4 (0.90)	2.87 (6.33)	14.3 (33.7)

TABLE XXXVIII. FUEL ECONOMY STUDY--THIRD-GEAR CONVERTER CLUTCH APPLIED--1.000:1

Vehicle speed, km/h (mph)	Transmission out, kW (hp)	Transmission out speed, rpm	Transmission out torque, N·m (lbf-ft)	Converter SR	Transmission input speed, rpm	Input to engine speed, %	Output spin loss, kW (hp)	Turbine power (gear and chain loss), kW (hp)	Input pump loss, kW (hp)
16 (10)	0.787 (1.055)	469.5	16.0 (11.8)						
24 (15)	1.270 (1.703)	704.3	17.2 (12.7)	1.0	790	23	0.162 (0.218)	1.43 (1.94)	0.145 (0.195)
32 (20)	1.867 (2.503)	939	19.0 (14.0)	1.0	1053	30.8	0.209 (0.280)	2.10 (2.81)	0.16 (0.22)
48 (30)	3.521 (4.72)	1409	23.8 (17.6)	1.0	1579	46.2	0.310 (0.415)	3.87 (5.19)	0.199 (0.267)
64 (40)	6.056 (8.118)	1878	30.8 (22.7)	1.0	2106	61.5	0.433 (0.581)	6.56 (8.79)	0.251 (0.337)
80 (50)	9.74 (13.05)	2348	39.6 (29.2)	1.0	2632	76.9	0.568 (0.762)	10.41 (13.95)	0.30 (0.40)
96 (60)	14.89 (19.96)	2817	50.4 (37.2)	1.0	3158	92.3	0.735 (0.986)	15.78 (21.16)	0.36 (0.48)

Vehicle speed, km/h (mph)	HPg into transmission, kW (hp)	Over all transmission efficiency, %	Accessory loss, kW (hp)	HPg net, kW (hp)	HPg to total, %	Turbine torque N·m (lbf-ft)	Engine torque N·m (lbf-ft)	SFC mg/Wh (lbm/hp-hr)	Fuel flow, kg/h (lbm/hr)	Fuel economy, km/L (mpg)
16 (10)										
24 (15)	1.80 (2.14)	80	0.20 (0.27)	1.80 (2.41)	2.8	17.5 (12.9)	21.7 (16)	596.1 (0.98)	1.07 (2.36)	19.3 (45.3)
32 (20)	2.26 (3.03)	83	0.27 (0.36)	2.53 (3.39)	3.9	19.0 (14.0)	22.9 (16.9)	474.5 (0.78)	1.20 (2.64)	22.9 (53.8)
48 (30)	4.07 (5.45)	87	0.42 (0.57)	4.50 (6.03)	7.0	23.5 (17.3)	27.1 (20)	316.3 (0.52)	1.42 (3.13)	28.9 (68.0)
64 (40)	6.30 (9.12)	89	0.62 (0.84)	7.43 (9.96)	11.6	29.7 (21.9)	33.6 (24.8)	292.0 (0.48)	2.17 (4.78)	25.3 (59.5)
80 (50)	10.71 (14.35)	91	0.85 (1.14)	11.6 (15.5)	18.0	37.7 (27.8)	41.9 (30.9)	346.7 (0.57)	4.01 (8.83)	17.1 (40.3)
96 (60)	16.14 (21.64)	92	1.10 (1.48)	17.2 (23.1)	26.9	47.7 (35.2)	52.2 (38.5)	589.3 (0.64)	6.71 (14.8)	12.2 (28.8)

TABLE XXXIX. FUEL ECONOMY STUDY--FOURTH-GEAR CONVERTER CLUTCH APPLIED--0.704:1

Vehicle speed, km/h (mph)	Transmission out, kW (hp)	Transmission out speed, rpm	Transmission out torque, N·m (lbf-ft)	Converter SR	Transmission input speed, rpm	Input to engine speed, %	Output spin loss, kW (hp)	Turbine power (gear and chain loss), kW (hp)	Input pump loss, kW (hp)
16 (10)	0.787 (1.055)	469.5	16.0 (11.8)						
24 (15)	1.270 (1.703)	704.3	17.2 (12.7)						
32 (20)	1.867 (2.503)	939	19.0 (14.0)	1.0	741	21.6	0.154 (0.206)	2.08 (2.79)	0.149 (0.20)
48 (30)	3.521 (4.72)	1409	23.8 (17.6)	1.0	1112	32.5	0.221 (0.296)	3.86 (5.17)	0.157 (0.21)
64 (40)	6.056 (8.118)	1878	30.8 (22.7)	1.0	1482	43.3	0.288 (0.386)	6.54 (8.77)	0.189 (0.254)
80 (50)	9.74 (13.05)	2348	39.6 (29.2)	1.0	1853	54.2	0.374 (0.501)	10.42 (13.97)	0.226 (0.303)
96 (60)	14.89 (19.96)	2817	50.4 (37.2)	1.0	2224	65	0.461 (0.618)	15.8 (21.2)	0.259 (0.347)

Vehicle speed, km/h (mph)	HPg into transmission, kW (hp)	Over all transmission efficiency, %	Accessory loss, kW (hp)	HPg net, kW (hp)	HPg to total, %	Turbine torque N·m (lbf-ft)	Engine torque N·m (lbf-ft)	SFC mg/Wh (lbm/hp-hr)	Fuel flow, kg/h (lbm/hr)	Fuel economy, km/L (mpg)
16 (10)										
24 (15)										
32 (20)	2.23 (2.99)	84	0.190 (0.255)	2.24 (3.25)	3.77	26.8 (19.8)	31.2 (23)	523.1 (0.86)	1.26 (2.79)	21.6 (50.9)
48 (30)	4.01 (5.38)	88	0.284 (0.381)	4.30 (5.76)	6.7	33.1 (24.4)	36.9 (27.2)	352.8 (0.58)	1.51 (3.34)	27.1 (63.8)
64 (40)	6.72 (9.02)	90	0.400 (0.536)	7.13 (9.56)	11.1	42.2 (31.1)	45.8 (33.8)	285.9 (0.47)	2.04 (4.49)	26.9 (63.3)
80 (50)	10.67 (14.3)	91.4	0.526 (0.705)	11.2 (15.0)	17.4	53.7 (39.6)	57.5 (42.4)	237.2 (0.39)	2.65 (5.84)	25.8 (60.8)
96 (60)	16.1 (21.6)	93	0.679 (0.910)	16.8 (22.5)	26.1	67.9 (50.1)	71.9 (53)	231.1 (0.38)	3.82 (8.42)	21.5 (50.6)

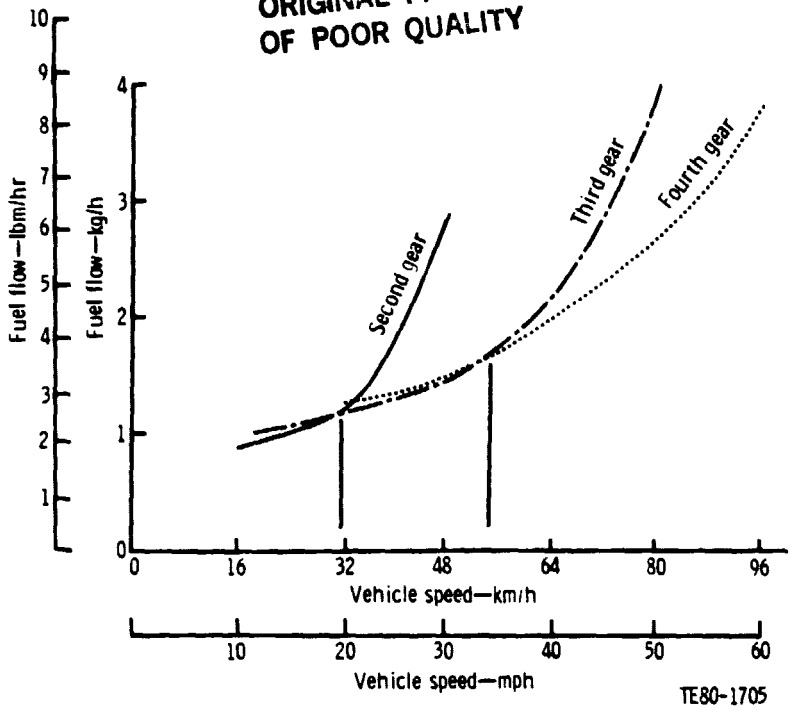

Figure 241. - Transmission Gear Range Fuel Economy at Steady-State Road Load.

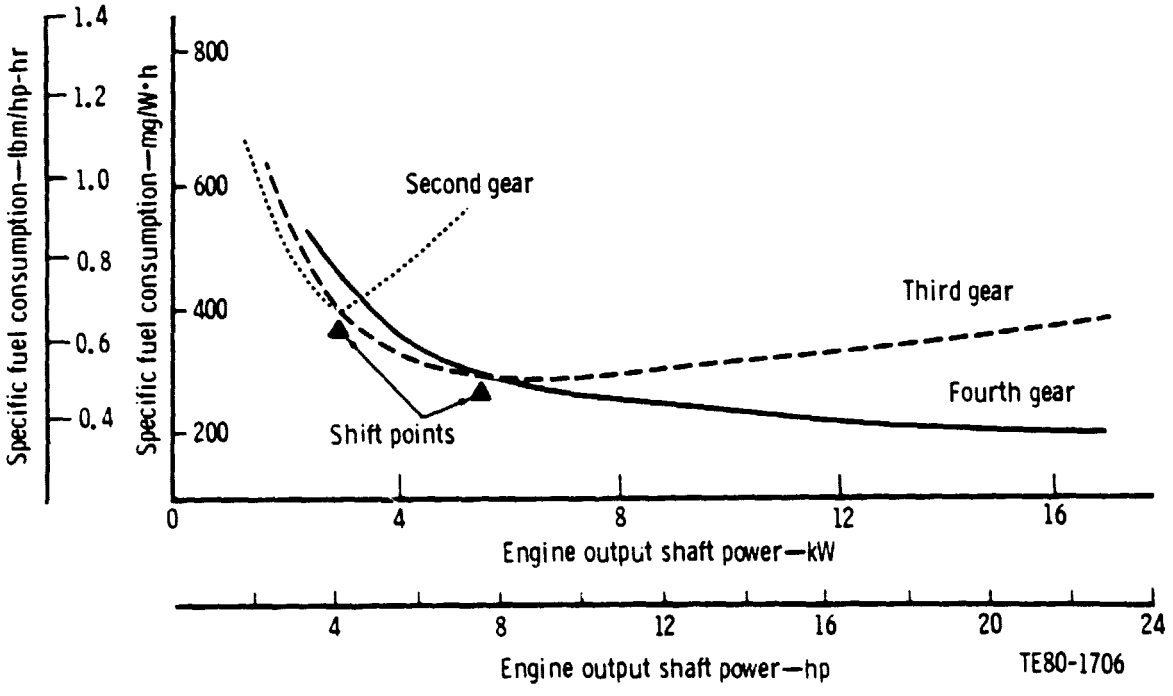

Figure 242. - SFC for Various Road-Load Power Requirements.

XII. SUPPPORTIVE MANUFACTURING, COST, AND MARKETABILITY

12.1 MANUFACTURING FEASIBILITY

Pontiac's effort in manufacturing feasibility studies has concentrated in three areas:

- o Analyzing components for machinability and assembly
- o Recommending changes to improve producibility
- o Initiating the tooling and piece-rate studies for determining cost

Results of the work to date are described in the following pages.

Engine Block

The basic feasibility of casting and machining the block has been determined. Core design appears amenable to conventional high-production machining techniques. The use of through-tapped holes was shown to be advantageous. In addition, an early design included a series of six square pads along the inner seal cross arm. These pads were to be machined on the block casting, which presented serious problems in machining the block inner seal surface flat and in achieving the height tolerance required, since the pads were inside the regenerator cavity and, therefore, not easily surface ground. Pontiac, therefore, suggested that these pads be made an integral part of the inner seal steel back up plate. This suggestion has been incorporated in the block design.

An aluminum block will be made as a visual aid to foundry people to determine the desired manufacturing processes. With added machining, this block can become the basis of a complete engine model. Parts, or models of parts, will be added to the block model as they become available. This assembled model will in turn be used in determinine the best orientations, sequences, and methods of assembling the engine on a production line.

Compressor/Gasifier Turbine Assembly

From the parts list provided, Pontiac has made preliminary make-or-buy determinations for all but a few parts in this assembly.

Item No.	Part No.	Name
C-0054	N/L	Seal, scroll E
C-0058	N/L	Vane, gas turbine--ceramic
C-0062	N/L	Rotor assembly, gas turbine
C-0064	N/L	Rotor, gas turbine--ceramic
C-0070	N/L	Scroll, GT inlet--RR--ceramic
C-0072	N/L	Insulator
C-0074	N/L	Yoke assembly
C-0188	N/L	Spacer, bevel pinion

Note: Several of these are ceramic parts.

Item No.	Part No.	Name
C-0012	AA-100058	Support assembly turbine bearing
C-0022	AA-100079	Plate assembly compressor seal--front
C-0028	AA-100076	Seal, compressor impeller
C-0030	AA-100078	Cap, compressor seal, front
C-0032	AA-100081	Retainer bearing--RR
C-0034	AA-100084	Housing assembly, seal-- R bearing
C-0036	AA-100082	Seal, turbine rotor
C-0040	AA-100083	Sleeve, RR bearing seal
*C-0048	AA-100101	Shield, bolt
C-0056	23003176	Scroll, GT inlet--front
C-0066	AA-100073	Shaft, GT rotor
C-0088	AA-100074	Spacer assembly compressor imp
C-0094	AA-100054	Diffuser, compressor
C-0096	AA-100056	Impeller assembly, compressor
C-0098	AA-100057	Shaft compressor imp
C-0100	AA-100055	

(23003178)

Shroud, compressor		
C-0104	AA-100054	Vane, inlet guide, compressor
C-0112	23003176	Scroll assembly, compressor
C-0124	AA-100060	Ring, scroll retainer
*C-0134	AA-100070	Separator assembly IGV--RR
C-0140	AA-100069	Separator, IGV--front
C-0162	AA-100087	Center body
C-0164	AA-100063	Seal ring
C-0172	AA-100061	Sleeve, isolater--front bearing
C-0194	23003175	Duct assembly compressor air inlet
C-0206	AA-100090 (2 parts)	Gear, bevel, upper--pinion & gear
C-0212	AA-100091 (2 parts)	Gear, bevel, lower--pinion & gear
*C-0232	AA-100093	Cover, upper bevel gear
C-0242	AA-100096	Support, bearing--lower bevel gear
C-0250	AA-100096	Spacer, bearing
C-0256	AA-100095	Housing assembly, lower bevel gear
C-0262	AA-100097	Cover, bevel gearbox

*To be quoted by PMD Sheet Metal Plant.

Machining of these parts are in various stages of geing estimated.

To date, items C-0056, C-0112, and C-0194 have had changes suggested by PMD to aid mass production manufacturability. The results of the suggestions follow:

Item No. C-0056 (23003176)--Scroll GT Inlet--Front

It was requested by PMD manufacturing engineering that the rear surface plane be free of outlet interference to facilitate machining that surface faster, at lower equipment cost and with the best flatness capability.

DDA decided that the part would remain as is for the test rig part but would be revised as requested by moving the outlet approximately 6.2 mm (0.25 in.) forward in the RPD final design.

Item No. C-10100--AA-100055 (23003178)--Shroud, Compressor

There is concern over the possible movement of the throat section when the boundary layer air groove is machined. It may be necessary to make the ribs of a heavy triangular cross section with a web of metal remaining in place into which the groove would extend. Close attention will be paid to such movement during the machining of the rig part. In addition, rig test will determine whether the groove is necessary at all. In any case, the RPD design will provide a stiff throat section for high-production machining.

Item No. C-0194 (23003175)--Duct Assembly Compressor Air Inlet

An air inlet design change was suggested to allow the power transfer shaft inner bearing pocket be a through bore from the outside rather than a back bore operation. This would ensure proper inner and outer bearing pocket concentricity and sturdier inner pocket boring tooling. The decision was accepted by DDA for the RPD. The method of achieving the straight through bore would be decided after rig testing.

Regenerator Assembly

The function and requirements of the various parts of the regenerator assembly have been reviewed.

Combustor Assembly

Combustor redesign provides additional space for insulation and incorporates many changes for manufacturability. These include:

- o Making the swirl vanes an investment casting rather than fabricated sheet metal
- o Redesigning the fuel and air rings to simplify assembly
- o Redesigning the main fuel tube to simplify assembly
- o Designing the idle-air chamber so that it could be easily preassembled prior to vacuum brazing
- o Designing the lower valve ring support so that the ceramic ring could be snapped in place
- o Simplifying the lever arm pocket blocks to prevent rotation and to provide attachment for the lower valve operating arms

The combustion chamber hold down rods were also changed to provide for easy assembly. Discussions have been held with machine vendors on machining the swirl vane side openings and the fuel distributor holes in the evaporator ring. These will be EDM machined.

Gear Train Assembly

Power Transfer Bevel Gears

Processing has been started on these gears using the layout drawing. These parts are listed in the compressor/gasifier turbine assembly which has been received. Further attention is required to the method of shimming to position these gears on their cone centers at assembly.

Regenerator Drive Gearing

These gears and their assembly have been studied as they appear on the layout. They present a difficult problem in assembly. PMD has suggested assembly procedure for these parts.

Oil System Assembly

After studying the layouts, PMD manufacturing engineering recommended the use of the same design and some of the actual parts that are used in the Pontiac L-4 engine. DDA accepted this recommendation.

Fuel System Assembly

Work has been done in this group as it relates to the combustor. In this respect, it has been determined that the actual starting and idle nozzles will be purchased items.

Engine Assembly

In studying the layouts, PMD manufacturing engineering keeps assembly constantly in mind and makes recommendations. Examples to date are:

- o All insulation should be designed as preformed pieces for snap-in assembly.
- o Insulating should have a protective coating to prevent damage and dislodging debris during subsequent assembly.
- o Subassemblies should be used so assemblers with minimum skills can perform individual operations in 15 to 20 s.

12.2 COST ANALYSIS

Initial make-or-buy analysis has been made on the parts (drawings) received from DDA, and the requests for quotation have been submitted to the outside suppliers or Pontiac manufacturing departments.

The Pontiac Industrial Engineering Department will be integrating the cost estimates of parts completed, along with extrapolated costs of parts not completed, to develop the vehicle cost for the first year RPD presentation.

The Pontiac Product Cost Analysis Department uses the cost data submitted by the Industrial Engineering Department to establish the vehicle price for comparison with the baseline vehicle. The pricing study will be based on 1981 vehicle cost and pricing.

REFERENCES

1. Johnson, R. A., "Conceptual Design Study of an Improved Gas Turbine (IGT) Powertrain," NASA CR-159604, prepared Lewis Research Center under Contract DEN 3-28 (July 1979).

2. "Advanced Gas Turbine (AGT) Powertrain System Initial Development Progress Report," NASA-CR-159804, prepared for NASA Lewis Research Center under Contract DEN-3-28 (March 1980).

3. Miller, D. S., "Internal Flow Systems," DHRA Fluid Engineering Series, Vol. 5, pp. 183-219 (1978).

4. Novick, A. S., et al., "Numerical Simulation of Combustor Flow Fields, A Primitive Variable Design Capability," Journal of Energy, Vol. 3, No. 2, p. 95 (March-April 1979).

5. "Comparison of the MOR--Channel Skew Correlations," Section 3.3.4A, reported in the July-January 1978 report for Ceramic Applications in Turbine Engines.

6. Widerhorn, S. M., and L. H. Bolz, "Stress Corrosion and Static Fatigue of Glass," Journal of the American Ceramics Society, Vol. 53, pp. 543, 547-548 (October 1970).

7. Wiederhorn, S. M., "High Temperature Fracture of Ceramic Materials," DOE Workshop, pp. 66-68 (February 1979).

8. Bausal, G. K., W. H. Duckworth, and D. E. Niesz, "Strength Analysis of Brittle Materials," Final Report, ONR, Contract No. 00014-73-C-0408, NR032-541, pp. B5-B9 (November 1977).

APPENDIX A

List of Symbols and Abbreviations

AGT	Advanced Gas Turbine
AGT-100	The AGT Model being developed by DDA
AS	Aluminum silicate
BIP	Burner inlet pressure
BIT	Burner inlet temperature
BOT	Burner outlet temperature
Btu	British thermal unit
B/U or BU	Build up
BVG	Burner variable geometry
C	Isentropic spouting velocity--$2gJ\ h_{is}$
°C	Degrees Celsius
C_p	Static pressure recovery coefficient; specific heat
CATE	A NASA/DOE development program "Ceramic Applications for Turbine Engines"
CBO	Carborundum Corporation
CCW	Counter clockwise (rotation)
CDP	Compressor discharge pressure
CGW	Corning Glass Works
CIT	Compressor inlet temperature
CM	Meridional chord
CO	Carbon monoxide
CVD	Chemical vapor deposition
CW	Clockwise (rotation)
CY	Calendar year
DF#2	Diesel fuel number 2
D_m	Mean bearing diameter
DDA	Detroit Diesel Allison Division of General Motors
DOE	US Department of Energy
ECU	Electronic control unit
EDR	Engineering Development Report (of DDA)
EO	Engine order
°F	Degrees Fahrenheit
F_1	Flow factor
F/A	Fuel air ratio
FDC	Federal driving cycle
ft	Foot
GM	General Motors Corporation
GT	Gas turbine
GMR	General Motors Research
GTE	General Telephone and Electronics Corp.
GPSIM	General purpose simulation
g	Gravitational constant
h	Hour; enthalpy
HP or hp	Horsepower
HRD	Harrison-Radiator Division of General Motors
Hz	Hertz (frequency)
ID	Inside diameter
in.	Inch

IGT	Industrial gas turbine (manufactured by DDA)
IGV	Inlet guide vane
J	Conversion factor, Btu to ft-lb; Joule
kg	Kilogram
km	Kilometre
ksi	Thousand pounds per square inch
L	Litre
LAS	Lithium aluminum silicate
lbm	Pound mass
LCF	Low cycle fatigue
L.E. or l.e.	Leading edge
M	Mega--(one million); meridional distance
M_N	Mach number
$M_{N_{ABS}}$	Absolute Mach number
MC	Meridional chord
m	Metre
mm	Milimetre
mpg	Miles per gallon
Mod I	The first design of AGT-100 using some metal hot section components
Mod II	The second AGT-100 design with ceramic hot section
MOR	Modulus of rupture
N	Newton; speed (rpm)
N_G	Gasifier speed
N_{Re}	Reynolds number
N_S	Specific speed
NASA	National Aeronautics and Space Administration
N/C	Normally closed
N/O	Normally opened
NDE	Non-destructive evaluation
Ni-Resist iron	A corrosion- and heat-resistant cast iron containing 2% Cr and 20% Ni
NO_x	Oxides of nitrogen
N1	Gasifier speed of rotation
N2	Power turbine speed of rotation
P	Pressure
P_T	Total pressure
Pa	Pascal
PMD	Pontiac Motors Division of General Motors
PRI	Primary Responsible Individual
P_S	Probability of Survival
Q	Volume flow
°R	Degrees Rankine
R_C	Pressure ratio
REGEN	Regenerator
RBSiC	Reaction bonded silicon carbide
RPD	Reference Powertrain Design
RTV	Room Temperature Vulcanizing
$R_{C_{T-S}}$	Compression ratio (total-to-static)
Sec or s	Second
SLAM	Scanning Laser Acoustic Microscopy
SLS	Sea level static; sea level standard

SPAM	Scanning Photoacoustic Spectroscopy
T	Temperature
T_8	Regenerator inlet temperature (hot side)
T.E. or t.e.	Trailing edge
THM 440-T4	Designation for a CM transmission for X-body cars
TOT	Turbine outlet temperature
U_T	Rotor tip speed
V	Viscosity, velocity
VG	Variable geometry
W	Watt; bearing thrust load; mass flow; relative velocity
W_c	Cooling flow rate
W_{CR}	Relative velocity (critical)
WOT	Wide open throttle
2-D	Two-dimensional (analysis)
3-D	Three-dimensional (analysis)
404	An industrial gas turbine engine by DDA
505	An industrial gas turbine engine by DDA
γ	Ratio of specific heats
$\gamma*$	Ratio of specific heats at U.S. standard sea level conditions of 1.013×10^2 kPa and 288.2°K
Δh	Specific work
Δh_{is}	Isentropic work
ϵ	Specific heat correction
η	Efficiency
η_{TT}	Efficiency (total-to-total)
θ	Temp/temp std
θ_{cr}	$(V_{cr}/V_{cr}std)^2$